

Calculation of nuclear reaction rates in astrophysical processes



A dissertation submitted to the
Department of Physics of the University of Lisbon
in partial fulfillment of the requirements
for the Degree of

Doctor of Philosophy

by

Bruno Marques Braizinha

SUPERVISORS:

Professor Ana Maria Eiró (University of Lisbon)

Professor Filipe Duarte Santos (University of Lisbon)

Professor Ian J. Thompson (University of Surrey)

Lisbon, 2004

Summary

The field of Nuclear Astrophysics is concerned with the study of nuclear reactions involved in the nucleosynthesis process inside stars (stellar nucleosynthesis) and in the early universe (primordial nucleosynthesis). This field flourished from the early work of Burbidge, Burbidge, Fowler and Hoyle [Bur57], which postulated a series of energy generating processes in stars.

In recent years, this field has seen a remarkable expansion and exciting developments, with the introduction of more sophisticated stellar models, and increased precision in the experimental determination of stellar reaction rates. However, it is still rare to find experimental values of nuclear reaction rates at the energies needed as inputs to stellar models, as these energies are almost always below the Coulomb barrier. Therefore, this field continues to be marked by the need of theoretical models that extrapolate, in a reliable way, the experimental data to the astrophysical relevant energies.

This work focuses precisely on this aspect of the Nuclear Astrophysics field, the theoretical analysis of nuclear reaction data, particularly in the low energy region. We propose and implement a framework for the systematic study of nuclear reactions, and attempt to address fundamental issues regarding the modeling of low energy nuclear reactions, namely the interplay between direct and resonant contributions to the reaction mechanism, and the accurate extrapolation of experimental data.

We focus on applications that involve transfer or photonuclear processes, and study a set of reactions, namely the $^{14}\text{N}(p,\gamma)^{15}\text{O}$, the $^3\text{He}(d,p)^4\text{He}$, the $^{12}\text{C}(\alpha,\gamma)^{16}\text{O}$ and the $^7\text{Li}(p,\gamma)^8\text{Be}$ reactions, that involve several types of processes (transfer and photonuclear processes, direct and resonant mechanisms, effects of tensor forces, etc), that are the object of much interest as modern topics of research.

We start with the introduction of the theoretical framework, where we focus on the coupled channels model and the R–matrix theory of nuclear reactions, both as a method of solving the coupled equations and in the pure phenomenological approach, and explore the possibility of including R–matrix poles in a coupled channels analysis, which we call the hybrid framework.

The first application of the theoretical framework is in the analysis of the $^3\text{He}(d,p)^4\text{He}$ transfer reaction. We study the available experimental low energy data (total and differential reaction cross section data, vector and tensor analyzing powers and polarization transfer observables) with DWBA, coupled channels and phenomenological R–matrix models. In this analysis we also include new experimental measurements of the A_{yy} and cross section observables at zero degrees, performed in the context of this work at TUNL (Triangle Universities Nuclear Laboratory), USA.

The study described in the last paragraph leads to the introduction of the hybrid R–matrix + potential analysis where the negative parity contributions, essentially arising from a direct reaction mechanism, are taken in consideration through a potential description, while the resonant contributions to the reaction mechanism are treated in the R–matrix framework. With this model we are able to describe the measured observables, fitting the potential and R–matrix parameters to the experimental data, and to disentangle the direct and resonant contributions to the reaction mechanism.

The range of applications of the theoretical framework developed is then expanded to include radiative capture processes. The analysis of these processes in the hybrid framework requires the introduction of photonuclear couplings in the coupled channels formalism, a development that has important application in the Nuclear Astrophysics field since many nuclear reactions important in Astrophysics involve photonuclear processes. We use the $^{12}\text{C}(\alpha,\gamma)^{16}\text{O}$ and $^7\text{Li}(\text{p},\gamma)^8\text{Be}$ reactions as a testing ground for the formalism, before studying the $^{14}\text{N}(\text{p},\gamma)^{15}\text{O}$ reaction.

Finally, the $^{14}\text{N}(\text{p},\gamma)^{15}\text{O}$ radiative capture reaction is studied with a phenomenological R–matrix model, showing the strengths and weaknesses of this approach, and with the hybrid framework. Both these models allow the correct description of the available experimental data, however, they yield different parameters for the set of ^{15}O resonances used in the analysis, and different values for the astrophysical S–factor. These differences can be attributed to a high degree of uncertainty in the low energy experimental data available, with large error bars affecting the data in this energy range.

We conclude that the hybrid framework developed has important applications in the analysis of low energy nuclear reaction data. With this model we are able to obtain information on the properties of the states that dominate the resonant contribution to the reaction mechanism, as well as on the strength of the direct process contributions. Furthermore, we are able to accurately extrapolate the theoretical curves to the energy region relevant for the astrophysical processes.

Acknowledgements

I would like to thank my parents and brothers for the encouragement and support, at all levels, I got from them during this lengthy process, and my grandfather for the model of rectitude in life that has always inspired me.

To my Portuguese friends, Catarina, Jorge, Gonçalo, Mota, Balacó, Gil and Sofia, a big thank you for all the help and encouragement, and to all the friends I meet during these four years, Young-A, Doug, Woekyoung, Arata, Veronique, Serge and Larissa, thank you for being so nice and supportive.

To my supervisors, Ian Thompson, Ana Eiró, Hugon Karwowski, Ed Ludwig and Filipe Santos, I wish to thank you for all you thought me, and the encouragement and commitment you always demonstrated. I hope I was worthy of your time.

Finally I would like to thank the Fundação para a Ciência e Tecnologia for the financial support through the scholarship SFRH/BD/1124/2000, and the Centro de Física Nuclear of the University of Lisbon, the University of North Carolina, Duke University and the University of Surrey for the excellent working environment they offered me.

Lisboa, Abril de 2004

Contents

I	Introduction	1
II	Reaction theory	7
1	The coupled equations	9
2	Solving coupled equations	17
2.1	Iterative solutions	17
2.2	R-matrix solutions	17
2.2.1	R-matrix model with reaction channels	18
2.2.2	The Scattering matrix	20
2.3	Phenomenological terms in the R-matrix	20
2.3.1	The hybrid method	20
2.3.2	Simple R-matrix phenomenology	21
III	The ${}^3\text{He}(\text{d,p}){}^4\text{He}$ transfer reaction	25
3	Features of the reaction	27
3.1	Reaction mechanism	27
3.2	Polarization formalism for the $\vec{1} + \frac{1}{2} \rightarrow \vec{1} + 0$ spin structure	30
3.2.1	General remarks	30
3.2.2	Form of the observables for $\vec{1} + \frac{1}{2} \rightarrow \vec{1} + 0$	33
3.2.3	Observables for $\theta=0^\circ$	37
3.3	Experimental data	38

4	New Measurements	41
4.1	Experimental study of the ${}^3\text{He}(\text{d},\text{p}){}^4\text{He}$ reaction	41
4.1.1	A_{yy} measurement	41
4.1.2	Cross section measurement	43
4.2	Scattering amplitudes	46
4.3	Conclusions	47
5	Analysis of the ${}^3\text{He}(\text{d},\text{p}){}^4\text{He}$ reaction	49
5.1	Analysis of the rank zero observables	49
5.1.1	DWBA and coupled channels analysis	50
5.1.2	Phenomenological R-matrix analysis	52
5.2	Analysis of rank zero, iT_{11} and T_{2q} observables	53
5.2.1	Phenomenological R-matrix analysis	53
5.2.2	Coupled channels analysis	55
5.2.3	Introduction of negative parity contributions	56
5.3	Study of the ${}^3\text{He}(\text{d},\text{p}){}^4\text{He}$ with the hybrid model	59
5.4	Conclusions	63
IV	Photonuclear couplings	65
6	R–matrix analysis of the ${}^{14}\text{N}(p,\gamma){}^{15}\text{O}$ reaction	67
6.1	R–matrix analysis	68
6.1.1	Radiative capture cross section in the R–matrix formalism	69
6.1.2	Results and discussion	70
6.2	Conclusions	75
7	Standard formalism for radiative capture reactions	77
7.1	General definitions	77
7.2	Matrix element for EL transitions	82
7.3	Matrix element for ML transitions	88
7.4	The cross section	92

8	The coupling interactions	95
8.1	The photon equation	95
8.2	Electric and magnetic couplings	99
8.3	Implementation	101
9	The $^{14}\text{N}(\text{p},\gamma)^{15}\text{O}$ reaction with the hybrid approach	105
9.1	SFRESKO definitions	105
9.2	R–matrix analysis with SFRESKO	111
9.3	Analysis of the $^{14}\text{N}(\text{p},\gamma)^{15}\text{O}$ reaction with the hybrid approach	113
9.3.1	Potential description of the negative parity background terms	113
9.3.2	Potential description of the $^{14}\text{N}(\text{p},\gamma)^{15}\text{O}$ background	115
9.4	Results and discussion	119
9.5	Conclusions	122
V	Conclusions	125
A	Elastic scattering of spinless particles by a central potential	129
B	R–matrix formalism: 2–channels	133
C	Transfer couplings	137
D	Madison and natural quantization frames	141
E	Properties of spherical harmonics and Racah algebra	143
F	Demonstration of expressions important for chapter 7	147

List of Figures

1	Scheme of the CNO cycle which is the main energy production mechanism for main sequence stars with $M > 1.1$ Solar Masses and $T > 1.6 \times 10^7$ K.	5
2	Scheme of the pp chain with the three main branches.	6
3.1	Energy level diagram for ${}^5\text{Li}$	28
3.2	The Madison convention coordinate system.	32
4.1	Experimental setup used in the A_{yy} measurement.	42
4.2	Experimental setup used in the cross section measurement.	44
5.1	Results of the fits to ${}^3\text{He}(d,p){}^4\text{He}$ total reaction cross section data of Geist <i>et al.</i> [Gei98] with DWBA and coupled channels fits, where S– and D–wave contributions to the $\frac{3}{2}^+$ resonance are considered.	51
5.2	Results of the fits to ${}^3\text{He}(d,p){}^4\text{He}$ differential elastic (right) and reaction cross section (left) data [Gei98, Jen79] with DWBA (full curves) and coupled channels (dashed curves) models, where S– and D–wave contributions to the $\frac{3}{2}^+$ resonance are considered.	51
5.3	Results of the fits to ${}^3\text{He}(d,p){}^4\text{He}$ total reaction cross section data of Geist <i>et al.</i> [Gei98] with the R–matrix model where S– and D–wave contributions to the $\frac{3}{2}^+$ resonance are considered.	52
5.4	Results of the fits to ${}^3\text{He}(d,p){}^4\text{He}$ differential elastic (right) and reaction cross section (left) data [Gei98, Jen79] with R–matrix model, where only the S–wave contribution to the $\frac{3}{2}^+$ resonance is considered.	53
5.5	R–matrix results with a $\frac{3}{2}^+$ S–wave resonance only for iT_{11} , T_{2q} , differential and total cross section measurements of Geist <i>et al.</i> [Gei98].	54
5.6	R–matrix results with S– and D–wave contributions to the $\frac{3}{2}^+$ resonance and a $\frac{3}{2}^+$ background term for the iT_{11} observable.	55

5.7	Results with a coupled channels fit, with S- and D-wave contributions to the $\frac{3}{2}^+$ resonance, to iT_{11} , T_{2q} , differential and total cross section measurements of Geist <i>et al.</i> [Gei98].	56
5.8	Results with a pure R-matrix fit with a $\frac{3}{2}^+$ S-wave resonance, the $\frac{3}{2}^-$ state at $E_d = 2.62$ MeV and a $\frac{1}{2}^-$ background term for iT_{11} , T_{2q} , differential and total cross section measurements of Geist <i>et al.</i> [Gei98].	57
5.9	Results with a pure R-matrix fit with a $\frac{3}{2}^+$ S-wave resonance, the $\frac{3}{2}^-$ state at $E_d = 2.62$ MeV and a $\frac{1}{2}^-$ background term for iT_{11} , T_{2q} , differential and total cross section measurements of Geist <i>et al.</i> [Gei98].	59
5.10	Comparison between the hybrid model results for the iT_{11} observable at $E_d=424$ keV and the results obtain with previous R-matrix fits which included the $J^\pi = \frac{3}{2}^+$ S-wave resonance only and a combination of this resonance with negative parity contributions from $\frac{1}{2}^-$ and $\frac{3}{2}^-$ states.	60
5.11	Hybrid model angular distributions for iT_{11} , T_{2q} differential and total cross section measurements of Geist <i>et al.</i> [Gei98].	61
5.12	Hybrid model results for the energy dependence of $A_{yy}(0^\circ)$, $\sigma(0^\circ)$ and $K_y'(0^\circ)$	62
6.1	Energy level diagram for ^{15}O	68
6.2	S-factor for radiative capture to the ground state of ^{15}O . The full curve represents the total S-factor, the dotted curves the contributions from the individual resonances, and the dashed curves the contributions from the background poles.	72
6.3	S-factor for radiative capture to the $E_x=6.18$ MeV state. The full curve represents the total S-factor, the dotted curves the contributions from the individual resonances, and the dashed curves the contributions from the background poles.	73
6.4	S-factor for radiative capture to the $E_x=6.79$ MeV state. The full curve represents the total S-factor, the dotted curves the contributions from the individual resonances, and the dashed curves the contributions from the background poles.	74
8.1	S-factor for $E1$ radiative capture in the $^7\text{Li}(p,\gamma)^8\text{Be}$ reaction. Comparison between the results obtained with eq. (7.67) - classical method, with the results obtained with the coupling interaction (8.50) - CC, the results obtained with Descouvemont Astrophysica code [Des00] and with Sampaio MSc thesis code [Sam99].	102

8.2	S-factor for $E1$ radiative capture in the $^{12}\text{C}(\alpha,\gamma)^{16}\text{O}$ reaction. Comparison between the results obtained with eq. (7.67) - classical method - and the results obtained with the coupling interaction (8.50) - CC. Descouvemont Astrophysica code [Des00] does not calculate this process due to the $E1$ cancellation effect in the $^{12}\text{C}-\alpha$ system [Bra00].	103
8.3	S-factor for $E2$ radiative capture in the $^7\text{Li}(p,\gamma)^8\text{Be}$ reaction. Comparison between the results obtained with eq. (7.67) - classical method, with the results obtained with the coupling interaction (8.50) - CC, and the results obtained with Descouvemont Astrophysica code [Des00].	103
8.4	S-factor for $E2$ radiative capture in the $^{12}\text{C}(\alpha,\gamma)^{16}\text{O}$ reaction. Comparison between the results obtained with eq. (7.67) - classical method, with the results obtained with the coupling interaction (8.50) - CC, and the results obtained with Descouvemont Astrophysica code [Des00].	104
8.5	S-factor for $M1$ radiative capture in the $^7\text{Li}(p,\gamma)^8\text{Be}$ reaction. Comparison between the results obtained with eq. (7.68) - classical method, with the results obtained with the coupling interaction (8.52) - CC, and the results obtained with Sampaio MSc thesis code [Sam99].	104
9.1	S-factor for radiative capture to the ground state. Comparison between the results obtained in chapter 6 and the results obtained with the SFRESCO code.	111
9.2	S-factor for radiative capture to the $E_x=6.18$ MeV state. Comparison between the results obtained in chapter 6 and the results obtained with the SFRESCO code.	112
9.3	S-factor for radiative capture to the $E_x=6.79$ MeV state. Comparison between the results obtained in chapter 6 and the results obtained with the SFRESCO code.	112
9.4	S-factor for radiative capture to the $E_x=6.79$ MeV state, with a hybrid description where the negative parity background is described through a potential model.	114
9.5	S-factor for radiative capture to the ground state, obtained with the hybrid framework where both negative and positive parity background poles are replaced by a potential model description.	116
9.6	S-factor for radiative capture to the $E_x=6.18$ MeV state, obtained with the hybrid framework where both negative and positive parity background poles are replaced by a potential model description.	116
9.7	S-factor for radiative capture to the $E_x=6.79$ MeV state, obtained with the hybrid framework where both negative and positive parity background poles are replaced by a potential model description.	117

- 9.8 S-factor for radiative capture to the ground state, obtained with a hybrid framework where the extended set of resonances was used. 118
- 9.9 S-factor for radiative capture to the $E_x=6.18$ MeV state, obtained with a hybrid framework where the extended set of resonances was used. 118
- 9.10 S-factor for radiative capture to the $E_x=6.79$ MeV state, obtained with a hybrid framework where the extended set of resonances was used. 119
- C.1 Graphical description of the transfer process $A(a,b)B$ 137
- C.2 Radial coordinates for the description of a transfer process $A(a,b)B$ 138

List of Tables

3.1	Matrix elements, M_n , for positive parity states, that contribute to the ${}^3\text{He}(\text{d,p}){}^4\text{He}$ reaction mechanism.	29
3.2	Matrix elements, M_n , for negative parity states, that contribute to the ${}^3\text{He}(\text{d,p}){}^4\text{He}$ reaction mechanism.	29
4.1	Values of measured A_{yy} , cross section and $K_y^{y'}$ at 0° and of calculated scattering amplitudes (errors quoted include statistical errors only). The amplitudes $ B ^2$ and $ F ^2$ have dimensions of cross section (mb/sr).	45
5.1	Potential parameters obtained from DWBA and coupled channels fits to the ${}^3\text{He}(\text{d,p}){}^4\text{He}$ rank zero observables. The values of the spectroscopic factor obtained from the DWBA and coupled channels analysis were 1.52 and 1.99 respectively.	50
5.2	Resonance parameters obtained from R–matrix analysis of rank zero, iT_{11} and T_{2q} observables. The width $\gamma_d^{(2)}$ refers to the coupling $\{(L = 2, S_p = 1)j = 2, S_t = \frac{1}{2}\}$ in the jj coupling scheme used by SFRESCO.	54
5.3	Potential parameters obtained from coupled channels analysis of rank zero, iT_{11} and T_{2q} observables of the ${}^3\text{He}(\text{d,p}){}^4\text{He}$ reaction. The value of the spectroscopic factor obtained from the analysis was 1.99.	55
5.4	Parameters from the R–matrix analysis of rank zero, iT_{11} and T_{2q} observables, for the $\frac{3}{2}^+$ resonance and the negative parity background terms where *1 indicates coupling to $j=1$, *2 coupling to $j=0$, and *3 coupling to $j=2$, in the jj coupling scheme.	58
5.5	Potential parameters obtained from coupled channels analysis of rank zero, iT_{11} and T_{2q} observables of the ${}^3\text{He}(\text{d,p}){}^4\text{He}$ reaction. The value of the spectroscopic factor obtained from the analysis was 1.93.	58
5.6	Potential parameters obtained from the hybrid analysis to rank zero, iT_{11} , T_{2q} and polarization transfer observables of the ${}^3\text{He}(\text{d,p}){}^4\text{He}$ reaction. The value of the spectroscopic factor obtained from the analysis was 0.87.	60

5.7	Parameters obtained from the hybrid analysis to rank zero, iT_{11} , T_{2q} and polarization transfer observables of the ${}^3\text{He}(d,p){}^4\text{He}$ reaction, where *1 indicates coupling to $j=1$, *2 coupling to $j=2$, and *3 coupling to $j=2$, in the jj coupling scheme.	61
6.1	Values for the resonance energies, formal proton and γ -widths at the position of the pole, and square root of reduced widths, from the R–matrix fit. The energies quoted correspond to the experimental values, and the proton widths for the subthreshold state and the background poles are simply the reduced proton widths, γ_p^2	70
9.1	Values for the position of the R–matrix poles and square roots of proton and γ reduced widths used in the SFRESCO analysis, obtained from the R–matrix analysis of chapter 6 and with eq. (9.35). The background terms were also converted.	113
9.2	Potential parameters obtained from the best fit to the ${}^{14}\text{N}(p,\gamma){}^{15}\text{O}$ radiative capture cross section data to the ground state, 6.18 MeV and 6.79 MeV states of ${}^{15}\text{O}$, corresponding to the curves labeled “fit d”.	119
9.3	Values for the resonance energies, proton and γ -widths at the position of the pole, and square root of reduced widths, obtained from the hybrid analysis. The energies quoted correspond to the fitted values and the proton width for the subthreshold state is a reduced width γ_p^2	120

Part I

Introduction

This work focuses on the theoretical analysis of nuclear reaction data, particularly in the low energy region. We propose and implement a framework for the systematic study of nuclear reactions, focusing on applications that involve transfer or photonuclear processes. This framework attempts to address fundamental issues regarding the modeling of low energy nuclear reactions, namely the interplay between direct and resonant contributions to the reaction mechanism and the accurate extrapolation of experimental data.

The immediate application of this work is in the field of Nuclear Astrophysics, which is concerned with the study of nuclear reactions involved in the nucleosynthesis process inside stars (stellar nucleosynthesis) and in the early universe (primordial nucleosynthesis). This field flourished from the early work of Burbidge, Burbidge, Fowler and Hoyle [Bur57], which postulated a series of energy generating processes in stars, and has recently been the object of intense experimental and theoretical work as the stellar models become more realistic. Additional motivation has come from projects of energy generation through nuclear fusion, which involve many of the nuclear reactions that take place in stellar nucleosynthesis.

An important characteristic of the Nuclear Astrophysics field is the energy range at which these nuclear reactions must be known, the Gamow window. These energies are almost always outside the energy range attainable through experimental work and theoretical methods are necessary to extrapolate the available data to the energy region of interest. This field is therefore marked by efforts to go lower in the experimental energy range covered and to develop nuclear reaction models that allow the accurate extrapolation of data. Another important feature of most nuclear reactions important in astrophysics is the interplay between direct and resonant mechanisms. These two processes are characterized by different energy behaviors and it is therefore important that the theoretical description of a reaction mechanism is able to capture and disentangle these processes.

Throughout this work the introduction of theoretical models will be guided by their applications to specific reactions, namely the $^{14}\text{N}(p,\gamma)^{15}\text{O}$, the $^3\text{He}(d,p)^4\text{He}$, the $^{12}\text{C}(\alpha,\gamma)^{16}\text{O}$ and the $^7\text{Li}(p,\gamma)^8\text{Be}$ reactions. These reactions were chosen due to the type of processes they involve (transfer and photonuclear processes, direct and resonant mechanisms, effects of tensor forces, etc), to their interest as modern topics of research, and due to the past studies done by the research groups involved in this work (namely the CFUNL at the University of Lisbon, TUNL at North Carolina, USA, and the Physics Department of the University of Surrey, UK).

Overview

We start with the introduction of the theoretical framework, in part II, that will be used throughout this dissertation. We focus on the coupled channels model and the R–matrix theory of nuclear reactions, both as a method of solving the coupled equations and in the pure phenomenological approach. The R–matrix theory was initially proposed

by Kapur and Peierls [Kap38] and developed by Wigner and Eisenbud [Wig47] and is, in the pure phenomenological form, probably the most widely applied model for analysis and extrapolation of low energy reaction data. Although rigorous and therefore capable of describing all types of reaction mechanisms, it is however particularly adapted for describing the compound nucleus mechanism. Indeed, although the R–matrix theory is able to accommodate the possibility that two colliding nuclei can interpenetrate each other without necessarily forming a compound nucleus and therefore describe the direct reaction mechanism, the theoretical description of a direct reaction mechanism is more efficiently and elegantly done within a coupled channels framework.

In part III we study the ${}^3\text{He}(\text{d},\text{p}){}^4\text{He}$ reaction. This reaction rate is important in the determination of the relative abundances of D, ${}^3\text{He}$, ${}^4\text{He}$ and ${}^7\text{Li}$ obtained from primordial nucleosynthesis and as a testing ground for nucleon-nucleon (N-N) interaction models, making this reaction a very modern topic of work. Moreover, the fact that this reaction has been investigated since the early days of accelerators to study various nuclear phenomena, and the amount of information available, makes it an ideal first step in the testing of new approaches to nuclear reaction modeling which is ultimately the objective of this work.

We start in chapter 3 with a description of the essential features of the ${}^3\text{He}(\text{d},\text{p}){}^4\text{He}$ reaction. After the analysis of the mechanism through which it occurs, we introduce the polarization formalism for reactions, focusing on the specific $\vec{1} + \frac{1}{2} \rightarrow \frac{1}{2} + 0$ spin structure, relevant for the study of the ${}^3\text{He}(\text{d},\text{p}){}^4\text{He}$ reaction. This chapter ends with the analysis of the available experimental data, focusing on the indications for the importance of non–resonant processes.

In chapter 4 we present the details of new experimental measurements of A_{yy} and cross section at zero degrees performed at TUNL. These results, together with recent measurements of the K_y^y observable, allow the calculation, for the first time, of all the linearly independent scattering amplitudes at a scattering angle of $\theta = 0^\circ$.

Finally, in chapter 5 we analyze all the available observables for the ${}^3\text{He}(\text{d},\text{p}){}^4\text{He}$ reaction (total and differential reaction cross section data, vector and tensor analyzing powers and polarization transfer observables) and the new data obtained in chapter 4, with the theoretical models introduced in part II. This study leads to the introduction of the hybrid R–matrix + potential framework. In the hybrid analysis the negative parity contributions, essentially arising from a direct reaction mechanism, are taken in consideration through a potential description [Bra04], while the resonant contributions to the reaction mechanism are described in the R–matrix framework. In this way one is able to describe the measured observables, fitting the potential and R–matrix parameters to the experimental data, and to disentangle the direct and resonant contributions to the reaction mechanism. The coupled channels code used in this analysis was the FRESKO code, developed by Ian Thompson [Tho04] and upgraded with χ^2 minimization, SFRESKO.

In part IV we focus on the introduction of photonuclear couplings in the coupled

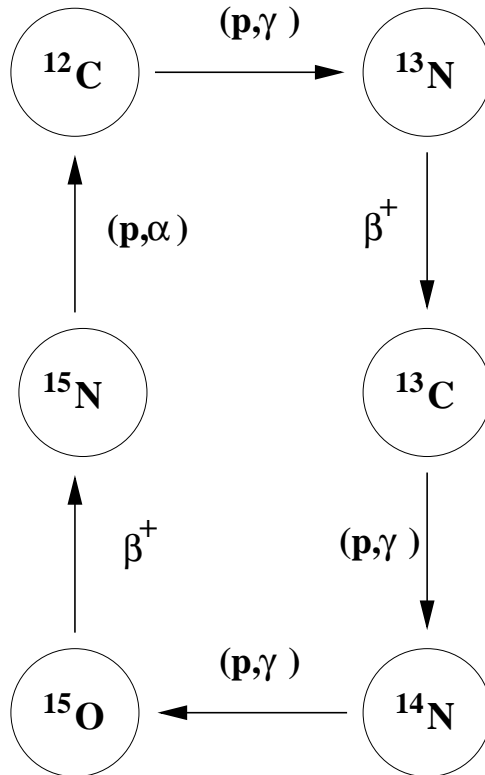


Figure 1: Scheme of the CNO cycle which is the main energy production mechanism for main sequence stars with $M > 1.1$ Solar Masses and $T > 1.6 \times 10^7$ K.

channels formalism. Although the $^3\text{He}(d,p)^4\text{He}$ reaction is an important application of the hybrid framework developed in chapter 5, many nuclear reactions of interest in astrophysics are radiative capture reactions that involve the calculation of electromagnetic couplings in order to be treated in a coupled channels framework. These were however not included in the FRESKO code.

We start in chapter 6 with the implementation of a phenomenological R–matrix code for radiative capture reactions, showing the strengths and weaknesses of this model through its application to the study of $^{14}\text{N}(p,\gamma)^{15}\text{O}$ reaction. This reaction is part of the CNO cycle, shown in figure 1, and it has recently been the focus of intense work, both experimental, with two competing experiments (from the LUNA collaboration and TUNL) publishing their results in 2004, and theoretical with new R–matrix fits to existing data by Angulo and Descouvemont [Ang01].

In chapter 7 we introduce the standard derivation of the radiative capture cross sections for electric, EL, and magnetic, ML, processes, and proceed to the derivation of the coupling interactions in chapter 8. This formalism is implemented and applied to the $^7\text{Li}(p,\gamma)^8\text{Be}$ and $^{12}\text{C}(\alpha,\gamma)^{16}\text{O}$ reactions. These reactions are important in the Hydrogen burning stage, where the $^7\text{Li}(p,\gamma)^8\text{Be}$ is relevant to the understanding of the capture mechanism in the $^7\text{Be}(p,\gamma)^8\text{B}$ reaction of the ppIII chain, and the Helium burning

stage of stellar evolution, respectively. They are used in this chapter as a testing ground for the formalism due to the background the Lisbon and Surrey groups have on these systems [Sam99, Bra00].

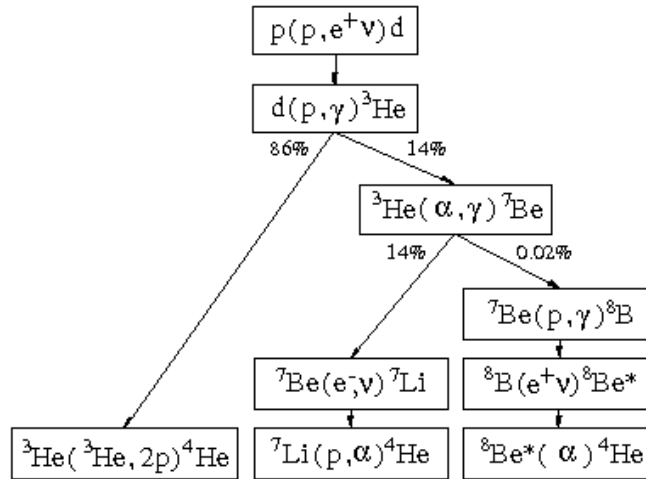


Figure 2: Scheme of the pp chain with the three main branches.

Finally, in chapter 9, we applied the formalism developed in chapters 6–8 to analyze the $^{14}\text{N}(p, \gamma)^{15}\text{O}$ reaction, already studied in chapter 6, in the context of the hybrid model framework, and obtain the astrophysical S-factor.

With the application of the hybrid framework developed in chapters 1 and 2 to the study of transfer and radiative capture reactions, in chapters 5 and 9, respectively, we prove the usefulness of this approach in the analysis of low energy nuclear reaction. Indeed, with this framework and the tool that was developed in the context of this work (the upgrade of the SFRESCO code), one is able to study the experimental data (total and differential cross section data, vector and tensor polarization observables, and polarization transfer data) for most nuclear reactions of interest in Astrophysics. It is possible to obtain information on resonance widths and energies, and to determine the strength of the direct contributions to the reaction mechanism, and furthermore it allows an accurate extrapolation of the theoretical curves to the low energy region. These are important features for a theoretician or experimentalist working in the fields of low energy nuclear reactions and Nuclear Astrophysics.

Part II

Reaction theory

Chapter 1

The coupled equations

When two nuclei interact with each other, they can scatter elastically, they may excite each other, or rearrangement processes may occur. We classify these possible outcomes in terms of different partitions, τ , of the total mass. In the $6A$ dimensional configuration space, where A is the number of constituents in the system and we included the spin degrees of freedom, one can define an internal region where all nucleons are within a volume of nuclear dimensions in physical space, and an external region where the nucleons are arranged in two body configurations.

For a nuclear process under study only a few of the available open configurations are significant. By imposing a truncation on the number of considered configurations, one is left with a finite number of partitions. In the partition τ of the projectile and target, $\tau = p + t$, the intrinsic nuclear Hamiltonian, H_τ , is

$$H_\tau = H_p + H_t \quad , \quad (1.1)$$

where

$$H_p \chi_p = E_p \chi_p \quad (1.2)$$

$$H_t \chi_t = E_t \chi_t \quad (1.3)$$

since H_p and H_t are the components relative to the projectile and target, respectively; the χ_p and χ_t are the wave functions for projectile and target, respectively.

The effective Hamiltonian is, considering the system in the *c.m.* coordinate frame:

$$H = H_\tau + T_\tau + V_\tau \quad (1.4)$$

where the effective interaction, V_τ , is obtained by summing the two body interactions between the constituents of projectile and target:

$$V_\tau = \sum_{i \in p, j \in t} V_{ij} \quad (1.5)$$

and T_τ the kinetic energy operator for the relative motion in partition τ . The nucleon coordinates $\{\mathbf{r}_1, \dots, \mathbf{r}_A\}$ can be written as $\{\mathbf{r}_1 \dots \mathbf{r}_{p-1}, \mathbf{R}_p, \mathbf{r}_{p+1} \dots \mathbf{r}_{A-1}, \mathbf{R}_t\}$ where \mathbf{R}_p and \mathbf{R}_t are the *c.m.* coordinates of the projectile and target respectively. \mathbf{R}_p and \mathbf{R}_t can in turn be written as $\mathbf{R} = \mathbf{R}_p - \mathbf{R}_t$ and \mathbf{R}_{cm} (the Jacobian of the transformation is 1) corresponding to the relative coordinate and the *c.m.* coordinate respectively; in a reference frame centered in the *c.m.* the \mathbf{R}_{cm} is zero. Integration with respect to the $\{\mathbf{r}_1 \dots \mathbf{r}_{p-1}, \mathbf{r}_{p+1} \dots \mathbf{r}_{A-1}, \mathbf{R}\}$ coordinates will be denoted by the subscript \mathbf{r}_{1A} or by $d\mathbf{r}_{1A}$, and the set of coordinates $\{\mathbf{r}_1, \dots, \mathbf{r}_{p-1}, \mathbf{r}_{p+1}, \dots, \mathbf{r}_{A-1}\}$ will be denoted for simplicity as $\bar{\mathbf{r}}_{1A}$.

The model wave function for the system, Ψ , can therefore be expanded in the set of internal states of the system $\chi_\tau \equiv \chi_p \chi_t$ in the corresponding partition

$$\Psi = \sum_{\tau'} \psi_{\tau'}(\mathbf{R}_{\tau'}) |\chi_{\tau'}(\bar{\mathbf{r}}_{1A}) \rangle \quad (1.6)$$

where $\mathbf{R}_{\tau'}$ is the relative coordinate of the τ' channel.

Inserting (1.6) in the Schrödinger equation for the system

$$(H - E) \sum_{\tau'} \psi_{\tau'}(\mathbf{R}_{\tau'}) |\chi_{\tau'}(\bar{\mathbf{r}}_{1A}) \rangle = 0 \quad (1.7)$$

and acting on the left with $\chi_{\tau'}^*$, and integrating on the internal coordinates one obtains, with $E_\tau = E - E_p - E_t$ and with the approximation $\langle \chi_\tau | \chi_{\tau'} \rangle = 0$ for $\tau' \neq \tau$:

$$\begin{aligned} & \langle \chi_\tau | (H_\tau + T_\tau + V_\tau - E) \sum_{\tau'} \psi_{\tau'}(\mathbf{R}_{\tau'}) |\chi_{\tau'} \rangle = 0 \\ \Leftrightarrow & (T_\tau - E_\tau) \sum_{\tau'} \psi_{\tau'}(\mathbf{R}_{\tau'}) \langle \chi_\tau | \chi_{\tau'} \rangle + \sum_{\tau'} \langle \chi_\tau | V_\tau | \chi_{\tau'} \rangle \psi_{\tau'} = 0 \\ \Leftrightarrow & (T_\tau - E_\tau) \psi_\tau(\mathbf{R}_\tau) + \sum_{\tau'} \langle \chi_\tau | V_\tau | \chi_{\tau'} \rangle \psi_{\tau'}(\mathbf{R}_{\tau'}) = 0 \\ \Leftrightarrow & (E_\tau - T_\tau - V_{\tau\tau}) \psi_\tau(\mathbf{R}_\tau) = \sum_{\tau' \neq \tau} V_{\tau\tau'}^{post} \psi_{\tau'}(\mathbf{R}_{\tau'}) \end{aligned} \quad (1.8)$$

which constitute a set of coupled equations for the wave functions of the relative motion, $\psi_{\tau'}(\mathbf{R}_{\tau'})$. The matrix elements represent integration over the internal coordinates:

$$\begin{aligned} V_{\tau\tau'}^{post} &= \langle \chi_\tau | V_\tau | \chi_{\tau'} \rangle \\ &\equiv \int \chi_\tau^*(\bar{\mathbf{r}}_{1A}) V_\tau(\mathbf{R}_\tau, \bar{\mathbf{r}}_{1A}) \chi_{\tau'}(\bar{\mathbf{r}}_{1A}) d\bar{\mathbf{r}}_{1A} \end{aligned} \quad (1.9)$$

Partial wave expansion

Since the integration of the angular part can be done analytically, through the properties of the spherical harmonics, one should introduce the coupled equations corresponding to the partial wave expansion of the solution of (1.7).

In the jj coupling scheme the spin-orbit wave functions in a given partition, τ , are defined by:

$$\mathcal{Y}_{LS_p j}^{m\tau}(\hat{\mathbf{R}}_\tau, \mathbf{r}_1 \dots \mathbf{r}_{p-1}) = \sum_{\mu, M_p} (L\mu, S_p M_p | jm) Y_L^\mu(\hat{\mathbf{R}}_\tau) \chi_{S_p}^{M_p \tau}(\mathbf{r}_1 \dots \mathbf{r}_{p-1}) \quad (1.10)$$

and the channel wave functions are constructed through:

$$\mathcal{Y}_{\alpha J}^{M\pi}(\hat{\mathbf{R}}_\tau, \bar{\mathbf{r}}_{1A}) = \sum_{m, M_t} (jm, S_t M_t | JM) \mathcal{Y}_{LS_p j}^{m\tau}(\hat{\mathbf{R}}_\tau, \mathbf{r}_1 \dots \mathbf{r}_{p-1}) \chi_{S_t}^{M_t \tau}(\mathbf{r}_{p+1} \dots \mathbf{r}_{A-1}) \quad (1.11)$$

where we introduced the definition of channel α , which corresponds to the set of quantum numbers defined with the τ partition $\{\tau, (L, S_p)j, S_t; JM\}$, J is the total angular momentum, and π the parity:

$$\pi = (-)^L \pi_{S_p} \pi_{S_t} \quad (1.12)$$

$$J = j + S_t = (L + S_p) + S_t \quad (1.13)$$

which corresponds to defining the channel α in the jj coupling scheme; alternatively one can use the LS coupling scheme, or channel spin representation, where $\alpha \equiv \{\tau, (S_p, S_t)S, L; JM\}$, in which case the parity is still given by (1.12) and $J = L + S = L + (S_p + S_t)$. One can expand the model wave function, Ψ , into partial waves:

$$\Psi_J^{M\pi} = \sum_{\alpha'} \frac{\psi_{\alpha' J}^\pi(R_{\tau'})}{R_{\tau'}} \mathcal{Y}_{\alpha' J}^{M\pi}(\hat{\mathbf{R}}_{\tau'}, \bar{\mathbf{r}}_{1A}) \quad (1.14)$$

corresponding to the decomposition (1.6).

Inserting the expansion (1.14) in the Schrödinger equation one obtains, like in (1.8):

$$[E_\alpha - T_\alpha - U^J(R_\tau)] \psi_{\alpha J}^\pi(R_\tau) = \sum_{\alpha' \neq \alpha} V_{\alpha\alpha'}^{J \text{ post}} \psi_{\alpha' J}^\pi(R_{\tau'}) \quad (1.15)$$

where:

$$T_\alpha = c_\tau \left[-\frac{d^2}{dR_\tau^2} + \frac{L_\alpha(L_\alpha + 1)}{R_\tau^2} \right] \quad (1.16)$$

$$V_{\alpha\alpha'}^{J \text{ post}} = \langle \mathcal{Y}_{\alpha J}^{M\pi} | V_\tau | \mathcal{Y}_{\alpha' J}^{M\pi} \rangle_{\bar{\mathbf{r}}_{1A}} \quad (1.17)$$

and $U(R)$ corresponds to the diagonal part of the coupling that is usually parametrized through an optical potential with nuclear and Coulomb terms; the indices $\{\alpha\pi J\}$ in ψ and Ψ represent the quantum numbers corresponding to the partial wave, and the subscript $\bar{\mathbf{r}}_{1A}$ in (1.17) denotes integration with respect to the internal coordinates. The coherent sum in (1.15) represents the contribution for the α channel from all the other channels of the model space, $\alpha' \neq \alpha$, with finite coupling interactions, $V_{\alpha\alpha'}$. The c_τ factor in eq. (1.16) allows for the possibility of particle channels with mass transfer, for which $c_\tau = \frac{\hbar^2}{2m_\tau}$ where m_τ is the reduced mass, or gamma channels, where $c_\tau = -\frac{E}{k^2}$ gives rise to Maxwell's equation as will be explained later in chapter 8.

Boundary condition

An important definition that should be introduced at this point is that of the channel radius a , which marks the frontier between the internal and external region and corresponds to the minimal radial distance of separation at which neither particle experiences polarizing forces from the other [Lan58].

In the external region, outside the range of the couplings, V and $U \rightarrow 0$ apart from the Coulomb interaction ($V_{\tau S_p S_t L} = \frac{Z_p Z_t e^2}{R_\tau}$), and one can write from eq. (1.15):

$$u_{\tau L}(\rho_\tau)'' - [L(L+1))\rho_\tau^{-2} + 2\eta_\tau\rho_\tau^{-1} \mp 1]u_{\tau L}(\rho_\tau) = 0 \quad (1.18)$$

where $\rho_\tau = k_\tau R_\tau$ ($k_\tau = \sqrt{\left|\frac{E}{c_\tau}\right|}$), $\eta_\tau = \frac{Z_p Z_t e^2}{\hbar v_\tau}$ is the Coulomb parameter for particles channels ($v_\tau = \frac{2}{\hbar} c_\tau k_\tau$) while $\eta_\tau = 0$ for gamma channels, and the differentiation is with respect to ρ_τ . The $- (+)$ sign refers to positive (negative) energy channels.

For positive energy channels the two linearly independent complex solutions of (1.18) usually chosen are the ones that represent incoming, I , and outgoing, O , waves (the solutions for closed channels can be found elsewhere [Lan58]). These can be written in terms of the real and linearly independent regular, F , and irregular, G , Coulomb functions:

$$I_\alpha = (G_\alpha - iF_\alpha)e^{i\omega_\alpha} \quad (1.19)$$

$$O_\alpha = (G_\alpha + iF_\alpha)e^{-i\omega_\alpha} \quad (1.20)$$

where $\omega_\alpha = \sigma_L - \sigma_0$ is the Coulomb phase shift.

The complete wave functions for positive energies, corresponding to incident and outgoing waves of unitary flux, are therefore:

$$\mathcal{I}_{\tau S_p S_t L} = (i^L Y_L^\mu) \frac{I_\alpha}{\sqrt{v_\alpha} R_\tau} \chi_p \chi_t \quad (1.21)$$

$$\mathcal{O}_{\tau S_p S_t L} = (i^L Y_L^\mu) \frac{O_\alpha}{\sqrt{v_\alpha} R_\tau} \chi_p \chi_t \quad (1.22)$$

where the $\sqrt{v_\alpha}$ factor normalizes the flux.

Wave functions at the boundary surface S

In order to match the radial part of the wave functions in the external and internal regions in the surface, S , at radius a , in the relative coordinate of each channel, we use the value and derivative quantities, V_α and D_α respectively:

$$V_\alpha = \left(\frac{c_\tau}{a}\right)^{\frac{1}{2}} u_\alpha(a) = \left(\frac{c_\tau}{a}\right)^{\frac{1}{2}} \int \varphi_\alpha^* \Psi^i dS \quad (1.23)$$

$$\begin{aligned} D_\alpha &= (ac_\tau)^{\frac{1}{2}} \left(\frac{du_\alpha}{dR_\tau}\right)_{R_\tau=a} = \left(\frac{c_\tau}{a}\right)^{\frac{1}{2}} \int \varphi_\alpha^* \nabla_n (R_\tau \Psi^i) dS \\ &= V_\alpha + (ac_\tau)^{\frac{1}{2}} \int \varphi_\alpha^* \nabla_n \Psi^i dS \end{aligned} \quad (1.24)$$

where Ψ^i is the total wave function of the system in the internal region, and $u_\alpha(a)$ the radial part of the wave function for channel α , as expressed in (1.14). The surface functions, φ_α , defined as the term that multiplies the normalized incoming and outgoing radial functions in (1.21) and (1.22), are normalized and mutually orthogonal in S :

$$\int \varphi_\alpha^* \varphi_{\alpha'} dS = \delta_{\alpha\alpha'} \quad . \quad (1.25)$$

In the external region, there are four quantities necessary to the specification of the wave functions on S : I , I' , O and O' (or F , F' , G and G'), which reduce to three through the Wronskian for positive energy channels [Lan58]:

$$\mathcal{W}_\alpha^+ = (O'_\alpha I_\alpha - I'_\alpha O_\alpha)_{R_\tau=a} = 2i(F'_\alpha G_\alpha - G'_\alpha F_\alpha)_{R_\tau=a} = 2i \quad (1.26)$$

These can be chosen as the shift factor, S_α , the penetrability, P_α and the hard-sphere scattering phase shift, ϕ_α , defined as:

$$L_\alpha \equiv \left(\rho_\alpha \frac{O'_\alpha}{O_\alpha}\right)_{R_\tau=a} = S_\alpha + iP_\alpha \quad (1.27)$$

$$\Omega_\alpha \equiv \left(\frac{I_\alpha}{O_\alpha}\right)_{R_\tau=a}^{\frac{1}{2}} = e^{[i(\omega_\alpha - \phi_\alpha)]} \quad (1.28)$$

$$\phi_\alpha = \text{tg}^{-1} \frac{F_\alpha}{G_\alpha} \quad (1.29)$$

The scattering matrix

The general solution of the wave equation in the external region is:

$$\Psi^e = \sum_\alpha (x_\alpha \mathcal{O}_\alpha + y_\alpha \mathcal{I}_\alpha) \quad (1.30)$$

where y_α and x_α are the amplitudes for incident and outgoing waves in various channels α , respectively. The scattering matrix \mathbf{U} relates the vectors \mathbf{x} and \mathbf{y} :

$$\mathbf{x} = -\mathbf{U}\mathbf{y} \quad (1.31)$$

In the case where there is only one incident channel (1.30) becomes

$$\Psi_{\text{incident in } \alpha}^e = \mathcal{I}_\alpha - \sum_{\alpha'} U_{\alpha'\alpha} \mathcal{O}_{\alpha'} \quad (1.32)$$

We now match the interior and exterior wave functions through the value and derivative quantities with (1.23), (1.24) and (1.30):

$$V_\alpha = \left(\frac{c_\tau}{a}\right)^{\frac{1}{2}} (v_\alpha^{-\frac{1}{2}} \mathcal{O}_\alpha x_\alpha + v_\alpha^{-\frac{1}{2}} I_\alpha y_\alpha) \quad (1.33)$$

$$D_\alpha = \left(\frac{\rho_\alpha^2 c_\tau}{a}\right)^{\frac{1}{2}} (v_\alpha^{-\frac{1}{2}} \mathcal{O}'_\alpha x_\alpha + v_\alpha^{-\frac{1}{2}} I'_\alpha y_\alpha) \quad (1.34)$$

The cross section

Writing the general solution in the external region, for unspecified coefficients of the incoming waves, as a function of the scattering matrix:

$$\Psi = \sum_{\alpha\alpha'} (\delta_{\alpha\alpha'} \mathcal{I}_\alpha - U_{\alpha'\alpha} \mathcal{O}_{\alpha'}) y_\alpha \quad (1.35)$$

and summing and subtracting the term Ψ' :

$$\Psi' = \sum_{\alpha\alpha'} (\delta_{\alpha\alpha'} \mathcal{I}_\alpha - e^{2i\omega_\alpha} \delta_{\alpha'\alpha} \mathcal{O}_\alpha) y_\alpha \quad (1.36)$$

one obtains

$$\Psi = \Psi' + \sum_{\alpha\alpha'} (e^{2i\omega_\alpha} \delta_{\alpha\alpha'} - U_{\alpha'\alpha}) \mathcal{O}_{\alpha'} y_\alpha \quad (1.37)$$

Choosing y_α so that Ψ' represents an incident plane moving along the z axis and disturbed only by the Coulomb field

$$y_\alpha \equiv y_{\tau S_p S_t L \mu} = \frac{i\pi^{\frac{1}{2}}}{k_\tau} (2L+1)^{\frac{1}{2}} \quad (1.38)$$

and using the channel spin representation, $\{(S_p, S_t)S, L\}$, one obtains for Ψ' :

$$\Psi'_{\tau S M_s} = v_\tau^{-\frac{1}{2}} k_\tau^{-1} \sum_L i^L (2L+1) e^{i\omega_\tau L} \frac{F_{\tau L}}{R_\tau} P_L(\cos\theta) \chi_{\tau S M_s} \quad (1.39)$$

which has the asymptotic form

$$\Psi'_{\tau S M_s} \sim v_\tau^{-\frac{1}{2}} \chi_{\tau S M_s} \left[\left(1 - \frac{\eta_\tau^2}{ik_\tau(R_\tau - z_\tau)} \right) \exp(ik_\tau z_\tau - i(\eta_\tau \log k_\tau(R_\tau - z_\tau) - \sigma_{\tau 0})) - \frac{\pi^{\frac{1}{2}}}{k_\tau R_\tau} C_\tau(\theta_\tau) \exp(i(\rho_\tau - \eta_\tau \log 2\rho_\tau - \sigma_{\tau 0})) \right] \quad (1.40)$$

$$C_\tau(\theta_\tau) = (4\pi)^{-\frac{1}{2}} \eta_\tau \operatorname{cosec}^2\left(\frac{\theta_\tau}{2}\right) \exp\left(-2i\eta_\tau \log \sin\left(\frac{\theta_\tau}{2}\right)\right) \quad (1.41)$$

The Ψ' represents an incident wave along the quantization axis, z , in a Coulomb field and a scattered wave with coefficient $C_\tau(\theta_\tau)$. On the other hand, one obtains for the asymptotic form of the particular solution that verifies (1.38):

$$\begin{aligned} \Psi &= \Psi' + \frac{i\pi^{\frac{1}{2}}}{k_\tau} \sum_{\tau'S'LL'M'_s\mu'} (2L+1)^{\frac{1}{2}} \frac{\exp(i(\rho_{\tau'} - \eta_{\tau'} \log 2\rho_{\tau'} - \sigma_{\tau'0}))}{v_{\tau'}^{\frac{1}{2}} R_{\tau'}} \\ &\quad (e^{2i\omega_{\tau'L'}} \delta_{\tau'S'L'M'_s\mu', \tau SLM_s0} - U_{\tau'S'L'M'_s\mu', \tau SLM_s0}) Y_{L'\mu'}(\hat{\mathbf{R}}_{\tau'}) \chi_{\tau'S'M'_s} \end{aligned} \quad (1.42)$$

In this way, one can define the amplitude for scattered waves in the asymptotic region, $\{\tau'S'M'_s\}$, corresponding to an incident plane wave, $\{\tau SM_s\}$, through the scalar product:

$$\begin{aligned} &A_{\tau'S'M'_s, \tau SM_s}(\hat{\mathbf{R}}_{\tau'}) \\ &= v_{\tau'}^{\frac{1}{2}} \exp(-i(\rho_{\tau'} - \eta_{\tau'} \log 2\rho_{\tau'} - \sigma_{\tau'0})) \lim_{R_{\tau'} \rightarrow \infty} \int R_{\tau'} \chi_{\tau'S'M'_s}^* \Psi d\bar{\mathbf{r}}_{1A\tau'} \\ &= \frac{\pi^{\frac{1}{2}}}{k_\tau} \left\{ -C_{\tau'}(\theta_{\tau'}) \delta_{\tau'S'M'_s, \tau SM_s} \right. \\ &\quad \left. + i \sum_{L'\mu'L} (2L+1)^{\frac{1}{2}} [e^{2i\omega_{\tau'L'}} \delta_{\tau'S'L'M'_s\mu', \tau SLM_s0} - U_{\tau'S'L'M'_s\mu', \tau SLM_s0}] Y_{L'\mu'}(\hat{\mathbf{R}}_{\tau'}) \right\} \end{aligned} \quad (1.43)$$

where $\bar{\mathbf{r}}_{1A\tau'}$ denotes the internal coordinates in partition τ' .

By writing the scattering matrix in the channel spin representation:

$$U_{\tau'S'L'M'_s\mu', \tau SLM_s\mu} = \sum_{JM} (SM_s L\mu | JM) U_{\tau'S'L', \tau SL}^J (S'M'_s L'\mu' | JM) \quad (1.44)$$

one obtains for the scattered waves amplitudes:

$$\begin{aligned} &A_{\tau'S'M'_s, \tau SM_s}(\hat{\mathbf{R}}_{\tau'}) \\ &= \frac{\pi^{\frac{1}{2}}}{k_\tau} \left\{ -C_{\tau'}(\theta_{\tau'}) \delta_{\tau'S'M'_s, \tau SM_s} \right. \\ &\quad \left. + i \sum_{JML'\mu'L} (2L+1)^{\frac{1}{2}} (SM_s L\mu | JM) (S'M'_s L'\mu' | JM) T_{\tau'S'L', \tau SL}^J Y_{L'\mu'}(\hat{\mathbf{R}}_{\tau'}) \right\} \end{aligned} \quad (1.45)$$

where we defined the T-matrix as:

$$T_{\tau'S'L', \tau SL}^J = e^{2i\omega_{\tau'L'}} \delta_{\tau'S'L', \tau SL} - U_{\tau'S'L', \tau SL}^J \quad (1.46)$$

In the case of unpolarized incident particles, the differential cross section is obtained from the scattering amplitudes by summing over M'_s and averaging over M_s . Furthermore, in the channel spin representation, the different values of the channel spin contribute incoherently to the unpolarized differential cross section [Sat83]. We can therefore write

$$\frac{d\sigma_{\tau, \tau'}}{d\hat{\mathbf{R}}_{\tau'}} = \frac{1}{(2S_p + 1)(2S_t + 1)} \sum_{S'M'_s, SM_s} |A_{\tau'S'M'_s, \tau SM_s}(\hat{\mathbf{R}}_{\tau'})|^2 \quad (1.47)$$

Using (1.45) in (1.47) and integrating over the solid angle, one obtains

$$\sigma_{\tau,\tau'} = \frac{\pi}{k_\tau^2} \sum_{JLL'SS'} g_J |T_{\tau'S'L',\tau SL}^J|^2 \quad (1.48)$$

$$g_J = \frac{2J+1}{(2S_p+1)(2S_t+1)} \quad (1.49)$$

To match up with the notation of [Tho01], one defines:

$$\begin{aligned} F_{\tau'} &= -\frac{\pi^{\frac{1}{2}}}{k_\tau} C_{\tau'}(\theta_{\tau'}) \\ &= -\frac{\eta_{\tau'} \exp\left(-2i\eta_{\tau'} \log \sin\left(\frac{\theta_{\tau'}}{2}\right)\right)}{k_\tau \sin^2\left(\frac{\theta_{\tau'}}{2}\right)} \end{aligned} \quad (1.50)$$

$$\begin{aligned} S_{\alpha',\alpha}^J &= e^{-i\omega_{\tau'L'}} e^{-i\omega_{\tau L}} U_{\alpha',\alpha}^J \sqrt{\frac{v_\tau}{v_{\tau'}}} \\ &= e^{-i(\sigma_{\tau'L'} - \sigma_{\tau'0})} e^{-i(\sigma_{\tau L} - \sigma_{\tau 0})} U_{\alpha',\alpha}^J \sqrt{\frac{v_\tau}{v_{\tau'}}} \end{aligned} \quad (1.51)$$

where (1.51) corresponds to a different definition of the incoming and outgoing solutions (1.19-1.22). Using alternatively the jj representation, where $\alpha = \{(S_p, L)j, S_t, JM\}$, one can obtain an alternative expression for the scattered waves amplitudes, with the T-matrix defined now as $\mathcal{T}_{\alpha',\alpha} = \frac{i}{2} \{\delta_{\alpha',\alpha} - S_{\alpha',\alpha}^J\}$:

$$\begin{aligned} &A_{\tau'M'_p M'_t, \tau M_p M_t}(\hat{\mathbf{R}}_{\tau'}) \\ &= F_{\tau'}(\theta_{\tau'}) \delta_{\alpha',\alpha} \\ &+ \sum_{LL'jj'J} (L0, S_p M_p | j M_p) (j M_p, S_t M_t | JM) (L' \mu', S'_p M'_p | j \mu' + M'_p) \\ & (j' \mu' + M'_p, S'_t M'_t | JM) \frac{4\pi}{k_\tau} e^{i(\sigma_{\tau'L'} - \sigma_{\tau'0})} e^{i(\sigma_{\tau L} - \sigma_{\tau 0})} \\ & \sqrt{\frac{2L+1}{4\pi}} \frac{i}{2} \mathcal{T}_{\alpha',\alpha} Y_{L'}^{M_p + M_t - M'_p - M'_t}(\hat{\mathbf{R}}_{\tau'}) \sqrt{\frac{v_{\tau'}}{v_\tau}} \end{aligned} \quad (1.52)$$

which corresponds to equation (38) of [Tho01].

With the definitions (1.50-1.52) the cross section for the process $\tau \rightarrow \tau'$ becomes, factorizing the flux factors out to the cross section expression:

$$\sigma_{\tau,\tau'} = \frac{4\pi}{k_\tau^2} \frac{v_{\tau'}}{v_\tau} \sum_{JLL'jj'} g_J |\mathcal{T}_{\tau'L'j',\tau Lj}^J|^2 \quad (1.53)$$

Both eqs. (1.53) and (1.48) are used in this work, according to the coupling scheme used in the calculations.

Chapter 2

Solving coupled equations

2.1 Iterative solutions

For given potentials and coupling interactions the coupled equations (1.15) need to be solved to obtain the scattering matrix. If the coupling interactions are weak, which is usually the case for photon channels, or if the back coupling effects of these interactions are already included in the optical potentials of the prior channel, it becomes reasonable to use the distorted wave Born approximation (DWBA). This is equivalent to solving the differential equations by calculating the T-matrix, as will be demonstrated in chapter 8.

If the couplings are stronger, the coupled equations may be solved iteratively, which is equivalent to n -step DWBA. When the couplings are too large, or the system is too near a resonance or a bound state pole, the procedure will diverge. Furthermore the iterative method only allows local couplings to be treated exactly, as non-local couplings from transfers have to be included iteratively.

2.2 R-matrix solutions

The R-matrix method of solving the coupled equations has the advantages of being more stable numerically than the iterative methods, and also allowing non-local components of the Hamiltonian in the interior region to be included to all orders. Furthermore, this method allows additional phenomenological terms to be included in the R-matrix, which is a useful feature in the analysis of resonant mechanisms, as will be shown later in this work.

One defines the real boundary condition as the ratio of value and derivative quantities introduced in the previous chapter:

$$\frac{\delta_{\lambda\alpha}}{\gamma_{\lambda\alpha}} = \frac{D_{\lambda\alpha}}{V_{\lambda\alpha}} \equiv B_{\alpha} \quad (2.1)$$

By satisfying this boundary condition on the boundary surface at channel radius, a , the solutions of the wave equation with eigenenergies $E_{\lambda J}$, $X_{\lambda JM}$:

$$HX_{\lambda JM} = E_{\lambda J}X_{\lambda JM} \quad (2.2)$$

constitute an orthonormal set over the internal region, $[0, a]$, and one can write the wave function for any particular energy, E , as a linear combination of the $X_{\lambda JM}$:

$$\Psi_{JM} = \sum_{\lambda} A_{\lambda J} X_{\lambda JM} \quad (2.3)$$

2.2.1 R-matrix model with reaction channels

In this section we introduce the R-matrix model in the multichannel case as a generalization of the 1-channel case developed in appendix A. The intermediate step, the two channels case, important for the understanding of the definition of reduced width for transfer and radiative capture reactions is presented in appendix B.

The R-matrix relates the value of the wave function at the channel radius, a , expanded in terms of eigenfunctions of the internal region as in eq. (2.3), with its derivative at a , where the matching between the wave functions of the internal and external regions is done. In the 1-channel case the R-function is given by:

$$R = G(a, a) = \frac{u_E(a)}{a \left(\frac{du_E}{dR} \right)_{R=a}} = \sum_{\lambda} \frac{\gamma_{\lambda}^2}{E_{\lambda} - E} \quad (2.4)$$

where the Green function, $G(R, a)$, relates the value of the wave function in the internal region with its derivative on the surface, and γ_{λ} are the square root of the reduced level widths (see appendix A). The generalization of eq. (2.4) to the two channels case corresponds to eq. (B.15) of appendix B.

For the multichannel case we start by generalizing the Green condition, eq. (A.3), replacing the surface term by a sum over participating channels:

$$(E_2 - E_1) \int_i \Psi_2^* \Psi_1 di = \sum_{\alpha} (V_{2\alpha}^* D_{1\alpha} - V_{1\alpha} D_{2\alpha}^*) \quad (2.5)$$

where i denotes integration over the interior region, and it is assumed that the interaction term, V , is self-adjoint.

The R-matrix

Considering that the general boundary condition (2.1) is satisfied by the complete set of states $X_{\lambda JM}$ of the internal region on the surface, S , and using eq. (2.5), one obtains for the coefficients of the Ψ_{JM} expansion in this basis, eq. (2.3), dropping the JM indices:

$$A_\lambda = \int_i X_\lambda^* \Psi di = (E_\lambda - E)^{-1} \sum_\alpha D_\alpha^0 \gamma_{\lambda\alpha} \quad (2.6)$$

where $D_\alpha^0 = D_\alpha - B_\alpha V_\alpha$. The Ψ expansion is therefore:

$$\Psi = \sum_\alpha \left[\sum_\lambda \frac{X_\lambda \gamma_{\lambda\alpha}}{E_\lambda - E} \right] D_\alpha^0 \quad (2.7)$$

which relates the value of Ψ in the internal region with its derivative on the surface S , D_α^0 . Multiplying (2.7) by the surface function, $\varphi_{\alpha'}^*$, and integrating on the surface S one obtains in matrix notation:

$$\mathbf{V} = \mathbf{R} \mathbf{D}^0 \quad (2.8)$$

where \mathbf{V} and \mathbf{D}^0 are column vectors of components $V_{\alpha'}$ and D_α^0 , respectively. The elements of the R-matrix, \mathbf{R} , are, generalizing eq. (2.4) (see appendix B):

$$\begin{aligned} R_{\alpha\alpha'}(E) &= \frac{c_{\tau'}}{a} \sum_\lambda \frac{u_\alpha^\lambda(a) u_{\alpha'}^\lambda(a)}{E - E_\lambda} \\ &= \sqrt{\frac{c_{\tau'}}{c_\tau}} \sum_\lambda \frac{\gamma_\alpha^\lambda \gamma_{\alpha'}^\lambda}{E_\lambda - E} \end{aligned} \quad (2.9)$$

where u_λ^α are the radial part of the elements of the basis for the expansion of the channel wave functions Ψ_{JM}^α in the internal region, X_λ^α , and

$$\gamma_\alpha^\lambda = \sqrt{\frac{c_\tau}{a}} u_\alpha^\lambda(a) \quad (2.10)$$

is the square root of the reduced level width. Defining the square matrix of the vector γ_λ with components $\gamma_{\lambda\alpha}$ as $(\gamma_\lambda \times \gamma_\lambda)$, we can write (2.9) in matrix notation

$$\mathbf{R} = \sum_\lambda \frac{\gamma_\lambda \times \gamma_\lambda}{E_\lambda - E} \mathcal{C} \quad (2.11)$$

where the matrix \mathcal{C} contains the information on particular channels (see appendix B); the R-matrix is real since the components of γ_λ are real.

2.2.2 The Scattering matrix

With the fundamental R–matrix relation (2.8) and the value and derivative quantities, (1.33) and (1.34), one obtains, with the boundary condition $\mathbf{B} = 0$ [Lan58]:

$$\sqrt{\frac{\mathcal{C}}{a}}(\mathbf{v}^{-\frac{1}{2}}\mathbf{O} - \mathbf{R}\rho\mathbf{v}^{-\frac{1}{2}}\mathbf{O}')\mathbf{x} = -\sqrt{\frac{\mathcal{C}}{a}}(\mathbf{v}^{-\frac{1}{2}}\mathbf{I} - \mathbf{R}\rho\mathbf{v}^{-\frac{1}{2}}\mathbf{I}')\mathbf{y} \quad (2.12)$$

where \mathcal{C} and \mathbf{v} are real matrices of elements c_τ and $v_\alpha \equiv v_\tau$, respectively. With (1.31) one obtains for the relation between the scattering matrix, \mathbf{U} , and the R–matrix:

$$\mathbf{U}^J = \left[\sqrt{\frac{\mathcal{C}}{a}}(\mathbf{v}^{-\frac{1}{2}}\mathbf{O} - \mathbf{R}^J\rho\mathbf{v}^{-\frac{1}{2}}\mathbf{O}') \right]^{-1} \left[\sqrt{\frac{\mathcal{C}}{a}}(\mathbf{v}^{-\frac{1}{2}}\mathbf{I} - \mathbf{R}^J\rho\mathbf{v}^{-\frac{1}{2}}\mathbf{I}') \right] \quad (2.13)$$

$$= \frac{\sqrt{\mathbf{v}}}{\mathbf{O}} \sqrt{\frac{a}{\mathcal{C}}} \left(\mathbf{1} - \mathbf{R}^J \frac{\rho\mathbf{O}'}{\mathbf{O}} \right)^{-1} \left(\mathbf{1} - \mathbf{R}^J \frac{\rho\mathbf{I}'}{\mathbf{I}} \right) \sqrt{\frac{\mathcal{C}}{a}} \frac{\mathbf{I}}{\sqrt{\mathbf{v}}} \quad (2.14)$$

$$= \sqrt{\frac{\mathbf{I}}{\mathbf{O}}} \sqrt{\frac{\mathbf{v}}{\mathbf{IO}}} \sqrt{\frac{a}{\mathcal{C}}} (\mathbf{1} - \mathbf{R}^J\mathbf{L})^{-1} (\mathbf{1} - \mathbf{R}^J\mathcal{L}) \sqrt{\frac{\mathcal{C}}{a}} \sqrt{\frac{\mathbf{IO}}{\mathbf{v}}} \sqrt{\frac{\mathbf{I}}{\mathbf{O}}} \quad (2.15)$$

where $\mathcal{L} = (\rho\frac{\mathbf{I}'}{\mathbf{I}})_{R_\tau=a}$. Using $\mathcal{B} = \frac{\mathbf{v}}{\mathbf{IO}} \frac{a}{\mathcal{C}}$ one can write the for eq. (2.15)

$$\mathbf{U}^J = \mathbf{\Omega}\mathcal{B}^{\frac{1}{2}} (\mathbf{1} - \mathbf{R}^J\mathbf{L})^{-1} (\mathbf{1} - \mathbf{R}^J\mathcal{L}) \mathcal{B}^{-\frac{1}{2}}\mathbf{\Omega} \quad (2.16)$$

$$= \mathbf{\Omega}\mathbf{W}^J\mathbf{\Omega} \quad (2.17)$$

which corresponds to eq. (VII-1.5) of Lane and Thomas [Lan58] when the particular case of particle channels is considered (in this case one defines $\mathcal{B} = \frac{\mathbf{v}}{\mathbf{IO}} \frac{a}{\mathcal{C}} \equiv \frac{ka}{\mathbf{IO}} \equiv \frac{\rho}{\mathbf{IO}}$ since the $\frac{\hbar}{2}$ factors from $\mathcal{B}^{-\frac{1}{2}}$ and $\mathcal{B}^{-\frac{1}{2}}$ cancel). The \mathbf{W} matrix is

$$\mathbf{W}^J = \mathcal{B}^{\frac{1}{2}}(\mathbf{1} - \mathbf{R}^J\mathbf{L}^0)^{-1}(\mathbf{1} - \mathbf{R}^J\mathcal{L}^0)\mathcal{B}^{-\frac{1}{2}} \quad (2.18)$$

$$= \mathbf{1} + \mathcal{B}^{\frac{1}{2}}(\mathbf{1} - \mathbf{R}^J\mathbf{L}^0)^{-1}\mathbf{R}^J\mathcal{B}^{\frac{1}{2}}\mathcal{W} \quad (2.19)$$

and can be easily generalized for a general boundary condition [Lan58]. The eq. (2.12) defines the scattering matrix \mathbf{U} as a function of the parameters $\{\gamma_{\lambda\alpha}, E_\lambda, \sigma_\alpha, \phi_\alpha, S_\alpha, P_\alpha\}$; although these quantities depend on the parameters a and B_α , the \mathbf{U} –matrix, which characterizes the physical system, should be independent of these parameters.

2.3 Phenomenological terms in the R-matrix

2.3.1 The hybrid method

By treating the potential contribution in the way described in the previous sections, one is able to add additional poles to the R–matrix, defined in eq. (2.9) as $R_{\alpha\alpha'}(E)$, with the form:

$$R_{\alpha\alpha'}^{total}(E) = R_{\alpha\alpha'}(E) + \sqrt{\frac{c_{\tau'}}{c_{\tau}}} \sum_{\nu} \frac{\gamma_{\alpha}^{\nu} \gamma_{\alpha'}^{\nu}}{E_{\nu} - E} \quad (2.20)$$

where γ_{α}^{ν} are the partial widths of channel α for the additional level ν . This equation is the fundamental relation of what will be referred in this work as the hybrid model, which was originally proposed by Johnson [Joh73] and first applied in the field of nuclear astrophysics to the analysis of the $^{12}\text{C}(\alpha,\gamma)^{16}\text{O}$ by Koonin *et al.* [Koo74].

In this model one is able to combine the coupled channels solutions with additional R-matrix poles that describe specific resonant contributions to the reaction mechanism and obtain the complete R-matrix. The scattering matrix can then be calculated from the R-matrix following the formalism introduced in chapter 1. This approach overcomes the usual difficulties of coupled channels analysis of nuclear reactions where a significant number of levels contribute to the reaction mechanism in the energy region being studied. The partial widths, γ_{α}^{ν} , are usually left as adjustable parameters in a χ^2 fit to experimental data.

2.3.2 Simple R-matrix phenomenology

The most widely applied model for analysis and extrapolation of low energy reaction data is probably the R-matrix theory of nuclear reactions in its pure phenomenological form, independent from the Hamiltonian. In these applications the R-matrix is simply:

$$\begin{aligned} \tilde{R}_{\alpha\alpha'}(E) &= C_{\alpha,\alpha'} \sum_{\lambda} \frac{\gamma_{\alpha}^{\lambda} \gamma_{\alpha'}^{\lambda}}{E_{\lambda} - E} \\ &= \sum_{\lambda} \frac{\tilde{\gamma}_{\alpha}^{\lambda} \tilde{\gamma}_{\alpha'}^{\lambda}}{E_{\lambda} - E} \end{aligned} \quad (2.21)$$

where the constant $C_{\alpha,\alpha'}$, which in eq. (2.20) takes the value $C_{\alpha,\alpha'} = \sqrt{\frac{c_{\tau'}}{c_{\tau}}}$, is usually chosen in this context to be $C_{\alpha,\alpha'} = 1$, corresponding to a definition for the partial widths of channel α from the additional level λ , $\tilde{\gamma}_{\alpha}^{\lambda}$, different from the used in eq. (2.20), $\gamma_{\alpha}^{\lambda}$ (see appendix B for details). This choice is valid in the weak coupling limit, discussed below, where the reverse couplings are not used.

This approach is used extensively by many authors. In the particular case of the reactions that are studied in this work, the analysis of the $^3\text{He}(\text{d,p})^4\text{He}$ reaction by Geist *et al.* [Gei99], of the $^{14}\text{N}(\text{p},\gamma)^{15}\text{O}$ reaction by Angulo and Descouvemont [Ang01], and of the $^{12}\text{C}(\alpha,\gamma)^{16}\text{O}$ reaction by Azuma [Azu94] should be mentioned. In these works the properties of the states, λ , included in the analysis (E_{λ} , $\tilde{\gamma}_{\alpha}^{\lambda}$ and $\tilde{\gamma}_{\alpha'}^{\lambda}$) are taken as adjustable parameters and fitted to existing experimental data.

An important feature of phenomenological R–matrix analysis [Ang01, Azu94, Gei99] is the introduction of background poles to account for the contributions arising from direct capture (DC) or low energy tails of high lying resonances. Indeed, contrary to the coupled channels approach, which allows the integrated treatment of the resonant and direct contributions to the reaction mechanism, describing the resonances through the interaction Hamiltonian, and also the explicit calculation of the direct contribution through a potential model, the phenomenological R–matrix approach takes the direct contributions into account by including background poles at high energies but with no direct connection to known resonances.

Two channels case in the weak coupling limit

The inversion of the $(\mathbf{1} - \mathbf{R}^J \mathbf{L}^0)$ matrix of eq. (2.19) is relatively simple in the case where one only considers two reaction channels (noted by 1 and 2). The components of the scattering matrix are:

$$W_{11} = 1 + 2iP_1[\tilde{R}_{11} - L_2^0(\tilde{R}_{11}\tilde{R}_{22} - \tilde{R}_{12}^2)]d^{-1} \quad (2.22)$$

$$W_{22} = 1 + 2iP_2[\tilde{R}_{22} - L_1^0(\tilde{R}_{11}\tilde{R}_{22} - \tilde{R}_{12}^2)]d^{-1} \quad (2.23)$$

$$W_{12} = W_{21} = 2iP_1^{\frac{1}{2}}\tilde{R}_{12}P_2^{\frac{1}{2}}d^{-1} \quad (2.24)$$

where $\mathbf{L}^0 = \mathbf{L} - \mathbf{B}$ results from the generalization of eq. (2.19) for a boundary condition \mathbf{B} , and d is the determinant:

$$d = (1 - \tilde{R}_{11}L_1^0)(1 - \tilde{R}_{22}L_2^0) - L_1^0\tilde{R}_{12}\tilde{R}_{21}L_2^0 \quad (2.25)$$

In the weak coupling limit one can treat the final channel perturbatively, which amounts to setting the corresponding column of the R–matrix to zero, and obtain:

$$d \approx 1 - \tilde{R}_{11}L_1^0 \quad (2.26)$$

In this way, using (2.24) in the cross section expression (1.48) one obtains

$$\sigma_{1,2} = \frac{4\pi}{k_1^2} \sum_{\substack{JSL \\ S'L'}} g_J \left| \frac{P_1^{\frac{1}{2}}\tilde{R}_{12}P_2^{\frac{1}{2}}}{1 - \tilde{R}_{11}L_1^0} \right|^2 \quad (2.27)$$

where the elements of the R-matrix are, from (2.21) (see appendix B):

$$\tilde{R}_{11} = \sum_{\lambda} \frac{\tilde{\gamma}_{\lambda 1}^2}{E_{\lambda} - E} \quad (2.28)$$

$$\tilde{R}_{12} = \sum_{\lambda} \frac{\tilde{\gamma}_{\lambda 1}\tilde{\gamma}_{\lambda 2}}{E_{\lambda} - E} \quad (2.29)$$

Replacing eqs. (2.28) and (2.29) in the cross section expression one obtains:

$$\sigma_{1,2} = \frac{\pi}{k_1^2} \sum_{\substack{JSL \\ S'L'}} g_J \left| \frac{\sum_{\lambda} \frac{\tilde{\Gamma}_{\lambda 1}^{\frac{1}{2}} \tilde{\Gamma}_{\lambda 2}^{\frac{1}{2}}}{E_{\lambda} - E}}{1 - L_1^0 \tilde{R}_{11}} \right|^2 \quad (2.30)$$

This approximation is particularly useful in the analysis of radiative capture reactions. In this case the summing indices $S'L'$ correspond to the channel spin of the final state, including the spin of the photon, and the multipolarity of the radiation, respectively.

The energy dependence of Γ -widths in eq. (2.30) is obtained in a general way from the penetrabilities according to the definition:

$$\tilde{\Gamma}_{\lambda i} = 2P_i \tilde{\gamma}_{\lambda i}^2 \quad (2.31)$$

however, in order to compare the formal Γ -widths obtained from an R-matrix analysis with experimental values, one should calculate the observed widths according to [Lan58, Til02]:

$$\tilde{\Gamma}_{\lambda i}^o = \frac{\tilde{\Gamma}_{\lambda i}}{1 + \sum_j \tilde{\gamma}_{\lambda j}^2 \left(\frac{dS_j}{dE} \right)_{E=E_{\lambda}}} \quad (2.32)$$

where S is the shift function.

Part III

The ${}^3\text{He}(\text{d},\text{p}){}^4\text{He}$ transfer reaction

Chapter 3

Features of the reaction

In the introduction we mentioned the importance of the ${}^3\text{He}(\text{d,p}){}^4\text{He}$ reaction rate in the primordial nucleosynthesis, in the context of fusion reactor processes [Kra87], and as a testing ground for nucleon-nucleon (N-N) interaction models [Bit90], which make this reaction a very much modern topic of work.

In this chapter we describe the essential features of the ${}^3\text{He}(\text{d,p}){}^4\text{He}$ reaction. We start with the description of the reaction mechanism. We then introduce the polarization formalism for reactions induced by deuterons, focusing on the particular spin structure relevant to the study of this reaction, $\vec{1} + \frac{1}{2} \rightarrow \frac{1}{2} + 0$. Finally, we describe the sets of data that will be used in the analysis of the ${}^3\text{He}(\text{d,p}){}^4\text{He}$ reaction presented in the following chapters.

3.1 Reaction mechanism

The ${}^3\text{He}(\text{d,p}){}^4\text{He}$ reaction rate is dominated at deuteron energies below 1 MeV by a broad $J^\pi = \frac{3}{2}^+ S$ -wave resonance in ${}^5\text{Li}$ at $E_d = 0.210$ MeV [Til02]. The analysis of the energy level diagram of ${}^5\text{Li}$, in figure 3.1, also shows that up to deuteron energies of 5 MeV, above the threshold of ${}^3\text{He}+\text{d}$, there are 4 other levels: $\frac{3}{2}^-$, $\frac{7}{2}^+$, $\frac{5}{2}^+$ and $\frac{1}{2}^+$. With this information one can identify the matrix elements that can contribute to the ${}^3\text{He}(\text{d,p}){}^4\text{He}$ reaction mechanism. For the positive parity states and considering relative angular momentum in the entrance channel up to $L_i = 2$ we have the contributions shown in Table 3.1, where we have used the notation ${}^{2S+1}L_J$ for the initial and final states ($S_i = S_d + S_{{}^3\text{He}}$ and $S_f = S_p + S_{{}^4\text{He}} = \frac{1}{2}$ are the channel spin for the initial and final states). If the reaction mechanism is predominantly resonant, then M_1 and M_2 are associated with the $\frac{1}{2}^+$ resonance at $E_d = 3.87$ MeV, M_3 , M_4 and M_5 to the $\frac{3}{2}^+$ resonance at $E_d = 0.21$ MeV which is the closest to the threshold, M_6 and M_7 to the $\frac{5}{2}^+$ resonance at $E_d = 3.05$ MeV, and M_8 with the $\frac{5}{2}^+$ resonance at $E_d = 2.79$ MeV. In the

case of the negative parity contributions, Table 3.2 shows the relevant matrix elements considering P -wave contributions from $J^\pi = \frac{1}{2}^-$ and $\frac{3}{2}^-$ states. Again in the case of a predominant resonant mechanism M_9 and M_{10} are associated with the $\frac{1}{2}^-$ subthreshold state at $E_d = -15.17$ MeV, while M_{11} and M_{12} are associated with the $\frac{3}{2}^-$ resonance at $E_d = 2.62$ MeV.

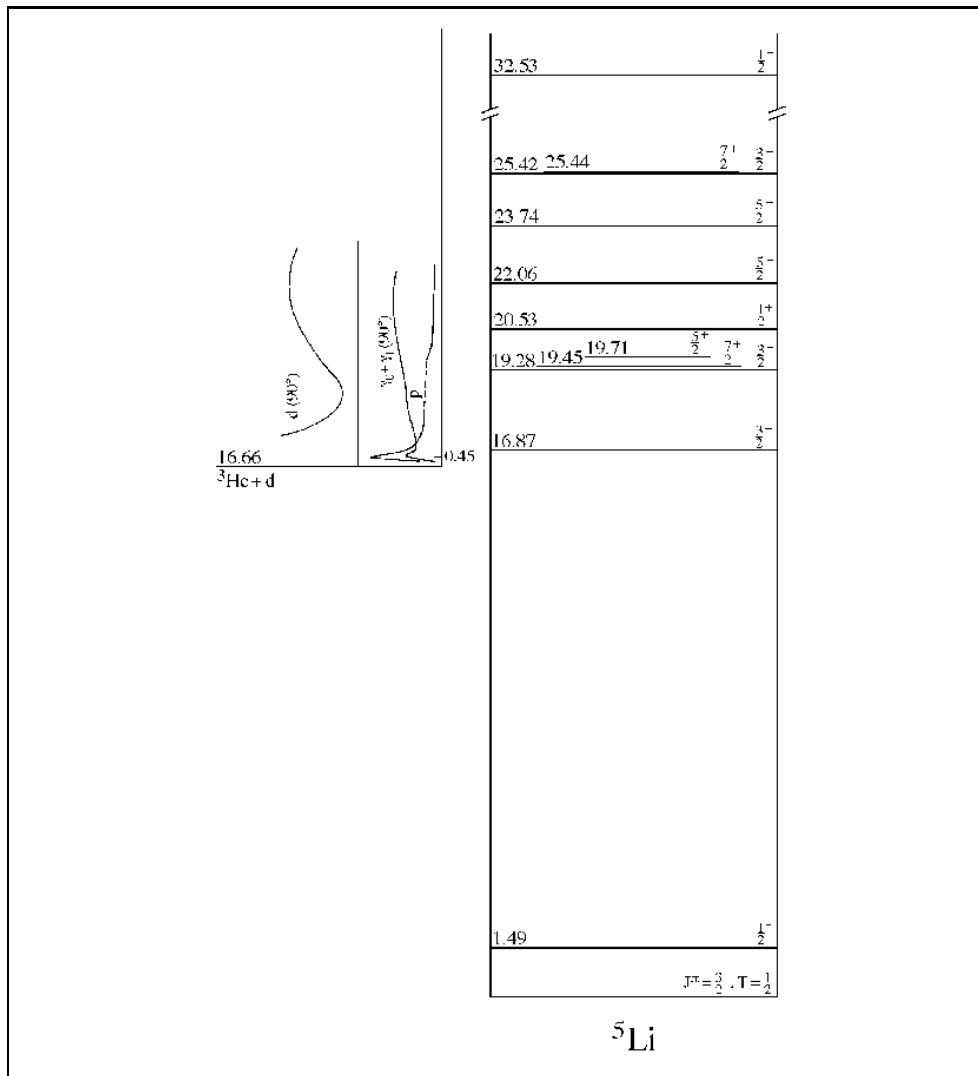


Figure 3.1: Energy level diagram for ${}^5\text{Li}$.

For very low energy deuterons, it is expected that the main contribution to the reaction mechanism arises from S-wave capture in the entrance channel. Tables 3.1 and 3.2 show that in this case there are only 2 matrix elements contributing, M_1 and M_3 , one of them corresponding to the lowest resonance ($\frac{3}{2}^+$) which is therefore expected to be the dominant component to the reaction.

However, recent measurements of polarization observables [Gei98], have shown significant deviation from the expected S-wave resonant behavior. These discrepancies may be due to $L > 0$ contributions to the reaction mechanism arising from direct transfer processes or tails of distant resonances, as the ones listed above. Indeed, the inclusion of P -waves amounts to considering the contribution of 4 additional matrix elements, M_{9-12} . It should be noted that the matrix elements M_9 and M_{10} should contribute predominantly through the direct reaction process in the energy range $0 < E_d < 1$ MeV, since the only possible $\frac{1}{2}^-$ resonant contributions are from distant states of ${}^5\text{Li}$ [Til02] (the closest being the subthreshold state at $E = -15.17$ MeV). Additional experimental information as well as appropriate models are required to identify these processes and obtain information on the relative importance of direct and resonant mechanism.

n	S_i	L_i	J	L_f	S_f	transition
1	1/2	0	1/2	0	1/2	${}^2S_{1/2} \rightarrow {}^2S_{1/2}$
2	3/2	2	1/2	0	1/2	${}^4D_{1/2} \rightarrow {}^2S_{1/2}$
3	3/2	0	3/2	2	1/2	${}^4S_{3/2} \rightarrow {}^2D_{3/2}$
4	1/2	2	3/2	2	1/2	${}^2D_{3/2} \rightarrow {}^2D_{3/2}$
5	3/2	2	3/2	2	1/2	${}^4D_{3/2} \rightarrow {}^2D_{3/2}$
6	1/2	2	5/2	2	1/2	${}^2D_{5/2} \rightarrow {}^2D_{5/2}$
7	3/2	2	5/2	2	1/2	${}^4D_{5/2} \rightarrow {}^4D_{5/2}$
8	3/2	2	7/2	4	1/2	${}^4D_{7/2} \rightarrow {}^2G_{7/2}$

Table 3.1: Matrix elements, M_n , for positive parity states, that contribute to the ${}^3\text{He}(d,p){}^4\text{He}$ reaction mechanism.

n	S_i	L_i	J	L_f	S_f	transition
9	1/2	1	1/2	1	1/2	${}^2P_{1/2} \rightarrow {}^2P_{1/2}$
10	3/2	1	1/2	1	1/2	${}^4P_{1/2} \rightarrow {}^2P_{1/2}$
11	1/2	1	3/2	1	1/2	${}^2P_{3/2} \rightarrow {}^2P_{3/2}$
12	3/2	1	3/2	1	1/2	${}^4P_{3/2} \rightarrow {}^2P_{3/2}$

Table 3.2: Matrix elements, M_n , for negative parity states, that contribute to the ${}^3\text{He}(d,p){}^4\text{He}$ reaction mechanism.

3.2 Polarization formalism for the $\vec{1} + \frac{1}{2} \rightarrow \frac{1}{2} + 0$ spin structure

In this sections we introduce the polarization formalism for reactions, following the article of Gerald Ohlsen [Ohl72]. We start with general remarks on the polarization formalism and then focus on the calculation of the observables for the specific $\vec{1} + \frac{1}{2} \rightarrow \frac{1}{2} + 0$ spin structure, relevant for the study of the ${}^3\text{He}(\text{d,p}){}^4\text{He}$ reaction. We obtain the density matrices for the initial and final states and the scattering amplitudes that relate them, and write the cross-section and outgoing polarization components as functions of these. Finally we write the scattering matrix, $\mathbf{M}(\hat{\mathbf{R}}) \equiv \mathbf{M}(\theta, \phi)$, in terms of a product of the 3×1 matrices and the Pauli operators. Since each of the zero-degree observables depend on a relatively small number of M-matrix amplitudes, thus allowing a relatively unambiguous determination of the properties of these elements, we calculate the M-matrix for the $\theta=0^\circ$ case and obtain the form of the observables at 0° degrees.

3.2.1 General remarks

Deuterons are spin 1 particles and therefore exist in three spin substates, $m_S = \pm 1$ and 0. A deuteron is unpolarized if there are equal populations of particles in each spin substate m_S : $N_1 = N_{-1} = N_0$.

To span the 3×3 space, nine hermitian operators are needed. Using the basic spin 1 angular momentum operators:

$$S_x = \frac{1}{\sqrt{2}} \begin{bmatrix} 0 & 1 & 0 \\ 1 & 0 & 1 \\ 0 & 1 & 0 \end{bmatrix} \quad S_y = \frac{1}{\sqrt{2}} \begin{bmatrix} 0 & -i & 0 \\ i & 0 & -i \\ 0 & i & 0 \end{bmatrix} \quad S_z = \begin{bmatrix} 1 & 0 & 0 \\ 0 & 0 & 0 \\ 0 & 0 & -1 \end{bmatrix} \quad (3.1)$$

(with the condition that each has zero trace so that each will be orthogonal to the unit matrix and the expectation value is zero for an unoriented ensemble), the set of operators:

$$P_{ij} = \frac{3}{2}(S_i S_j + S_j S_i) - 2\delta_{ij} \quad (3.2)$$

(where $2\delta_{ij}$ makes the second rank tensor traceless) and the unit matrix, I , form an over-complete set from where the nine operators can be obtained by choosing any of the pairs:

$$\begin{array}{ll} (P_{xx} - P_{yy}) & P_{zz} \\ (P_{yy} - P_{zz}) & P_{xx} \\ (P_{zz} - P_{xx}) & P_{yy} \end{array} \quad (3.3)$$

in place of the three operators P_{ii} .

The density matrix for an ensemble of spin 1 particles

We use the notation $P_i = S_i$, with $i = x, y$, and z , and define the set of orthogonal operators, Ω_i , required to be normalized so that:

$$\text{Tr}(\Omega_i \Omega_j) = 3\delta_{ij} \quad (3.4)$$

which corresponds to the set:

$$\begin{aligned} \Omega_0 &= I & \Omega_4 &= \sqrt{\frac{2}{3}} P_{xy} \\ \Omega_1 &= \sqrt{\frac{3}{2}} P_x & \Omega_5 &= \sqrt{\frac{2}{3}} P_{xz} \\ \Omega_2 &= \sqrt{\frac{3}{2}} P_y & \Omega_6 &= \sqrt{\frac{2}{3}} P_{yz} \\ \Omega_3 &= \sqrt{\frac{3}{2}} P_z & \Omega_7 &= \sqrt{\frac{1}{6}} (P_{xx} - P_{yy}) \\ \Omega_8 &= \sqrt{\frac{1}{2}} P_{zz} \end{aligned} \quad (3.5)$$

These expressions correspond to the Cartesian form of the most commonly used spherical basis [Gom01, Mad71].

The density matrix for an ensemble of spin 1 particles can be expanded in terms of the complete set of operators defined in the previous section:

$$\begin{aligned} \rho &= \frac{1}{3} \left\{ I + \frac{3}{2} (p_x P_x + p_y P_y + p_z P_z) + \frac{2}{3} (p_{xy} P_{xy} + p_{yz} P_{yz} + p_{xz} P_{xz}) + \right. \\ &\quad \left. \frac{1}{6} (p_{xx} - p_{yy}) (P_{xx} - P_{yy}) + \frac{1}{2} p_{zz} P_{zz} \right\} \end{aligned} \quad (3.6)$$

where the polarization quantity, p_i , is the expectation value of P_i :

$$p_i = \text{Tr}(\rho P_i). \quad (3.7)$$

Using the fact that:

$$p_{xx} + p_{yy} + p_{zz} = 0 \quad (3.8)$$

$$P_{xx} + P_{yy} + P_{zz} = 0_{3 \times 3} \quad (3.9)$$

the last two terms of the density matrix expression can be written in the form:

$$\frac{1}{6} (p_{xx} - p_{yy}) (P_{xx} - P_{yy}) + \frac{1}{2} p_{zz} P_{zz} = \frac{1}{3} (p_{xx} P_{xx} + p_{yy} P_{yy} + p_{zz} P_{zz}) \quad (3.10)$$

The beam polarization in the projectile helicity frame

Various production schemes for polarized deuteron beams produce different types of polarization. All schemes, however, produce beams with axial symmetry. It is convenient to take the axis of quantization along this axis, so that all but two tensors vanish, and to denote this coordinate system by X, Y, Z, where Z is along the quantization axis (thus $p_Z = N_1 + N_{-1}$ and $p_{ZZ} = N_1 + N_{-1} - 2N_0$ are non-zero, where $N_{\pm 1, 0}$ are the fractional populations of the $m_S = \pm 1$ and 0 states) and X and Y are arbitrary. Therefore, only four quantities are needed to describe such a beam: two angles to determine the direction of the quantization axis in space, the rank-one polarization, p_Z , and the rank-two polarization, p_{ZZ} (p_{XX} and p_{YY} do not vanish but because of the axial symmetry they are determined by the relation $p_{XX} = p_{YY} = -\frac{1}{2}p_{ZZ}$).

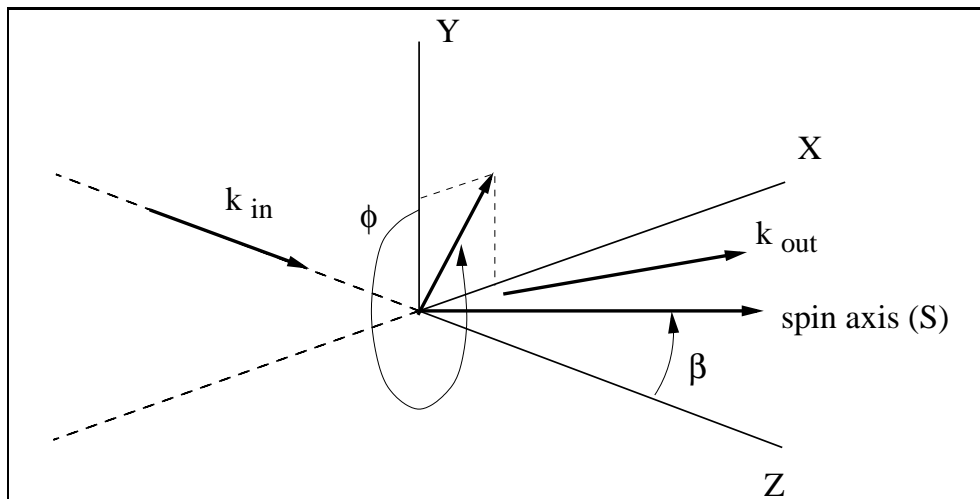


Figure 3.2: The Madison convention coordinate system.

Scattering or reactions induced by spin 1 particles can be best described in the projectile helicity frame, the Madison convention coordinate system [Mad71] represented in figure 3.2. In this coordinate system, the axis of quantization (z axis) is taken along the direction of the projectile motion, \mathbf{k}_{in} ; the y axis is taken along the $\mathbf{k}_{in} \times \mathbf{k}_{out}$, where \mathbf{k}_{out} represents the direction of scattered particle or reaction product motion; and x is chosen to form a right-hand coordinate system. Unit vectors along the x , y , z directions are referred to as $\hat{\mathbf{p}}$, $\hat{\mathbf{n}}$, $\hat{\mathbf{k}}$.

Let $\hat{\mathbf{S}}$ be the natural quantization axis of the incident polarized beam. This axis can be described in the projectile helicity frame by the angles β and ϕ , such that:

$$\cos \beta = \hat{\mathbf{S}} \cdot \hat{\mathbf{k}}_{in} \quad (3.11)$$

$$\cos \phi = (\hat{\mathbf{S}} \times \hat{\mathbf{k}}_{in}) \cdot (\hat{\mathbf{n}} \times \hat{\mathbf{k}}_{in}) \quad (3.12)$$

where β is the angle between $\hat{\mathbf{S}}$ and \mathbf{k}_{in} and ϕ is the angle between the projection of $\hat{\mathbf{S}}$ on the x, y plane and the y axis. One can therefore obtain the polarizations in the projectile helicity frame ($p_x, p_y, p_z, p_{xx}, p_{yy}, p_{zz}, p_{xy}, p_{yz}$ and p_{xz}) from the polarizations defined in the reference frame of the natural quantization axis of the incident beam (p_z and p_{zz}) through the angles β and ϕ (see appendix D).

For measuring polarizations in the outgoing channel, one defines the x', y', z' coordinate system similarly with z' along its momentum, \mathbf{k}_{out} ; y' still along $\mathbf{k}_{in} \times \mathbf{k}_{out}$; and x' again chosen to form a right-handed system.

3.2.2 Form of the observables for $\vec{1} + \frac{1}{2} \rightarrow \frac{1}{2} + 0$

The initial state is composed of a projectile of spin $S_p = 1$ and a target of spin $S_t = \frac{1}{2}$, and therefore it is a direct product of a spin 1 and a spin $\frac{1}{2}$ space, thus the spin function of any initial state can be described, with respect to a particular z axis, in terms of a six-component column vector. Using the uncoupled representation for the initial state we can write

$$\chi_i = \sum_{j=1}^6 a_j \phi_j \quad (3.13)$$

where $\phi_1 = \chi_{11}\chi_{\frac{1}{2}\frac{1}{2}}$, $\phi_2 = \chi_{10}\chi_{\frac{1}{2}\frac{1}{2}}$, $\phi_3 = \chi_{1-1}\chi_{\frac{1}{2}\frac{1}{2}}$, $\phi_4 = \chi_{11}\chi_{\frac{1}{2}-\frac{1}{2}}$, $\phi_5 = \chi_{10}\chi_{\frac{1}{2}-\frac{1}{2}}$ and $\phi_6 = \chi_{1-1}\chi_{\frac{1}{2}-\frac{1}{2}}$. The χ_{1M_p} are the eigenfunctions of the spin 1 operator S_z and $\chi_{\frac{1}{2}M_t}$ are the eigenfunctions of the spin $\frac{1}{2}$ operator σ_z .

The final state consists of a spin $\frac{1}{2}$ and a spin 0 particle, so it can be represented by

$$\chi_f = \sum_{j=1}^2 b_j \phi'_j \quad (3.14)$$

where $\phi'_1 = \chi_{\frac{1}{2}\frac{1}{2}}$ and $\phi'_2 = \chi_{\frac{1}{2}-\frac{1}{2}}$.

The j th final state is related to the k th initial state by the M_{jk} element of the scattering matrix, when we only consider spin variables:

$$b_j = \sum_k M_{jk} a_k$$

$$\Leftrightarrow \begin{bmatrix} b_1 \\ b_2 \end{bmatrix} = \begin{bmatrix} M_{11} & M_{12} & M_{13} & M_{14} & M_{15} & M_{16} \\ M_{21} & M_{22} & M_{23} & M_{24} & M_{25} & M_{26} \end{bmatrix} \begin{bmatrix} a_1 \\ a_2 \\ a_3 \\ a_4 \\ a_5 \\ a_6 \end{bmatrix} \quad (3.15)$$

When we describe the whole wave functions in the entrance and outgoing channels, this matrix is in fact the scattering matrix of elements $A_{M'_p M'_t, M_p M_t}(\theta, \phi)$ defined in eq. (1.52), corresponding in this case to the elements shown below:

$$\mathbf{A}(\theta, \phi) = \begin{bmatrix} A_{\frac{1}{2}0,1\frac{1}{2}} & A_{\frac{1}{2}0,0\frac{1}{2}} & A_{\frac{1}{2}0,-1\frac{1}{2}} & A_{\frac{1}{2}0,1-\frac{1}{2}} & A_{\frac{1}{2}0,0-\frac{1}{2}} & A_{\frac{1}{2}0,-1-\frac{1}{2}} \\ A_{-\frac{1}{2}0,1\frac{1}{2}} & A_{-\frac{1}{2}0,0\frac{1}{2}} & A_{-\frac{1}{2}0,-1\frac{1}{2}} & A_{-\frac{1}{2}0,1-\frac{1}{2}} & A_{-\frac{1}{2}0,0-\frac{1}{2}} & A_{-\frac{1}{2}0,-1-\frac{1}{2}} \end{bmatrix} \quad (3.16)$$

Density matrices for the initial and final states

The 6×6 and 2×2 density matrices that describe the initial and final states are defined, respectively, for an ensemble of N particles:

$$(\rho_i)_{jk} = \frac{1}{N} \sum_{n=1}^N a_j^n a_k^{n*} \quad (3.17)$$

$$(\rho_f)_{jk} = \frac{1}{N} \sum_{n=1}^N b_j^n b_k^{n*} \quad (3.18)$$

The initial and final density matrices are related by

$$\rho_f = M \rho_i M^+ \quad (3.19)$$

As in (3.6), the density matrix for the initial state, ρ_i , can now be expanded in terms of a direct product of appropriate spin 1 operators and the spin $\frac{1}{2}$ operators I , σ_x , σ_y and σ_z . Using the notation $\sigma_0 = I$, $\sigma_1 = \sigma_x$, $\sigma_2 = \sigma_y$ and $\sigma_3 = \sigma_z$ and the normalized spin 1 operators defined previously in (3.5), one obtains:

$$\rho_i = \frac{1}{6} \sum_{jk} \omega_j p_k \Omega_j \sigma_k \quad (3.20)$$

where ω_j and p_k are the expectation values of the operators Ω_j and σ_k respectively: $\omega_j = \langle \Omega_j \rangle$ and $p_k = \langle \sigma_k \rangle$. If the spin $\frac{1}{2}$ particle is unpolarized, $p_k=1$ for $k=0$ and $p_k=0$ for $k=1, 2, 3$, so that

$$\rho_i = \frac{1}{6} \sum_j \omega_j \Omega_j I \quad (3.21)$$

Cross-section and outgoing polarization components

If ρ_i is normalized to unity, the differential cross-section for a polarized beam is given by:

$$I(\theta, \phi) = \text{Tr } \rho_f = \frac{1}{6} \sum_j \omega_j \text{Tr}(M \Omega_j I M^+) \quad (3.22)$$

where θ is the scattering angle. If the beam is unpolarized so that

$$\rho_i = \frac{1}{6}I \quad (3.23)$$

this reduces to

$$I_0(\theta) = \text{Tr } \rho_f = \frac{1}{6}\text{Tr}(MIM^+) \quad (3.24)$$

To calculate the polarization of the scattered particles, we first notice that $\rho_f/\text{Tr}\rho_f$ is normalized to have trace unity so that

$$\begin{aligned} p_{k'} &\equiv \langle \sigma_{k'} \rangle = \text{Tr} \left(\frac{\rho_f \sigma_{k'}}{\text{Tr}\rho_f} \right) \\ &= \frac{\sum \omega_j \text{Tr}(M\Omega_j I M^+ \sigma_{k'})}{\sum \omega_j \text{Tr}(M\Omega_j M^+)} \end{aligned} \quad (3.25)$$

or

$$p_{k'} I(\theta, \phi) = I_0(\theta) \left(\frac{\sum \omega_j \text{Tr}(M\Omega_j I M^+ \sigma_{k'})}{\text{Tr}(MM^+)} \right) \quad (3.26)$$

Suppressing the unit matrix I in the trace expressions and using eq. (3.10), the previous expressions can be written in compact form, corresponding to eq. (34) of [Gom01], as

$$I(\theta, \phi) = I_0(\theta) \left(1 + \frac{3}{2} \sum_j p_j A_j(\theta) + \frac{1}{3} \sum_{jk} p_{jk} A_{jk} \right) \quad (3.27)$$

$$p_{l'} I(\theta, \phi) = I_0(\theta) \left(P_{l'}(\theta) + \frac{3}{2} \sum_j p_j K_j^{l'} + \frac{1}{3} \sum_{jk} p_{jk} K_{jk}^{l'} \right) \quad (3.28)$$

where $A_j(\theta)$ and $A_{jk}(\theta)$ are the analyzing powers

$$A_j(\theta) = \frac{\text{Tr}(MP_j M^+)}{\text{Tr}(MM^+)} \quad (3.29)$$

$$A_{jk}(\theta) = \frac{\text{Tr}(MP_{jk} M^+)}{\text{Tr}(MM^+)} \quad (3.30)$$

$P_{l'}(\theta)$ the l' th component of outgoing polarization which would be produced by an unpolarized beam

$$P_{l'}(\theta) = \frac{\text{Tr}(MM^+ \sigma_{l'})}{\text{Tr}(MM^+)} \quad (3.31)$$

and $K_j^{l'}$ and $K_{jk}^{l'}$ are the polarization transfer coefficients that relate the initial polarization component to the final polarization component

$$K_j^{l'}(\theta) = \frac{\text{Tr}(MP_j M^+ \sigma_{l'})}{\text{Tr}(MM^+)} \quad (3.32)$$

$$K_{jk}^{l'}(\theta) = \frac{\text{Tr}(MP_{jk} M^+ \sigma_{l'})}{\text{Tr}(MM^+)} \quad (3.33)$$

Parity conservation and rotation invariance allow the simplification of expressions (3.22) and (3.26). Choosing coordinate frames with y, y' along $\mathbf{k}_{in} \times \mathbf{k}_{out}$, parity conservation requires that an observable vanish unless $n_x + n_z$ is an even number, and rotational invariance requires an observable to be odd or even function of θ as $n_x + n_y$ is odd or even (n_i with $i = x, y, \text{ or } z$ refers to the number of times i appears in an observable notation). Thus the expressions for the observables reduce to the form given in the following equations, where terms odd in the scattering angle, θ , are underlined

$$I = I_0 \left(1 + \frac{3}{2} p_y \underline{A_y} + \frac{2}{3} p_{xz} \underline{A_{xz}} + \frac{1}{3} p_{xx} A_{xx} + \frac{1}{3} p_{yy} A_{yy} + \frac{1}{3} p_{zz} A_{zz} \right) \quad (3.34)$$

$$p_{x'} I = I_0 \left(\frac{3}{2} p_x K_x^{x'} + \frac{3}{2} p_z \underline{K_z^{x'}} + \frac{2}{3} p_{xy} \underline{K_{xy}^{x'}} + \frac{2}{3} p_{yz} K_{yz}^{x'} \right) \quad (3.35)$$

$$p_{y'} I = I_0 \left(\underline{P_{y'}} + \frac{3}{2} p_y K_y^{y'} + \frac{2}{3} p_{xz} K_{xz}^{y'} + \frac{1}{3} p_{xx} \underline{K_{xx}^{y'}} \right. \\ \left. + \frac{1}{3} p_{yy} \underline{K_{yy}^{y'}} + \frac{1}{3} p_{zz} \underline{K_{zz}^{y'}} \right) \quad (3.36)$$

while, because of symmetry, $p_{z'}$ is analogous to $p_{x'}$ with $x' \rightarrow z'$.

From eq. (3.34), using eqs. (3.10) and (D.6–D.11), one can write the observables as a function of the one- and two-rank polarization, p_Z and p_{ZZ} , and the angles β and ϕ . For the cross-section one obtains the expression:

$$I(\theta, \phi) = I_0 \left[1 + \frac{3}{2} p_y \underline{A_y}(\theta) + \frac{2}{3} p_{xz} \underline{A_{xz}}(\theta) - \frac{2}{6} (p_{xx} - p_{yy}) A_{yy}(\theta) \right. \\ \left. + \left(\frac{1}{2} p_{zz} - \frac{1}{6} (p_{xx} - p_{yy}) \right) A_{zz}(\theta) \right] \\ = I_0 \left[1 + \frac{3}{2} \sin \beta \cos \phi p_Z \underline{A_y}(\theta) - \sin \beta \cos \beta \sin \phi p_{ZZ} \underline{A_{xz}}(\theta) \right. \\ \left. + \frac{1}{2} \sin^2 \beta \cos 2\phi p_{ZZ} A_{yy}(\theta) \right. \\ \left. + \frac{1}{4} (3 \cos^2 \beta - 1 + \sin^2 \beta \cos 2\phi) p_{ZZ} A_{zz}(\theta) \right] \quad (3.37)$$

3.2.3 Observables for $\theta=0^\circ$

After obtaining the cross-section and outgoing polarization as a function of analyzing powers, outgoing polarization produced by an unpolarized beam and polarization transfer coefficients, one should obtain the relations between these last ones, and the elements of the M–matrix, the scattering amplitudes. We start by writing the M–matrix in terms of a product of the 3×1 matrices and the Pauli operators. Since each of the zero-degree observables depend on a relatively small number of scattering amplitudes, thus allowing a relatively unambiguous determination of the properties of these elements, we calculate the M–matrix for the $\theta=0^\circ$ case and obtain the form of the observables at 0° degrees.

The M–matrix

The 6×2 M–matrix of (3.15) can be written quite generally in terms of a direct product matrix of the form

$$\mathbf{M} = \sum_{i=x,y,z} C_i \chi_i^+ I + \sum_{j=x',y',z'} C_{ij} \chi_i^+ \sigma_j \quad (3.38)$$

Note that each term is a 6×2 matrix, as required; the χ^+ are the complete set of spinors in the 3×1 space, I the 2×2 unit matrix and $\sigma_{x'}$, $\sigma_{y'}$, $\sigma_{z'}$ the Pauli operators. Assuming parity conservation we can write

$$\mathbf{M} = A \underline{\chi_y^+} I + B \underline{\chi_y^+} \sigma_{y'} + C \underline{\chi_x^+} \sigma_{x'} + D \underline{\chi_x^+} \sigma_{z'} + E \underline{\chi_z^+} \sigma_{x'} + F \underline{\chi_z^+} \sigma_{z'} \quad (3.39)$$

since all the other 6 terms vanish ($n_x + n_z$ is odd). The terms underlined are odd functions of θ ($n_x + n_y$ is odd).

In this formulation there is freedom to choose the x , y , z and x' , y' , z' coordinate systems differently as long as they share a common y axis along $\mathbf{k}_{in} \times \mathbf{k}_{out}$. If the x , y , z and x' , y' , z' are chosen to be the same, the scattering matrix assumes the simple form:

$$\mathbf{M} = \begin{bmatrix} \frac{-iA-D}{\sqrt{2}} & F & \frac{-iA+D}{\sqrt{2}} & \frac{-B-C}{\sqrt{2}} & E & \frac{-B+C}{\sqrt{2}} \\ \frac{B-C}{\sqrt{2}} & E & \frac{B+C}{\sqrt{2}} & \frac{-iA+D}{\sqrt{2}} & -F & \frac{-iA-D}{\sqrt{2}} \end{bmatrix} \quad (3.40)$$

The observables for $\theta=0^\circ$

The rotational invariance of the scattering matrix implies that the quantities A , D and E are odd functions of θ , and therefore at 0° $A=D=E=0$. Furthermore, since at 0° no preferential transverse direction is defined then $B=C$. In this case the scattering matrix takes the form

$$\mathbf{M} = \begin{bmatrix} 0 & F & 0 & \frac{-2B}{\sqrt{2}} & 0 & 0 \\ 0 & 0 & \frac{2B}{\sqrt{2}} & 0 & -F & 0 \end{bmatrix} \quad (3.41)$$

With the M–matrix at 0° , a straightforward evaluation of the traces in the equations (3.19) and (3.24-3.26) relevant for the calculation of the observables (3.29-3.33) can be done, yielding the results

$$6I_0 = 4|B|^2 + 2|F|^2 \quad (3.42)$$

$$6I_0A_{xx} = 6I_0A_{yy} = -2|B|^2 + 2|F|^2 \quad (3.43)$$

$$6I_0A_{zz} = 4|B|^2 - 4|F|^2 \quad (3.44)$$

$$6I_0K_x^{x'} = 6I_0K_y^{y'} = 4\text{Re}(BF^*) \quad (3.45)$$

$$6I_0K_{yz}^{x'} = -6I_0K_{xz}^{y'} = 6\text{Im}(BF^*) \quad (3.46)$$

$$6I_0K_z^{z'} = 4\text{Re}(|B|^2) = 4|B|^2 \quad (3.47)$$

$$6I_0K_{xy}^{z'} = -6\text{Im}(|B|^2) = 0 \quad (3.48)$$

All the remaining terms are odd terms in θ in equation (3.29-3.33) and therefore are zero at 0° . In this set of non-vanishing observables, there are only three independent ones. These can be chosen as I_0 , A_{yy} and $K_y^{y'}$, and the others can be written in terms of these as:

$$A_{xx} = -\frac{1}{2}A_{zz} = A_{yy} \quad (3.49)$$

$$K_x^{x'} = K_y^{y'} \quad (3.50)$$

$$K_z^{z'} = \frac{2}{3}(1 - A_{yy}) \quad (3.51)$$

$$K_{yz}^{x'} = -K_{xz}^{y'} = \left[(1 - A_{yy})(1 + 2A_{yy}) - \left(\frac{3}{2}K_y^{y'} \right)^2 \right]^{\frac{1}{2}} \quad (3.52)$$

With the previous relations the 2 amplitudes in the M–matrix, corresponding to 3 real numbers since one relative phase factor can be chosen arbitrarily, can be written as $B = |B|$ and $F = |F|e^{i\phi}$ and are determined as functions of the three independent observables

$$|F|^2 = I_0(1 + 2A_{yy}) \quad (3.53)$$

$$|B|^2 = I_0(1 - A_{yy}) \quad (3.54)$$

$$\phi = \arccos \left(\frac{3I_0K_y^{y'}}{2|B||F|} \right) \quad (3.55)$$

3.3 Experimental data

The ${}^3\text{He}(d,p){}^4\text{He}$ reaction has been investigated since the early days of accelerators to study various nuclear phenomena [Kra87], and therefore the amount of information available, makes it an ideal first step in the testing of new approaches to nuclear reaction modeling, which is ultimately the objective of this work.

Particular attention has been paid over the years to the measurement of polarization observables [Bro66, Bit90, Gei99, Fle02]. Polarization effects are very small in N-N scattering, however, in few-nucleon systems polarization observables can increase by one or two orders of magnitude. The complexity of the structure of few-nucleon systems with $A > 3$ is increased by the existence of resonances and the measurement of polarization observables allows to detect in an analysis of the data the tiny effects of the underlying interaction [Bit90] and, in what concerns us more in this work, to disentangle the resonant contributions to the reaction mechanism from the direct process.

In recent studies Geist *et al.* [Gei99] obtained precise measurements of vector and tensor analyzing powers, and of total and differential cross sections at several energies up to 1 MeV, and Fletcher *et al.* [Fle02] measured the polarization transfer $K_y^{y'}(0^\circ)$ at $E_d = 0.52, 0.89$ and 1.49 MeV.

In chapter 4, new experimental results for the cross section and A_{yy} tensor analyzing power observables of the ${}^3\text{He}(d,p){}^4\text{He}$ reaction at a scattering angle of $\theta = 0^\circ$ will be presented, allowing the calculation, for the first time, of all the linearly independent elements of the scattering matrix at $\theta = 0^\circ$ from eqs. (3.53-3.55).

The new measurements, together with the experimental data of Geist *et al.* [Gei99], the $K_y^{y'}(0^\circ)$ measurements of Fletcher *et al.* [Fle02], and elastic differential cross section of Jenny [Jen79], constituting 25% of the available data in the energy range $E_d < 1\text{MeV}$, are analyzed with a hybrid R-matrix + potential model in chapter 5.

Chapter 4

New Measurements

In this chapter new experimental results for the cross section and A_{yy} tensor analyzing power observables of the ${}^3\text{He}(\text{d},\text{p}){}^4\text{He}$ reaction at a scattering angle of $\theta = 0^\circ$ are obtained, complementing the existing $K_y^{y'}(0^\circ)$ data [Fle02]. As shown previously, from these results one is able to calculate all the linearly independent elements of the scattering matrix at $\theta = 0^\circ$, through eqs. (3.53-3.55). Moreover, the new tensor observable measured, being very sensitive to the reaction process, provides an excellent tool to test a theoretical study of the mechanism of the reaction.

4.1 Experimental study of the ${}^3\text{He}(\text{d},\text{p}){}^4\text{He}$ reaction

In this section we describe the experimental setups, procedures and data reduction used to determine the tensor analyzing power, A_{yy} , and cross section values at zero degrees. The experiment was performed in the 61-cm-diameter scattering chamber at the Triangle Universities Nuclear Laboratory (TUNL) using the FN Tandem accelerator.

4.1.1 A_{yy} measurement

The A_{yy} analyzing power at $\theta = 0^\circ$ was measured with a polarized deuteron beam incident on a ${}^3\text{He}$ gas cell target. The setup is shown schematically in Figure 4.1.

The gas target was a 2.54 cm diameter cell with a 6.3 μm Havar-foil cylindrical window. This cell was filled with ${}^3\text{He}$ gas and the pressure (1 atm for runs at $E_d = 0.52$ MeV and 2 atm for runs at $E_d = 0.89$ and 1.49 MeV) monitored to be constant during the experiment.

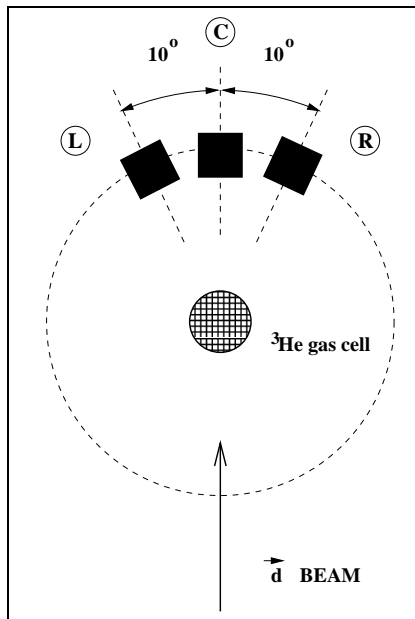


Figure 4.1: Experimental setup used in the A_{yy} measurement.

The polarized deuteron beam was obtained from the atomic beam polarized ion source (ABPIS) [Cle95] at TUNL via a three polarization state method with fast state switching [Gei98]. During the measurements the beam current on target ranged from 100 nA to 200 nA, depending on the energy.

Three silicon detectors were positioned inside the chamber, a central detector (labeled C) at $\theta = 0^\circ$ and the others at 10° left (L), and right (R), from the 0° detector. Consecutive runs at the deuteron energies of interest were intercalated with runs at $E_d = 4$ MeV to determine the tensor beam polarization p_{zz} .

The beam current was integrated from the gas cell and a tantalum foil in front of the 0° detector. Calculations with SRIM [Zie00] were performed to obtain the beam energies corresponding to the mean reaction energies at the center of the gas cell. This procedure was also used for the self supported targets described later in Section 4.1.2.

For the determination of the analyzing power, $A_{yy}(0^\circ)$, the normalized yield Y^i for a detector in the i th polarization state is determined by normalizing the number of reaction counts collected in that detector and state to the charge collected. These yields also include a correction for dead-time in the data acquisition system. A value of $i=0$ is used to represent the unpolarized state.

For this measurement, the alignment of the spin quantization axis is perpendicular to the reaction plane, in the direction of the y axis (figure 3.2). The left detector corresponds to $(\beta = 90^\circ, \phi = 0^\circ)$, while the right detector to $(\beta = 90^\circ, \phi = 180^\circ)$. From eq. (3.37) one obtains therefore [Gei99]:

$$\frac{I(\theta, 0^\circ)}{I_0(\theta)} \equiv \frac{Y_L^i}{Y_L^0} = 1 + \frac{3}{2}p_z A_y + \frac{1}{2}p_{zz}^i A_{yy} \quad (4.1)$$

$$\frac{I(\theta, 180^\circ)}{I_0(\theta)} \equiv \frac{Y_R^i}{Y_R^0} = 1 - \frac{3}{2}p_z A_y + \frac{1}{2}p_{zz}^i A_{yy} \quad (4.2)$$

Y_L and Y_R denote the yields for the left, $Y(\theta, 0^\circ)$, and right, $Y(\theta, 180^\circ)$, detectors respectively, and p_{zz}^i is the beam polarization in the i th polarized state. From (4.1) and (4.2) we obtain the expression for $A_{yy}(\theta)$

$$A_{yy}(\theta) = \frac{Y_L^i/Y_L^0 + Y_R^i/Y_R^0 - 2}{p_{zz}^i} \quad (4.3)$$

which at $\theta = 0^\circ$ corresponds to

$$A_{yy}(0^\circ) = \frac{2(Y_C^i/Y_C^0 - 1)}{p_{zz}^i} \quad (4.4)$$

where the subscript C denotes the central detector.

The beam polarization was calculated from the 4 MeV runs from eq. (4.3):

$$p_{zz}^i = \frac{Y_L^i/Y_L^0 + Y_R^i/Y_R^0 - 2}{A_{yy}(10^\circ)} \quad (4.5)$$

where $A_{yy}(10^\circ) = 0.818 \pm 0.004$ is the value obtained from Bittcher *et al.* [Bit90]. During the experiment, the on target beam polarizations were determined to be stable for both polarization states. The average of the magnitudes of the two polarizations was 75%.

The final values, given in Table 4.1, are the averages of both spin states.

4.1.2 Cross section measurement

The cross section at $\theta = 0^\circ$ was measured in inverse kinematics with a ^3He beam incident on a deuterated carbon target. The setup is shown schematically in Figure 4.2.

The self-supported deuterated carbon targets were produced using the plasma-assisted chemical vapor deposition technique with deuterated-methane gas: ferro-type slides were placed in an evaporation chamber where NaCl was evaporated in order to produce a thin (approximately 400Å) film on the slides; these slides were then moved to the plasma-associated chemical vapor deposition chamber where they were put between two electrodes; a small amount of deuterated methane gas was flowed into the chamber while also being pumped by a mechanical pump; once the pressure equalized, a high potential was applied between the electrodes until a plasma ignited; the current was then read from

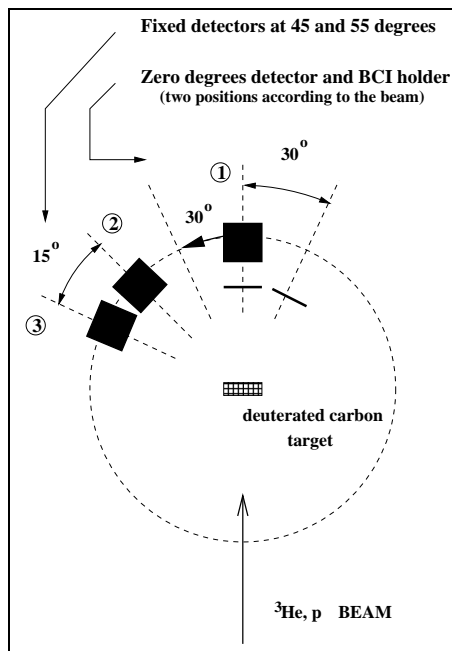


Figure 4.2: Experimental setup used in the cross section measurement.

the plates until the desired thickness (collected charge) was reached; finally, water was used to dissolve the salt layer out from under the deuterated amorphous carbon layer, and this one was separated from the slide and placed on target holders. These targets have been shown [Gei98] to be stable and to have a slow decrease of deuterium thickness.

To normalize the results to the $p - d$ elastic cross section, the ${}^3\text{He}$ runs were intercalated with proton runs for the same value of the magnetic field in the analyzing magnet (at $E_p = \frac{3}{4}E_d$). The proton beam was obtained from the direct extraction negative ion source (DENIS). Typical beam currents on target were 40 nA for the proton beam and 70 nA for the ${}^3\text{He}$ beam.

Three detectors were positioned inside the chamber, two fixed detectors (monitors) at 45° and 55° (detectors 2 and 3 respectively), and a central detector (detector 1), positioned at $\theta = 0^\circ$ for the ${}^3\text{He}$ beam and sliding to 30° when running with the proton beam. In this way, one avoids radiation damage of the detector during the proton runs and is able to avoid solid angle corrections.

During the ${}^3\text{He}$ runs beam current integration was performed from the target and a tantalum foil in front of detector 1. During the proton runs the current was measured from the target and a Havar foil that slid rigidly with the central detector and was located at 0° .

The differential cross section at 0° for the ${}^3\text{He}(d,p)\alpha$ reaction, $\sigma(0^\circ)$, is determined using:

$$\sigma(0^\circ) = \frac{\Delta\Omega_m}{\Delta\Omega_1} \frac{Q}{Q'} \frac{N_1^\alpha}{N_m^p} \sigma_{el}(\theta_m) \quad (4.6)$$

where Q' and Q are the collected charges obtained during ${}^3\text{He}$ runs and proton runs respectively, and N^α and N^p are the dead-time-corrected integrals of the counts in the α peak and proton elastic peak respectively. The subscripts denote the detectors, as shown in Figure 4.2, and m refers to the detector used for p-d elastic scattering. The elastic p-d cross section, $\sigma_{el}(\theta_m)$, is obtained from Kievsky [Kie01]. These calculations, which have been shown to be in excellent agreement with experimental data in this energy range [Woo02, Bru01], use correlated hyperspherical harmonics (CHH) to calculate the continuum wavefunctions [Viv98] corresponding to a realistic Hamiltonian consisting of the Argonne V18 two-nucleon [Wir95] and Urbana IX three nucleon interactions [Pud95]. A Kohn variational principle is used to determine the scattering matrix elements. Equation (4.6) is applied to consecutive ${}^3\text{He}$ and proton runs, assuming that the target thickness does not change during these runs.

For $E_d = 1.49$ MeV, one can use detector 1 for p-d elastic yields; thus $m = 1$, $\theta_m = 30^\circ$, and the ratio of solid angles in equation (4.6) vanishes. However, for the lower energy the scattered particles are absorbed by the foil in front of detector 1. The ratio of solid angles $\Delta\Omega_m/\Delta\Omega_1$ is then obtained from the proton runs at $E_p = 1.68$ MeV using:

$$\frac{\Delta\Omega_m}{\Delta\Omega_1} = \frac{N_m^p \sigma_{el}(30^\circ)}{N_1^p \sigma_{el}(\theta_m)} \quad (4.7)$$

The angles in Equations (4.6) and (4.7) are laboratory angles.

The final values, given in Table 4.1, are the average of the values obtained from normalizing to different detectors.

Table 4.1: Values of measured A_{yy} , cross section and $K_y^{y'}$ at 0° and of calculated scattering amplitudes (errors quoted include statistical errors only). The amplitudes $|B|^2$ and $|F|^2$ have dimensions of cross section (mb/sr).

E_d (MeV)	$A_{yy}(0^\circ)$	$\sigma(0^\circ)$ (mb/sr)	$K_y^{y'}(0^\circ)^1$	$ B ^2$	$ F ^2$	ϕ (degrees)
0.52	0.47 ± 0.02	54.9 ± 0.7^2	-0.68 ± 0.03	35.5 ± 0.7	9.7 ± 0.4	180.0 ± 10.1
0.89	0.35 ± 0.02	31.9 ± 0.4	-0.67 ± 0.05	18.1 ± 0.4	6.9 ± 0.2	162.9 ± 9.7
1.49	0.32 ± 0.03	18.8 ± 0.4	-0.62 ± 0.05	10.3 ± 0.3	4.3 ± 0.2	151.7 ± 11.3

Uncertainties

To estimate the systematic errors introduced in the analyzing power measurement by the uncertainties in the reaction energies and gas leaking effects in the target, SRIM [Zie00] calculations were performed. The systematic errors in the A_{yy} values associated with the uncertainties in the reaction energies are 2.2%, 2.1% and 0.9% for $E_d = 0.52, 0.89$ and

1.49 MeV, respectively. Furthermore, it was found that 5% uncertainty in the gas pressure during a run corresponds to a 0.5% systematic error in the values of A_{yy} obtained in this experiment. Also, the systematic error in the value of $A_{yy}(10^\circ)$ obtained from Bittcher *et al.* [Bit90] corresponds to a 0.5% systematic error in the values of A_{yy} . The systematic error associated with the angular acceptance introduced by the collimators was found to be negligible (less than 0.1%).

Detector position, energy loss in the target and beam motion effects were found to be the main sources of systematic uncertainties involved in the determination of the cross section. The errors in the detector angles were determined, through the peak positions, to be accurate within 0.25° . Based on angular dependence data [Gei99, Bit90, Kie01], the systematic errors associated with the positions of the detectors were found to be 0.9% and 1.1% for $E_d = 0.89$ and 1.49 MeV, respectively. Based on a previous experiment [Gei98], the upper limit to the systematic errors in the cross section values introduced by the uncertainties in the reaction energies is 2%. Horizontal 3 mm beam motion effects were found to introduce a 2.9% systematic uncertainty in the cross section value at $E_d = 0.89$ MeV. The systematic error in the cross section values associated with the angular acceptance introduced by the collimators was found to be negligible.

4.2 Scattering amplitudes

As we saw in section chapter 3, in some cases, when the number of independent polarization observables is sufficient, the experimental data can be used to obtain information about the M-matrix amplitudes. This is the case for the scattering angle $\theta = 0^\circ$, where no preferential transverse direction is defined and \mathbf{M} must be invariant under rotation along the z axis. The two amplitudes (three real numbers) that determine completely the scattering matrix can be calculated from the three measured quantities, $K_y^{y'}$, A_{yy} and the cross section, which are linearly independent observables. From eqs. (3.53-3.55) we can write:

$$|B|^2 = \frac{\sigma(0^\circ)}{3} [1 + 2A_{yy}(0^\circ)] \quad (4.8)$$

$$|F|^2 = \frac{\sigma(0^\circ)}{3} [1 - A_{yy}(0^\circ)] \quad (4.9)$$

$$\phi = \arccos \left[\frac{\sigma(0^\circ) K_y^{y'}(0^\circ)}{2 |B||F|} \right] \quad (4.10)$$

The experimental results obtained in this work, together with recent measurements [Fle02] for the $K_y^{y'}(0^\circ)$ observable, which relates the polarization of the outgoing reactant with the projectile polarization and is defined as

$$K_y^{y'}(0^\circ) = \frac{2 p_Z^{(p)}}{3 p_Z^{(d)}} \quad (4.11)$$

where $p_Z^{(d)}$ and $p_Z^{(p)}$ are the vector polarization of the deuteron beam and outgoing proton respectively, allow the determination of all the scattering matrix elements at $\theta = 0^\circ$. The results are given in Table 4.1.

From the $K_y^{y'}(0^\circ)$ measurements Fletcher *et al.* [Fle02] concluded that the reaction mechanism is dominated by the $\frac{3}{2}^+$ S-wave resonance in ${}^5\text{Li}$ at $E_d = 0.430$ MeV with no sizeable non-resonant contributions at deuteron energies below 1 MeV. In fact, the results are consistent with the predictions of a pure S-wave resonant behavior of $K_y^{y'}(0^\circ) = -\frac{2}{3}$. The same model predicts $iT_{11} = 0$ and $A_{yy} = -\frac{1}{\sqrt{2}}T_{20} - \sqrt{3}T_{22} = 0.5$. Although the measured result for $A_{yy}(0^\circ)$ at $E_d = 0.52$ MeV is consistent with that prediction, at higher energies, $E_d = 0.89$ and 1.49 MeV, the discrepancy is of the order of 30%, suggesting that the reaction mechanism is not purely resonant. This conclusion is also supported by iT_{11} vector analyzing power measurements of Geist *et al.* [Gei98], who obtained positive iT_{11} inconsistent with zero for $E_d < 1$ MeV. These results reveal the importance of negative parity contributions in the entrance channel.

4.3 Conclusions

New measurements of the $A_{yy}(0^\circ)$ and $\sigma(0^\circ)$ observables of the ${}^3\text{He}(d,p){}^4\text{He}$ reaction were taken at $E_d = 0.52, 0.89$ and 1.49 MeV, complementing the existing $K_y^{y'}(0^\circ)$ data at those energies. These measurements allow, for the first time, the determination of all the linearly independent scattering matrix elements at 0° .

In order to calculate the remaining scattering amplitudes necessary to describe the ${}^3\text{He}(d,p){}^4\text{He}$ reaction observables at all angles, and to determine the relative importance of direct and resonant mechanisms, it is necessary to develop a model that extracts this information from the available experimental data. This is the focus of the next chapter.

Chapter 5

Analysis of the ${}^3\text{He}(\text{d,p}){}^4\text{He}$ reaction

In this chapter we analyze the experimental results obtained in the previous chapter along with vector and tensor analyzing powers, total and differential cross sections [Gei98], polarization transfer [Fle02], and elastic differential cross section data [Jen79] for the ${}^3\text{He}(\text{d,p}){}^4\text{He}$ reaction in the energy range $E_d < 1$ MeV. We start with the assumption of a reaction mechanism dominated by the broad $J^\pi = \frac{3}{2}^+$ S-wave resonance in ${}^5\text{Li}$ at $E_d = 0.430$ MeV, and analyze the rank zero observables with DWBA, coupled channels, and a phenomenological R-matrix model, comparing the three approaches. We then introduce the iT_{11} , T_{2q} and $K_y'(0^\circ)$ data and analyze the complete set of experimental results with the coupled channels and the phenomenological R-matrix models. The prediction of these models for the vector analyzing power observable, iT_{11} , leads to the introduction of negative parity contributions to the reaction mechanism and motivates the adoption of a hybrid R-matrix+potential model.

5.1 Analysis of the rank zero observables

In this section we focus on the analysis of rank zero observables of the ${}^3\text{He}(\text{d,p}){}^4\text{He}$, total and differential reaction cross section, and elastic differential cross section. We analyze the data with three distinct approaches: DWBA, coupled channels, and a phenomenological R-matrix model. These calculations include the effect of the dominant $J^\pi = \frac{3}{2}^+$ resonance only, corresponding to matrix elements M_3 – M_5 of Table 3.1.

5.1.1 DWBA and coupled channels analysis

The DWBA and the coupled channels analysis were performed with the code FRESKO developed by Ian Thompson [Tho88] and upgraded with χ^2 minimization using the MINUIT routine [Jam94], SFRESKO [Tho04]. The results are shown in Figures 5.1–5.2.

The coupled channels calculation is done in the post form, which corresponds to solving eq. (1.8). The transfer coupling necessary for the analysis of the ${}^3\text{He}(\text{d},\text{p}){}^4\text{He}$ is introduced in appendix C, and the post form of the coupling interaction corresponds to eq. (C.3). The potentials used are the following: the entrance channel, $U_i(R_i)$ in the notation of appendix C, is a sum of a central Woods-Saxon potential with projectile and target spin-orbit, and spin-spin terms; the p - n potential that binds the projectile (deuteron) in the initial state, $V_{(L'_i s)j'_i}(\mathbf{r}_i)$, is a Reid soft-core potential [Rei68]; the ${}^4\text{He}$ - p exit channel potential is the sum of a Woods-Saxon potential with a target spin-orbit term; and the ${}^3\text{He}$ - p “core-core” potential used in the calculation is chosen to be the same as the exit channel potential. The parameters of the entrance channel potential are left as adjustable parameters in the calculation; the values obtained from the analysis are shown in Table 5.1.

Whereas in the coupled channels calculation the effective imaginary potential is obtained exactly from the transfer couplings, in DWBA analysis the imaginary potential that accounts for the loss of flux from the elastic channel is fitted by the search procedure. In this analysis we choose to fit only the depth of the imaginary potential. The parameters of the entrance channel potential obtained from the fit, including the imaginary potential, iW , are shown in Table 5.1. The expected value of the spectroscopic amplitude is $\sqrt{CS^2} = \sqrt{2}$ (two ways of removing a neutron from the alpha particle), however the values in this work were 1.52 and 1.99 for the DWBA and coupled channels analysis, respectively.

model	potential	depth	radius	diffuseness
DWBA	V	87.9	1.23	0.25
	iW	4.4	0.70	0.40
	VSO _P	0.1	0.4	0.01
	VSO _T	14.0	1.90	0.95
	V _{SS}	9.7	2.58	0.97
CC	V	72.5	1.01	0.09
	VSO _P	6.2	0.73	0.09
	VSO _T	12.0	1.90	0.90
	V _{SS}	11.7	2.91	0.98

Table 5.1: Potential parameters obtained from DWBA and coupled channels fits to the ${}^3\text{He}(\text{d},\text{p}){}^4\text{He}$ rank zero observables. The values of the spectroscopic factor obtained from the DWBA and coupled channels analysis were 1.52 and 1.99 respectively.

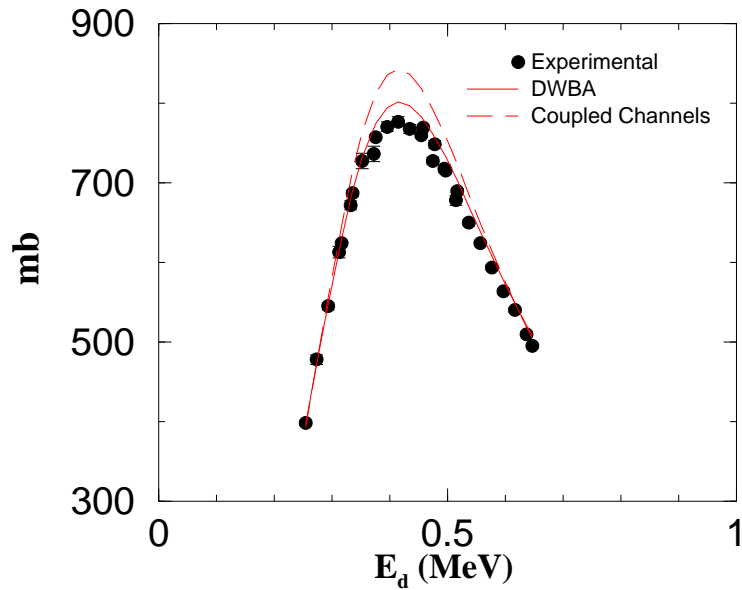


Figure 5.1: Results of the fits to ${}^3\text{He}(d,p){}^4\text{He}$ total reaction cross section data of Geist *et al.* [Gei98] with DWBA and coupled channels fits, where S- and D-wave contributions to the $\frac{3}{2}^+$ resonance are considered.

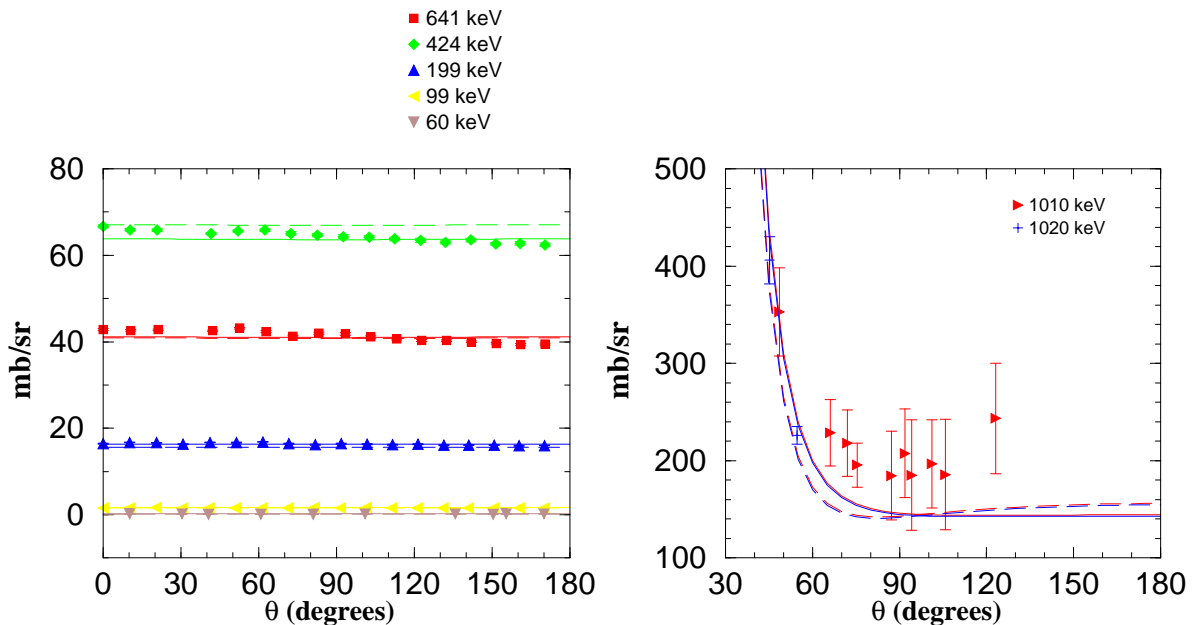


Figure 5.2: Results of the fits to ${}^3\text{He}(d,p){}^4\text{He}$ differential elastic (right) and reaction cross section (left) data [Gei98, Jen79] with DWBA (full curves) and coupled channels (dashed curves) models, where S- and D-wave contributions to the $\frac{3}{2}^+$ resonance are considered.

5.1.2 Phenomenological R-matrix analysis

The code SFRESCO [Tho04] was updated to include the capability to perform two-channels multilevel R-matrix analysis, explained in detail in chapter 2 and appendix B. In this analysis the rank zero observables were studied with a simple two-channels 1-level model, where the energy of the R-matrix pole, the S-wave contribution to the $J^\pi = \frac{3}{2}^+$ resonance, and the exit channel width were all fitted to the experimental data. The channel radius was set to $a = 5$ fm.

The results for the total and differential reaction cross section and elastic differential cross section are shown in Figures 5.3 and 5.4. The resonance parameters obtained from this analysis are: $E_d=0.186$ MeV, $\gamma_d^{(0)}=0.407$ MeV $^{\frac{1}{2}}$ and $\gamma_p^{(2)}=0.208$ MeV $^{\frac{1}{2}}$ (corresponding to observed $\Gamma_d^{(0)}=0.009$ MeV and $\Gamma_p^{(2)}=0.361$ MeV, obtained from eq. (2.32)), where the superscripts (0) and (2) indicate the partial wave to which the widths refer to, S- and D-wave, respectively. The values obtained from the compilation of Tilley *et al.* [Til02] are $E_d=0.23$ MeV, $\Gamma_d=0.134$ MeV and $\Gamma_p=0.055$ MeV, where the particle widths are defined by (2.31). These are significantly different from the values obtained in this work, but this much is expected since the values of this compilation are obtained with a much larger set of levels and more partial waves (the total width, Γ is simply the sum of partial widths $\Gamma = \sum_i \Gamma^{(i)}$). The agreement is expected to improve when we extend the analysis to the inclusion of the remaining observables.

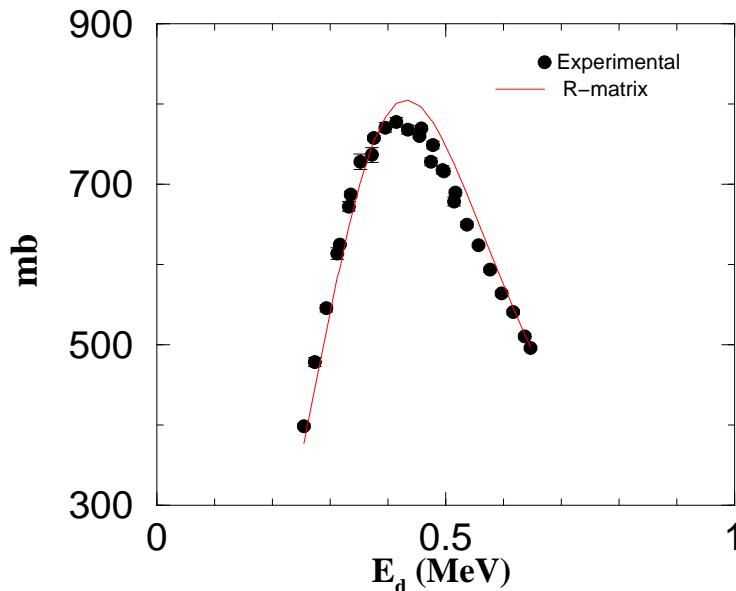


Figure 5.3: Results of the fits to ${}^3\text{He}(\text{d,p}){}^4\text{He}$ total reaction cross section data of Geist *et al.* [Gei98] with the R-matrix model where S- and D-wave contributions to the $\frac{3}{2}^+$ resonance are considered.

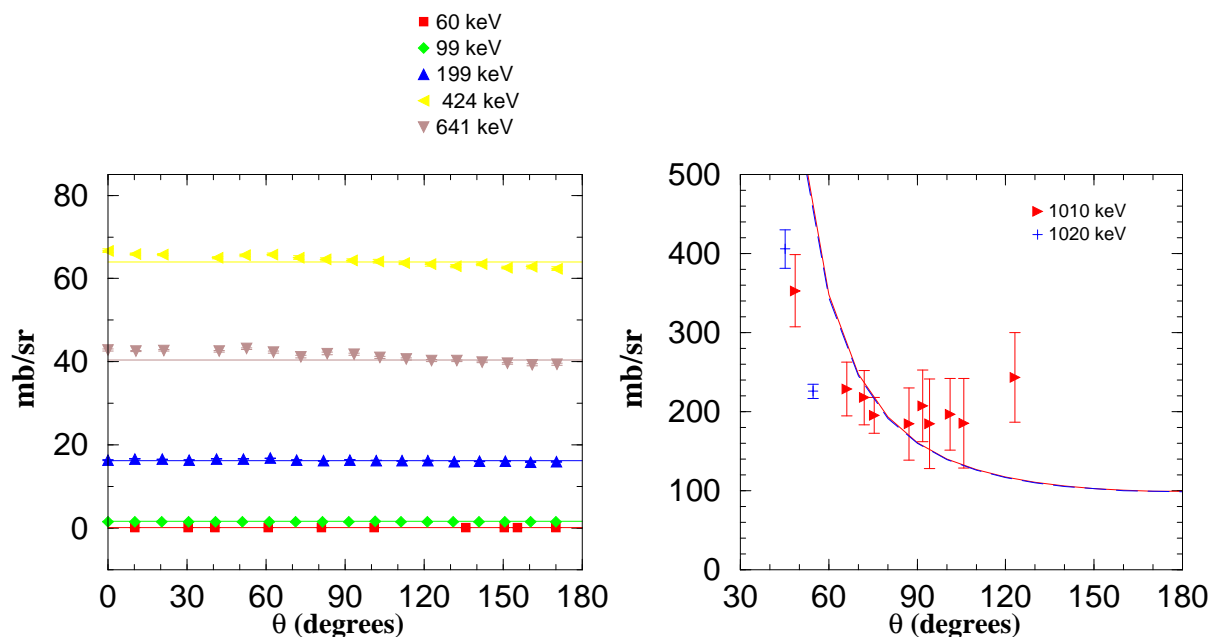


Figure 5.4: Results of the fits to ${}^3\text{He}(d,p){}^4\text{He}$ differential elastic (right) and reaction cross section (left) data [Gei98, Jen79] with R–matrix model, where only the S–wave contribution to the $\frac{3}{2}^+$ resonance is considered.

5.2 Analysis of rank zero, iT_{11} and T_{2q} observables

In this section we include the polarization observables iT_{11} and T_{2q} in the previous analysis. We study this set of observables with a coupled channels and a phenomenological R–matrix model.

5.2.1 Phenomenological R-matrix analysis

An R-matrix analysis where only a $\frac{3}{2}^+$ S-wave resonance is considered, like the one shown in the previous section, predicts values for tensor analyzing powers and $K_y^{y'}$ in good agreement with most of the measured data [Gei98, Fle02]. However, in this simplified model iT_{11} is zero, as shown in Figure 5.5, in clear disagreement with the measurements of Geist *et al.* [Gei98]. The resonance parameters obtained from this analysis (analysis I) are given in table 5.2.

Although the dominant mechanism of the reaction is clearly resonant, being well described by an R–matrix procedure, positive vector analyzing power data are a clear signature of other competing processes, namely those related to odd partial waves. Indeed, the addition of other positive parity contributions in the form D–wave components

in the $\frac{3}{2}^+$ resonance, as reference in the Table 3.1, or background terms, do not improve the fit significantly or the description of the $i\text{T}_{11}$ observable. The results from this analysis (analysis II) for the $i\text{T}_{11}$ observable are shown in Figure 5.6, and the corresponding parameters for the $\frac{3}{2}^+$ resonance and background terms are given in table 5.2.

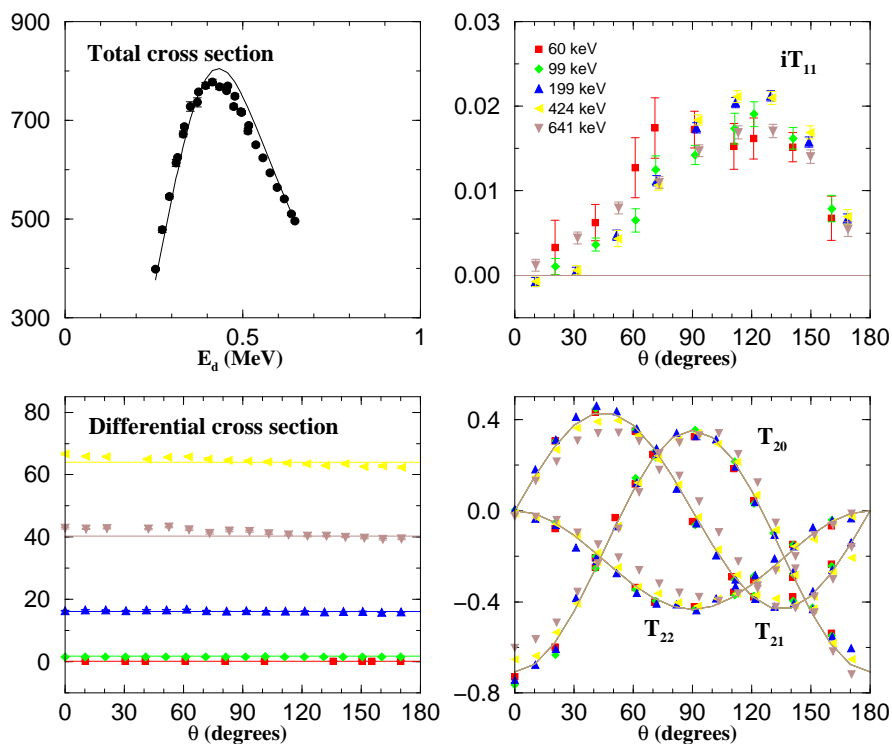


Figure 5.5: R–matrix results with a $\frac{3}{2}^+$ S–wave resonance only for $i\text{T}_{11}$, T_{2q} , differential and total cross section measurements of Geist *et al.* [Gei98].

analysis	states	Energy (MeV)	$\gamma_d^{(0)}$ ($\text{MeV}^{\frac{1}{2}}$)	$\gamma_d^{(2)}$ ($\text{MeV}^{\frac{1}{2}}$)	$\gamma_p^{(2)}$ ($\text{MeV}^{\frac{1}{2}}$)
I	$\frac{3}{2}^+$	0.19	0.407		0.209
II	$\frac{3}{2}^+$	0.20	0.435		0.216
	$\frac{3}{2}^+$	5.0	0.994	0.065	0.279

Table 5.2: Resonance parameters obtained from R–matrix analysis of rank zero, $i\text{T}_{11}$ and T_{2q} observables. The width $\gamma_d^{(2)}$ refers to the coupling $\{(L = 2, S_p = 1)j = 2, S_t = \frac{1}{2}\}$ in the jj coupling scheme used by SFRESCO.

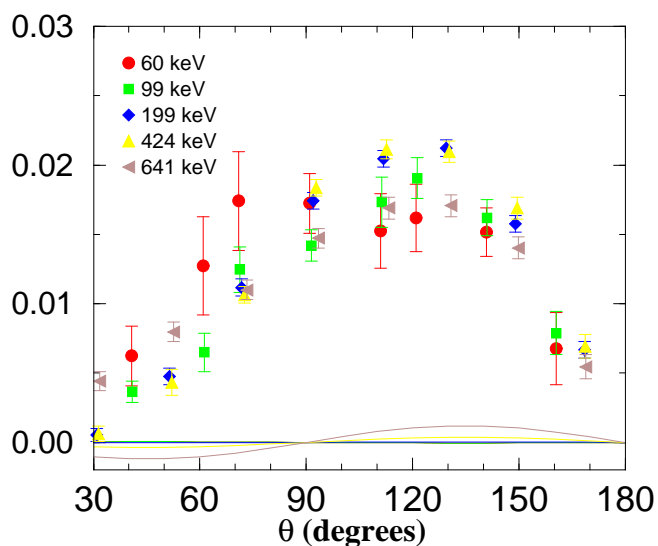


Figure 5.6: R–matrix results with S– and D–wave contributions to the $\frac{3}{2}^+$ resonance and a $\frac{3}{2}^+$ background term for the iT_{11} observable.

5.2.2 Coupled channels analysis

The extension of the coupled channels analysis described previously to include the polarization observables faces similar problems. The description of the zero and rank two observables is reasonable with the assumption of a dominant $\frac{3}{2}^+$ S–wave mechanism where D–waves are included, which improves the quality of the fit. However, the magnitude obtained for the iT_{11} observable does not match the measured results of Geist *et al.* [Gei98], as shown in Figure 5.7. As before, the parameters of the entrance channel potential were fitted to the experimental data and the resulting values are given in Table 5.3. The spin-orbit forces are significantly different from the ones of table 5.1, but we should note that we consider in this analysis a much larger set of observables.

model	potential	depth	radius	diffuseness
CC	V	72.6	1.01	0.09
	VSO _P	31.0	2.10	0.90
	VSO _T	0.1	0.50	0.10
	V _{SS}	11.7	2.91	0.99

Table 5.3: Potential parameters obtained from coupled channels analysis of rank zero, iT_{11} and T_{2q} observables of the ${}^3\text{He}(d,p){}^4\text{He}$ reaction. The value of the spectroscopic factor obtained from the analysis was 1.99.

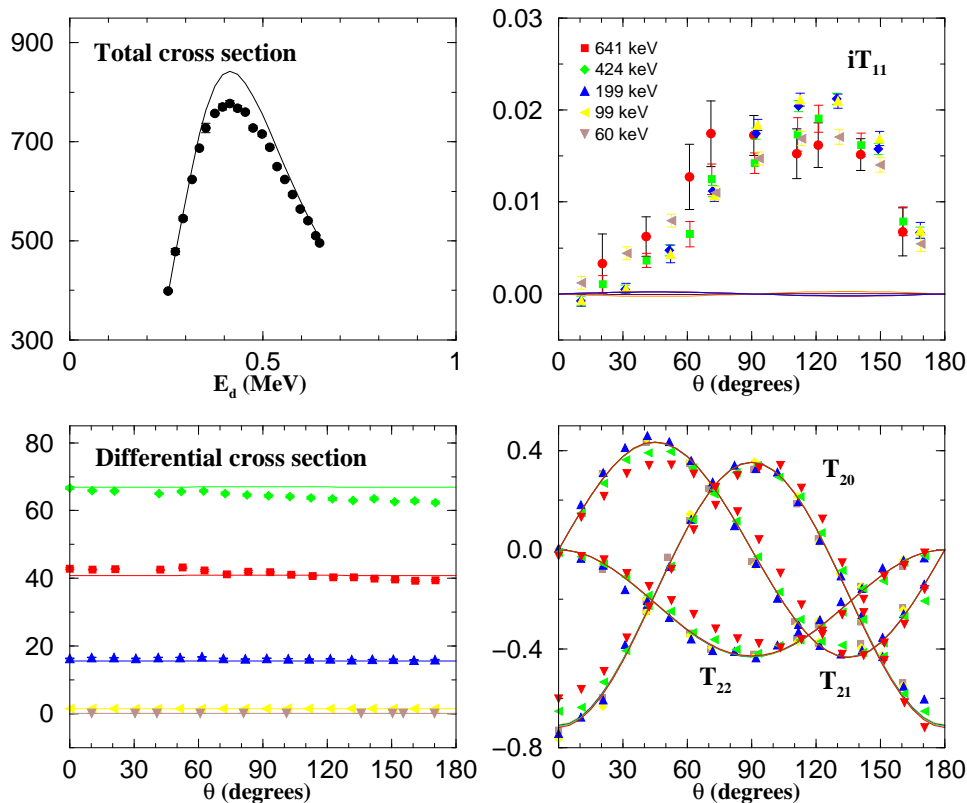


Figure 5.7: Results with a coupled channels fit, with S- and D-wave contributions to the $\frac{3}{2}^+$ resonance, to iT_{11} , T_{2q} , differential and total cross section measurements of Geist *et al.* [Gei98].

5.2.3 Introduction of negative parity contributions

The previous analysis shows the deviations from expected S-wave resonant behavior in the recent measurements of Geist *et al.* [Gei98]. These discrepancies may be due to $L > 0$ contributions to the reaction mechanism arising from direct transfer processes or tails of distant resonances. However, the study of the the iT_{11} observable demonstrates that D-wave contributions do not improve significantly the description of the iT_{11} observable.

We therefore expand the previous analysis with the inclusion of $\frac{3}{2}^-$ and $\frac{1}{2}^-$ negative parity contributions, corresponding to the matrix elements T_9 – T_{11} of Table 3.2. Indeed, the next excited state in the energy level diagram of ${}^5\text{Li}$ is the $\frac{3}{2}^-$ state at $E_d = 2.62$ MeV [Til02]. However, the inclusion of this contribution in the phenomenological R-matrix approach needs to be carefully considered, since adding terms in the R-matrix without being supported by experimental data amounts simply to the inclusion of a background term. We therefore include these two contributions in the R-matrix analysis through background terms outside the range of energies considered in the study.

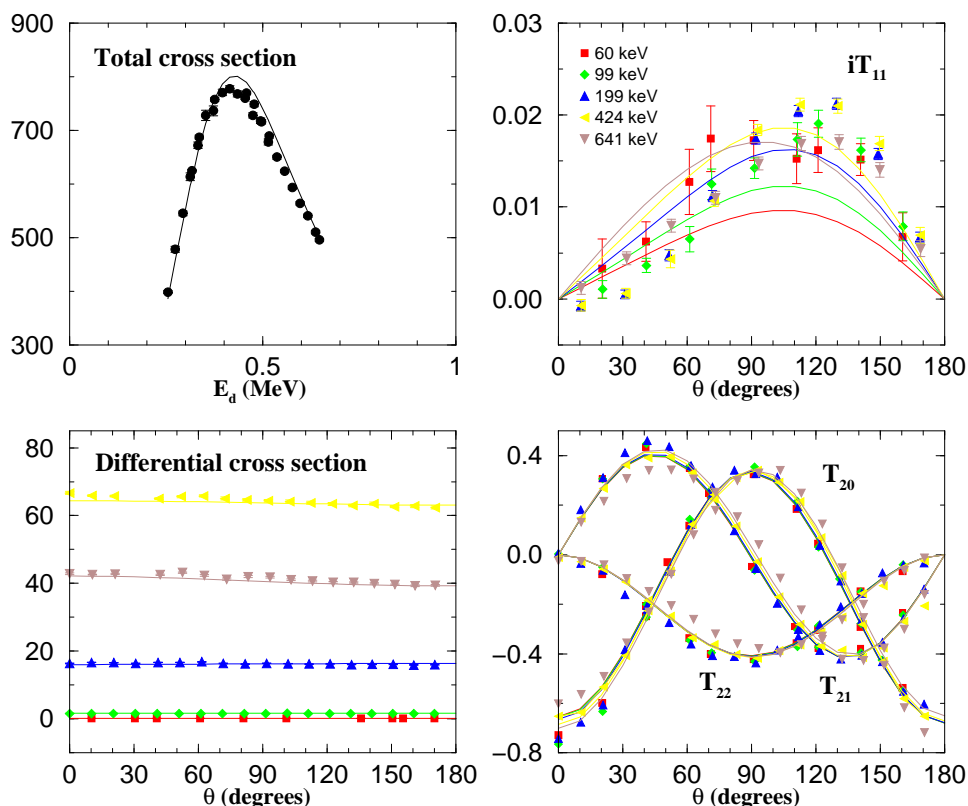


Figure 5.8: Results with a pure R-matrix fit with a $\frac{3}{2}^+$ S-wave resonance, the $\frac{3}{2}^-$ state at $E_d = 2.62$ MeV and a $\frac{1}{2}^-$ background term for iT_{11} , T_{2q} , differential and total cross section measurements of Geist *et al.* [Gei98].

The results obtained with the R-matrix fit with the $\frac{3}{2}^+$ resonance, and the $\frac{3}{2}^-$ and $\frac{1}{2}^-$ background contributions, are shown in Figure 5.8. The T_{2q} and rank zero observables are still well described, but the predictions for iT_{11} , although non-zero, do not reproduce the angular dependence of the data. This behavior however, indicates the strong sensitivity of this observable to negative parity contributions to the reaction mechanism. The parameters obtained from this analysis are shown in table 5.4

The inclusion of the $\frac{3}{2}^-$ and $\frac{1}{2}^-$ negative parity contributions in the coupled channels formalism requires the solution of the coupled equations through the R-matrix basis. Only in this approach are we able to remove the contribution from couplings to the $\frac{1}{2}^+$ state that is naturally included with the $\frac{1}{2}^-$ contribution. We start by determining the number of basis states necessary for this method to converge to the iterative method used in the previous analysis. We find that for a channel radius of $a=20$ fm, 20 basis states are required for the convergence between the two methods. The results obtained with the coupled channels analysis, where $\frac{3}{2}^+$, $\frac{3}{2}^-$ and $\frac{1}{2}^-$ contributions to the reaction mechanism are considered, of the rank zero, iT_{11} and T_{2q} observables are shown in Figure 5.9. The entrance channel parameters obtained from this analysis are given in table 5.5.

states	Energy (MeV)	$\gamma_d^{(0)}$ ($\text{MeV}^{\frac{1}{2}}$)	$\gamma_d^{(1)}$ ($\text{MeV}^{\frac{1}{2}}$)	$\gamma_d^{(1)}$ ($\text{MeV}^{\frac{1}{2}}$)	$\gamma_p^{(2)}$ ($\text{MeV}^{\frac{1}{2}}$)	$\gamma_p^{(1)}$ ($\text{MeV}^{\frac{1}{2}}$)
$\frac{3}{2}^+$	0.19	0.407			0.209	
$\frac{3}{2}^-$	2.6		-0.951 ^{*1}	0.500 ^{*3}		-0.001
$\frac{1}{2}^-$	5.0		-0.871 ^{*2}			0.131

Table 5.4: Parameters from the R–matrix analysis of rank zero, iT_{11} and T_{2q} observables, for the $\frac{3}{2}^+$ resonance and the negative parity background terms where ^{*1} indicates coupling to $j=1$, ^{*2} coupling to $j=0$, and ^{*3} coupling to $j=2$, in the jj coupling scheme.

These results demonstrate that we are unable in the coupled channels approach to describe the magnitude and the angular dependence of the iT_{11} observable. Moreover, the inclusion of the negative parity states worsens the description of the other observables considered in the analysis.

Conclusions and motivation for an hybrid approach

The analysis presented in this section demonstrates the importance of $L > 0$ contributions, namely those related to odd partial waves, to the reaction mechanism arising from direct transfer processes or from tails of distant resonances. In particular, the inclusion of P–wave contributions in the phenomenological R–matrix analysis indicates the strong sensitivity of the iT_{11} observable to negative parity contributions to the reaction mechanism. We are however unable to reproduce the angular dependence of the data.

In the coupled channels analysis, the inclusion of $\frac{1}{2}^-$ and $\frac{3}{2}^-$ contributions does not improve significantly the description of the iT_{11} observable, and significantly worsens the description of the other observables. An alternative approach needs therefore to be considered for the analysis of the ${}^3\text{He}(\text{d,p}){}^4\text{He}$ reaction. Given the way the phenomenological R–matrix deals with the resonant contributions, and the capability of the coupled channels model to calculate explicitly the direct contributions to the reaction mechanism, it is natural to consider a hybrid R–matrix + potential analysis of the ${}^3\text{He}(\text{d,p}){}^4\text{He}$ reaction.

model	potential	depth	radius	diffuseness
CC	V	72.5	1.02	0.09
(R–matrix basis)	V_{SO_P}	30.0	2.00	0.80
	V_{SO_T}	0.1	0.50	0.10
	V_{SS}	11.7	2.91	0.98

Table 5.5: Potential parameters obtained from coupled channels analysis of rank zero, iT_{11} and T_{2q} observables of the ${}^3\text{He}(\text{d,p}){}^4\text{He}$ reaction. The value of the spectroscopic factor obtained from the analysis was 1.93.

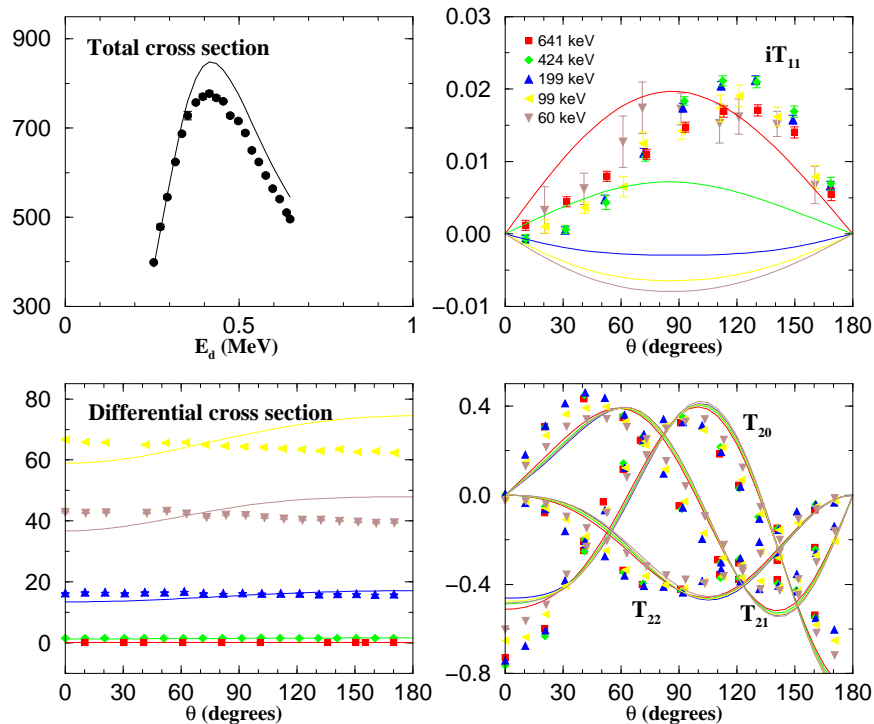


Figure 5.9: Results with a pure R-matrix fit with a $\frac{3}{2}^+$ S-wave resonance, the $\frac{3}{2}^-$ state at $E_d = 2.62$ MeV and a $\frac{1}{2}^-$ background term for iT_{11} , T_{2q} , differential and total cross section measurements of Geist *et al.* [Gei98].

5.3 Study of the ${}^3\text{He}(d,p){}^4\text{He}$ with the hybrid model

The inclusion of negative parity contributions in the R-matrix framework has been done before [Til02] and resulted in very large widths, with very large error bars, which are essential to obtain the correct magnitude of the iT_{11} observable. It is reasonable to assume however, based on the analysis of the previous section and the energy level diagram of Tilley *et al.* [Til02] that these negative parity contributions arise essentially from a direct mechanism.

To account for these negative parity contributions we develop a model that takes into consideration the direct component of the reaction through a potential description [Bra04], while the resonant contributions to the reaction mechanism are described in an R-matrix framework. This hybrid model, allows the combination of important features of the R-matrix theory (the ability to include a large number of states in the analysis) and the coupled channels model (the capacity to treat the direct contribution explicitly).

In the analysis presented here, we introduce the new measurements obtained in chapter 5 of $A_{yy}(0^\circ)$ and $\sigma(0^\circ)$, and the recent $K_y^y(0^\circ)$ measurements of Fletcher *et al.* [Fle02], along with the set of observables studied before (rank zero, iT_{11} and T_{2q} observables).

In the hybrid model, the dominant $J^\pi = \frac{3}{2}^+$ resonance is introduced through an R-matrix pole, and all the negative parity contributions to the reaction mechanism are obtained through a fitted potential. To improve the quality of the fits we also include $\frac{1}{2}^+$, $\frac{3}{2}^+$ and $\frac{5}{2}^+$ background poles at energies above $E_d = 3$ MeV. The results of this model for the iT_{11} observable at the energy closest to the $\frac{3}{2}^+$ resonance are shown in Figure 5.10.

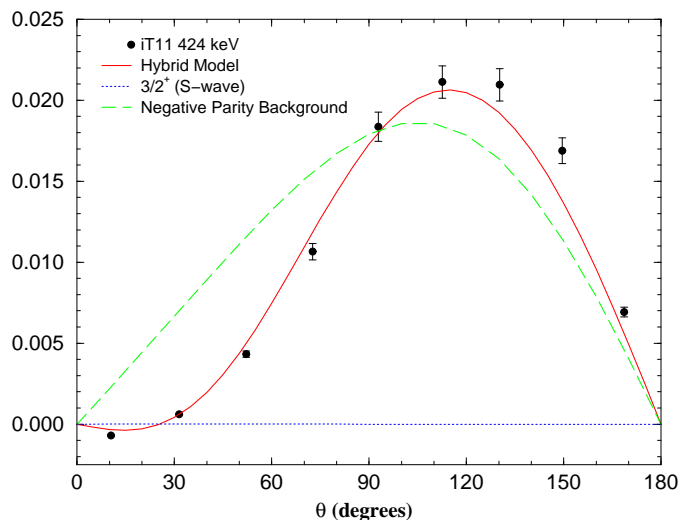


Figure 5.10: Comparison between the hybrid model results for the iT_{11} observable at $E_d=424$ keV and the results obtain with previous R–matrix fits which included the $J^\pi = \frac{3}{2}^+$ S–wave resonance only and a combination of this resonance with negative parity contributions from $\frac{1}{2}^-$ and $\frac{3}{2}^-$ states.

The improvement in terms of the description of the iT_{11} observable is significant. With this hybrid R-matrix + potential model we are also able to describe successfully [Bra03] the vector and tensor analyzing powers, and the total and differential cross section data for the ${}^3\text{He}(\text{d,p}){}^4\text{He}$ reaction at the whole energy range measured by Geist *et al.* [Gei98]. The results obtained for all these observables are shown in Figure 5.11. The parameters obtained from this fit are given in tables 5.6 and 5.7.

model	potential	depth	radius	diffuseness
CC	V	60.0	0.87	0.61
(R–matrix basis)	V_{SO_P}	0.68	0.53	0.04
	V_{SO_T}	0.04	0.50	0.10
	V_{SS}	13.0	2.00	1.05

Table 5.6: Potential parameters obtained from the hybrid analysis to rank zero, iT_{11} , T_{2q} and polarization transfer observables of the ${}^3\text{He}(\text{d,p}){}^4\text{He}$ reaction. The value of the spectroscopic factor obtained from the analysis was 0.87.

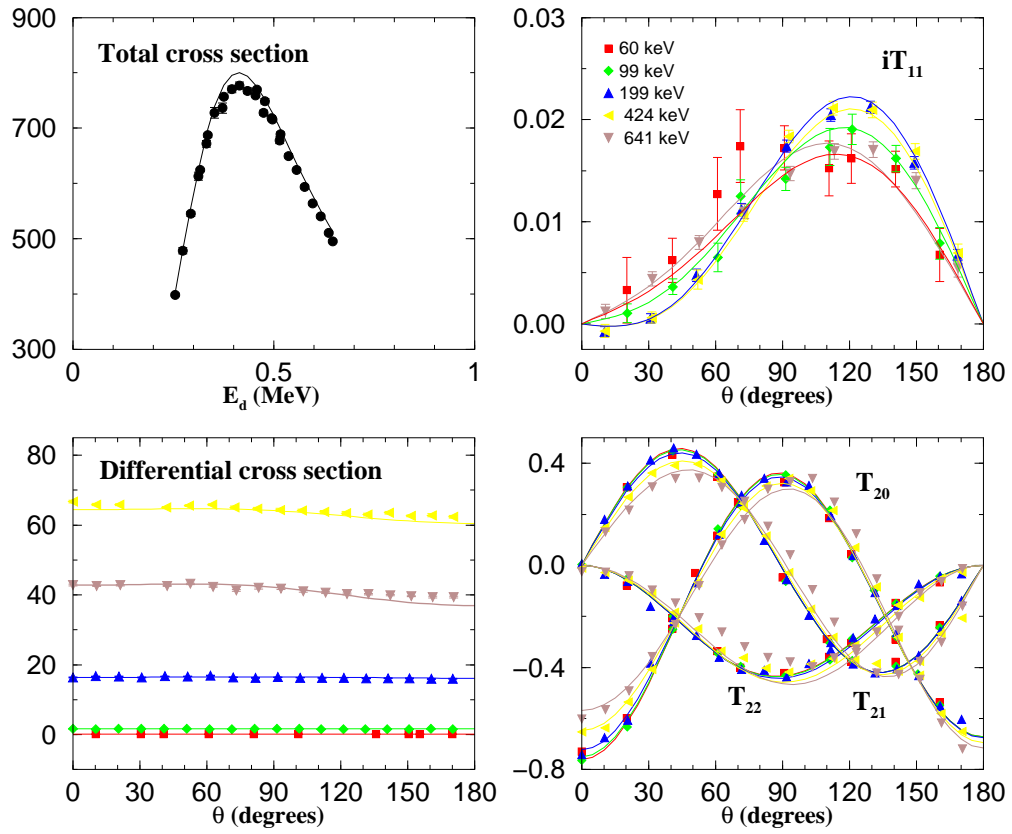


Figure 5.11: Hybrid model angular distributions for iT_{11} , T_{2q} differential and total cross section measurements of Geist *et al.* [Gei98].

states	Energy (MeV)	$\gamma_d^{(0)}$ ($\text{MeV}^{\frac{1}{2}}$)	$\gamma_d^{(2)}$ ($\text{MeV}^{\frac{1}{2}}$)	$\gamma_d^{(2)}$ ($\text{MeV}^{\frac{1}{2}}$)	$\gamma_p^{(2)}$ ($\text{MeV}^{\frac{1}{2}}$)	$\gamma_p^{(0)}$ ($\text{MeV}^{\frac{1}{2}}$)
$\frac{3}{2}^+$	0.24	-0.334			0.043	
$\frac{1}{2}^+$	3.0	0.053	-2.052			-0.040
$\frac{3}{2}^+$	3.0	-0.817	0.071 ^{*1}	-0.154 ^{*3}	-0.057	
$\frac{5}{2}^+$	4.0		5.931 ^{*2}		0.145	

Table 5.7: Parameters obtained from the hybrid analysis to rank zero, iT_{11} , T_{2q} and polarization transfer observables of the ${}^3\text{He}(d,p){}^4\text{He}$ reaction, where ^{*1} indicates coupling to $j=1$, ^{*2} coupling to $j=2$, and ^{*3} coupling to $j=2$, in the jj coupling scheme.

The predictions of this model for the energy dependence of $A_{yy}(0^\circ)$, $\sigma(0^\circ)$ and $K_y^{y'}(0^\circ)$, shown in Figure 5.12, are also in good agreement with the experimental data. The hybrid model results for $K_y^{y'}(0^\circ)$ are -0.69 and -0.68 for 0.52 and 0.89 MeV respectively, in excellent agreement with the measurements of reference [Fle02]. It is known [San74] that if the reaction proceeds by a direct mechanism and only the S-state of the deuteron is considered, $K_y^{y'}(0^\circ) = +\frac{2}{3}$. The inclusion of the deuteron D-state lowers this result, but it will still be positive. This feature is clearly seen in the data shown in reference [Fle02] in the energy region where the direct process dominates. The results obtained for the spin transfer coefficient with this model are therefore particularly interesting because they allow us to conclude that values of $K_y^{y'}(0^\circ)$ close to $-\frac{2}{3}$ can still be consistent with a mixed mechanism of the reaction. Furthermore, the strong sensitivity of this observable to the direct mechanism sets a limit on the amount of mixing.

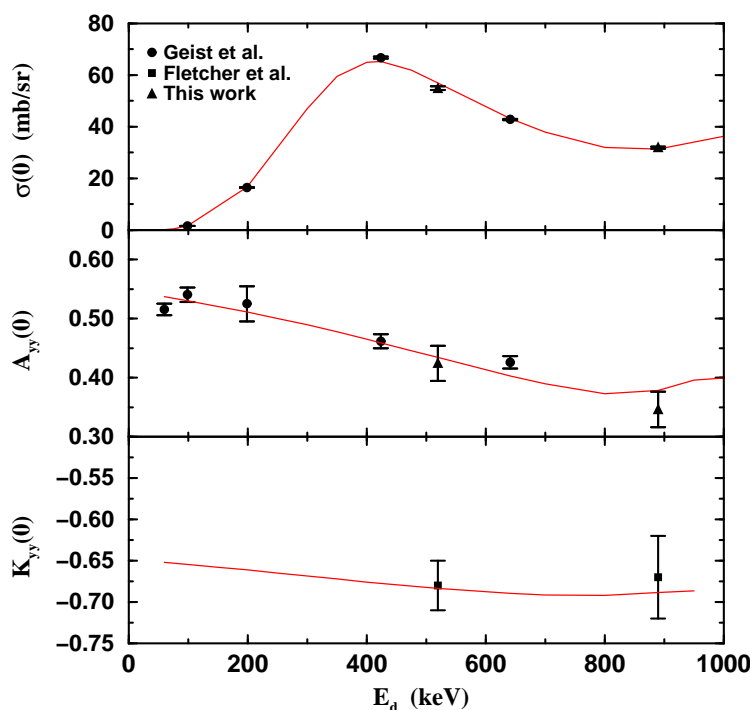


Figure 5.12: Hybrid model results for the energy dependence of $A_{yy}(0^\circ)$, $\sigma(0^\circ)$ and $K_y^{y'}(0^\circ)$.

This analysis indicates that direct process contributions to the reaction mechanism should not be neglected as they compete with the resonant mechanism through P and F-waves in the entrance channel [Bra03], accounting for up to 15% of the total cross section in the energy range below 1 MeV.

5.4 Conclusions

In this chapter we applied the phenomenological R–matrix model and the coupled channels model to the analysis of the ${}^3\text{He}(\text{d,p}){}^4\text{He}$ reaction. These analyses show the importance of $L > 0$ contributions, namely those related to odd partial waves, to the reaction mechanism arising from direct transfer processes or tails of distant resonances.

Faced with the problems of the description of the $i\text{T}_{11}$ observable, which is strongly sensitive to P–wave contributions in the entrance channel, we adopted a hybrid treatment of the ${}^3\text{He}(\text{d,p}){}^4\text{He}$ reaction mechanism.

With this R–matrix + potential model, that accounts for both resonant and direct mechanisms by combining R-matrix poles and a potential description, we were able to successfully describe the rank zero, $i\text{T}_{11}$, T_{2q} and $\text{K}_y^{\prime}(0^\circ)$ reaction observables. The parameters for the dominant $\frac{3}{2}^+$ resonance obtained by the hybrid analysis were $E_d = 0.24$ MeV, $\gamma_d^{(0)} = -0.334$ MeV $^{\frac{1}{2}}$ and $\gamma_p^{(2)} = 0.043$, which correspond to observed widths of $\Gamma_d^{(0)} = 0.209$ MeV and $\Gamma_p^{(2)} = 0.046$ MeV, obtained from eq. (2.32). These values are very close to the ones quoted by Tilley *et al.* [Til02] ($E_d = 0.23$ MeV, $\Gamma_d = 0.134$ MeV and $\Gamma_p = 0.055$ MeV)

We conclude that a consistent description of the different polarization observables, vector and tensor analyzing powers, and spin transfer coefficients can be achieved by assuming that the reaction proceeds by a mixed mechanism where the dominant resonant component competes with a non negligible direct component.

Part IV

Photonuclear couplings

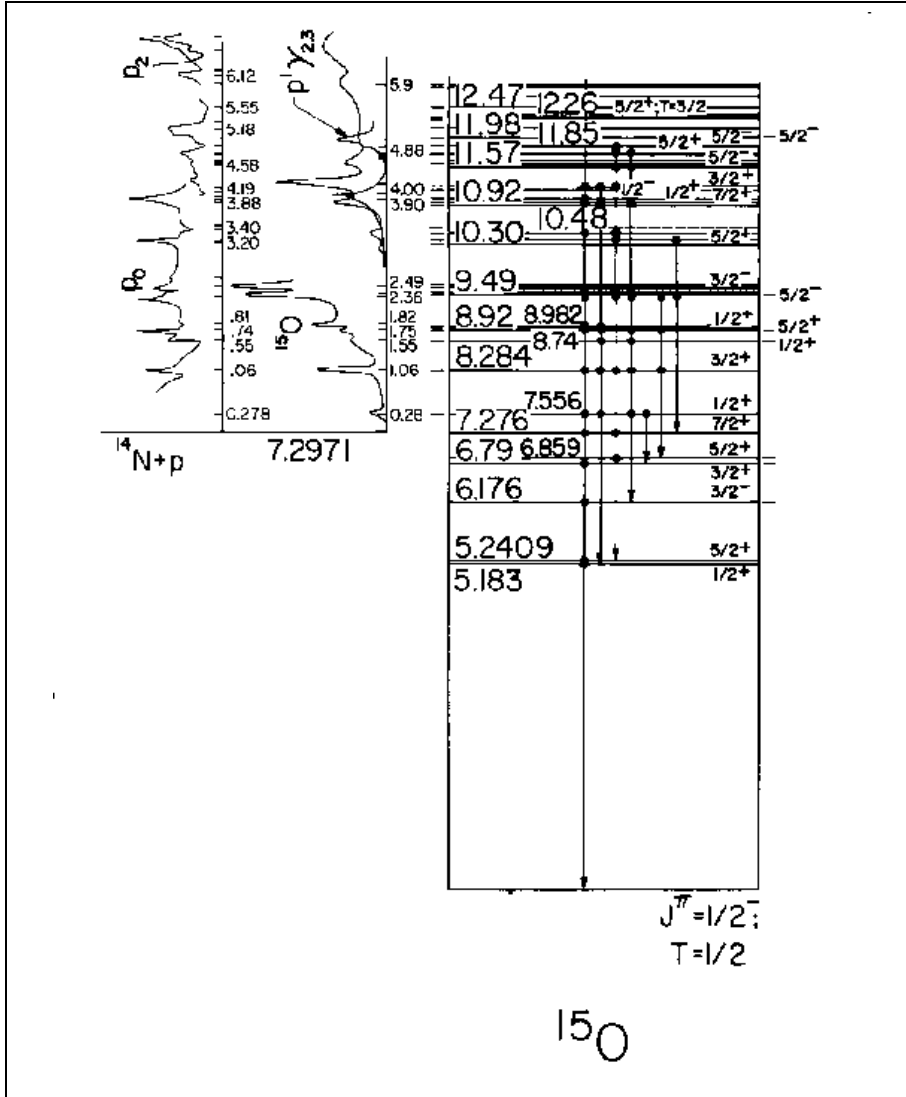
Chapter 6

R–matrix analysis of the $^{14}\text{N}(p, \gamma)^{15}\text{O}$ reaction

The $^{14}\text{N}(p, \gamma)^{15}\text{O}$ is the slowest reaction in the CN cycles and as such plays a crucial role in the energy production of main sequence stars. However, as most other reactions relevant to astrophysics, the reaction cross section in the Gamow window cannot be determined experimentally and has to be obtained from extrapolation of experimental data.

Presently the main set of experimental data published on this reaction is the work of Schröder *et al.* [Sch87]. In this work, the transitions to the $\frac{1}{2}^-$ ground state, the $\frac{3}{2}^-$ state at $E_x=6.18$ MeV, and the $\frac{3}{2}^+$ state at $E_x=6.79$ MeV were found to yield the main contributions (more than 95%) to the astrophysical S-factor (see Figure 6.1 for the level diagram of ^{15}O). Using a Breit–Wigner fit, with the direct contribution calculated explicitly from a Woods–Saxon potential, these authors obtained an astrophysical S-factor of $S(0)=3.10\pm 0.34$ keV.b.

In a recent work, Angulo and Descouvemont [Ang01] reanalyzed the Schröder data using an R–matrix model, and calculating explicitly the external contribution to the reaction mechanism and the asymptotic normalization constant. In this work they obtained an astrophysical S–factor of $S(0)=1.77\pm 0.20$ keV.b. This significant discrepancy with respect to previous results has been the reason for most of the recent work on this reaction, including the two experiments under way at the Triangle Universities Nuclear Laboratories (USA) and the LUNA collaboration [LUN04]. These experiments focus on the energy range below $E_x < 0.2$ MeV and the results are expected to reduced significantly the level of uncertainty of the $^{14}\text{N}(p, \gamma)^{15}\text{O}$ S-factor at astrophysical energies. They should not, however, make the need for the extrapolation of experimental data to the Gamow peak redundant, and this is one of the reasons for the study presented in this chapter.

Figure 6.1: Energy level diagram for ^{15}O .

6.1 R-matrix analysis

In this section we consider the data of Schröder *et al.* [Sch87] for transitions to the $\frac{1}{2}^-$ ground state of ^{15}O , the $\frac{3}{2}^-$ state at $E_x=6.18$ MeV, and the $\frac{3}{2}^+$ state at $E_x=6.79$ MeV. We analyze these data in the framework of the phenomenological R-matrix theory described in chapter 2, examining the contributions to the transition amplitudes from the $\frac{3}{2}^+$ and $\frac{1}{2}^+$ states of ^{15}O at (figure 6.1 for the energy level diagram) $E = -0.504$, 0.985 and 2.187 MeV (not shown explicitly in the diagram) and $E = 0.259$ and 1.446 MeV, respectively.

The spin and parity of the target and projectile ground states are $S_t^\pi = 1^+$ and $S_p^\pi = \frac{1}{2}^+$, respectively, which correspond to a channel spin of $S^\pi = \frac{1}{2}^+$ or $\frac{3}{2}^+$. The reaction mechanism for the transition to the $\frac{1}{2}^-$ ground state and the $\frac{3}{2}^-$ state at $E_x=6.18$ MeV is therefore dominated by the E1 process corresponding to S –wave radiative capture.

For transitions to the $\frac{3}{2}^+$ state at $E_x=6.79$ MeV the reaction mechanism is dominated by the E2 process corresponding also to S –wave radiative capture (possible M1 contributions are not considered in this work). However, E1 process contributions arising from direct capture (DC) or low energy tails of high lying $\frac{1}{2}^-$, $\frac{3}{2}^-$ or $\frac{5}{2}^-$ resonances may contribute through P –wave radiative capture.

6.1.1 Radiative capture cross section in the R–matrix formalism

In the case of radiative capture cross section, $\sigma_{p\gamma}$, one can remove the sum over S' of eq. (2.30) and write:

$$\sigma_{p\gamma} = \frac{\pi}{k_p^2} \sum_{JSL L'} g_J \left| \frac{\sum_{\lambda} \frac{(\tilde{\Gamma}_{\lambda p} \tilde{\Gamma}_{\lambda \gamma})^{\frac{1}{2}}}{E_{\lambda} - E}}{1 - L_p^0 \tilde{R}_{pp}} \right|^2 \quad (6.1)$$

with the energy dependence of $\tilde{\Gamma}_{\lambda p}(E)$ and $\tilde{\Gamma}_{\lambda \gamma}(E)$ defined by the penetrability, eq. (2.31):

$$\tilde{\Gamma}_{\lambda p}(E) = 2P_p^L \gamma_{\lambda p}^2 \quad (6.2)$$

$$\tilde{\Gamma}_{\lambda \gamma}(E) = 2\gamma_{\lambda \gamma}^2 \left(\frac{E - E_f}{E_{\lambda} - E_f} \right)^{2L_{\gamma}+1} \quad (6.3)$$

where L and L_{γ} denote the dependence of these quantities on the relative angular momentum of the entrance channel and the multipolarity of the radiation; and E_f is the energy of the final state [Azu94, Bra00]. In eq. (6.3) we used a relative definition of penetrability, normalized to unit in the position of the pole, E_{λ} ; this definition will be discussed later in this work.

For the $^{14}\text{N}(p, \gamma)^{15}\text{O}$ S –wave radiative capture, equation (6.1) takes the form:

$$\sigma_{p\gamma}^{L=0}(E1(2)) = \frac{2}{6} \frac{\pi}{k_p^2} \left| \frac{\sum_{\lambda} \frac{(\tilde{\Gamma}_{\lambda p}^{L=0} \tilde{\Gamma}_{\lambda \gamma}^{L_{\gamma}=1(2)})^{\frac{1}{2}}}{E_{\lambda} - E}}{1 - L_p^0 \tilde{R}_{pp}} \right|^2 + \frac{4}{6} \frac{\pi}{k_p^2} \left| \frac{\sum_{\lambda'} \frac{(\tilde{\Gamma}_{\lambda' p}^{L=0} \tilde{\Gamma}_{\lambda' \gamma}^{L_{\gamma}=1(2)})^{\frac{1}{2}}}{E_{\lambda'} - E}}{1 - L_p^0 \tilde{R}_{pp}} \right|^2 \quad (6.4)$$

for E1(2) cross sections, respectively. The first term in (6.4) corresponds to summing λ over $J^\pi = \frac{1}{2}^+$ states and the second term to summing λ' over $J^\pi = \frac{3}{2}^+$ states.

6.1.2 Results and discussion

The results obtained for the astrophysical S–factor corresponding to capture to the ground state, $E_x=6.18$ and 6.79 MeV states will be shown in figures 6.2–6.4, respectively (black curves represent the overall result and colored curves the contributions from the individual states and the background). In the fitting procedure the channel radius was chosen to be $a=6.5$ fm, and the boundary condition used corresponded to the shift function at the position of the subthreshold state at $E = -0.504$ MeV, which allows us to fix the energy of this state at the experimentally observed value. The fitting is reasonably insensitive to the channel radius.

Table 6.1: Values for the resonance energies, formal proton and γ -widths at the position of the pole, and square root of reduced widths, from the R–matrix fit. The energies quoted correspond to the experimental values, and the proton widths for the subthreshold state and the background poles are simply the reduced proton widths, γ_p^2 .

Transition	J^π	E_λ (MeV)	γ_p (MeV $^{\frac{1}{2}}$)	$\tilde{\Gamma}_p$ (keV)	γ_γ (MeV $^{\frac{1}{2}}$)	$\tilde{\Gamma}_\gamma$ (eV)	interference
g.s.	$\frac{1}{2}^+$	0.259	0.071	0.02	0.0002	0.036	–
		3.0	0.805	648	0.0026	7.0	–
		–0.504	0.412	170	0.0005	0.263	+
	$\frac{3}{2}^+$	0.985	0.063	3.2	0.0004	0.165	+
		2.187	0.167	66	0.0027	7.077	+
		4.5	0.933	871	0.0021	4.4	+
6.18 MeV	$\frac{1}{2}^+$	0.259	0.071	0.02	0.0009	0.850	+
		1.446	0.022	0.79	0.0006	0.376	+
		3.0	0.805	648	0.0004	0.141	+
	$\frac{3}{2}^+$	–0.504	0.412	170	0.0001	0.008	+
		0.985	0.063	3.2	0.0001	0.010	–
		4.5	0.933	871	0.0048	23.0	+
6.79 MeV	$\frac{1}{2}^+$	0.259	0.071	0.02	0.0006	0.313	+
	$\frac{1}{2}^-$	3.5	8.4	3.3×10^4	0.0425	1813	+
	$\frac{3}{2}^-$	3.5	2.4×10^{-6}	0.02	0.0004	0.196	–

The overall agreement between the R–matrix model and the data is very good, however, the total χ^2 per degree of freedom is 14.7. This is essentially due to a set of experimental points on the resonances that are not accurately described by the theoretical curve, since there are no horizontal error bars on the experimental data. The removal of these 11 points (7 on the ground state capture, 2 on the capture to the $E_x=6.18$ MeV state, and 2 on the capture to the $E_x=6.79$ MeV state) lowers the total χ^2 per degree of freedom to 9.3.

The resonance parameters corresponding to the best fit to the experimental data are shown in table 6.1. Particularly important in this table is the γ –width value of the $\frac{3}{2}^+$ subthreshold state at $E_x=6.79$ MeV, due to the sensitivity of the low energy astrophysical S–factor to this value. Schröder *et al.* [Sch87] obtained $\Gamma_\gamma=6.3$ eV, however, the analysis of Angulo and Descouvemont [Ang01] gives the width $\tilde{\Gamma}_\gamma=1.75\pm 0.60$ eV. Recent experiments on the properties of this state by Yamada *et al.* [Yam04] and Bertone *et al.* [Ber02] obtained $\Gamma_\gamma=0.41^{+0.34}_{-0.13}$ eV and $\Gamma_\gamma=0.95^{+0.60}_{-0.95}$ eV, respectively. The result obtained in this work, $\tilde{\Gamma}_\gamma=0.263$ eV, although not consistent with the value obtained from R–matrix analysis of Angulo and Descouvemont [Ang01], is in good agreement with the recent experimental results [Yam04, Ber02].

Capture to the ground state ($\frac{1}{2}^-$)

In the analysis of the ground state capture S–factor we use the $J^\pi = \frac{1}{2}^+$ state at $E=0.259$ MeV and the $J^\pi = \frac{3}{2}^+$ states at $E= -0.504, 0.985$ and 2.187 MeV. To account for contributions from direct process or low lying tails of high lying resonances we include two background poles, $J^\pi = \frac{1}{2}^+$ and $\frac{3}{2}^+$ above 3 MeV.

In the context of this model the proton $\tilde{\Gamma}_p$ and gamma widths $\tilde{\Gamma}_\gamma$ of these states are adjustable parameters and the values corresponding to the best fit are given in Table 6.1. As already mentioned, the values obtained for the parameters of the subthreshold state, $\gamma_p^2 = 170$ keV and $\tilde{\Gamma}_\gamma = 0.263$ eV, are in reasonable agreement with the values obtained by Angulo and Descouvemont [Ang01] ($\gamma_p^2 = 140$ keV and $\tilde{\Gamma}_\gamma = 1.75$ eV) and other works [AS91, Yam04, Ber02]. For the other $\frac{3}{2}^+$ states the values obtained ($\tilde{\Gamma}_p = 3.2$ keV and $\tilde{\Gamma}_\gamma = 0.165$ eV for the $E=0.985$ MeV state, and $\tilde{\Gamma}_p = 66$ keV and $\tilde{\Gamma}_\gamma = 7.08$ eV for the $E=2.187$ MeV state) are also in good agreement with the values referenced in other works [Ang01, Sch87, AS91].

For the $\frac{1}{2}^+$ state at $E=0.259$ MeV the values obtained in this work, $\tilde{\Gamma}_p = 0.02$ keV and $\tilde{\Gamma}_\gamma = 0.036$ eV, are significantly different from those obtained by Angulo and Descouvemont [Ang01] ($\tilde{\Gamma}_p = 1$ keV and $\tilde{\Gamma}_\gamma = 1.6 \times 10^{-3}$ eV), which may be explained by the different interference sign obtained.

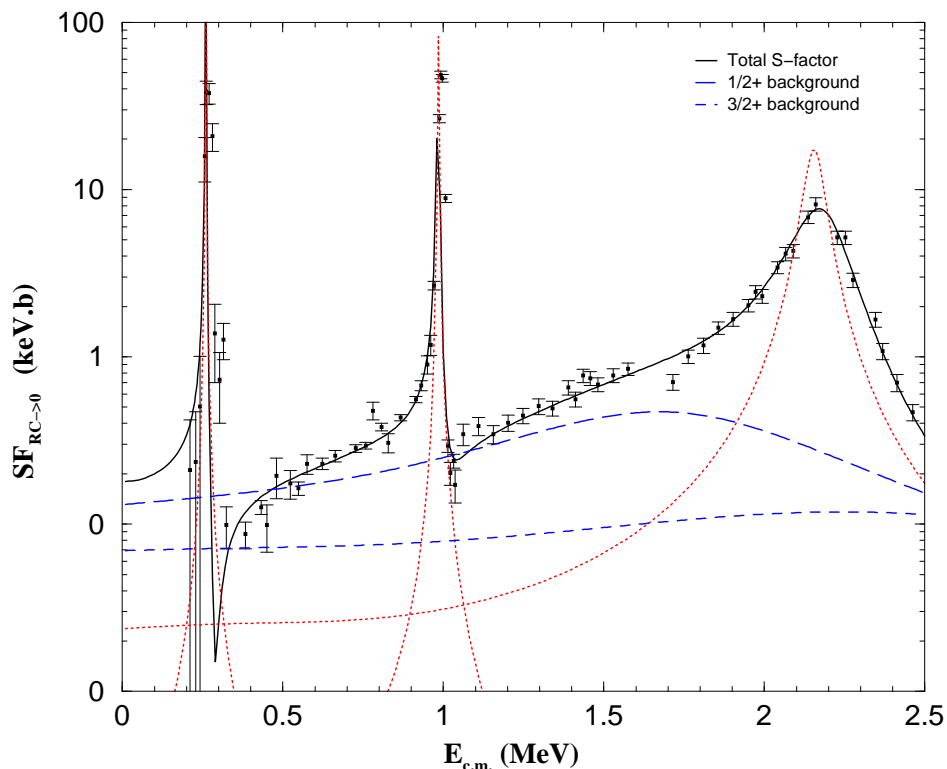
RC \rightarrow ground state

Figure 6.2: S-factor for radiative capture to the ground state of ^{15}O . The full curve represents the total S–factor, the dotted curves the contributions from the individual resonances, and the dashed curves the contributions from the background poles.

Given the boundary condition used, the energy of the subthreshold state is fixed to the value obtained from literature [AS91, Ang01]. The resonance energies are fitted to the experimental data. The values obtained in this work for the two $\frac{3}{2}^+$ resonances at $E=0.985$ and 2.187 MeV are $E=0.990$ and 2.220 MeV respectively. The fitted resonance energies for the $\frac{1}{2}^+$ states at $E=0.259$ and 1.446 MeV are $E=0.262$ and 1.449 MeV respectively. Fitting the energies considerably improves the result of the fitting procedure and results obtained are within 1% of the values quoted in the literature [AS91, Ang01].

The value obtained for the S–factor at astrophysical energies, $S(0)=0.17$ keV.b, is a factor of two larger than the one obtained by Angulo and Descouvemont [Ang01] but within the confidence interval quoted in this work ($S(0)=0.08^{+0.13}_{-0.06}$ keV.b), and significantly different from the one obtained by Schröder *et al.* [Sch87] ($S(0)=1.55$ keV.b). This reflects the uncertainty of the low energy experimental data and emphasizes the need for new and more accurate experimental data. Indeed, based on the available data, the R–matrix procedure and the S–factor obtained are very sensitive to the parameters of the subthreshold state and the $\frac{1}{2}^+$ resonance.

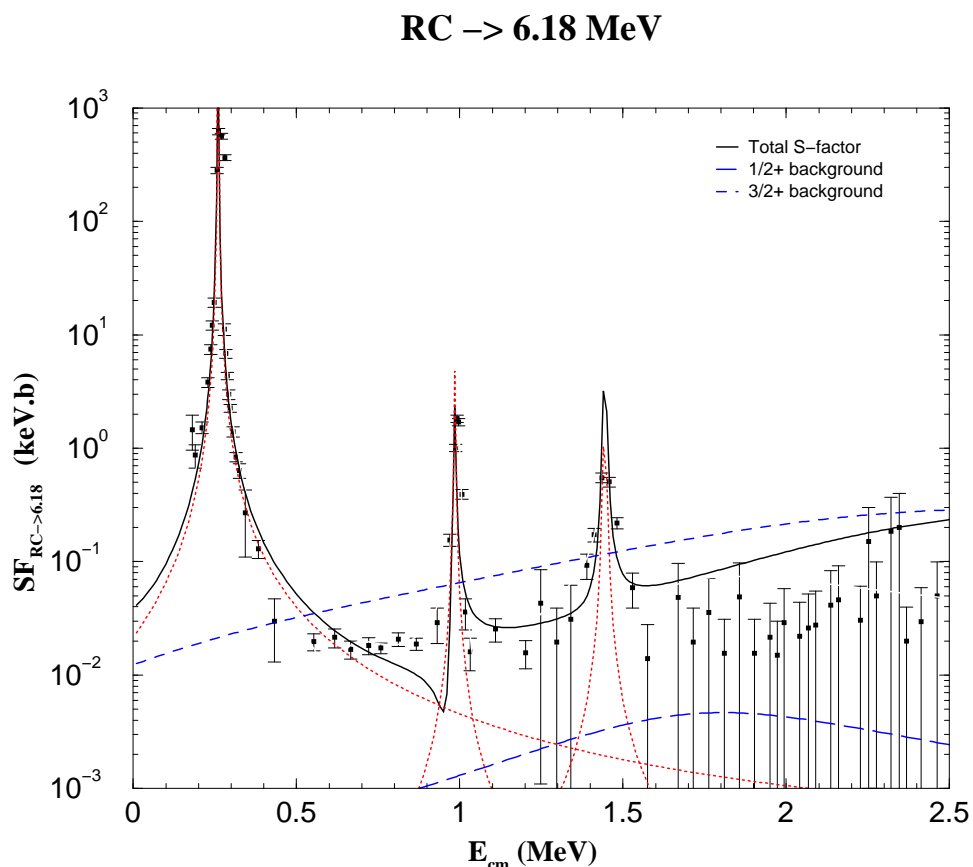


Figure 6.3: S–factor for radiative capture to the $E_x=6.18$ MeV state. The full curve represents the total S–factor, the dotted curves the contributions from the individual resonances, and the dashed curves the contributions from the background poles.

Capture to the $E_x=6.18$ MeV state ($\frac{3}{2}^-$)

In the analysis of the capture to the $E_x=6.18$ MeV state we used the $J^\pi = \frac{1}{2}^+$ states at $E=0.259$ and 1.446 MeV, the $J^\pi = \frac{3}{2}^+$ states at $E=-0.504$ and 0.985 MeV, and the background poles, $J^\pi = \frac{1}{2}^+$ and $\frac{3}{2}^+$ above 3 MeV.

The values obtained for the γ –widths of the subthreshold and $E=0.985$ MeV states, $\tilde{\Gamma}_\gamma=0.008$ and 0.010 eV respectively, are in reasonable agreement with the results from Angulo and Descouvemont [Ang01] ($\tilde{\Gamma}_\gamma = 5.0 \times 10^{-3}$ and 4.0×10^{-3} eV respectively).

For the γ –widths of the $\frac{1}{2}^+$ resonances at $E=0.259$ MeV and 1.446 MeV we obtain $\tilde{\Gamma}_\gamma=0.850$ and 0.376 eV. The fitted proton width of the $E=1.446$ MeV is $\tilde{\Gamma}_p=0.79$ keV. These values are significantly different from those obtained by the analysis of Angulo and Descouvemont [Ang01] ($\tilde{\Gamma}_p=42.0$ keV and $\tilde{\Gamma}_\gamma=0.11$ eV for the $E=1.446$ MeV state, and $\tilde{\Gamma}_\gamma = 2.0 \times 10^{-2}$ eV for the $E=0.259$ MeV resonance).

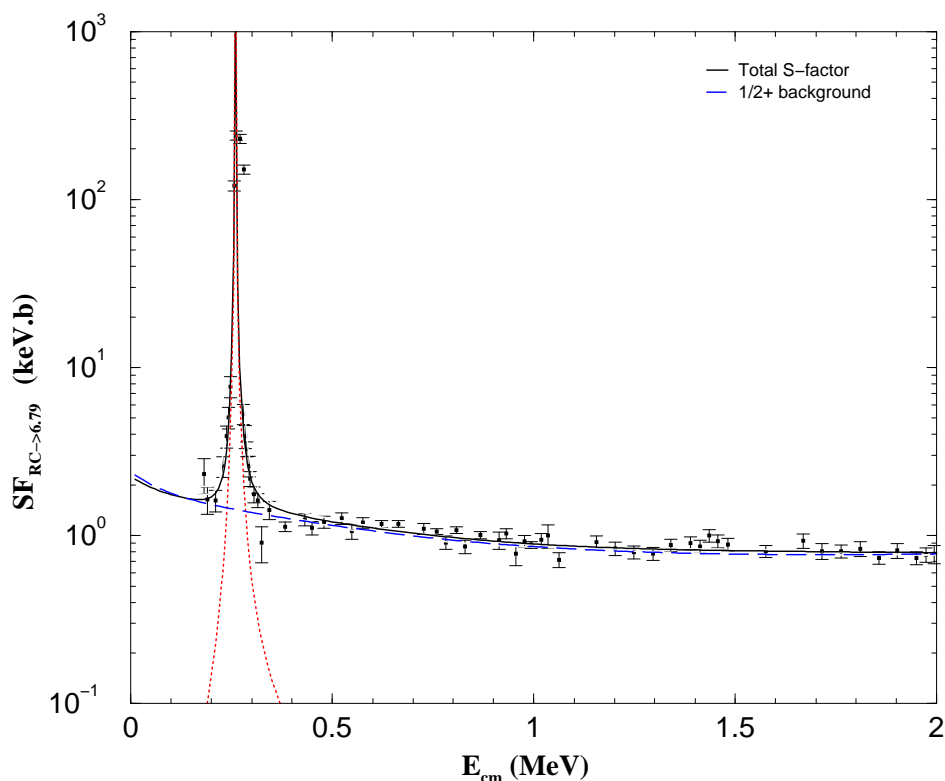
RC \rightarrow 6.79 MeV

Figure 6.4: S–factor for radiative capture to the $E_x=6.79$ MeV state. The full curve represents the total S–factor, the dotted curves the contributions from the individual resonances, and the dashed curves the contributions from the background poles.

The value obtained for the S–factor at astrophysical energies, $S(0)=0.04$ keV.b, is 30% smaller than the one obtained by Angulo and Descouvemont [Ang01] but again within the confidence interval quoted in this work ($S(0)=0.06^{+0.01}_{-0.02}$ keV.b).

Capture to the $E_x = 6.79$ MeV state ($\frac{3}{2}^+$)

The analysis of the capture to the $E_x = 6.79$ MeV state was performed with the $J^\pi = \frac{1}{2}^+$ state at $E=0.259$ MeV, and two negative parity background poles, $J^\pi = \frac{1}{2}^-$ and $J^\pi = \frac{3}{2}^-$ above 3 MeV to simulate the E1 process arising from direct contributions and low energy tails of high lying negative parity resonances.

The value obtained for the γ –widths of the $E=0.259$ MeV resonance, $\tilde{\Gamma}_\gamma = 0.313$ eV, differs significantly from the one obtained by the R–matrix analysis of Angulo and Descouvemont [Ang01], which consider the contribution from negative parity states through a potential model ($\tilde{\Gamma}_\gamma = 1.0 \times 10^{-2}$ eV).

The value obtained for the S–factor at astrophysical energies, $S(0)=2.21$ keV.b, is 35% larger than the one obtained by Angulo and Descouvemont [Ang01] ($S(0)=1.63\pm 0.17$ keV.b). This discrepancy is also related to the way the background contribution for the capture to the $E_x=6.79$ MeV state is treated. Later in this work we introduce a potential description of this background and attempt to clarify this issue.

Total S–factor

The analysis performed in this chapter reveals that the contribution from capture to the $E_x=6.79$ MeV state dominates the astrophysical S–factor at zero energy. The total S–factor at astrophysical energies obtained in this work, $S(0)=2.42$ keV.b, is 36% higher than the value obtained by Angulo and Descouvemont [Ang01] ($S(0)=1.77\pm 0.20$ keV.b).

6.2 Conclusions

In this chapter we applied a phenomenological R–matrix model, introduced in chapters 1 and 2, to the analysis of the radiative capture reaction $^{14}\text{N}(p, \gamma)^{15}\text{O}$ and the determination of its S–factor at energies relevant in astrophysics.

The total S–factor at astrophysical energies obtained in this work, $S(0)=2.42$ keV.b, is significantly higher than the value obtained by Angulo and Descouvemont [Ang01], although both studies used the experimental data obtained by Schröder *et al.* [Sch87]. This results from small differences of the fitted properties of the resonances and the $\frac{3}{2}^+$ subthreshold state, and is a consequence of the uncertainty of the low energy experimental data.

An important feature of this study, often used in R–matrix analysis [Ang01], is the introduction of background poles to account for the contributions arising from direct capture (DC) or low energy tails of high lying resonances. Indeed, as can be seen from figures 6.2–6.4, the contribution from these background poles in the R–matrix is certainly non-negligible.

The explicit treatment of the direct contribution is important to clarify the interplay between the two reaction mechanisms, resonant and direct, and reduce the ambiguity in the fitted properties of the resonances or subthreshold states considered in the model space. This effort is the motivation for the hybrid treatment that will be introduced in chapter 9. However, before the introduction of this model, it is important to study the formalism that allows the treatment of photonuclear processes in the coupled channels framework. This is the objective of the following two chapters.

Chapter 7

Standard formalism for radiative capture reactions

In this chapter we derive the general formalism for the calculation of radiative capture reaction rates, proceeding via both electric and magnetic processes. We study the radiative capture process with a two body approximation for the particle+target system.

The transition rate between an initial state $|i\rangle$ and a final state $|f\rangle$ is given by Fermi's golden rule of time-dependent perturbation theory [Eis88, Gre95]:

$$w_{f\leftarrow i} = \frac{2\pi}{\hbar} |\langle f|H_{int}|i\rangle|^2 \rho_f \quad (7.1)$$

where ρ_f is the density of final states for the system and H_{int} is the interaction Hamiltonian. We derive detailed expressions for the cross section of electric and magnetic radiative capture. We start by introducing the elements necessary to calculate the transition rate (initial and final state wave functions, interaction Hamiltonian and density of states) and proceed to calculate the matrix elements for electric and magnetic transitions, and finally the cross sections. We calculate the electric transition rates from the interaction Hamiltonian using the Siegert theorem and the long wavelength approximation (LWA).

7.1 General definitions

For emission of radiation we have for the initial and final states:

$$|i\rangle \equiv |\Phi_i(t), 0\rangle = |\Phi_{J_i, S_p, S_t}^{M_i, M_p, M_t} e^{-i\frac{E_i t}{\hbar}}, 0\rangle \quad (7.2)$$

$$|f\rangle \equiv |\Psi_f(t), \mathbf{k}\mu\rangle = |\Psi_{J_f}^{M_f} e^{-i\frac{E_f t}{\hbar}}, \mathbf{k}\mu\rangle \quad (7.3)$$

since these are stationary states; where $\mathbf{k}\mu$ are the photon wave vector and polarization, and E_i and E_f are the energies of the initial and final state respectively, with $E_i > E_f$.

We consider transitions between an initial scattering state, $\Phi_{J_i, S_p, S_t}^{M_i, M_p, M_t}$, and a final bound state, $\Psi_{J_f}^{M_f}$. These are defined in the jj coupling scheme. The possibility of inelastic excitations of particle and target is considered.

Bound state

In a general way, the bound state formed with in a particle+target system can be described by, using the notation for the set of quantum numbers $\alpha_f = \{(L_f, S_p'')j_f, S_t''\}$:

$$|\Psi_{J_f}^{M_f}\rangle = \sum_{\substack{S_p'', M_p'', S_t'', M_t'' \\ j_f, m_f, L_f, \mu_f}} (L_f \mu_f, S_p'' M_p'' | j_f m_f) (j_f m_f, S_t'' M_t'' | J_f M_f) Y_{L_f}^{\mu_f}(\hat{R}) \frac{\psi_{\alpha_f}^{J_f}(R)}{R} \chi_{S_p''}^{M_p''}(\mathbf{r}_1, \dots, \mathbf{r}_{p-1}) \chi_{S_t''}^{M_t''}(\mathbf{r}_{p+1}, \dots, \mathbf{r}_{A-1}) \quad (7.4)$$

$$= \sum_{S_p'', S_t'', j_f, L_f} |(L_f S_p'') j_f S_t''; J_f M_f\rangle_{\mathbf{r}_{1,p-1}}^{\mathbf{r}_{p+1,A-1}} \frac{\psi_{\alpha_f}^{J_f}(R)}{R} \quad (7.5)$$

where $\psi_{\alpha_f}^{J_f}(R)$ and $Y_{L_f}^{\mu_f}(\hat{R})$ correspond to the radial and angular parts of the wave function respectively, J_f is the total angular momentum of the bound state, L_f is the relative angular momentum between particle and target, and R the relative coordinate. The χ are the wave functions of projectile and target including spin and depend on their internal coordinates; this dependence is included in the *ket* of the above expression and is denoted by the subscript $\mathbf{r}_{1,p-1}$ and superscript $\mathbf{r}_{p+1,A-1}$.

As explained in chapter 1, the nucleon coordinates $\{\mathbf{r}_1, \dots, \mathbf{r}_A\}$ can be written as $\{\mathbf{r}_1 \dots \mathbf{r}_{p-1}, \mathbf{R}_p, \mathbf{r}_{p+1} \dots \mathbf{r}_{A-1}, \mathbf{R}_t\}$ where \mathbf{R}_p and \mathbf{R}_t are the *cm* coordinates of the projectile and target respectively. \mathbf{R}_p and \mathbf{R}_t can in turn be written as $\mathbf{R} = \mathbf{R}_p - \mathbf{R}_t$ and \mathbf{R}_{cm} (the Jacobian of the transformation is 1) corresponding to the relative coordinate and the *cm* coordinate respectively; in a reference frame centered in the *cm* the \mathbf{R}_{cm} is zero. Integration with respect to the $\{\mathbf{r}_1 \dots \mathbf{r}_{p-1}, \mathbf{r}_{p+1} \dots \mathbf{r}_{A-1}, \mathbf{R}\}$ coordinates will be denoted by the subscript \mathbf{r}_{1A} or by $d\mathbf{r}_{1A}$.

Scattering state

Generally, the scattering state between an incoming particle and the target can be expanded in partial waves with relative angular momentum L_i , and therefore using the notation for the sets of quantum numbers $\alpha_i = \{(L_i, S_p)j_i, S_t\}$ and $\alpha'_i = \{(L'_i, S'_p)j'_i, S'_t\}$:

$$|\Phi_{J_i, S_p, S_t}^{M_i, M_p, M_t}, k_p \rangle = \sum_{L_i, \mu_i, j_i, m_i} \frac{4\pi}{k_p} (L_i \mu_i, S_p M_p | j_i m_i) (j_i m_i, S_t M_t | J_i M_i) e^{i\sigma_{L_i}} Y_{L_i}^{\mu_i}(\hat{k}_p) \Phi_{J_i, L_i}^{M_i}(\mathbf{R}) \quad (7.6)$$

$$= \sum_{L_i, \mu_i, j_i, m_i} \frac{4\pi}{k_p} (L_i \mu_i, S_p M_p | j_i m_i) (j_i m_i, S_t M_t | J_i M_i) e^{i\sigma_{L_i}} Y_{L_i}^{\mu_i}(\hat{k}_p) \sum_{\substack{L'_i, \mu'_i, j'_i, m'_i \\ S'_p, M'_p, S'_t, M'_t}} (L'_i \mu'_i, S'_p M'_p | j'_i m'_i) (j'_i m'_i, S'_t M'_t | J_i M_i) i^{L'_i} Y_{L'_i}^{\mu'_i}(\hat{R}) \frac{\phi_{\alpha'_i, \alpha_i}^{J_i}(R)}{R} \chi_{S'_p}^{M'_p}(\mathbf{r}_1, \dots, \mathbf{r}_{p-1}) \chi_{S'_t}^{M'_t}(\mathbf{r}_{p+1}, \dots, \mathbf{r}_{A-1}) \quad (7.7)$$

$$= \sum_{L_i, \mu_i, j_i, m_i} \frac{4\pi}{k_p} (L_i \mu_i, S_p M_p | j_i m_i) (j_i m_i, S_t M_t | J_i M_i) e^{i\sigma_{L_i}} Y_{L_i}^{\mu_i}(\hat{k}_p) \sum_{L'_i, j'_i, S'_p, S'_t} |(L'_i S'_p) j'_i S'_t; J_i M_i \rangle_{\mathbf{r}_{1,p-1}^{\mathbf{r}_{p+1,A-1}}} i^{L'_i} \frac{\phi_{\alpha'_i, \alpha_i}^{J_i}(R)}{R} \quad (7.8)$$

where $\phi_{\alpha'_i, \alpha_i}^{J_i}(R)$ and $Y_{L'_i}^{\mu'_i}(\hat{R})$ correspond to the radial and angular parts of the scattering wave function respectively, and χ are the wave functions for projectile and target spin that, like before, depend on their internal coordinates with this dependence included in the *ket*; prime indicate quantities after the interaction while unprimed indicates quantities before the interaction; because of rotational invariance the coupling does not change total angular momentum and therefore $J_i M_i$ are the same before and after the coupling.

Interaction Hamiltonian

In (7.1) H_{int} is the Hamiltonian for the interaction between radiation and matter [Eis88, Gre95]:

$$H_{int} = -\frac{1}{c} \int \mathbf{j}(\mathbf{r}, t) \cdot \mathbf{A}(\mathbf{r}, t) d\mathbf{r} \quad (7.9)$$

where $\mathbf{j}(\mathbf{r}, t)$ and $\mathbf{A}(\mathbf{r}, t)$ are the nuclear current and electromagnetic field operators.

The $\mathbf{A}(\mathbf{r}, t)$ matrix element between the photon vacuum and a one photon-state is

$$\langle \mathbf{k}\mu | \mathbf{A}(\mathbf{r}, t) | 0 \rangle = c \sqrt{\frac{2\pi\hbar}{\omega V}} \boldsymbol{\epsilon}_\mu^* e^{-i\mathbf{k}\cdot\mathbf{r} + i\omega t} \quad (7.10)$$

where the $\boldsymbol{\epsilon}_\mu$ are the unit vectors that indicate the polarization of the field.

There is a degree of arbitrariness in the definition of the vector potential from the electric and magnetic fields, since Maxwell's equations are invariant to the introduction of any scalar function which is called a gauge transformation. The freedom implied by this invariance means one can choose a set of vector and scalar potentials vector potential that fulfill a gauge condition. A useful gauge is the so-called Coulomb or transverse gauge, $\nabla \cdot \mathbf{A} = 0$, yielding the transverse nature of the electromagnetic field. By aligning the momentum \mathbf{k} with ϵ_3 we are left with only two independent polarization directions $\mu = 1, 2$ both fulfilling $\epsilon_\mu \cdot \mathbf{k} = 0$. Then

$$\begin{aligned} \langle f | H_{int} | i \rangle &\equiv \langle \Psi_f(t), \mathbf{k}\mu | H_{int} | \Phi_i(t), 0 \rangle \\ &= - \int d^3r \sqrt{\frac{2\pi\hbar}{\omega V}} \epsilon_{k\mu}^* \cdot e^{-i\mathbf{k}\cdot\mathbf{r}+i\omega t} \langle \Psi_f(t) | \mathbf{j}(\mathbf{r}, t) | \Phi_i(t) \rangle_{\mathbf{r}_{1A}} \end{aligned} \quad (7.11)$$

Density of states

The final state involves a discrete state or narrow resonance of the nucleus combined with a photon state of given energy, $E = \hbar\omega = \hbar ck$, but variable direction, so that the density of available states is determined by the photon energy [Gre95]. The density of final states is therefore

$$\rho(E) = \frac{V}{(2\pi)^3} \frac{k^2}{\hbar c} d\Omega_k \quad , \quad (7.12)$$

where $d\Omega_k$ is the solid angle into which the photon is ejected. Inserting eqs. (7.12) and (7.11) into (7.1), the transition rate is

$$w_{f \leftarrow i} = \frac{k}{2\pi\hbar c^2} \left| \int d^3r \langle \Psi_f(t) | \mathbf{j}(\mathbf{r}, t) | \Phi_i(t) \rangle_{\mathbf{r}_{1A}} \cdot \epsilon_{k\mu}^* e^{-i\mathbf{k}\cdot\mathbf{r}+i\omega t} \right|^2 d\Omega_k \quad (7.13)$$

Multipole expansion

By assuming that the time dependence of the matrix element of the nuclear current, which describes the current density in the nucleus, exists only through the wave functions, one can write

$$\langle \Psi_f(t) | \mathbf{j}(\mathbf{r}, t) | \Phi_i(t) \rangle = \langle \Psi_{J_f}^{M_f} | \mathbf{j}(\mathbf{r}) | \Phi_{J_i, S_p, S_t}^{M_i, M_p, M_t} \rangle e^{i\frac{(E_f - E_i)t}{\hbar}} \quad . \quad (7.14)$$

In Fermi's golden rule the time-dependent phase of the matrix element vanishes to ensure energy conservation. By combining the phases of the nuclear states and the photon operator one obtains the condition for photon emission

$$i\frac{(E_f - E_i)t}{\hbar} + i\omega t = 0 \Leftrightarrow E_f = E_i - \hbar\omega \quad , \quad (7.15)$$

and the transition rate (7.13) becomes

$$w_{f \leftarrow i} = \frac{k}{2\pi\hbar c^2} \left| \int d^3r \langle \Psi_{J_f}^{M_f} | \mathbf{j}(\mathbf{r}) | \Phi_{J_i, S_p, S_t}^{M_i, M_p, M_t} \rangle \cdot \boldsymbol{\xi}_\mu^* e^{-i\mathbf{k}\cdot\mathbf{r}} \right|^2 d\Omega_k, \quad \mu = \pm 1 \quad (7.16)$$

where we changed $\boldsymbol{\epsilon}_{k\mu}$ to the system of spherical basis vectors, $\boldsymbol{\xi}_\mu$, with ξ_0 along \mathbf{k} , and $\xi_{\pm 1}$ corresponding to circularly polarized photons.

Using the well known expansion of the plane wave into fields of good angular momentum [Eis88, Gre95]:

$$\begin{aligned} \mathbf{A}(\mathbf{r}) &= \boldsymbol{\xi}_\mu e^{i\mathbf{k}\cdot\mathbf{r}} \\ &= \mu\sqrt{2\pi} \sum_{L\nu} \sqrt{2L+1} i^L D_{\nu\mu}^L(\phi, \theta, 0) [\mathbf{A}_{L\nu}(\mathbf{r}; M) + i\mu\mathbf{A}_{L\nu}(\mathbf{r}; E)] \end{aligned} \quad (7.17)$$

where θ and ϕ are the polar and azimuthal angles that describe \mathbf{k} ; we can write (7.16) as

$$\begin{aligned} w_{f \leftarrow i} &= \frac{k}{2\pi\hbar c^2} \left| \int d^3r \mu\sqrt{2\pi} \sum_{L\nu} \sqrt{2L+1} i^L D_{\nu\mu}^L(\phi, \theta, 0) \right. \\ &\quad \left. \langle \Psi_{J_f}^{M_f} | \mathbf{j}(\mathbf{r}) | \Phi_{J_i, S_p, S_t}^{M_i, M_p, M_t} \rangle [\mathbf{A}_{L\nu}(\mathbf{r}; M) + i\mu\mathbf{A}_{L\nu}(\mathbf{r}; E)] \right|^2 d\Omega_k \end{aligned} \quad (7.18)$$

where the explicit expressions for $\mathbf{A}_{L\nu}(\mathbf{r}; E)$ and $\mathbf{A}_{L\nu}(\mathbf{r}; M)$ are in terms of Bessel functions will be written below.

A multipole field is a solution of the free-space Maxwell equations which is an eigenfunction of the square and one component of the angular momentum, and of the parity [Bla58]. Thus the potentials in a multipole field must be irreducible tensors of rank L with definite parity. The parity is determined by the parity of the magnetic field \mathbf{H} . A multipole field is an electric field if the parity of the magnetic field is $(-1)^L$ and a magnetic field if the parity of the magnetic field is $(-1)^{L+1}$.

Now, we consider the vector spherical harmonics which are simultaneous eigenfunctions of L_z and $L^2 = L_x^2 + L_y^2 + L_z^2$. For each value of $L^2 = L(L+1)$ with $L \geq 1$, there are three kinds of vector harmonics, corresponding to $\lambda = L, L \pm 1$:

$$\mathbf{Y}_{L1,\lambda}^\nu = \sum_{m=-1}^1 (\lambda\nu - m, 1m | L\nu) Y_\lambda^{\nu-m}(\theta, \phi) \boldsymbol{\xi}_m \quad (7.19)$$

where 1 corresponds to the spin of the photon. The vector functions $\mathbf{Y}_{L1,\lambda}^\nu$ have parity $(-1)^\lambda$. Since the scalar spherical harmonics $Y_\lambda^{\nu-m}$ form a complete set for scalar functions and the $\boldsymbol{\xi}_m$ a complete set of basis vectors for the spin, the vector spherical harmonics are also a complete set, and any vector field $\mathbf{A}(\mathbf{r})$ can be written as a linear combination of the $\mathbf{Y}_{L1,\lambda}^\nu(\theta, \phi)$ with coefficients which depend on the radial coordinate r only. The three independent vector fields are therefore:

$$j_L(kr)\mathbf{Y}_{L1,L}^\nu(\hat{r}), \quad j_{L-1}(kr)\mathbf{Y}_{L1,L-1}^\nu(\hat{r}), \quad \text{and} \quad j_{L+1}(kr)\mathbf{Y}_{L1,L+1}^\nu(\hat{r})$$

From these one can build the fields of good parity, $\mathbf{A}_{L\nu}(\mathbf{r}; M)$ and $\mathbf{A}_{L\nu}(\mathbf{r}; E)$ with parities $(-1)^L$ and $(-1)^{L+1}$ respectively:

$$\begin{aligned}\mathbf{A}_{L\nu}(\mathbf{r}; M) &= j_L(kr)\mathbf{Y}_{L1,L}^\nu(\hat{r}) \\ &\equiv \frac{1}{\sqrt{L(L+1)}} \mathbf{L}j_L(kr)Y_L^\nu(\hat{r})\end{aligned}\quad (7.20)$$

$$\begin{aligned}\mathbf{A}_{L\nu}(\mathbf{r}; E) &= c_{L-1} j_{L-1}(kr)\mathbf{Y}_{L1,L-1}^\nu(\hat{r}) + c_{L+1} j_{L+1}(kr)\mathbf{Y}_{L1,L+1}^\nu(\hat{r}) \\ &= \sqrt{\frac{L+1}{2L+1}} j_{L-1}(kr)\mathbf{Y}_{L1,L-1}^\nu(\hat{r}) - \sqrt{\frac{L}{2L+1}} j_{L+1}(kr)\mathbf{Y}_{L1,L+1}^\nu(\hat{r}) \\ &\equiv \frac{-i}{k\sqrt{L(L+1)}} \nabla \times (\mathbf{L}j_L(kr)Y_L^\nu(\hat{r}))\end{aligned}\quad (7.21)$$

where the coefficients $c_{L\pm 1}$ are determined from the transversality condition for the field, $\nabla \cdot \mathbf{A}_{L\nu}(\mathbf{r}; E) = 0$ [Eis88, Boh69]; and $\mathbf{L} = -i\mathbf{r} \times \nabla$ is the orbital angular momentum operator.

From the gradient formula (E.9) and eqs. (E.11) and (E.11) one can also obtain the expression for the longitudinal component of the field (since $\nabla \cdot \mathbf{A}_{L\nu}(\mathbf{r}; Long) \neq 0$):

$$\begin{aligned}\mathbf{A}_{L\nu}(\mathbf{r}; Long) &= \frac{1}{k} \nabla (j_L(kr)Y_L^\nu(\hat{r})) \\ &= \sqrt{\frac{L}{2L+1}} j_{L-1}(kr)\mathbf{Y}_{L1,L-1}^\nu(\hat{r}) + \sqrt{\frac{L+1}{2L+1}} j_{L+1}(kr)\mathbf{Y}_{L1,L+1}^\nu(\hat{r})\end{aligned}\quad (7.22)$$

where the coefficients guarantee the condition $\nabla \times \mathbf{A}_{L\nu}(\mathbf{r}; Long) = 0$ [Eis88].

7.2 Matrix element for EL transitions

The matrix element relevant to the calculation of electric transitions of a specific multipolarity L is, from (7.18)

$$M_{f \leftarrow i}(E) = \sqrt{2\pi} \hat{L} i^{L+1} \sum_{\nu} D_{\nu\mu}^L(\phi, \theta, 0) \int d^3r \langle \Psi_{J_f}^{M_f} | \mathbf{j}(\mathbf{r}) | \Phi_{J_i, S_p, S_t}^{M_i, M_p, M_t} \rangle_{\mathbf{r}_{1A}} \cdot \mathbf{A}_{L\nu}(\mathbf{r}; E) \quad (7.23)$$

where we have made the additional assumption that \mathbf{k} is aligned with the z direction; and $\hat{L} = \sqrt{2L+1}$. The nuclear current is made up of a convective part and a magnetization part [Eis88]:

$$\begin{aligned}&\langle \Psi_{J_f}^{M_f} | \mathbf{j}(\mathbf{r}) | \Phi_{J_i, S_p, S_t}^{M_i, M_p, M_t} \rangle \\ &= \sum_{i=1}^A \int \left\{ \frac{1 + \tau_{zi}}{2} \frac{e\hbar}{2m_i} \left[\Psi_{J_f}^{M_f*} \left(\nabla_i \Phi_{J_i, S_p, S_t}^{M_i, M_p, M_t} \right) - \left(\nabla_i \Psi_{J_f}^{M_f*} \right) \Phi_{J_i, S_p, S_t}^{M_i, M_p, M_t} \right] \right. \\ &\quad \left. + \frac{e\hbar}{m_i} K_i \nabla_i \times \left[\Psi_{J_f}^{M_f*} \mathbf{S}_i \Phi_{J_i, S_p, S_t}^{M_i, M_p, M_t} \right] \right\} \delta(\mathbf{r} - \mathbf{r}_i) d\mathbf{r}_1 \dots d\mathbf{r}_A\end{aligned}\quad (7.24)$$

where τ_{zi} is the Z -axis component of the isospin operator of the i nucleon, and the operator $\frac{1+\tau_{zi}}{2}$ projects onto the proton states; K_i is the empirical magnetic moment for protons and neutrons, $K_p = 2.79$ and $K_n = -1.91$; and m_i denotes the mass of each nucleon. The first term, the convective part, dominates electric transitions and can be simplified by using the Siegert theorem in the long wavelength approximation, while the second term, the magnetization (spin dependent) part, has to be calculated explicitly.

The convective term and Siegert theorem

For many radiating systems the wavelength of the emitted radiation is much larger than the typical length scale of the system in question, $kr \ll 1$. As the nuclear radii are typically less than 10 fm, this corresponds to energies

$$E = \hbar ck \approx (197 \text{ MeV}\cdot\text{fm})k \ll \frac{197}{10} \approx 20 \text{ MeV}$$

Under this condition, and as a result of the behavior of the Bessel functions of small arguments, the second terms in eqs. (7.21) and (7.22) are much smaller than the first

$$j_L(kr) \approx \frac{(kr)^L}{(2L+1)!!} \quad \Rightarrow \quad \frac{j_{L+1}(kr)}{j_{L-1}(kr)} \approx \frac{(kr)^2}{(2L+1)(2L+3)} \ll 1 \quad (7.25)$$

and one can simplify the radiation fields:

$$\mathbf{A}_{L\nu}(\mathbf{r}; E) \approx \sqrt{\frac{L+1}{L}} \mathbf{A}_{L\nu}(\mathbf{r}; Long) = \frac{1}{k} \nabla (j_L(kr) Y_L^\nu(\hat{r})) \quad (7.26)$$

and write the convection part of the electric L multipole matrix element as:

$$M_{f \leftarrow i}^c = \frac{\sqrt{2\pi} i^{L+1}}{k} \sqrt{\frac{(2L+1)(L+1)}{L}} \sum_{\nu} D_{\nu\mu}^L(\phi, \theta, 0) \int d^3r \langle \Psi_{J_f}^{M_f} | \mathbf{j}^c(\mathbf{r}) | \Phi_{J_i, S_p, S_t}^{M_i, M_p, M_t} \rangle_{\mathbf{r}_{1A}} \nabla (j_L(kr) Y_L^\nu(\hat{r})) \quad (7.27)$$

Using the continuity equation

$$\nabla \cdot \langle f | \mathbf{j}^c(\mathbf{r}, t) | i \rangle + \frac{d}{dt} \langle f | \rho(\mathbf{r}, t) | i \rangle = 0 \quad (7.28)$$

(where the wave functions of the initial and final state depend neither on \mathbf{r} , the fixed position in space where the density and current density are being evaluated, nor on time) and by transforming into the Schrödinger picture, one is able to insert the time dependence of the states explicitly [Gre95]

$$\begin{aligned} \nabla \cdot \langle f(t) | \mathbf{j}^c(\mathbf{r}) | i(t) \rangle + \frac{d}{dt} \langle f(t) | \rho(\mathbf{r}) | i(t) \rangle &= 0 \\ \Leftrightarrow \nabla \cdot \langle f | \mathbf{j}^c(\mathbf{r}) | i \rangle - \frac{i}{\hbar} (E_i - E_f) \langle f | \rho(\mathbf{r}) | i \rangle &= 0 \end{aligned} \quad (7.29)$$

and obtain the divergence of the matrix elements of the nuclear current from the matrix elements of the density operator, which constitutes the Siegert theorem.

With the previous relation and integrating (7.23) by parts one obtains (noting that $(E_i - E_f) = \hbar ck$ for photon emission):

$$\begin{aligned}
M_{f \leftarrow i}^c(E) &= \frac{\sqrt{2\pi} i^{L+1}}{k} \sqrt{\frac{(2L+1)(L+1)}{L}} \sum_{\nu} D_{\nu\mu}^L(\phi, \theta, 0) \\
&\quad \int d^3r \nabla \cdot \langle \Psi_{J_f}^{M_f} | \mathbf{j}^c(\mathbf{r}) | \Phi_{J_i, S_p, S_t}^{M_i, M_p, M_t} \rangle j_L(kr) Y_L^{\nu}(\hat{r}) \\
&= -\sqrt{2\pi} i^L c \sqrt{\frac{(2L+1)(L+1)}{L}} \sum_{\nu} D_{\nu\mu}^L(\phi, \theta, 0) \\
&\quad \int d^3r \langle \Psi_{J_f}^{M_f} | \rho(\mathbf{r}) | \Phi_{J_i, S_p, S_t}^{M_i, M_p, M_t} \rangle j_L(kr) Y_L^{\nu}(\hat{r}) \quad (7.30)
\end{aligned}$$

$$\begin{aligned}
&= -\sqrt{2\pi} i^L c \sqrt{\frac{(2L+1)(L+1)}{L}} \sum_{\nu} D_{\nu\mu}^L(\phi, \theta, 0) \\
&\quad \int d^3r \langle \Psi_{J_f}^{M_f} | \rho(\mathbf{r}) | \Phi_{J_i, S_p, S_t}^{M_i, M_p, M_t} \rangle \frac{(kr)^L}{(2L+1)!!} Y_L^{\nu}(\hat{r}) \quad (7.31)
\end{aligned}$$

where the last step used the expression for the Bessel functions in the long wavelength limit (7.25).

The magnetization term

Using eq. (7.23) and

$$\langle \Psi_{J_f}^{M_f} | \mathbf{j}^m(\mathbf{r}) | \Phi_{J_i, S_p, S_t}^{M_i, M_p, M_t} \rangle = \sum_{i=1}^A \int \frac{e\hbar}{m_i} K_i \nabla_i \times \left[\Psi_{J_f}^{M_f*} \mathbf{S}_i \Phi_{J_i, S_p, S_t}^{M_i, M_p, M_t} \right] \delta(\mathbf{r} - \mathbf{r}_i) d\mathbf{r}_{1A} \quad (7.32)$$

and also eq. (F.1), one can obtain the magnetization part of electric L multipole matrix element:

$$\begin{aligned}
M_{f \leftarrow i}^m(E) &= -\sqrt{2\pi} \hat{L} i^{L+1} \sum_{\nu} D_{\nu\mu}^L(\phi, \theta, 0) \sum_{i=1}^A \frac{e\hbar}{m_i} K_i \frac{k^{L+1}}{\sqrt{L(L+1)}(2L+1)!!} \\
&\quad \int d^3r \left\{ \int \left[\Psi_{J_f}^{M_f*} \mathbf{S}_i \Phi_{J_i, S_p, S_t}^{M_i, M_p, M_t} \right] \times \mathbf{r}_i \cdot \nabla (r_i^L Y_L^{\nu}(\hat{r}_i)) \delta(\mathbf{r} - \mathbf{r}_i) d\mathbf{r}_{1A} \right\} \quad (7.33)
\end{aligned}$$

Due to the dominant effect of the convective part of the nuclear current we will neglect this magnetization term in the subsequent calculations of electric transitions.

Transition rate

The density operator can be written in terms of the coordinates of the field sources, i.e., the elements of the particle and target system, $\mathbf{r}_1, \mathbf{r}_2, \dots, \mathbf{r}_A$:

$$\rho(\mathbf{r}) = \sum_{i=1}^A \frac{1 + \tau_{zi}}{2} e \delta(\mathbf{r} - \mathbf{r}_i) \quad (7.34)$$

where $A = A_p + A_t$ is total number of constituents in the particle+target system.

Using the density operator of (7.34) in (7.31) and integrating over \mathbf{r} , one can write the convective matrix element for electric transitions as

$$\begin{aligned} M_{f \leftarrow i}^c(E) &= -\sqrt{2\pi} c i^L \frac{k^L}{(2L+1)!!} \sqrt{\frac{(2L+1)(L+1)}{L}} \sum_{\nu} D_{\nu\mu}^L(\phi, \theta, 0) \\ &\quad \langle \chi_{S_p''}^{M_p''} \chi_{S_t''}^{M_t''} \Psi_{J_f}^{M_f} | \sum_{i=1}^A \frac{1 + \tau_{zi}}{2} e r_i^L Y_L^{\nu}(\hat{r}_i) | \Phi_{J_i, S_p, S_t}^{M_i, M_p, M_t} \chi_{S_p'}^{M_p'} \chi_{S_t'}^{M_t'} \rangle_{\mathbf{r}_{1A}} \end{aligned} \quad (7.35)$$

where the dependence on the internal coordinates of the particle and target was factorized from the matrix element through the spin functions, χ .

From the transition rate (7.18), and integrating over the photon direction using:

$$\int d\Omega D_{\mu,\nu}^L * D_{\mu',\nu'}^L = \frac{4\pi}{2L+1} \delta_{\mu\mu'} \delta_{\nu\nu'} \quad (7.36)$$

one obtains the convective transition rate for electric photo-emission of multipolarity L :

$$\begin{aligned} T_{fi}^c(EL) &= \frac{8\pi(L+1)}{L[(2L+1)!!]^2} \frac{k^{2L+1}}{\hbar} \\ &\quad \left| \langle \chi_{S_p''}^{M_p''} \chi_{S_t''}^{M_t''} \Psi_{J_f}^{M_f} | \sum_{i=1}^A \frac{1 + \tau_{zi}}{2} e r_i^L Y_L^{\mu}(\hat{r}_i) | \Phi_{J_i, S_p, S_t}^{M_i, M_p, M_t} \chi_{S_p'}^{M_p'} \chi_{S_t'}^{M_t'} \rangle_{\mathbf{r}_{1A}} \right|^2 \end{aligned} \quad (7.37)$$

where we have also summed over the photon polarization, yielding a factor of 2. The index μ is not a free index, since the Wigner-Eckart theorem (E.12) requires $\mu = M_f - M_i$.

Transition operator

The generic form for the electric operator in the long wavelength approximation is, from (7.37):

$$QE_L^{\mu} = \sum_{i=1}^A \frac{1 + \tau_{zi}}{2} r_i^L Y_L^{\mu}(\hat{r}_i) \quad (7.38)$$

By changing from *c.m.* coordinates of the individual constituents to internal and *c.m.* coordinates of particle and target ($\mathbf{r}_i = \mathbf{R}_p + \xi_i^p$ and $\mathbf{r}_i = \mathbf{R}_t + \xi_i^t$), one obtains:

$$QE_L^\mu = \sum_{i=1}^{Z_p} (R_p + \xi_i^p)^L Y_L^\mu(\hat{R}_p) + \sum_{i=Z_p+1}^Z (R_t + \xi_i^t)^L Y_L^\mu(\hat{R}_t) \quad (7.39)$$

with Z_p and Z_t the particle and target charges respectively, and $Z = Z_p + Z_t$. In (7.39) we used the first order approximation in the spherical harmonics, eq. (E.6). For the coefficients of the spherical harmonics we can use the binomial expansion:

$$(R + \xi)^L = R^L + \sum_{n=1}^L \binom{L}{n} R^{L-n} \xi^n \quad (7.40)$$

With (7.40) into (7.39) one obtains:

$$\begin{aligned} QE_L^\mu &= Z_p R_p^L Y_L^\mu(\hat{R}_p) + \sum_{i=1}^{Z_p} \left(\sum_{n=1}^L \binom{L}{n} R_p^{L-n} (\xi_i^p)^n \right) Y_L^\mu(\hat{R}_p) \\ &+ Z_t R_t^L Y_L^\mu(\hat{R}_t) + \sum_{i=Z_p+1}^Z \left(\sum_{n=1}^L \binom{L}{n} R_t^{L-n} (\xi_i^t)^n \right) Y_L^\mu(\hat{R}_t) \end{aligned} \quad (7.41)$$

It is important to note that the odd powers of ξ in this expansion average out to zero, so that the expressions for the $E1$ and $E2$ transition operators simplify substantially:

$$QE_1^\mu = Z_p R_p Y_1^\mu(\hat{R}_p) + Z_t R_t Y_1^\mu(\hat{R}_t) \quad (7.42)$$

$$\begin{aligned} QE_2^\mu &= Z_p R_p^2 Y_2^\mu(\hat{R}_p) + \sum_{i=1}^{Z_p} (\xi_i^p)^2 Y_2^\mu(\hat{R}_p) \\ &+ Z_t R_t^2 Y_2^\mu(\hat{R}_t) + \sum_{i=Z_p+1}^Z (\xi_i^t)^2 Y_2^\mu(\hat{R}_t) \end{aligned} \quad (7.43)$$

Indeed, since the set of low lying states of a compact nucleus are almost always of the same parity there are no odd power couplings between these states.

Using the transformation of *c.m.* coordinates of particle and target to relative coordinates, R , and the properties (E.1) and (E.2) of the spherical harmonics, one obtains for the previous expressions:

$$\begin{aligned}
QE_1^\mu &= Z_p \frac{m_t}{M} RY_1^\mu(\hat{R}) - Z_t \frac{m_p}{M} RY_1^\mu(\hat{R}) \\
&= mR \left[\frac{Z_p}{m_p} - \frac{Z_t}{m_t} \right] Y_1^\mu(\hat{R})
\end{aligned} \tag{7.44}$$

$$\begin{aligned}
QE_2^\mu &= m^2 R^2 \left[\frac{Z_p}{m_p^2} + (-1)^2 \frac{Z_t}{m_t^2} \right] Y_2^\mu(\hat{R}) \\
&\quad + \sum_{i=1}^{Z_p} (\xi_i^p)^2 Y_2^\mu(\hat{R}_p) + \sum_{i=Z_p+1}^Z (\xi_i^t)^2 Y_2^\mu(\hat{R}_t) \\
&= QE_2^\mu(R) + QE_2^\mu(p) + QE_2^\mu(t)
\end{aligned} \tag{7.45}$$

where m_p and m_t are the particle and target masses, respectively, and m is the reduced mass of the system. In general, the main part of the electric transition operator has the form:

$$\begin{aligned}
QE_L^\mu(R) &= m^L R^L \left[\frac{Z_p}{m_p^L} + (-1)^L \frac{Z_t}{m_t^L} \right] Y_L^\mu(\hat{R}) \\
&\equiv C_L R^L Y_L^\mu(\hat{R})
\end{aligned} \tag{7.46}$$

The matrix element

From eqs. (7.5), (7.8), and (7.37), and considering only the main part of the interaction (7.46), one obtains for the matrix element

$$\begin{aligned}
&\langle \chi_{S_p''}^{M_p''} \chi_{S_t''}^{M_t''} \Psi_{J_f}^{M_f} | QE_L^\mu(\mathbf{R}) | \Phi_{J_i, S_p, S_t}^{M_i, M_p, M_t} \chi_{S_p'}^{M_p'} \chi_{S_t'}^{M_t'} \rangle_{\mathbf{r}_{1A}} \\
&= \frac{4\pi}{k_p} \sum_{S_p'', S_t'', j_f, L_f} \sum_{\substack{L_i, \mu_i, j_i, m_i \\ L_i', j_i', S_p', S_t'}} e^{i\sigma_{L_i}} Y_{L_i}^{\mu_i}(\hat{k}_p) i^{L_i'} (L_i \mu_i, S_p M_p | j_i m_i)(j_i m_i, S_t M_t | J_i M_i) \\
&\quad C_L \frac{(J_i M_i, L \mu | J_f M_f)}{\hat{J}_f} \int R^2 \frac{\psi_{\alpha_f}^{J_f}(R)}{R} R^L \frac{\phi_{\alpha_i, \alpha_i}^{J_i}(R)}{R} dR \\
&\quad \langle \chi_{S_p''}^{M_p''} \chi_{S_t''}^{M_t''} | \chi_{S_p'}^{M_p'} \chi_{S_t'}^{M_t'} \rangle_{\mathbf{r}_{1, p-1}}^{\mathbf{r}_{p+1, A-1}} \\
&\quad \langle (L_f S_p'') j_f S_t''; J_f M_f || Y_L(\hat{R}) || (L_i' S_p') j_i S_t'; J_i M_i \rangle_{\hat{\mathbf{R}}}
\end{aligned} \tag{7.47}$$

where we have used the Wigner-Eckart theorem (E.12) to obtain the reduced matrix element from the matrix element. Working out the reduced matrix element in terms of Racah algebra, eqs. (F.2–F.4), this can be written as:

$$\begin{aligned}
& \langle \chi_{S_p}^{M_p''} \chi_{S_t}^{M_t''} \Psi_{J_f}^{M_f} | Q E_L^\mu(\mathbf{R}) | \Phi_{J_i, S_p, S_t}^{M_i, M_p, M_t} \rangle_{\mathbf{r}_{1A}} \chi_{S_p}^{M_p'} \chi_{S_t}^{M_t'} \rangle_{\mathbf{r}_{1A}} \\
&= \frac{\sqrt{4\pi}}{k_p} \sum_{j_f, L_f} \sum_{L_i, \mu_i, j_i, m_i} e^{i\sigma_{L_i}} Y_{L_i}^{\mu_i}(\hat{k}_p) i^{L_i'} (L_i \mu_i, S_p M_p | j_i m_i) (j_i m_i, S_t M_t | J_i M_i) \\
& \quad C_L(J_i M_i, L \mu | J_f M_f) \int R^2 \frac{\psi_{\alpha_f}^{J_f}(R)}{R} R^L \frac{\phi_{\alpha_i, \alpha_i}^{J_i}(R)}{R} dR \\
& \quad \hat{J}_i \hat{j}_i \hat{j}_f \hat{L} \hat{L}_i \hat{L}_f (-1)^{S_p + S_t - j_i' - L_i' + L_f} \\
& \quad W(j_i' J_i j_f J_f; S_t L) W(L_i' j_i' L_f j_f; S_p L) \begin{pmatrix} L_f & L & L_i' \\ 0 & 0 & 0 \end{pmatrix} \quad (7.48)
\end{aligned}$$

7.3 Matrix element for ML transitions

The matrix element for magnetic transitions of specific multipolarity L is, from (7.18)

$$M_{f \leftarrow i}(M) = \mu \sqrt{2\pi} \hat{L} i^L \sum_{\nu} D_{\nu\mu}^L(\phi, \theta, 0) \int d^3r \langle \Psi_{J_f}^{M_f} | \mathbf{j}(\mathbf{r}) | \Phi_{J_i, S_p, S_t}^{M_i, M_p, M_t} \rangle \cdot \mathbf{A}_{L\nu}(\mathbf{r}; M) \quad (7.49)$$

Using the nuclear current from (7.24) and eq. (F.5), one obtains for the convection current contribution to the magnetic L multipole matrix element:

$$\begin{aligned}
M_{f \leftarrow i}^c(M) &= -\mu \sqrt{2\pi} \hat{L} i^L \sum_{\nu} D_{\nu\mu}^L(\phi, \theta, 0) \sum_{i=1}^A \frac{1 + \tau_{zi}}{2} \frac{e\hbar}{2m_i} \frac{2k^L}{\sqrt{L(L+1)}(2L+1)!!} \\
& \quad \int d^3r \left\{ \int (\Psi_{J_f}^{M_f*} \mathbf{L}_i \Phi_{J_i, S_p, S_t}^{M_i, M_p, M_t}) \cdot \nabla_i (r_i^L Y_L^\nu(\hat{r}_i)) \delta(\mathbf{r} - \mathbf{r}_i) d\mathbf{r}_{1A} \right\} \quad (7.50)
\end{aligned}$$

Analogously, using eq. (F.6), the magnetization current contribution to the magnetic L multipole matrix element is:

$$\begin{aligned}
M_{f \leftarrow i}^m(M) &= \mu \sqrt{2\pi} \hat{L} i^{L+1} \sum_{\nu} D_{\nu\mu}^L(\phi, \theta, 0) \sum_{i=1}^A \frac{e\hbar}{m_i} K_i \sqrt{\frac{L+1}{L}} \frac{k^L}{(2L+1)!!} \\
& \quad \int d^3r \left\{ \int (\Psi_{J_f}^{M_f*} \mathbf{S}_i \Phi_{J_i, S_p, S_t}^{M_i, M_p, M_t}) \cdot \nabla_i (r_i^L Y_L^\nu(\hat{r}_i)) \delta(\mathbf{r} - \mathbf{r}_i) d\mathbf{r}_{1A} \right\} \quad (7.51)
\end{aligned}$$

Transition rate

The transition rate for magnetic photo-emission of multipolarity L is, from eqs. (7.18), (7.37), (7.50) and (7.51):

$$T_{fi}(ML) = \frac{8\pi(L+1)}{L[(2L+1)!!]^2} \frac{k^{2L+1}}{\hbar} \left| \langle \chi_{S_p}^{M_p''} \chi_{S_t}^{M_t''} \Psi_{J_f}^{M_f} | QM_L^\mu + \tilde{Q}M_L^\mu | \Phi_{J_i, S_p, S_t}^{M_i, M_p, M_t} \chi_{S_p}^{M_p'} \chi_{S_t}^{M_t'} \rangle_{\mathbf{r}_{1A}} \right|^2 \quad (7.52)$$

with the generic form of the magnetic transition operators:

$$\begin{aligned} QM_L^\mu &= \frac{2}{L+1} \sum_{i=1}^A \frac{e\hbar}{2m_i c} \frac{1 + \tau_{zi}}{2} \mathbf{L}_i \cdot \nabla_i (r_i^L Y_L^\mu(\hat{r}_i)) \\ &= \frac{2\mu_N}{L+1} \sum_{i=1}^A \frac{p_{mass}}{m_i} \frac{1 + \tau_{zi}}{2} \mathbf{L}_i \cdot \nabla_i (r_i^L Y_L^\mu(\hat{r}_i)) \end{aligned} \quad (7.53)$$

$$\tilde{Q}M_L^\mu = \sum_{i=1}^A \frac{e\hbar}{m_i c} K_i \mathbf{S}_i \cdot \nabla_i (r_i^L Y_L^\mu(\hat{r}_i)) \quad (7.54)$$

where $\mu_N = \frac{e\hbar}{2p_{mass}c}$ is the nuclear magneton and p_{mass} is the mass of the proton. As in the case of electric transitions, we only use the dominant convective part, QM_L^μ , in the subsequent calculations of magnetic transitions.

Transition operator QM_L^μ

From (7.53) one can obtain in the expression for the transition operator in the two-body model:

$$QM_L^\mu = \frac{2\mu_N}{L+1} \left\{ \sum_{i=1}^{Z_p} \frac{p_{mass}}{m_p} \mathbf{L}_p \cdot \nabla_p (r_p^L Y_L^\mu(\hat{r}_p)) + \sum_{i=Z_p+1}^Z \frac{p_{mass}}{m_t} \mathbf{L}_t \cdot \nabla_t (r_t^L Y_L^\mu(\hat{r}_t)) \right\} \quad (7.55)$$

A more complex derivation of this expression that also yields, like in (7.41), the intrinsic terms of the transition operator can be done by changing from *c.m.* coordinates of the individual constituents to internal and *c.m.* coordinates of particle and target ($\mathbf{r}_i = \mathbf{R}_p + \xi_i^p$ and $\mathbf{r}_i = \mathbf{R}_t + \xi_i^t$) and noting that in the particle and target terms the relevant masses are the masses of the projectile and target (consistent with $g_L = Z_{p(t)} \frac{p_{mass}}{m_{p(t)}}$ from [Sam99]):

$$\begin{aligned}
QM_L^\mu &= \frac{2}{L+1} \left\{ \sum_{i=1}^{Z_p} \frac{e\hbar}{2m_p c} \mathbf{L}_i \cdot \nabla_i (r_i^L Y_L^\mu(\hat{r}_i)) + \sum_{i=Z_p+1}^{Z_p+Z_t} \frac{e\hbar}{2m_t c} \mathbf{L}_i \cdot \nabla_i (r_i^L Y_L^\mu(\hat{r}_i)) \right\} \\
&= \frac{2\mu_N p_{mass} \sqrt{L(2L+1)}}{L+1} \left\{ \frac{1}{m_p} \sum_{i=1}^{Z_p} (R_p + \xi_i^p)^L \mathbf{Y}_{L1,L-1}^\mu(R_p \hat{+} \xi_i^p) \cdot \mathbf{L}_{R_p + \xi_i^p} \right. \\
&\quad \left. + \frac{1}{m_t} \sum_{i=Z_p+1}^{Z_p+Z_t} (R_t + \xi_i^t)^L \mathbf{Y}_{L1,L-1}^\mu(R_t \hat{+} \xi_i^t) \cdot \mathbf{L}_{R_t + \xi_i^t} \right\} \tag{7.56}
\end{aligned}$$

where we have used the approximation

$$\nabla_i (r_i^L Y_L^\mu(\hat{r}_i)) = \sqrt{L(2L+1)} r_i^{L-1} \mathbf{Y}_{L1,L-1}^\mu(\hat{r}_i) \tag{7.57}$$

With the approximation for the vector spherical harmonics analogous to (E.6), and using (7.40) and

$$\begin{aligned}
\mathbf{L}_{R_{p(t)} + \xi_i^{p(t)}} &= (\mathbf{R}_{p(t)} + \xi_i^{p(t)}) \times (\mathbf{p}_{p(t)} + \mathbf{p}_{\xi_i^{p(t)}}^{p(t)}) \\
&\approx \mathbf{R}_{p(t)} \times \mathbf{p}_{p(t)} = \mathbf{L}_{p(t)} \tag{7.58}
\end{aligned}$$

one can obtain for (7.56)

$$\begin{aligned}
QM_L^\mu &= \frac{2\mu_N p_{mass} \sqrt{L(2L+1)}}{L+1} \left\{ \frac{Z_p}{m_p} R_p^{L-1} \mathbf{Y}_{L1,L-1}^\mu(\hat{R}_p) \cdot \mathbf{L}_p + \frac{Z_t}{m_t} R_t^{L-1} \mathbf{Y}_{L1,L-1}^\mu(\hat{R}_t) \cdot \mathbf{L}_t \right. \\
&\quad + \frac{1}{m_p} \sum_{i=1}^{Z_p} \left(\sum_{n=1}^{L-1} \binom{L-1}{n} R_p^{L-1-n} (\xi_i^p)^n \right) \mathbf{Y}_{L1,L-1}^\mu(\hat{r}_i) \cdot \mathbf{L}_p \\
&\quad \left. + \frac{1}{m_t} \sum_{i=Z_p+1}^{Z_p+Z_t} \left(\sum_{n=1}^{L-1} \binom{L-1}{n} R_t^{L-1-n} (\xi_i^t)^n \right) \mathbf{Y}_{L1,L-1}^\mu(\hat{r}_i) \cdot \mathbf{L}_t \right\} \\
&= \frac{2\mu_N p_{mass} \sqrt{L(2L+1)}}{L+1} \left\{ \frac{Z_p}{m_p} \left(\frac{m_t}{M} \right)^L R^{L-1} \mathbf{Y}_{L1,L-1}^\mu(\hat{R}) \cdot \mathbf{L}_R \right. \\
&\quad - (-1)^L \frac{Z_t}{m_t} \left(\frac{m_p}{M} \right)^L R^{L-1} \mathbf{Y}_{L1,L-1}^\mu(\hat{R}) \cdot \mathbf{L}_R \\
&\quad + \frac{1}{m_p} \sum_{i=1}^{Z_p} \left(\sum_{n=1}^{L-1} \binom{L-1}{n} R_p^{L-1-n} (\xi_i^p)^n \right) \mathbf{Y}_{L1,L-1}^\mu(\hat{r}_i) \cdot \mathbf{L}_p \\
&\quad \left. + \frac{1}{m_t} \sum_{i=Z_p+1}^{Z_p+Z_t} \left(\sum_{n=1}^{L-1} \binom{L-1}{n} R_t^{L-1-n} (\xi_i^t)^n \right) \mathbf{Y}_{L1,L-1}^\mu(\hat{r}_i) \cdot \mathbf{L}_t \right\} \\
&= QM_L^\mu(R) + QM_L^\mu(p) + QM_L^\mu(t) \tag{7.59}
\end{aligned}$$

where $QM_L^\mu(R)$ has the form:

$$\begin{aligned}
QM_L^\mu(R) &= \frac{2\mu_N p_{mass} \sqrt{L(2L+1)}}{L+1} R^{L-1} \mathbf{Y}_{L1,L-1}^\mu(\hat{R}) \cdot \mathbf{L}_R \\
&\quad \left\{ \frac{Z_p}{m_p} \left(\frac{m_t}{M}\right)^L - (-1)^L \frac{Z_t}{m_t} \left(\frac{m_p}{M}\right)^L \right\} \\
&= \frac{2\mu_N p_{mass}}{L+1} \nabla_R \left(R^L Y_L^\mu(\hat{R}) \right) \cdot \mathbf{L}_R \\
&\quad \left\{ \frac{Z_p}{m_p} \left(\frac{m_t}{M}\right)^L - (-1)^L \frac{Z_t}{m_t} \left(\frac{m_p}{M}\right)^L \right\} \\
&= \frac{2\mu_N}{L+1} \nabla_R \left(R^L Y_L^\mu(\hat{R}) \right) \cdot \mathbf{L}_R C_L^m
\end{aligned} \tag{7.60}$$

with

$$C_L^m = p_{mass} m^L \left\{ \frac{Z_p}{m_p^{L+1}} - (-1)^L \frac{Z_t}{m_t^{L+1}} \right\} \tag{7.61}$$

The matrix element

Considering only the first term of the interaction, $QM_L^\mu(R)$, from (7.60) and the wave functions for the initial and final states from (7.5) and (7.8), one obtains for the matrix element in (7.52):

$$\begin{aligned}
&\langle \chi_{S_p''}^{M_p''} \chi_{S_t''}^{M_t''} \Psi_{J_f}^{M_f} | QM_L^\mu(\mathbf{R}) | \Phi_{J_i, S_p, S_t}^{M_i, M_p, M_t} \chi_{S_p'}^{M_p'} \chi_{S_t'}^{M_t'} \rangle_{\mathbf{r}_{1A}} \\
&= \frac{4\pi}{k_p} \sum_{S_p'', S_t'', j_f, L_f} \sum_{L_i, \mu_i, j_i, m_i}^{L_i, \mu_i, j_i, m_i} e^{i\sigma_{L_i}} Y_{L_i}^{\mu_i}(\hat{k}_p) i^{L_i} (L_i \mu_i, S_p M_p | j_i m_i)(j_i m_i, S_t M_t | J_i M_i) \\
&\quad \frac{2\mu_N}{L+1} C_L^m \frac{(J_i M_i, L \mu | J_f M_f)}{\hat{J}_f} \int R^2 \frac{\psi_{\alpha_f}^{J_f}(R)}{R} R^{L-1} \frac{\phi_{\alpha_i, \alpha_i}^{J_i}(R)}{R} dR \\
&\quad \langle \chi_{S_p''}^{M_p''} \chi_{S_t''}^{M_t''} | \chi_{S_p'}^{M_p'} \chi_{S_t'}^{M_t'} \rangle_{\mathbf{r}_{1,p-1}} \sqrt{L(2L+1)} \\
&\quad \langle (L_f S_p'') j_f S_t''; J_f M_f || \left[\mathbf{Y}_{L1,L-1}(\hat{R}) \cdot \mathbf{L}_R \right] || (L_i' S_p') j_i S_t'; J_i M_i \rangle_{\hat{\mathbf{R}}}
\end{aligned} \tag{7.62}$$

where we have used the Wigner-Eckart theorem (E.12) to obtain the reduced matrix element from the matrix element. Working out the reduced matrix element in terms of Racah algebra, eqs. (F.7–F.10) of appendix F, one obtains for the matrix element:

$$\begin{aligned}
& \langle \chi_{S_p''}^{M_p''} \chi_{S_t''}^{M_t''} \Psi_{J_f}^{M_f} | Q M_L^\mu(\mathbf{R}) | \Phi_{J_i, S_p, S_t}^{M_i, M_p, M_t} \rangle_{\mathbf{r}_{1A}} \chi_{S_p'}^{M_p'} \chi_{S_t'}^{M_t'} \rangle_{\mathbf{r}_{1A}} \\
&= \frac{4\pi}{k_p} \sum_{j_f, L_f} \sum_{\substack{L_i, \mu_i, j_i, m_i \\ L_i', j_i'}} e^{i\sigma_{L_i}} Y_{L_i}^{\mu_i}(\hat{k}_p) i^{L_i'} (L_i \mu_i, S_p M_p | j_i m_i) (j_i m_i, S_t M_t | J_i M_i) \\
&\quad \frac{2\mu_N}{L+1} C_L^m (J_i M_i, L \mu | J_f M_f) \int R^2 \frac{\psi_{\alpha_f}^{J_f}(R)}{R} R^{L-1} \frac{\phi_{\alpha_i', \alpha_i}^{J_i}(R)}{R} dR \\
&\quad \hat{J}_i \hat{j}_i \hat{j}_f (-1)^{S_p + S_t - j_i' - j_f - L_i' - J_f} W(j_i' J_i j_f J_f; S_t L) W(L_i' j_i' L_f j_f; S_p L) \\
&\quad \frac{(2L_i' + 1)(k - 1)\hat{k}\sqrt{L_i'(L_i' + 1)}}{\sqrt{4\pi}} (L_f 0, L - 10 | L_i' 0) W(L_i' 1 L_f L - 1; L_i' L) \quad (7.63)
\end{aligned}$$

7.4 The cross section

The cross section for electric (magnetic) transitions is obtained by dividing the transition rate, (7.37) and (7.52), by the incident flux v :

$$\begin{aligned}
\sigma_{if}(E(M)L) &= \frac{8\pi(L+1)}{L[(2L+1)!!]^2} \frac{k^{2L+1}}{\hbar v} \\
&\quad \left| \langle \chi_{S_p''}^{M_p''} \chi_{S_t''}^{M_t''} \Psi_{J_f}^{M_f} | Q E(M)_L^\mu + Q \tilde{E}(M)_L^\mu | \Phi_{J_i, S_p, S_t}^{M_i, M_p, M_t} \chi_{S_p'}^{M_p'} \chi_{S_t'}^{M_t'} \rangle_{\mathbf{r}_{1A}} \right|^2 \\
&= \frac{8\pi(L+1)}{L[(2L+1)!!]^2} \frac{mc^2}{(\hbar c)^2} \frac{k^{2L+1}}{k_p} \\
&\quad \left| \langle \chi_{S_p''}^{M_p''} \chi_{S_t''}^{M_t''} \Psi_{J_f}^{M_f} | Q E(M)_L^\mu + Q \tilde{E}(M)_L^\mu | \Phi_{J_i, S_p, S_t}^{M_i, M_p, M_t} \chi_{S_p'}^{M_p'} \chi_{S_t'}^{M_t'} \rangle_{\mathbf{r}_{1A}} \right|^2 \quad (7.64)
\end{aligned}$$

With the matrix elements for electric and magnetic multipole operators, (7.48) and (7.63) respectively, one obtains for the cross section for electric EL transitions and magnetic ML transitions:

$$\begin{aligned}
\sigma_{if}(EL) &= \frac{8\pi(L+1)}{L[(2L+1)!!]^2} \frac{mc^2}{(\hbar c)^2} \frac{k^{2L+1}}{k_p^3} \frac{(eC_L)^2}{(2S_p+1)(2S_t+1)} \sum_{\substack{M_p M_t \\ \mu M_i M_f}} \\
&\left| \sqrt{4\pi} \sum_{j_f, L_f} \sum_{\substack{L_i, \mu_i, j_i, m_i \\ L'_i, j'_i}} e^{i\sigma_{L_i}} Y_{L_i}^{\mu_i}(\hat{k}_p) i^{L'_i} \int R^2 \frac{\psi_{\alpha_f}^{J_f}(R)}{R} R^L \frac{\phi_{\alpha'_i, \alpha_i}^{J_i}(R)}{R} dR \right. \\
&(J_i M_i, L \mu | J_f M_f)(L_i \mu_i, S_p M_p | j_i m_i)(j_i m_i, S_t M_t | J_i M_i) \\
&W(j'_i J_i j_f J_f; S_t L) W(L'_i j'_i L_f j_f; S_p L) \begin{pmatrix} L_f & L & L'_i \\ 0 & 0 & 0 \end{pmatrix} \\
&\left. \hat{J}_i \hat{j}'_i \hat{j}_f \hat{L} \hat{L}'_i \hat{L}_f (-1)^{S_p+S_t-j'_i-L'_i+L_f} \right|^2 \quad (7.65)
\end{aligned}$$

$$\begin{aligned}
\sigma_{if}(ML) &= \frac{8\pi(L+1)}{L[(2L+1)!!]^2} \frac{mc^2}{(\hbar c)^2} \frac{k^{2L+1}}{k_p^3} \frac{(\mu_N C_L^m)^2}{(2S_p+1)(2S_t+1)} \sum_{\substack{M_p M_t \\ \mu M_i M_f}} \\
&\left| \frac{2\sqrt{4\pi}}{L+1} \sum_{j_f, L_f} \sum_{\substack{L_i, \mu_i, j_i, m_i \\ L'_i, j'_i}} e^{i\sigma_{L_i}} Y_{L_i}^{\mu_i}(\hat{k}_p) i^{L'_i} \int R^2 \frac{\psi_{\alpha_f}^{J_f}(R)}{R} R^{L-1} \frac{\phi_{\alpha'_i, \alpha_i}^{J_i}(R)}{R} dR \right. \\
&(J_i M_i, L \mu | J_f M_f)(L_i \mu_i, S_p M_p | j_i m_i)(j_i m_i, S_t M_t | J_i M_i)(L_f 0, L-10 | L'_i 0) \\
&W(L'_i 1 L_f L-1; L'_i L) W(j'_i J_i j_f J_f; S_t L) W(L'_i j'_i L_f j_f; S_p L) \hat{J}_i \hat{j}'_i \hat{j}_f \\
&\left. (-1)^{S_p+S_t-j'_i-j_f-L'_i-J_f} (2L'_i+1) (L-1) (2L+1) \sqrt{L} \sqrt{L'_i(L'_i+1)} \right|^2 \quad (7.66)
\end{aligned}$$

respectively.

Summing (7.65) and (7.66) over the angular momentum and spin projections one obtains finally:

$$\begin{aligned}
\sigma_{if}(EL) &= \frac{8\pi(L+1)(2L+1)}{L[(2L+1)!!]^2} \frac{mc^2}{(\hbar c)^2} \frac{k^{2L+1}}{k_p^3} \frac{(2J_i+1)(2J_f+1)}{(2S_p+1)(2S_t+1)} (eC_L)^2 \\
&\sum_{j_f, L_f} \left| \sum_{L_i j_i, L'_i j'_i} e^{i\sigma_{L_i}} i^{L'_i} (-1)^{j'_i-L'_i-j_f} \int R^2 \frac{\psi_{\alpha_f}^{J_f}(R)}{R} R^L \frac{\phi_{\alpha'_i, \alpha_i}^{J_i}(R)}{R} dR \right. \\
&\left. \hat{j}'_i \hat{j}_f \hat{L}_f W(j'_i J_i j_f J_f; S_t L) W(L'_i j'_i L_f j_f; S_p L) (L_f 0, L_0 | L'_i 0) \right|^2 \quad (7.67)
\end{aligned}$$

$$\begin{aligned}
\sigma_{if}(ML) = & \frac{8\pi(L+1)(2L+1)}{L[(2L+1)!!]^2} \frac{mc^2}{(\hbar c)^2} \frac{k^{2L+1}}{k_p^3} \frac{(2J_i+1)(2J_f+1)}{(2S_p+1)(2S_t+1)} (\mu_N C_L^m)^2 \\
& \sum_{j_f, L_f} \left| \sum_{L_i j_i, L_i' j_i'} e^{i\sigma_{L_i}} i^{L_i'} (-1)^{j_i' - L_i' - j_f} \int R^2 \frac{\psi_{\alpha_f}^{J_f}(R)}{R} R^{L-1} \frac{\phi_{\alpha_i, \alpha_i}^{J_i}(R)}{R} dR \right. \\
& \frac{2 \hat{j}_i' \hat{j}_f (2L_i' + 1) (L - \hat{1}) \hat{L} \sqrt{L} \sqrt{L_i'(L_i' + 1)}}{L + 1} (L_f 0, L - 10 | L_i' 0) \\
& \left. W(j_i' J_i j_f J_f; S_i L) W(L_i' j_i' L_f j_f; S_p L) W(L_i' 1 L_f L - 1; L_i' L) \right|^2 \quad (7.68)
\end{aligned}$$

Chapter 8

The coupling interactions

In the previous chapter we calculated the cross section expressions for magnetic ML and electric EL radiative capture cross sections. In this chapter we will obtain the form of the photonuclear couplings that allow the calculation of these cross section in the coupled channels framework. By calculating the coupling interactions we are able to calculate the cross sections with two equivalent methods: coupled channels and T-matrix. We start, however, by writing the photon equation from Maxwell's equations, and justifying the choice of $c_\tau = -\frac{E}{k^2}$ gamma channels introduced in chapter 2.

8.1 The photon equation

Maxwell's electromagnetic field equations are [Ros58]:

$$\nabla \times \hat{\mathbf{H}} = \frac{4\pi}{c} \hat{\mathbf{j}} + \frac{1}{c} \frac{d\hat{\mathbf{E}}}{dt} \quad (8.1)$$

$$\nabla \times \hat{\mathbf{E}} = -\frac{1}{c} \frac{d\hat{\mathbf{H}}}{dt} \quad (8.2)$$

$$\nabla \cdot \hat{\mathbf{H}} = 0 \quad (8.3)$$

$$\nabla \cdot \hat{\mathbf{E}} = 4\pi \hat{\rho} \quad (8.4)$$

where hats indicate real observed quantities. For monochromatic radiation of frequency ω we introduce complex, time-independent, amplitudes. For the field strengths we write:

$$\hat{\mathbf{H}}_\omega(\mathbf{r}, t) = \mathbf{H}_\omega(\mathbf{r})e^{-i\omega t} + \mathbf{H}_\omega^*(\mathbf{r})e^{i\omega t} \quad (8.5)$$

$$\hat{\mathbf{E}}_\omega(\mathbf{r}, t) = \mathbf{E}_\omega(\mathbf{r})e^{-i\omega t} + \mathbf{E}_\omega^*(\mathbf{r})e^{i\omega t} \quad (8.6)$$

and for the current and charged densities we introduce

$$\hat{\mathbf{j}}_\omega(\mathbf{r}, t) = \mathbf{j}_\omega(\mathbf{r})e^{-i\omega t} + \mathbf{j}_\omega^*(\mathbf{r})e^{i\omega t} \quad (8.7)$$

$$\hat{\rho}_\omega(\mathbf{r}, t) = \rho_\omega(\mathbf{r})e^{-i\omega t} + \rho_\omega^*(\mathbf{r})e^{i\omega t} \quad (8.8)$$

In the following discussion the subscript ω will be dropped. Introducing the wave number $k=\omega/c$, Maxwell's equations became:

$$\nabla \times \mathbf{H} = \frac{4\pi}{c}\mathbf{j} - ik\mathbf{E} \quad (8.9)$$

$$\nabla \times \mathbf{E} = ik\mathbf{H} \quad (8.10)$$

$$\nabla \cdot \mathbf{H} = 0 \quad (8.11)$$

$$\nabla \cdot \mathbf{E} = 4\pi\rho \quad (8.12)$$

We can obtain equations for \mathbf{E} and \mathbf{H} alone by eliminating one or the other of the fields from (8.9) and (8.10). We get

$$\nabla \times \nabla \times \mathbf{H} - k^2\mathbf{H} = \frac{4\pi}{c}\nabla \times \mathbf{j} \quad (8.13)$$

$$\nabla \times \nabla \times \mathbf{E} - k^2\mathbf{E} = \frac{4\pi ik}{c}\mathbf{j} \quad (8.14)$$

In a source-free region, the Maxwell's electromagnetic field equations are:

$$\nabla \times \mathbf{H} = - ik\mathbf{E} \quad (8.15)$$

$$\nabla \times \mathbf{E} = ik\mathbf{H} \quad (8.16)$$

$$\nabla \cdot \mathbf{H} = 0 \quad (8.17)$$

$$\nabla \cdot \mathbf{E} = 0 \quad (8.18)$$

Vector and scalar potentials

It is usual to introduce the vector potential $\hat{\mathbf{A}}$, as implied by (8.3):

$$\hat{\mathbf{H}} = \nabla \times \hat{\mathbf{A}} \quad (8.19)$$

and with (8.2) we can use a scalar potential $\hat{\phi}$, such that

$$\hat{\mathbf{E}} = -\nabla\hat{\phi} - \frac{1}{c}\frac{d\hat{\mathbf{A}}}{dt} \quad (8.20)$$

As before, we can write the vector and scalar potentials as

$$\hat{\mathbf{A}}(\mathbf{r}, t) = \mathbf{A}(\mathbf{r})e^{-i\omega t} + \mathbf{A}^*(\mathbf{r})e^{i\omega t} \quad (8.21)$$

$$\hat{\phi}(\mathbf{r}, t) = \phi(\mathbf{r})e^{-i\omega t} + \phi^*(\mathbf{r})e^{i\omega t} \quad (8.22)$$

which allow us to write (8.19) and (8.20) as:

$$\mathbf{H} = \nabla \times \mathbf{A} \quad (8.23)$$

$$\mathbf{E} = -\nabla\phi + ik\mathbf{A} \quad (8.24)$$

The gauge transformation

The electric and magnetic fields are therefore determined by the vector and scalar potentials. On the other hand, the fields do not completely determine the potential, since any scalar function S can be introduced such that \mathbf{A}_τ and ϕ_τ , defined by

$$\mathbf{A}_\tau = \mathbf{A} + \nabla S \quad (8.25)$$

$$\phi_\tau = \phi + ikS \quad (8.26)$$

are satisfactory vector and scalar potentials if \mathbf{A} and ϕ are. That is, Maxwell's equations (8.9–8.12) are invariant to the introduction of the function S , which is called a gauge transformation. The substitution of (8.25) and (8.26) into (8.9) and (8.10) yields the following equations for \mathbf{A} and ϕ

$$\nabla^2 \mathbf{A} + k^2 \mathbf{A} = -\frac{4\pi}{c} \mathbf{j} + \nabla(\nabla \cdot \mathbf{A} - ik\phi) \quad (8.27)$$

$$\nabla^2 \phi = -4\pi\rho + ik(\nabla \cdot \mathbf{A}) \quad (8.28)$$

The freedom implied by (8.25) and (8.26) means that we can choose the vector field such that

$$\nabla \cdot \mathbf{A} = 0 \quad (8.29)$$

which is the so-called Coulomb or transverse gauge. From (8.28) we see that the scalar potential satisfies Poisson's equation

$$\nabla^2 \phi = -4\pi\rho \quad (8.30)$$

while the vector potential satisfies the inhomogeneous wave equation

$$\nabla^2 \mathbf{A} + k^2 \mathbf{A} = -\frac{4\pi}{c} \mathbf{j} - ik\nabla\phi \quad (8.31)$$

The Coulomb or transverse gauge is often used when no sources are present. In source-free regions, $\rho=0$ and $\mathbf{j}=0$ over some part of the space, the vector and scalar potentials are solutions of the homogeneous vector and scalar Helmholtz equations

$$\nabla^2 \mathbf{A} + k^2 \mathbf{A} = 0 \quad (8.32)$$

$$\nabla^2 \phi + k^2 \phi = 0 \quad (8.33)$$

Multipole fields

The vector field $\mathbf{A}(\mathbf{r})$ can be expanded into a series:

$$\mathbf{A}(\mathbf{r}) = \sum_{J=0}^{\infty} \sum_{M=-J}^J \mathbf{A}_J^M(\mathbf{r}) \quad (8.34)$$

where each term $\mathbf{A}_J^M(\mathbf{r})$ is a pure multipole field and is an eigenfunction of the operators J^2 and J_z .

Since the vector spherical harmonics form a complete set of basis functions, one can write a pure multipole field as

$$\mathbf{A}_J^M(\mathbf{r}) = \sum_{L=J, J\pm 1} F_{LJ}(r) \mathbf{Y}_{JL1}^M \quad (8.35)$$

It is useful to define the radial function $f_{LJ}(r)$ as

$$F_{LJ}(r) = r^{-1} f_{LJ}(r) \quad (8.36)$$

which, in the case of the photon in the exit channel, as the asymptotic form:

$$f_{LJ}(r) \cong \frac{i}{2} S_{LJ}^\gamma H_L^+(kr) \quad (\text{for } r \rightarrow \infty) \quad (8.37)$$

where S_{LJ}^γ is the S-matrix and $H_L^+(r)$ the Hankel function. In the case of the photon in the entrance channel with L_0 and J_0 , the boundary condition is:

$$f_{LJ}^{L_0 J_0}(r) \cong \frac{i}{2} (H_L^-(kr) \delta_{L_0 L} \delta_{J_0 J} - S_{LJ, L_0 J_0}^p H_L^+(kr)) \quad (\text{for } r \rightarrow \infty) \quad (8.38)$$

Photon equation

The time independent wave equation for the \mathbf{A} field equation is:

$$\nabla^2 \mathbf{A} + k^2 \mathbf{A} = -\tilde{\mathbf{j}} \quad (8.39)$$

for some source term $\tilde{\mathbf{j}}$, which will be discussed in detail in the next section. Using eqs. (8.34) and (8.35) the wave equation can be written as

$$\sum_{L=J, J\pm 1} \{\nabla_{r,L}^2 + k^2\} \frac{f_{LJ}(r)}{r} \mathbf{Y}_{JL1}^M(\mathbf{r}) = -\tilde{\mathbf{j}} \quad (8.40)$$

Acting on the left with $\mathbf{Y}_{JL'1}^{M'}(\mathbf{r})$ one obtains:

$$\{\nabla_{r,L'}^2 + k^2\} \frac{f_{L'J}(r)}{r} = -\langle \mathbf{Y}_{JL'1}^{M'}(\mathbf{r}) | \tilde{\mathbf{j}} \rangle \quad (8.41)$$

where the right side involves an integration over angular coordinates. Using

$$\{\nabla_{r,L}^2 + k^2\} \frac{f(r)}{r} = \frac{1}{r} \left\{ \frac{d^2}{dr^2} - \frac{L(L+1)}{r^2} + k^2 \right\} f(r)$$

in (8.41) one obtains finally:

$$\left\{ \frac{d^2}{dr^2} - \frac{L'(L'+1)}{r^2} + k^2 \right\} f_{L'J}(r) = - \langle \mathbf{Y}_{JL'1}^{M'}(\mathbf{r}) | \tilde{\mathbf{j}} \rangle \quad (8.42)$$

By multiplying the previous equation by $c_\tau = -\frac{E}{k^2}$ (which has the same dimensions as $\frac{\hbar^2}{2\mu}$, MeV.fm²), one obtains an equation,

$$c_\tau \left\{ \frac{d^2}{dr^2} - \frac{L'(L'+1)}{r^2} + k^2 \right\} f_{L'J}(r) = -c_\tau \langle \mathbf{Y}_{JL'1}^{M'}(\mathbf{r}) | \tilde{\mathbf{j}} \rangle \quad (8.43)$$

where the left side has the same dimensions as the Schrödinger equation. This allows us to treat the photon equation on an equal footing with the particle equation in the coupled channels framework, and is the basis of the next section where we determine the right side of eq. (8.43) from the expressions of chapter 7.

8.2 Electric and magnetic couplings

From (1.53) one obtains for the case of photons in the final state:

$$\begin{aligned} \sigma_{if} &= \frac{4\pi}{k_i^2} \frac{v_f}{v_i} g_{J_i} |\mathcal{T}_{L_f J_f, L_i J_i}^{J_i}|^2 \\ &= \frac{4\pi}{k_i^2} \frac{m_i c^2}{(\hbar c) k_i} \frac{2J_i + 1}{(2S_p + 1)(2S_t + 1)} |\mathcal{T}_{L_f J_f, L_i J_i}^{J_i}|^2 \end{aligned} \quad (8.44)$$

since the total angular momentum J in (1.53) is $J \equiv J_i$.

On the other hand, the radial integral in the cross section expression (7.67) can be written as

$$\begin{aligned} & \frac{1}{k} \frac{k^{2L+2}}{[(2L+1)!!]^2} \left\{ \int \frac{\psi_{\alpha_f}^{J_f}(R)}{R} R^{L+1} \phi_{\alpha_i, \alpha_i}^{J_i}(R) dR \right\}^2 \\ &= \frac{1}{k} \left\{ \frac{k^{L+1}}{(2L+1)!!} \int \frac{\psi_{\alpha_f}^{J_f}(R)}{R} R^{L+1} \phi_{\alpha_i, \alpha_i}^{J_i}(R) dR \right\}^2 \\ &= \frac{1}{k} \left\{ \int F_L(kR) \frac{\psi_{\alpha_f}^{J_f}(R)}{R} \phi_{\alpha_i, \alpha_i}^{J_i}(R) dR \right\}^2 \end{aligned} \quad (8.45)$$

where the long wavelength approximation for $F_L(kR)$ was used. One can therefore write the radiative capture cross section for electric EL transitions, (7.67), in the form:

$$\begin{aligned}
\sigma_{if}(EL) &= \frac{(2J_i + 1)(2J_f + 1)}{(2S_p + 1)(2S_t + 1)} \frac{8\pi(L + 1)(2L + 1)}{L} \frac{k}{k_p^3} \frac{mc^2}{(\hbar c)} \alpha \\
&\left| -\frac{1}{k} \int dR F_L(kR) \left\{ \sum_{\substack{L_f j_f, L_i j_i \\ L'_i j'_i}} e^{i\sigma_{L_i}} i^{L'_i} \hat{j}'_i \hat{j}_f \hat{L}_f (-1)^{j'_i - L'_i - j_f} (L_f 0, L 0 | L'_i 0) \right. \right. \\
&\quad \left. \left. C_L W(j'_i J_i j_f J_f; S_t L) W(L'_i j'_i L_f j_f; S_p L) \frac{\psi_{\alpha_f}^{J_f}(R)}{R} \phi_{\alpha'_i, \alpha_i}^{J_i}(R) \right\} \right|^2 \\
&= 4\pi \frac{1}{k_p^3} \frac{mc^2}{\hbar c} \frac{(2J_i + 1)}{(2S_p + 1)(2S_t + 1)} \left[(2J_f + 1) \frac{2(L + 1)(2L + 1)}{L} \alpha k \right. \\
&\quad \left. \left| -\frac{1}{k} \int dR F_L(kR) \left\{ \sum_{\substack{L_f j_f, L_i j_i \\ L'_i j'_i}} e^{i\sigma_{L_i}} i^{L'_i} \hat{j}'_i \hat{j}_f \hat{L}_f (-1)^{j'_i - L'_i - j_f} (L_f 0, L 0 | L'_i 0) \right. \right. \right. \\
&\quad \left. \left. \left. C_L W(j'_i J_i j_f J_f; S_t L) W(L'_i j'_i L_f j_f; S_p L) \frac{\psi_{\alpha_f}^{J_f}(R)}{R} \phi_{\alpha'_i, \alpha_i}^{J_i}(R) \right\} \right|^2 \right] \quad (8.46)
\end{aligned}$$

which has the same form as (8.44).

The T-matrix is defined as [Rod67]:

$$\mathcal{T}_L = -\frac{1}{k} \int dR F_L(kR) S(R) \quad (8.47)$$

so the source term, $S(R)$, can be written in the form:

$$\begin{aligned}
S &= \left[(2J_f + 1) \frac{2(L + 1)(2L + 1)}{L} \alpha k \right]^{\frac{1}{2}} \\
&\quad \sum_{\substack{L_f j_f, L_i j_i \\ L'_i j'_i}} e^{i\sigma_{L_i}} i^{L'_i} \hat{j}'_i \hat{j}_f \hat{L}_f (-1)^{j'_i - L'_i - j_f} (L_f 0, L 0 | L'_i 0) \\
&\quad C_L W(j'_i J_i j_f J_f; S_t L) W(L'_i j'_i L_f j_f; S_p L) \frac{\psi_{\alpha_f}^{J_f}(R)}{R} \phi_{\alpha'_i, \alpha_i}^{J_i}(R) \quad (8.48)
\end{aligned}$$

With the source term, S , we can then write the photon equation:

$$c_\gamma \left\{ \frac{d^2}{dR^2} - \frac{L(L + 1)}{R^2} + k^2 \right\} \chi_L(R) = \sum_{L'_i j'_i} V_{L'_i j'_i}^e(R) \phi_{\alpha'_i, \alpha_i}^{J_i}(R) \quad (8.49)$$

where $c_\gamma = -\frac{E}{k^2}$, and

$$\begin{aligned}
V_{fi}^e &= \left[(2J_f + 1) \frac{2(L+1)(2L+1)}{L} \alpha k \right]^{\frac{1}{2}} c_\gamma \\
&\sum_{L_f j_f, L_i j_i} e^{i\sigma_{L_i}} \hat{i}^{L_i'} \hat{j}_i' \hat{j}_f \hat{L}_f (-1)^{j_i' - L_i' - j_f} (L_f 0, L 0 | L_i' 0) \\
&C_L W(j_i' J_i j_f J_f; S_t L) W(L_i' j_i' L_f j_f; S_p L) \frac{\psi_{\alpha_f}^{J_f}(R)}{R}
\end{aligned} \tag{8.50}$$

is the coupling interaction.

In the case of the magnetic ML transitions, proceeding analogously from (7.68) one obtains the photon equation:

$$c_\gamma \left\{ \frac{d^2}{dR^2} - \frac{L(L-1)}{R^2} + k^2 \right\} \chi_L(R) = \sum_{L_i', j_i'} V_{L_i' j_i'}^m(R) \phi_{\alpha_i', \alpha_i}^{J_i}(R) \tag{8.51}$$

where we have used the LWA for $F_{L-1}(kR)$. The coupling interaction for magnetic ML transitions is

$$\begin{aligned}
V_{fi}^m &= \left[(2J_f + 1) \frac{2(L+1)(2L+1)}{L} \frac{\mu_N^2}{\hbar c} k^3 \right]^{\frac{1}{2}} c_\gamma \\
&\sum_{L_f j_f, L_i j_i} e^{i\sigma_{L_i}} \hat{i}^{L_i'} \frac{2 \hat{j}_i' \hat{j}_f (2L_i' + 1) (L - \hat{1}) \hat{L} \sqrt{L} \sqrt{L_i'(L_i' + 1)}}{(L+1)(2L+1)} \\
&(-1)^{j_i' - L_i' - j_f} (L_f 0, L - 10 | L_i' 0) C_L^m \\
&W(j_i' J_i j_f J_f; S_t L) W(L_i' j_i' L_f j_f; S_p L) W(L_i' 1 L_f L - 1; L_i' L) \frac{1}{R} \frac{\psi_{\alpha_f}^{J_f}(R)}{R}
\end{aligned} \tag{8.52}$$

8.3 Implementation

The calculation of electric and magnetic radiative capture cross sections through the solution of the coupled equations with the coupling interactions (8.50) and (8.52), respectively, is equivalent to calculating these cross sections with eqs. (7.67) and (7.68). These two methods were implemented and the results for $E1$ and $E2$ radiative capture in the ${}^7\text{Li}(p,\gamma){}^8\text{Be}$ and ${}^{12}\text{C}(\alpha,\gamma){}^{16}\text{O}$ reactions are compared in Figures 8.1–8.4.

The scattering and bound state wave functions necessary for the calculation of the cross section from (7.67) were obtained with optical potentials. In order to generate the bound state the potential depths were adjusted to reproduce the binding energies of the ^{16}O and ^8Be ground states, 7.16 and 17.25 MeV respectively; these wave functions were obtained with the code FRESKO [Tho04]. The same potential radius and diffuseness were used to obtain the bound state necessary in the cross section calculation through the coupling interaction (8.50). The potentials used in these calculations are not realistic potentials and the cross sections obtained are not intended to reproduce available experimental data but only to demonstrate the equivalence of the methods.

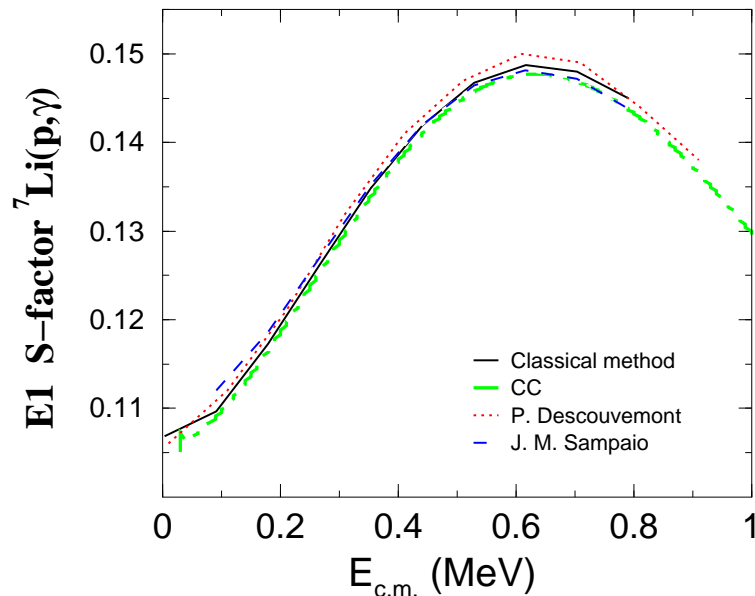


Figure 8.1: S-factor for $E1$ radiative capture in the $^7\text{Li}(p,\gamma)^8\text{Be}$ reaction. Comparison between the results obtained with eq. (7.67) - classical method, with the results obtained with the coupling interaction (8.50) - CC, the results obtained with Descouvemont Astrophysica code [Des00] and with Sampaio MSc thesis code [Sam99].

The same procedure was used for the comparison of the results obtained from the coupling interaction (8.52) and eq. (7.68) for the $M1$ radiative capture cross in the $^7\text{Li}(p,\gamma)^8\text{Be}$ reaction. The results shown in Figure (8.5) are compared with the results obtained with Sampaio MSc thesis code [Sam99]. To obtain the agreement shown the S-factor obtained from Sampaio [Sam99] must be multiplied by a factor of $3/2$, resulting from inconsistencies its definition of the reduced matrix element for $M1$ transitions.

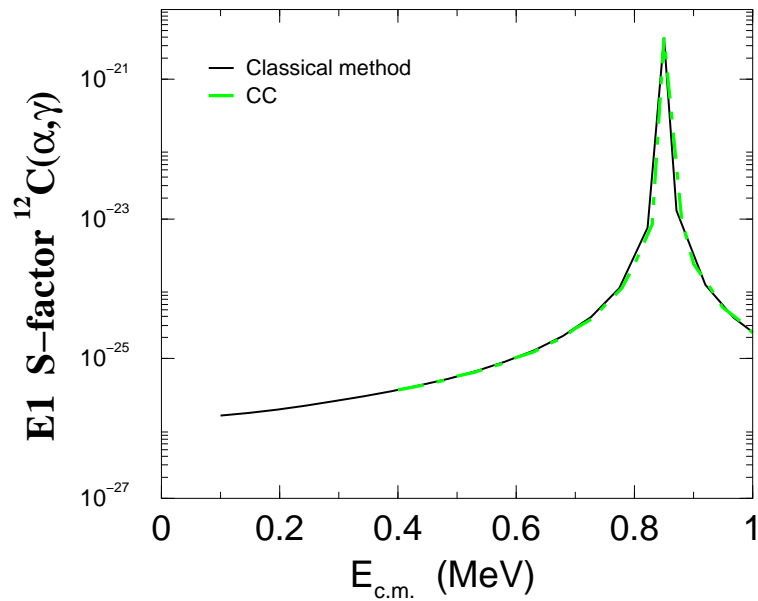


Figure 8.2: S-factor for $E1$ radiative capture in the $^{12}\text{C}(\alpha, \gamma)^{16}\text{O}$ reaction. Comparison between the results obtained with eq. (7.67) - classical method - and the results obtained with the coupling interaction (8.50) - CC. Descouvemont Astrophysica code [Des00] does not calculate this process due to the $E1$ cancellation effect in the $^{12}\text{C}-\alpha$ system [Bra00].

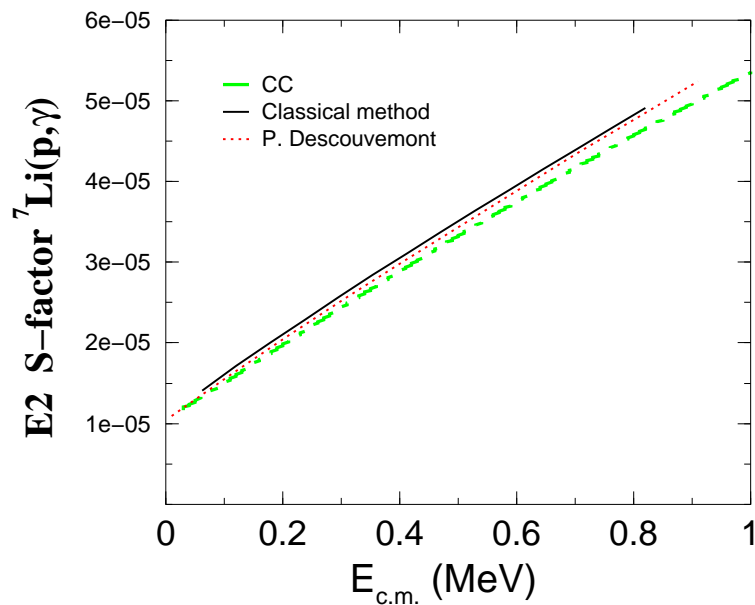


Figure 8.3: S-factor for $E2$ radiative capture in the $^7\text{Li}(p, \gamma)^8\text{Be}$ reaction. Comparison between the results obtained with eq. (7.67) - classical method, with the results obtained with the coupling interaction (8.50) - CC, and the results obtained with Descouvemont Astrophysica code [Des00].

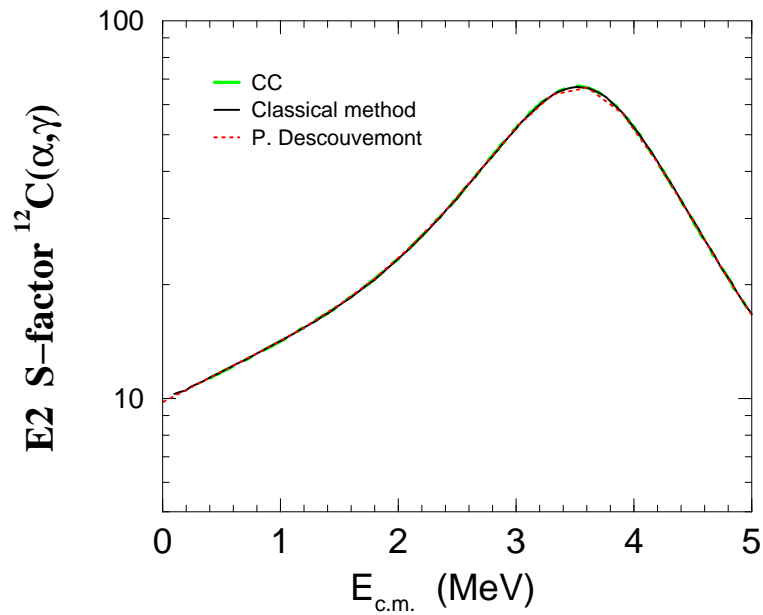


Figure 8.4: S-factor for $E2$ radiative capture in the $^{12}\text{C}(\alpha, \gamma)^{16}\text{O}$ reaction. Comparison between the results obtained with eq. (7.67) - classical method, with the results obtained with the coupling interaction (8.50) - CC, and the results obtained with Descouvemont Astrophysica code [Des00].

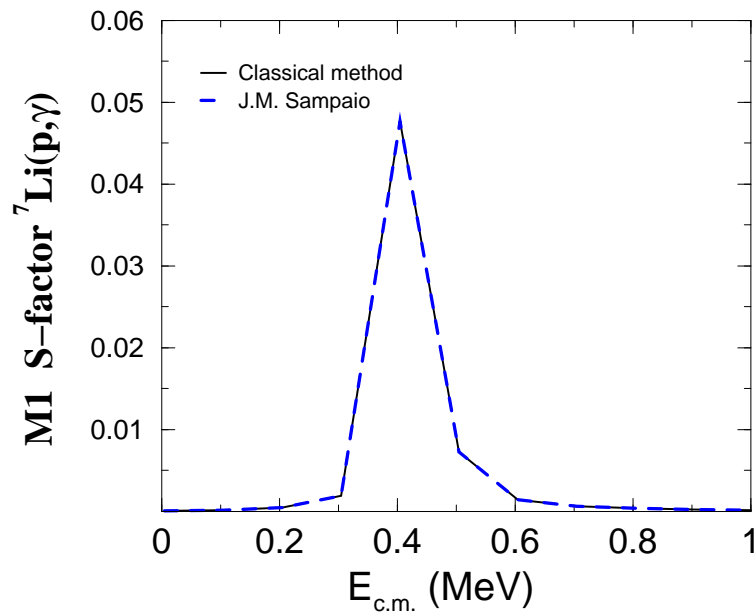


Figure 8.5: S-factor for $M1$ radiative capture in the $^7\text{Li}(p, \gamma)^8\text{Be}$ reaction. Comparison between the results obtained with eq. (7.68) - classical method, with the results obtained with the coupling interaction (8.52) - CC, and the results obtained with Sampaio MSc thesis code [Sam99].

Chapter 9

The $^{14}\text{N}(\text{p},\gamma)^{15}\text{O}$ reaction with the hybrid approach

In this chapter we apply the hybrid approach developed previously to the analysis of the $^{14}\text{N}(\text{p},\gamma)^{15}\text{O}$ reaction. As noted before, the contributions from negative parity states are significant in the case of transitions to the excited state of ^{15}O at 6.79 MeV. In chapter 6, these contributions were considered through the introduction $\frac{1}{2}^-$ and $\frac{3}{2}^-$ negative parity poles. In this chapter these background contributions are treated through a potential model.

The hybrid model is implemented with the SFRESCO code, however, before introducing the hybrid analysis of the $^{14}\text{N}(\text{p},\gamma)^{15}\text{O}$ reaction, it is important to reproduce the results of chapter 6 using this code and to introduce the definitions of reduced width, penetrability and R-matrix as used in this code, which are slightly different from the ones used in chapters 1, 2 and 6.

9.1 SFRESCO definitions

Particle channels

From eqs. (B.16) and (B.17) of appendix B one obtains in the case of entrance and exit particle channels, where $c_i = -\frac{\hbar^2}{2\mu_i}$ with μ_i the reduced mass in channel i

$$R_{11} = \frac{\hbar^2}{2\mu_1 a} \sum_{\lambda} \frac{(f_1^{\lambda})^2}{E_{\lambda} - E} \quad (9.1)$$

$$R_{21} = \frac{\hbar^2}{2\mu_1 a} \sum_{\lambda} \frac{f_1^{\lambda} f_2^{\lambda}}{E_{\lambda} - E} \quad (9.2)$$

By defining the squared root of the reduce widths as $\gamma_i^\lambda = \sqrt{\frac{\hbar^2}{2\mu_i a}} f_i^\lambda$ one obtains for the elements of the R–matrix:

$$R_{11} = \sum_{\lambda} \frac{(\gamma_1^\lambda)^2}{E_\lambda - E} \quad (9.3)$$

$$R_{21} = \sqrt{\frac{\mu_2}{\mu_1}} \sum_{\lambda} \frac{\gamma_1^\lambda \gamma_2^\lambda}{E_\lambda - E} = \sqrt{\frac{c_1}{c_2}} \sum_{\lambda} \frac{\gamma_1^\lambda \gamma_2^\lambda}{E_\lambda - E} \quad (9.4)$$

The particle width is defined from the reduced gamma width as

$$\Gamma_i^\lambda = 2P_i (\gamma_i^\lambda)^2 \quad (9.5)$$

where P_i is the penetrability in channel i .

Gamma channels

As mentioned in chapter 2, in R–matrix phenomenology the constant $C_{\alpha,\alpha'}$ is usually chosen to be $C_{\alpha,\alpha'} = 1$. This choice is valid in the weak coupling limit where the reverse couplings are not used, and is particularly relevant in the treatment of γ channels. With this definition one obtains for the elements of the R–matrix:

$$\tilde{R}_{11} = \sum_{\lambda} \frac{(\tilde{\gamma}_1^\lambda)^2}{E_\lambda - E} \quad (9.6)$$

$$\tilde{R}_{12} = \sum_{\lambda} \frac{\tilde{\gamma}_1^\lambda \tilde{\gamma}_2^\lambda}{E_\lambda - E} \quad (9.7)$$

which correspond to eqs. (2.28) and (2.29), respectively.

In this work, we have used therefore two different definitions of reduced width: the standard definition of R–matrix phenomenology corresponding to eqs. (9.6) and (9.7), commonly used in phenomenological fits and used in the $^{14}\text{N}(\text{p},\gamma)^{15}\text{O}$ analysis presented in chapter 6; and the definition used in eqs. (9.3) and (9.4), corresponding to eq. (2.10), which is used in the code SFRESCO [Tho04]. It becomes necessary therefore to obtain the relation between the standard definition of reduced widths, used in chapter 6, and the definition used in the code SFRESCO [Tho04], taking into account the different definitions for the T–matrix used in the former and in chapter 6.

We consider the case of radiative capture reactions, where $1 \equiv p$ and $2 \equiv \gamma$. The relation between $\tilde{\gamma}_\gamma$ and γ_γ can be found by examining the cross-section expressions for radiative capture. In chapter 2 we obtained the cross-section for electric radiative capture, in the weak coupling limit, as a function of the reduced widths:

$$\sigma_{p\gamma} = \frac{\pi}{k_p^2} \sum_{JSL L'} g_J \left| \frac{\sum_{\lambda} \frac{(2P_p)^{\frac{1}{2}} \tilde{\gamma}_p^{\lambda} \tilde{\gamma}_{\gamma}^{\lambda} (2\mathcal{P}_{\gamma})^{\frac{1}{2}}}{E_{\lambda} - E}}{1 - L_p^0 \tilde{R}_{pp}} \right|^2 \quad (9.8)$$

It is important to note the definitions of penetrability used in this equation. Indeed, whereas for the particle channel, p , the penetrabilities are calculated according to the absolute definition of penetrability, which from (1.27) corresponds to

$$P_p = \left(\frac{\rho_p}{F_p^2 + G_p^2} \right)_{R_p=a} \quad (9.9)$$

where $\rho_p = k_p R_p$, and F_p and G_p are the regular and irregular Coulomb functions for channel p , we used in chapter 6 the definition of relative photon penetrability, which will be denoted as \mathcal{P} to distinguish from the absolute penetrability, normalized to unity at the position of the R–matrix pole, eq. (6.3):

$$\mathcal{P}_{\gamma, L_{\gamma}} = \left(\frac{E - E_f}{E_{\lambda} - E_f} \right)^{2L_{\gamma}+1} = \left(\frac{E_{\gamma}}{E_{\lambda} - E_f} \right)^{2L_{\gamma}+1} \quad (9.10)$$

where L_{γ} is the multipolarity of the emitted electric radiation (this definition is derived from the asymptotic behavior of the absolute penetrability, eq. (9.9), later in this chapter). Eqs. (9.8-9.10) were used in chapter 6 in the analysis of the $^{14}\text{N}(p, \gamma)^{15}\text{O}$ reaction.

SFRESCO definitions

The cross-section expression used in the code SFRESCO for radiative capture reactions corresponds to (8.44) [Tho01]:

$$\sigma_{if} = \frac{4\pi}{k_i^2} \frac{v_f}{v_i} \sum_{JL_i L_f j_i j_f} g_{J_i} |\mathcal{T}_{L_f j_f, L_i j_i}^{J_i}|^2 \quad (9.11)$$

$$= \frac{\pi}{k_i^2} \frac{v_f}{v_i} \sum_{JL_i L_f j_i j_f} g_{J_i} |S_{L_f j_f, i L_i j_i}^{J_i}|^2 \quad (9.12)$$

where the definition of the T–matrix, $\mathcal{T}_{f,i}^J = \frac{i}{2} \{ \delta_{f,i} - S_{f,i}^J \}$, was used.

The S–matrix is defined in terms of the R–matrix by the matrix relation [Tho01]:

$$\mathbf{S} = \left[\mathbf{H}^+ - \mathbf{R}^F (\mathbf{H}'^+ - \mathbf{B}\mathbf{H}^+) \right]^{-1} \left[\mathbf{H}^- - \mathbf{R}^F (\mathbf{H}'^- - \mathbf{B}\mathbf{H}^-) \right] \quad (9.13)$$

where the derivatives are with respect to R , $\mathbf{R}^F = a\mathbf{R}$ (the superscript F denotes the SFRESCO definition for the \mathbf{R} -matrix), and \mathbf{H}^- and \mathbf{H}^+ are diagonal matrices of Coulomb functions with incoming and outgoing boundary conditions, respectively:

$$\mathbf{H}^- = \mathbf{G} - i\mathbf{F} \quad (9.14)$$

$$\mathbf{H}^+ = \mathbf{G} + i\mathbf{F} \quad (9.15)$$

corresponding to eqs. (1.19) and (1.20) without the Coulomb phase shift.

Proceeding in analogy with the eqs. (2.13–2.19) for the matrix eq. (9.13) one obtains, for the boundary conditions $\mathbf{B} = \mathbf{0}$

$$\mathbf{S} = \left[\mathbf{H}^+ - \mathbf{R}^F \mathbf{H}'^+ \right]^{-1} \left[\mathbf{H}^- - \mathbf{R}^F \mathbf{H}'^- \right] \quad (9.16)$$

$$= \mathbf{H}^{+^{-1}} \left[\mathbf{1} - \mathbf{R}^F \frac{\mathbf{H}'^+}{\mathbf{H}^+} \right]^{-1} \left[\mathbf{1} - \mathbf{R}^F \frac{\mathbf{H}'^-}{\mathbf{H}^-} \right] \mathbf{H}^- \quad (9.17)$$

$$= \sqrt{\frac{\mathbf{H}^-}{\mathbf{H}^+}} \sqrt{\frac{\mathbf{1}}{\mathbf{H}^- \mathbf{H}^+}} \left[\mathbf{1} - \mathbf{R}^F \frac{\mathbf{H}'^+}{\mathbf{H}^+} \right]^{-1} \left[\mathbf{1} - \mathbf{R}^F \frac{\mathbf{H}'^-}{\mathbf{H}^-} \right] \sqrt{\mathbf{H}^- \mathbf{H}^+} \sqrt{\frac{\mathbf{H}^-}{\mathbf{H}^+}} \quad (9.18)$$

$$= \Omega \sqrt{\frac{\mathbf{1}}{\mathbf{H}^- \mathbf{H}^+}} \left[\mathbf{1} - \mathbf{R}^F \frac{\mathbf{H}'^+}{\mathbf{H}^+} \right]^{-1} \left[\mathbf{1} - \mathbf{R}^F \frac{\mathbf{H}'^-}{\mathbf{H}^-} \right] \sqrt{\mathbf{H}^- \mathbf{H}^+} \Omega \quad (9.19)$$

The expression for the \mathbf{W} matrix in SFRESCO is therefore, from (9.19) and (2.17)

$$\mathbf{W}^F = \sqrt{\frac{\mathbf{1}}{\mathbf{H}^- \mathbf{H}^+}} \left[\mathbf{1} - \mathbf{R}^F \frac{\mathbf{H}'^+}{\mathbf{H}^+} \right]^{-1} \left[\mathbf{1} - \mathbf{R}^F \frac{\mathbf{H}'^-}{\mathbf{H}^-} \right] \sqrt{\mathbf{H}^- \mathbf{H}^+} \quad (9.20)$$

$$= \sqrt{\frac{\mathbf{1}}{\mathbf{IO}}} \left[\mathbf{1} - \frac{\mathbf{R}^F}{a} ka \frac{\mathbf{O}'}{\mathbf{O}} \right]^{-1} \left[\mathbf{1} - \frac{\mathbf{R}^F}{a} ka \frac{\mathbf{I}'}{\mathbf{I}} \right] \sqrt{\mathbf{IO}} \quad (9.21)$$

The velocity factors in the cross-section expression (9.12) can be included in the square modulus, corresponding to defining \mathbf{W} as:

$$\mathbf{W} = \sqrt{\frac{\mathbf{v}a}{\mathbf{IO}}} \left[\mathbf{1} - \frac{\mathbf{R}^F}{a} L \right]^{-1} \left[\mathbf{1} - \frac{\mathbf{R}^F}{a} \mathcal{L} \right] \sqrt{\frac{\mathbf{IO}}{\mathbf{v}}} a \quad (9.22)$$

where we multiplied and divided by the channel radius, a , and \mathbf{v} is the matrix of elements v_c for channel c .

By defining the velocity as $v_c = d_c k_c$ where d_c is

$$d_{particle\ channels} \equiv d_p = \frac{\hbar}{\mu_c} \quad (9.23)$$

$$d_{gamma\ channels} \equiv d_\gamma = \frac{\hbar c^2}{E_\gamma} \quad (9.24)$$

for particles and gammas respectively, one can write (9.22) as

$$\begin{aligned}
\mathbf{W} &= \sqrt{\mathbf{d}} \sqrt{\frac{\rho}{\mathbf{IO}}} \left[\mathbf{1} - \frac{\mathbf{R}^F}{a} L \right]^{-1} \left[\mathbf{1} - \frac{\mathbf{R}^F}{a} \mathcal{L} \right] \sqrt{\frac{\mathbf{IO}}{\rho}} \frac{1}{\sqrt{\mathbf{d}}} \\
&= \sqrt{\mathbf{d}} \left(\mathbf{1} + \mathcal{B}^{\frac{1}{2}} \left[\mathbf{1} - \frac{\mathbf{R}^F}{a} L \right]^{-1} \frac{\mathbf{R}^F}{a} \mathcal{B}^{\frac{1}{2}} \mathcal{W} \right) \frac{1}{\sqrt{\mathbf{d}}} \\
&= \mathbf{1} + \sqrt{\mathbf{d}} \mathcal{B}^{\frac{1}{2}} \left[\mathbf{1} - \frac{\mathbf{R}^F}{a} L \right]^{-1} \frac{\mathbf{R}^F}{a} \mathcal{B}^{\frac{1}{2}} \mathcal{W} \frac{1}{\sqrt{\mathbf{d}}}
\end{aligned} \tag{9.25}$$

where $\mathcal{B} = \frac{\rho}{\mathbf{IO}}$. In the two-channels case, by inverting the (2×2) matrix $\left[\mathbf{1} - \frac{\mathbf{R}^F}{a} L \right]$, one obtains, similarly to (2.24), for (p, γ) reactions:

$$W_{\gamma p} = 2i \sqrt{d_\gamma} P_\gamma^{\frac{1}{2}} \frac{R_{\gamma p}^F}{a} P_p^{\frac{1}{2}} \frac{1}{\sqrt{d_p}} \det^{-1} \tag{9.26}$$

where \det is the determinant

$$\det = \left(1 - \frac{R_{pp}^F}{a} L_p \right) \left(1 - \frac{R_{\gamma\gamma}^F}{a} L_\gamma \right) - \frac{1}{a^2} L_p R_{\gamma p}^F R_{p\gamma}^F L_\gamma \tag{9.27}$$

and P_p and P_γ are the elements of the \mathcal{B} matrix, the penetrabilities for the particle and gamma channels respectively.

In the case of the treatment of photon channels in SFRESCO, we set $c_2 = -\frac{E}{k^2}$ in eq. (B.1) which corresponds to describing the final channel with Maxwell's equation. In the phenomenological R-matrix approach, SFRESCO uses for the elements of the R-matrix eqs. (9.3) and (9.4) multiplied by the channel radius, a :

$$R_{pp}^F = a \frac{(\gamma_p^\lambda)^2}{E_\lambda - E} = a \tilde{R}_{pp} \tag{9.28}$$

$$\begin{aligned}
R_{\gamma p}^F &= a \sqrt{c_1} \frac{\gamma_p^\lambda \gamma_\gamma^\lambda}{E_\lambda - E} \\
&\equiv a \sqrt{\frac{c_p}{c_\gamma}} \frac{\gamma_p^\lambda}{E_\lambda - E} \frac{f_\gamma^\lambda}{\sqrt{a}}
\end{aligned} \tag{9.29}$$

and therefore the reduced gamma width defined in SFRESCO, γ_γ^2 , has dimensions of MeV, as the reduced gamma width, $\tilde{\gamma}_\gamma^2$, in (9.8). The R-matrix however is no longer dimensionless, having dimensions of length (fm).

Replacing (9.26) into the cross-section expression (9.12) (the velocity factors are included in the expression for \mathbf{W}), and considering (9.28) and (9.29) one obtains, in the weak coupling limit

$$\sigma_{p\gamma} = \frac{\pi}{k_i^2} \sum_{JL_i L_f j_i j_f} g_{J_i} \left| \frac{\sum_{\lambda} \sqrt{\frac{c_p d_{\gamma}}{c_{\gamma} d_p} \frac{(2P_p)^{\frac{1}{2}} \gamma_p^{\lambda} \gamma_{\gamma}^{\lambda} (2P_{\gamma})^{\frac{1}{2}}}{E_{\lambda} - E}}}{1 - L_p \tilde{R}_{pp}} \right|^2 \quad (9.30)$$

From the definition of \mathcal{B}

$$\begin{aligned} \mathcal{B} &= \left(\frac{\rho}{\mathbf{IO}} \right)_{R=a} \\ &= \left(\frac{\rho}{\mathbf{F}^2 + \mathbf{G}^2} \right)_{R=a} \end{aligned} \quad (9.31)$$

and eq. (9.10) we observe that eqs. (9.8) and (9.30) involve different kinds of gamma penetrability, P_{γ} and \mathcal{P}_{γ} . Indeed the gamma penetrability is defined in the SFRESCO as

$$P_{\gamma,q} = \left(\frac{\rho}{F_{\gamma,q}^2 + G_{\gamma,q}^2} \right)_{R_{\gamma}=a} \quad (9.32)$$

where the subscript q references not the multipolarity of the emitted radiation but rather the angular momentum from the centrifugal barrier (as we saw previously, the two might not be the same as in the case of magnetic transitions). The asymptotic behavior of the penetrability for the gamma channels is therefore

$$P_{\gamma,q} \approx \frac{(k_{\gamma} a)^{2q+1}}{[(2q-1)!!]^2} = \frac{1}{[(2q-1)!!]^2} \left(E_{\gamma} \frac{a}{\hbar c} \right)^{2q+1} \quad (9.33)$$

From eqs. (9.8), (9.10), (9.30) and (9.33) one obtains the relation between the reduced gamma widths in the case of electric $\text{EL}_{L_{\gamma}}$ transitions, for which $q = L_{\gamma}$:

$$\begin{aligned} (\tilde{\gamma}_{\gamma}^{\lambda})^2 \left(\frac{E_{\gamma}}{E_{\lambda} - E_f} \right)^{2L_{\gamma}+1} &= (\gamma_{\gamma}^{\lambda})^2 \frac{1}{[(2L_{\gamma}-1)!!]^2} \left(E_{\gamma} \frac{a}{\hbar c} \right)^{2L_{\gamma}+1} \frac{c_p d_{\gamma}}{c_{\gamma} d_p} \\ &= (\gamma_{\gamma}^{\lambda})^2 \frac{1}{[(2L_{\gamma} + \gamma - 1)!!]^2} \left(E_{\gamma} \frac{a}{\hbar c} \right)^{2L_{\gamma}+1} \frac{\hbar^2 k_{\gamma}^2 \hbar c^2 \mu_p}{2\mu_p E_{\gamma} E_{\gamma} \hbar} \\ &= (\gamma_{\gamma}^{\lambda})^2 \frac{1}{2[(2L_{\gamma}-1)!!]^2} \left(E_{\gamma} \frac{a}{\hbar c} \right)^{2L_{\gamma}+1} \end{aligned} \quad (9.34)$$

and therefore, the relationship between the reduced level widths is

$$(\gamma_{\gamma}^{\lambda})^2 = (\tilde{\gamma}_{\gamma}^{\lambda})^2 \left[2[(2L_{\gamma}-1)!!]^2 \left(\frac{\hbar c}{a(E_{\lambda} - E_f)} \right)^{2L_{\gamma}+1} \right] \quad (9.35)$$

9.2 R–matrix analysis with SFRESCO

With the reduced widths of table 6.1, and eq. (9.35) one is able to reproduce the results of chapter 6 with the SFRESCO code. The results of this analysis, together with the fits obtained in chapter 6, are shown in figures 9.1–9.3. The consistency of the results obtained with the two codes, the one used in chapter 6 and SFRESCO, should be emphasized. The SFRESCO parameters are shown in table 9.1.

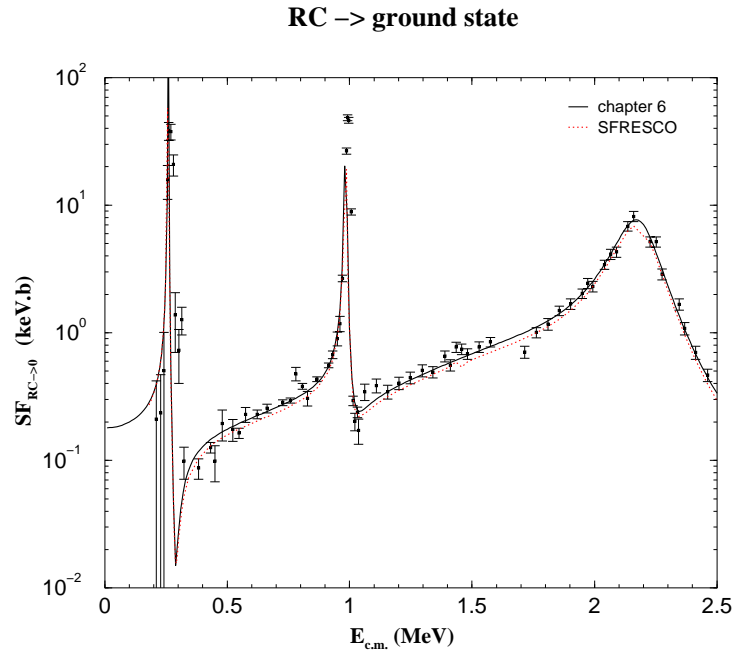


Figure 9.1: S–factor for radiative capture to the ground state. Comparison between the results obtained in chapter 6 and the results obtained with the SFRESCO code.

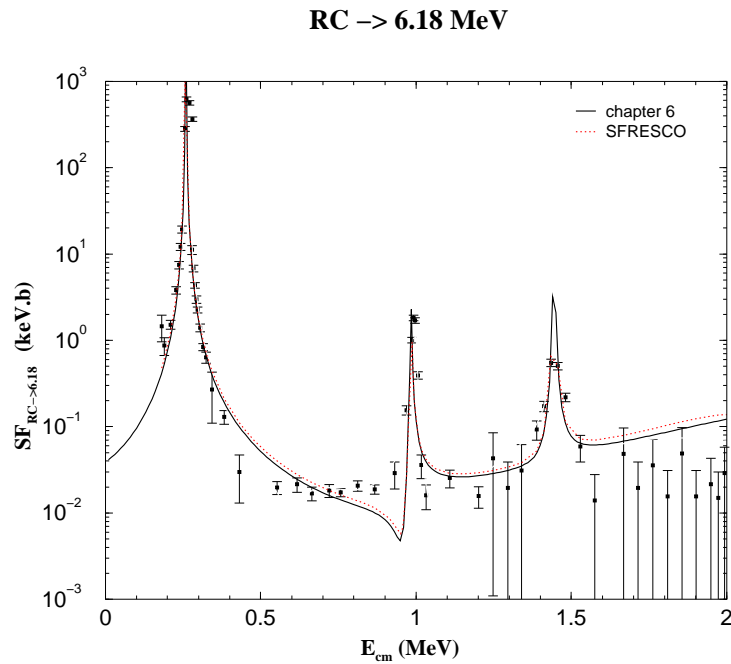


Figure 9.2: S-factor for radiative capture to the $E_x=6.18$ MeV state. Comparison between the results obtained in chapter 6 and the results obtained with the SFRESCO code.

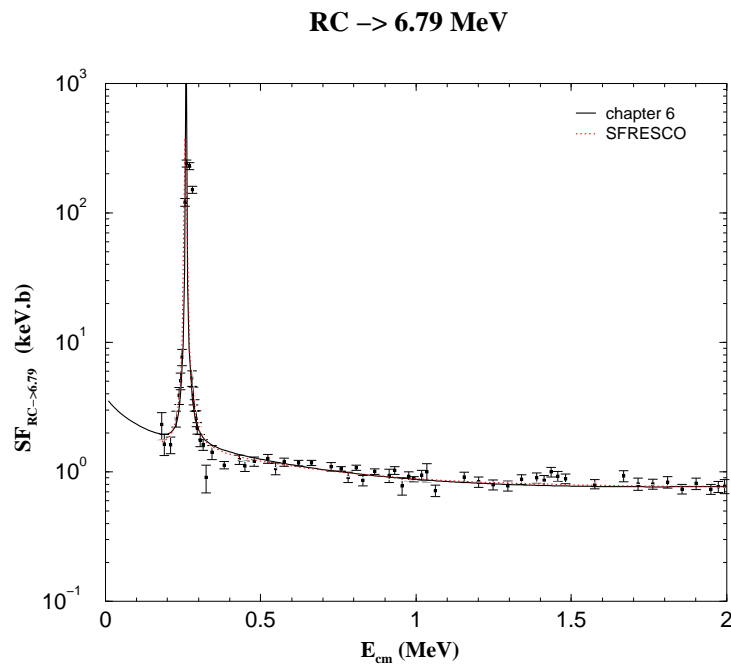


Figure 9.3: S-factor for radiative capture to the $E_x=6.79$ MeV state. Comparison between the results obtained in chapter 6 and the results obtained with the SFRESCO code.

Table 9.1: Values for the position of the R–matrix poles and square roots of proton and γ reduced widths used in the SFRESCO analysis, obtained from the R–matrix analysis of chapter 6 and with eq. (9.35). The background terms were also converted.

Transition	J^π	E_λ (MeV)	γ_p (MeV $^{\frac{1}{2}}$)	γ_γ (MeV $^{\frac{1}{2}}$)	interference
g.s.	$\frac{1}{2}^+$	0.262	0.0778	0.0015	–
	$\frac{3}{2}^+$	–0.504	0.4123	0.0049	+
		0.990	0.0632	0.0028	+
		2.200	0.1674	0.0152	+
6.18 MeV	$\frac{1}{2}^+$	0.262	0.0778	0.0955	+
		1.445	0.0224	0.0251	+
	$\frac{3}{2}^+$	–0.504	0.4123	0.0305	+
		0.990	0.0632	0.0054	–
		$\frac{1}{2}^+$	0.262	0.0778	16.58

9.3 Analysis of the $^{14}\text{N}(\text{p},\gamma)^{15}\text{O}$ reaction with the hybrid approach

With the formalism developed in chapters 7 and 8 we can now replace the background terms in the R–matrix description of the $^{14}\text{N}(\text{p},\gamma)^{15}\text{O}$ of chapter 6, and the previous section of this chapter, by a potential description of the direct contributions to the reaction mechanism. We start by replacing only the contribution from the negative parity $\frac{1}{2}^-$ and $\frac{3}{2}^-$ states, P–waves in the entrance channel, and later extend this procedure to the treatment of all background contributions.

9.3.1 Potential description of the negative parity background terms

The negative parity background terms contribute to the $^{14}\text{N}(\text{p},\gamma)^{15}\text{O}$ reaction mechanism predominantly through E1 capture to the $\frac{3}{2}^+$ subthreshold state at $E=-0.504$ MeV. We perform the coupled channels calculation with a potential that has a central, target and projectile spin–orbit terms, and a spin–spin term. The parameters of the entrance channel potential are adjusted to the experimental data for radiative capture to the $\frac{3}{2}^+$ subthreshold state, when combined with the the R–matrix parameters fixed at the values shown in table 9.1.

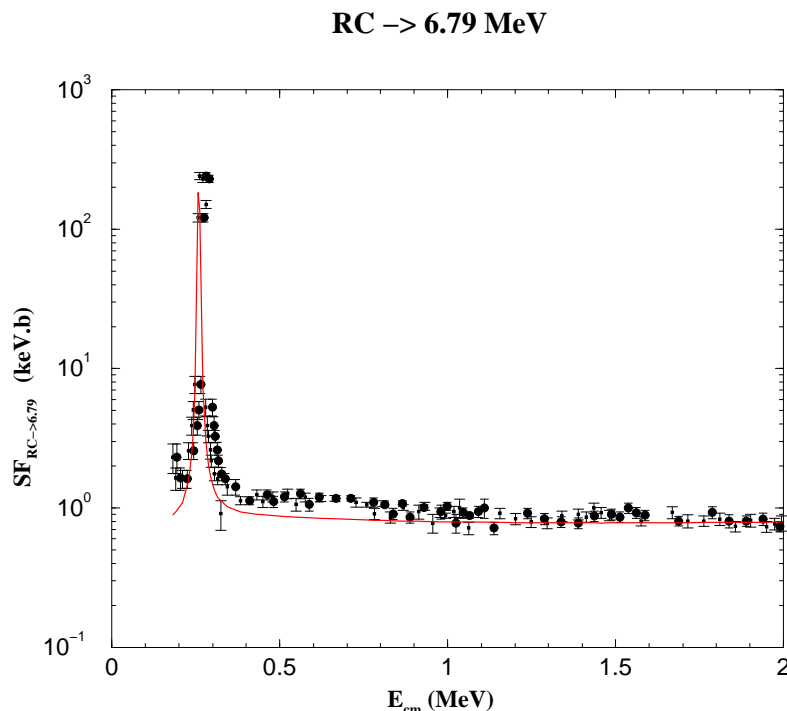


Figure 9.4: S-factor for radiative capture to the $E_x=6.79$ MeV state, with a hybrid description where the negative parity background is described through a potential model.

This P-wave potential was varied independently of the properties of the known bound states. In the next section we extend this analysis to all partial waves and we are more consistent and consider the known constraints on the potential.

We are able to use the R-matrix parameters obtained from the fits of chapter 6, which were obtained for a channel radius of $a = 6.5$ fm, because of the way the wave functions in the exterior region are calculated. The potential contribution to the R-matrix is evaluated at $a = 6.5$ fm to be added to the contribution from the additional poles. However, the matching between the wave functions obtained from the full interaction and the Coulomb wave functions is done at the maximum coupling radius of $R_m = 50$ fm. As a result, the Coulomb matrices for $a < R < R_m$, $\tilde{\mathbf{H}}^+$ and $\tilde{\mathbf{H}}^-$, are non-diagonal, and include the effects of the nuclear and Coulomb interactions [Chr82]. These non-diagonal Coulomb matrices are then matched at the channel radius a with the internal wave functions.

The result of the best fit is presented in figure 9.4 and the corresponding potential parameters are (53.69,1.58,0.41) for the central term, (7.93,2.84,0.40) and (10.0,3.64,1.30) for the target and projectile spin-orbit terms, respectively, and (8.39,1.74,0.60) for the spin-spin term – in this notation the first element corresponds to the potential depth, the second to the radius, and the third to the diffuseness. The spectroscopic amplitude for the transition to the $\frac{3}{2}^+$ subthreshold state obtained in this fit was $\sqrt{CS^2}=1.75$.

The results obtained for the transitions to the ground state and the 6.18 MeV state are the ones shown in figures 9.1 and 9.2, since the R–matrix parameters were left unchanged and the E2 contribution from the potential is negligible compared with the E1 resonant contributions.

Figure 9.4 shows that one is able to describe reasonably the experimental data for the transition to the 6.79 MeV state by replacing the negative parity background poles by a potential model. However, the discrepancy between the fit and the experimental data around the low energy resonance is a clear indication that the R–matrix parameters need to be refitted along with the potential parameters. This will be done next, by extending to positive parities the treatment of the background terms through a potential model.

9.3.2 Potential description of the $^{14}\text{N}(\mathbf{p},\gamma)^{15}\text{O}$ background

The extension of the previous analysis to the treatment of both positive and negative parity backgrounds is done by the use of two optical potentials for each contribution. Both potentials include central and projectile spin-orbit Woods-Saxon terms, since the capture to the ground state and the 6.18 MeV state of ^{15}O , although proceeding predominantly through S–wave E1 capture, are expected to have small D–wave contributions. We constrained the positive parity potential to have an S–wave bound state at $E = -0.504$ Mev and the negative parity potential to have a $P_{\frac{3}{2}}$ bound state at the ground state energy. This removes the possibility of these eigenstates appearing at positive energies and interfering with the set of resonances.

The results obtained from an analysis where the potential parameters for the negative and positive parity potentials are fitted, while the the R–matrix parameters are left unchanged to the values of table 9.1, correspond to the curves “fit a” in figures 9.5–9.7. These results show again the need for refitting the R–matrix parameters along with the potential parameters. In a second iteration, after obtaining the potential parameters corresponding to the best fit to the data, the overall set of parameters, potential and R–matrix levels parameters, was allowed to vary to obtain the final curves labeled “fit b” in the same figures.

Although the transitions to the 6.18 and 6.79 MeV states are reasonably well described by the model, figures 9.6 and 9.7, we observe from figure 9.5 that we are not able in this framework to reproduce the experimental data for the transition to the ground state in the energy range between 1 and 2 MeV. We note however that we used a reduced set of states in this analysis, and that the energy level diagram of ^{15}O has other states in this energy range which are not included in this set.

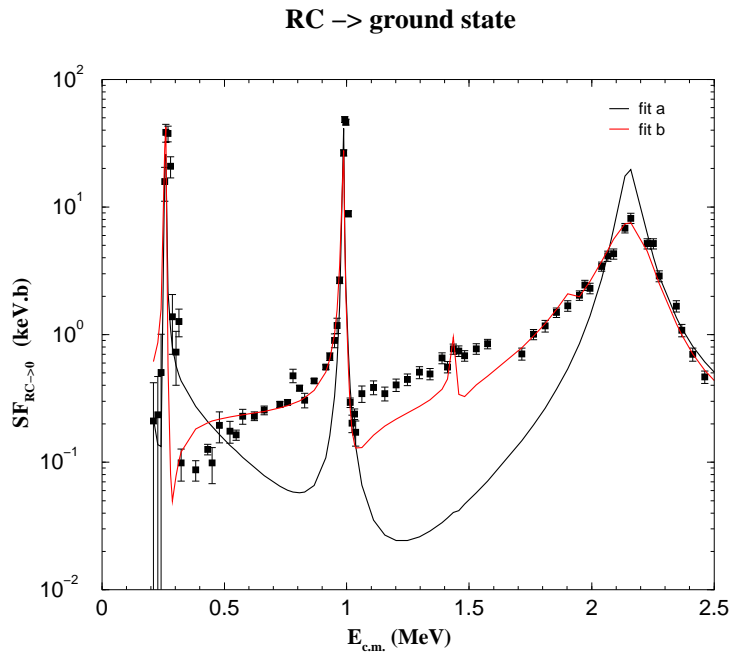


Figure 9.5: S-factor for radiative capture to the ground state, obtained with the hybrid framework where both negative and positive parity background poles are replaced by a potential model description.

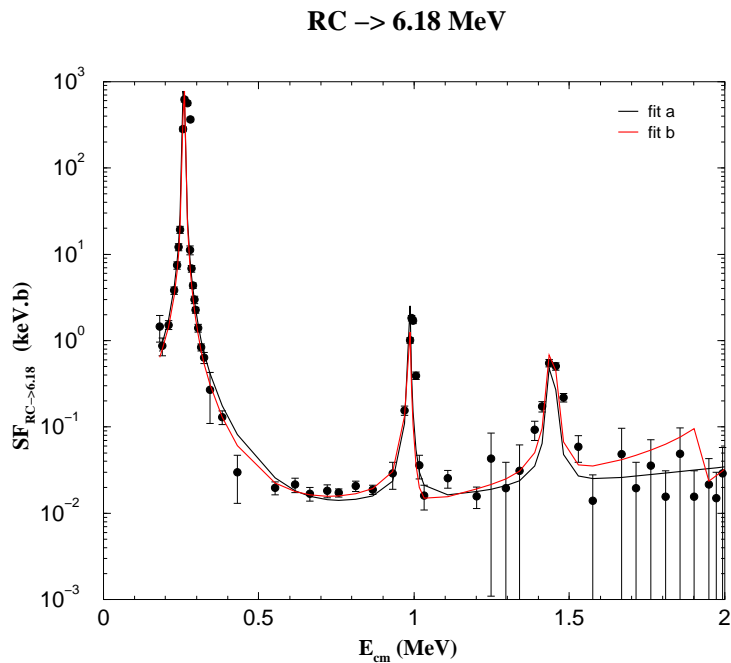


Figure 9.6: S-factor for radiative capture to the $E_x=6.18$ MeV state, obtained with the hybrid framework where both negative and positive parity background poles are replaced by a potential model description.

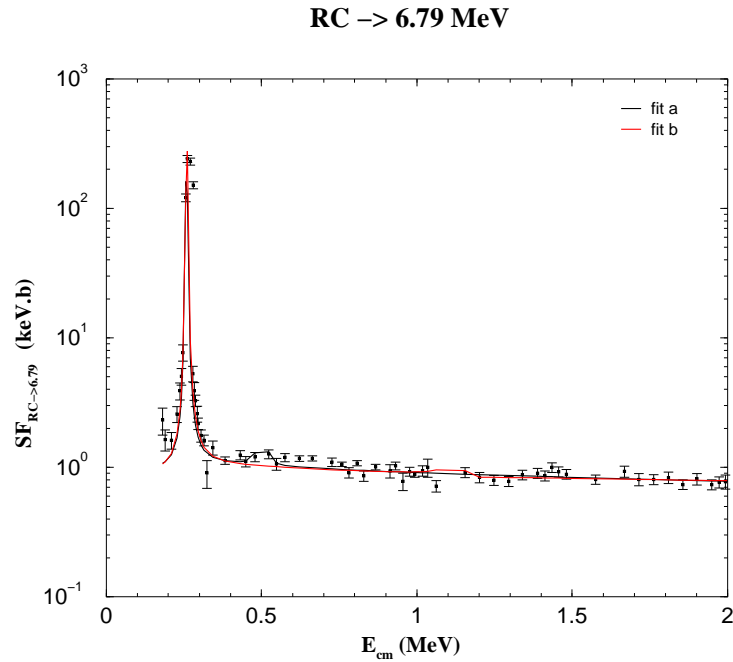


Figure 9.7: S-factor for radiative capture to the $E_x=6.79$ MeV state, obtained with the hybrid framework where both negative and positive parity background poles are replaced by a potential model description.

We consider therefore an extended set of resonances that includes the levels introduced previously plus the $\frac{1}{2}^+$ state at 1.63 MeV and the $\frac{3}{2}^+$ states at 3.21 MeV. By following the same procedure as before and adjusting the energies and the reduced proton and gamma widths for the transition to the ground state of the two states introduced, along with the potential parameters, while maintaining the remaining level parameters fixed at the values of table 9.1, one obtains the curves labeled “fit c” in figures 9.8–9.10. The curves “fit d” in the same figures are obtained in a second iteration by allowing some of the parameters of the new set of R-matrix poles used in the analysis to vary.

The analysis corresponding to “fit d” yields the smallest χ^2 of all the fits shown in this section, $\chi_{fit\ d}^2 = 12.0$, and the potential and R-matrix parameters obtained are shown in tables 9.3 and 9.2, respectively. The energies quoted in these tables are the fitted energies. The spectroscopic amplitudes obtained for the transitions to the ground state, the 6.18 MeV state and the 6.79 MeV state were $\sqrt{CS^2} = 0.07$, -0.77 and 1.90 , respectively.

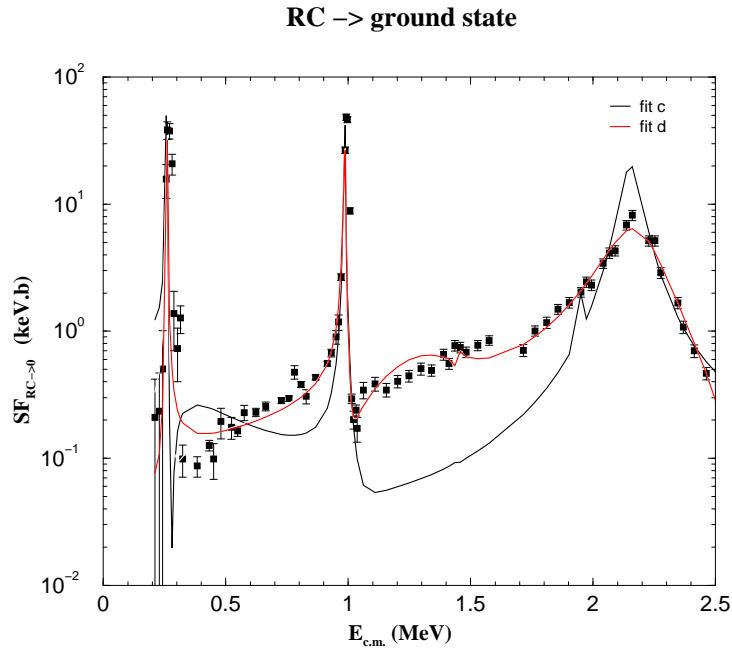


Figure 9.8: S-factor for radiative capture to the ground state, obtained with a hybrid framework where the extended set of resonances was used.

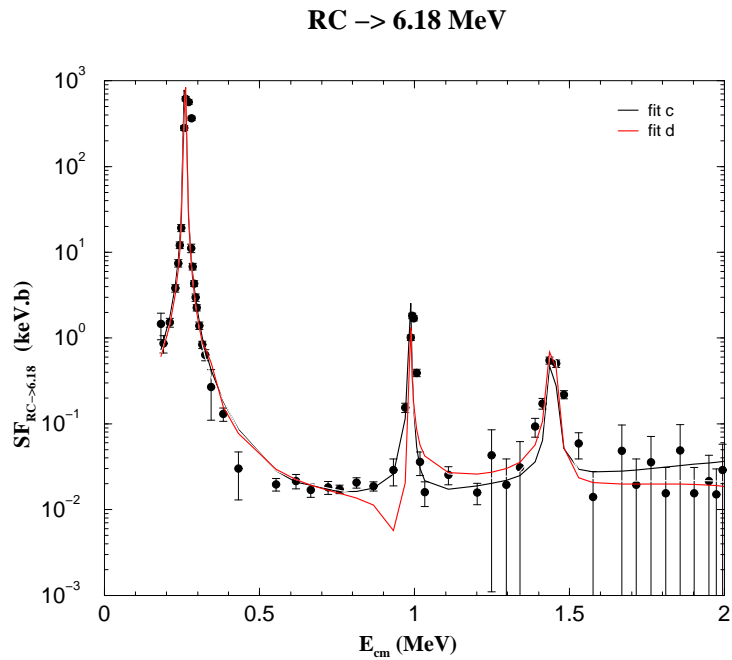


Figure 9.9: S-factor for radiative capture to the $E_x=6.18$ MeV state, obtained with a hybrid framework where the extended set of resonances was used.

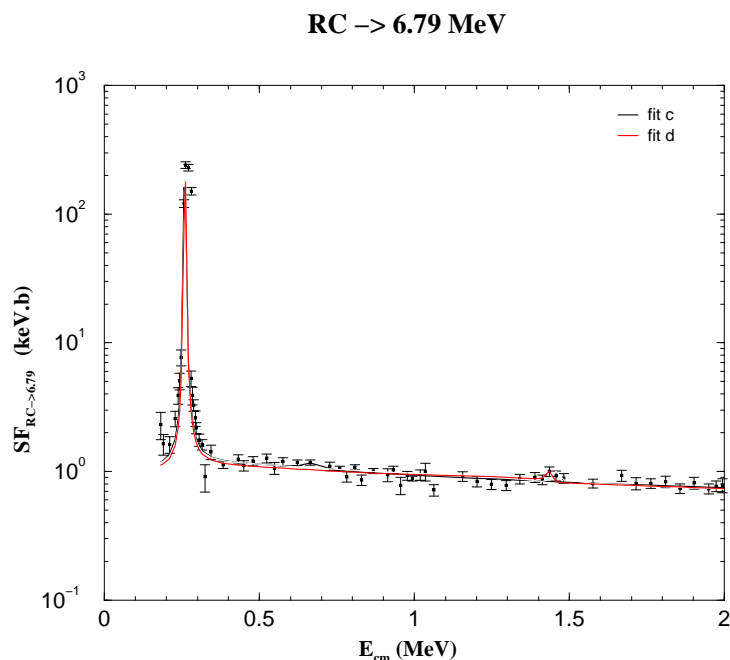


Figure 9.10: S-factor for radiative capture to the $E_x=6.79$ MeV state, obtained with a hybrid framework where the extended set of resonances was used.

9.4 Results and discussion

In the analysis presented in this chapter, as in chapter 6, the channel radius was fixed at 6.5 fm and the boundary condition used corresponded to the shift function at the position of the subthreshold state at $E = -0.504$ MeV, which allows us to fix the energy of this state at the experimentally observed value. We have not studied the sensitivity of the fit to the channel radius, however, since this was already done in context of the analysis presented in chapter 6.

parity	potential	depth	radius	diffuseness
negative	V	48.7	2.18	0.31
	VSO_P	0.74	2.49	0.65
positive	V	48.7	2.55	0.66
	VSO_P	9.56	3.00	0.73

Table 9.2: Potential parameters obtained from the best fit to the $^{14}\text{N}(p,\gamma)^{15}\text{O}$ radiative capture cross section data to the ground state, 6.18 MeV and 6.79 MeV states of ^{15}O , corresponding to the curves labeled “fit d”.

Table 9.3: Values for the resonance energies, proton and γ -widths at the position of the pole, and square root of reduced widths, obtained from the hybrid analysis. The energies quoted correspond to the fitted values and the proton width for the subthreshold state is a reduced width γ_p^2 .

Transition	J^π	E_λ (MeV)	γ_p (MeV $^{\frac{1}{2}}$)	Γ_p (keV)	γ_γ (MeV $^{\frac{1}{2}}$)	Γ_γ (eV)	interference
g.s.	$\frac{1}{2}^+$	0.262	0.062	0.016	0.0015	0.070	–
		1.445	0.030	1.413	0.0001	0.001	–
		1.800	0.526	580	0.0041	0.904	+
	$\frac{3}{2}^+$	–0.504	0.412	170	0.0485	0.244	+
		0.987	0.045	1.634	0.0033	0.443	+
		2.239	0.206	113	0.0124	9.531	+
		3.213	0.481	848	0.0107	9.501	+
6.18 MeV	$\frac{1}{2}^+$	0.262	0.062	0.016	0.0955	0.096	+
		1.445	0.030	1.413	0.0234	0.658	–
	$\frac{3}{2}^+$	–0.504	0.412	170	0.0481	0.038	+
		0.987	0.045	1.634	0.0054	0.019	–
6.79 MeV	$\frac{1}{2}^+$	0.262	0.062	0.016	16.58	0.317	+
		1.445	0.030	1.413	0.9314	0.210	–

The overall agreement between the hybrid model and the data is good, with a total χ^2 per degree of freedom of 12.0, corresponding to “fit d”. This result is better than the one obtained with the R–matrix analysis of chapter 6 ($\chi^2 = 14.7$). There are, however, some discrepancies between the values obtained with the hybrid model for the parameters of the resonances, and the ones obtained in the study of chapter 6 and by the the R–matrix fit of Angulo and Descouvemont [Ang01]. These are discussed in detail next.

Capture to the ground state ($\frac{1}{2}^-$)

In the fitting procedure we found the results to be relatively insensitive to the product $\gamma_p \times \gamma_\gamma$ for the $\frac{3}{2}^+$ subthreshold state. We therefore fixed the proton width at the values obtained from chapter 6, $\gamma_p^2 = 170$, and adjust only the γ -width of this state. The value obtained for the γ -width was $\Gamma_\gamma = 0.244$ eV, which is in reasonable agreement with the value obtained in chapter 6 ($\Gamma_\gamma = 0.263$ eV), and with the recent measurements of Yamada *et al.* [Yam04] and Bertone *et al.* [Ber02] ($\Gamma_\gamma = 0.41_{-0.13}^{+0.34}$ eV and $\Gamma_\gamma = 0.95_{-0.95}^{+0.60}$ eV, respectively).

For the other $\frac{3}{2}^+$ states the values obtained with the hybrid analysis ($\Gamma_p = 1.634$ keV and $\Gamma_\gamma = 0.443$ eV for the $E=0.987$ MeV state, and $\Gamma_p = 113$ keV and $\Gamma_\gamma = 9.532$ eV for the $E=2.239$ MeV state) are in reasonable agreement with the values referenced in other works [Ang01, Sch87, AS91]. In Angulo and Descouvemont, for example, $\Gamma_p = 3.0$ keV and $\Gamma_\gamma = 0.10$ eV for the state at $E=0.985$ MeV and $\Gamma_p = 270$ keV and $\Gamma_\gamma = 9.0$ eV for the state at $E=2.187$ MeV.

For the $\frac{1}{2}^+$ state at $E=0.262$ MeV the values obtained in this work, $\Gamma_p = 0.016$ keV and $\Gamma_\gamma = 0.070$ eV, are significantly different from those obtained by Angulo and Descouvemont [Ang01] ($\Gamma_p = 1$ keV and $\Gamma_\gamma = 0.0016$ eV), but are in reasonable agreement with the ones obtained in the R–matrix analysis of chapter 6 ($\Gamma_p = 0.02$ keV and $\Gamma_\gamma = 0.036$ eV).

The resonance energies were also fitted to the experimental data. The values obtained in this work for the two $\frac{3}{2}^+$ resonances at $E=0.985$ and 2.187 MeV are $E=0.987$ and 2.239 MeV respectively. The fitted resonance energies for the $\frac{1}{2}^+$ states at $E=0.259$ and 1.446 MeV are $E=0.262$ and 1.445 MeV respectively. Fitting the energies considerably improves the result of the fitting procedure and results obtained are within 2% of the values quoted in the literature [AS91, Ang01].

The two states introduced in this analysis, the $\frac{1}{2}^+$ resonance at $E=1.800$ MeV and the $\frac{3}{2}^+$ resonance at $E=3.213$ MeV have large proton and gamma widths, which indicates that these states are possibly accounting for resonance contributions not taken into account explicitly by the set of states used in the analysis.

The value obtained for the S–factor at astrophysical energies, $S(0)=0.05$ keV.b, is very close to the value obtained by the R–matrix analysis of Angulo and Descouvemont [Ang01], $S(0)=0.08_{-0.06}^{+0.13}$ keV.b. It is, however significantly different from the value obtained by Schröder *et al.* [Sch87], $S(0)=1.55$ keV.b, and the result obtained in chapter 6.

Capture to the $E_x = 6.18$ MeV state ($\frac{3}{2}^-$)

The values obtained for the γ –widths of the subthreshold and $E=0.987$ MeV states, $\Gamma_\gamma = 0.038$ and 0.019 eV respectively, are in reasonable agreement with the results obtained in chapter 6 ($\Gamma_\gamma^{-0.504} = 0.015$ eV and $\Gamma_\gamma^{0.985} = 0.019$ eV) and by the work of Angulo and Descouvemont [Ang01] ($\Gamma_\gamma^{-0.504} = 0.005$ eV and $\Gamma_\gamma^{0.985} = 0.004$ eV).

For the γ –widths of the $\frac{1}{2}^+$ resonances at $E=0.262$ MeV and 1.445 MeV we obtain $\Gamma_\gamma = 0.096$ and 0.658 eV, respectively. The fitted proton width of the $E=1.445$ MeV is $\Gamma_p = 1.413$ keV. These values are significantly different from the ones obtained in chapter 6 ($\Gamma_\gamma^{0.262} = 0.850$ eV, $\Gamma_\gamma^{1.449} = 0.376$ eV and $\Gamma_p^{1.446} = 0.79$ keV), and from those obtained by the analysis of Angulo and Descouvemont [Ang01] ($\Gamma_\gamma^{0.259} = 0.02$ eV, $\Gamma_\gamma^{1.445} = 0.11$ eV, and $\Gamma_p^{1.445} = 42.0$ keV)

The value obtained for the S–factor at astrophysical energies, $S(0)=0.12$ keV.b, is considerably higher than the one obtained in chapter 6, $S(0)=0.04$ keV.b, and the one obtained by Angulo and Descouvemont [Ang01], $S(0)=0.06^{+0.01}_{-0.02}$ keV.b.

Capture to the $E_x=6.79$ MeV state ($\frac{3}{2}^+$)

The value obtained for the γ –widths of the $E=0.262$ MeV resonance, $\Gamma_\gamma=0.317$ eV, although very close to the value obtained in chapter 6, $\Gamma_\gamma=0.313$ eV, differs significantly from the one obtained by the R–matrix analysis of Angulo and Descouvemont [Ang01], $\Gamma_\gamma=0.01$ eV. In this analysis, we introduce the contribution from the $\frac{1}{2}^+$ state at $E=1.445$ MeV, which is not considered in the phenomenological R–matrix analysis of chapter 6, or by Angulo and Descouvemont [Ang01]. The value obtained for the γ –width of this state was $\Gamma_\gamma=0.210$ eV.

The contribution from capture to the $E_x=6.79$ MeV state still dominates the astrophysical S–factor at zero energy, however, the value obtained in this analysis, $S(0)=0.95$ keV.b, is much smaller than the one obtained in chapter 6, $S(0)=2.21$ keV.b, and smaller than the one obtained by Angulo and Descouvemont [Ang01], $S(0)=1.63\pm 0.17$ keV.b).

Total S–factor

The total S–factor at astrophysical energies obtained in this work, $S(0)=1.12$ keV.b (corresponding to the sum of the contributions $S(0)=0.05$, 0.12 and 0.95 keV.b from the capture to the ground state, the 6.18 and the 6.79 MeV states, respectively), is significantly lower than the one obtained in the analysis of chapter 6, $S(0)=2.42$ keV.b, or the value obtained by Angulo and Descouvemont [Ang01], $S(0)=1.77\pm 0.20$ keV.b.

9.5 Conclusions

In this chapter we applied a hybrid R–matrix + potential model, to the analysis of the radiative capture reaction $^{14}\text{N}(p,\gamma)^{15}\text{O}$ and the determination of its S–factor at energies relevant in astrophysics.

We started with a potential description for the contribution to the background from negative parity states, and were able to successfully describe the data for radiative capture to the 6.79 MeV state, as well as for the ground state and 6.18 MeV state of ^{15}O .

We then extended the hybrid analysis to the treatment of all the background contributions. In this study we observed some discrepancies between the resonance parameters obtained and the values obtained by Angulo and Descouvemont [Ang01]. Furthermore, the large proton and gamma widths obtained for the two states introduced the analysis (the $\frac{1}{2}^+$ and $\frac{3}{2}^+$ resonances at $E=1.800$ MeV and $E=3.213$ MeV, respectively) indicate that these states are accounting for resonance contributions not taken into account explicitly by the set of states used in the analysis. The total S-factor at astrophysical energies obtained in this analysis, $S(0)=1.12$ keV.b, is significantly lower than the one obtained in the analysis of chapter 6, $S(0)=2.42$ keV.b, and the value obtained by Angulo and Descouvemont [Ang01], $S(0)=1.77\pm 0.20$ keV.b.

The two analysis of the $^{14}\text{N}(p, \gamma)^{15}\text{O}$ shown in this work, the phenomenological R-matrix analysis of chapter 6 and the hybrid analysis presented in this chapter, and the R-matrix analysis of Angulo and Descouvemont [Ang01], obtain very different values for the S-factor at astrophysical energies, although all these studies used the experimental data obtained by Schröder *et al.* [Sch87]. The reason for these differences, as for the discrepancies observed in the values of the resonance parameters, is related to the uncertainties of the low energy experimental data, which do not allow a proper definition of the properties of the 6.79 MeV subthreshold state or the $\frac{1}{2}^+$ resonance at $E=0.262$ MeV.

The new experimental data being made available by the TUNL and the LUNA collaboration experiments will significantly reduce the uncertainties in the low energy region and allow for a much more reliable analysis of the $^{14}\text{N}(p, \gamma)^{15}\text{O}$ reaction.

Part V

Conclusions

In this work we proposed and implemented a hybrid R–matrix + potential framework for the systematic study of nuclear reactions, and focusing on applications that involve transfer or photonuclear processes.

In order to accomplish this, we started by rederiving the R–matrix theory for transfer and photon channels, focusing on the 2–channel case. We studied the R–matrix theory both as a method of solving the coupled equations and in the pure phenomenological approach, and explore the possibility of including R–matrix poles in a coupled channels analysis, which constitutes the hybrid framework.

This model was then applied to the analysis of the ${}^3\text{He}(\text{d},\text{p}){}^4\text{He}$ transfer reaction, and the set of observables available (rank zero, $i\Gamma_{11}$, T_{2q} and $K_y'(0^\circ)$ reaction observables), together with new measurements presented in this work, were successfully described in this framework. The parameters obtained from this hybrid analysis for the dominant $\frac{3}{2}^+$ resonance were $E_d = 0.24$ MeV, $\Gamma_d^{(0)} = 0.209$ MeV and $\Gamma_p^{(2)} = 0.046$ MeV, which are in good agreement with the values quoted by Tilley *et al.* [Til02] ($E_d = 0.23$ MeV, $\Gamma_d = 0.134$ MeV and $\Gamma_p = 0.055$ MeV). Furthermore, this analysis reveals the importance of $L > 0$ contributions, namely those related to odd partial waves (essentially P–waves), to the reaction mechanism, arising from direct transfer processes or tails of distant resonances. We conclude that a consistent description of the different polarization observables can be achieved by assuming that the reaction proceeds by a mixed mechanism where the dominant resonant component competes with a non negligible direct component.

With the new experimental measurements presented in this work for the $A_{yy}(0^\circ)$ and $\sigma(0^\circ)$ observables of the ${}^3\text{He}(\text{d},\text{p}){}^4\text{He}$ reaction, we were able to calculate, for the first time, all the linearly independent scattering matrix elements at 0° .

We then focused on the study of radiative capture reactions, particularly the ${}^{14}\text{N}(p, \gamma){}^{15}\text{O}$ reaction. We started by using the phenomenological R–matrix model to study the ${}^{14}\text{N}(p, \gamma){}^{15}\text{O}$ radiative radiative capture data to the ground state, the 6.18 MeV and the 6.79 MeV states of ${}^{15}\text{O}$. With this model we were able to determine the S–factor at energies relevant in astrophysics. The value obtained, $S(0) = 2.42$ keV.b, is 36% higher than the one obtained by Angulo and Descouvemont [Ang01]. This is the result of small differences of the fitted resonance properties and the $\frac{3}{2}^+$ subthreshold state, and is a consequence of the uncertainties in the low energy experimental data. This study also revealed the importance of background poles to account for the contributions arising from direct capture or low energy tails of high lying resonances, suggesting the relevance of a hybrid treatment of the ${}^{14}\text{N}(p, \gamma){}^{15}\text{O}$ in order to clarify the interplay between the resonant and the direct reaction mechanism.

The hybrid analysis of the ${}^{14}\text{N}(p, \gamma){}^{15}\text{O}$ required the development of a formalism where the photon equation could be treated on an equal footing with the particle equation in the coupled channels framework, which was accomplished in chapter 8. This development that has important application in the Nuclear Astrophysics field since many nuclear reactions important in Astrophysics involve photonuclear processes.

We started the hybrid analysis of the $^{14}\text{N}(p, \gamma)^{15}\text{O}$ with a potential description of the contribution to the background from negative parity states only, and were able with this simple model to successfully describe the data for radiative capture to the 6.79 MeV state, as well as for the ground state and 6.18 MeV state of ^{15}O . We then extended the hybrid analysis to the treatment of all the background contributions. In this study we also observed some discrepancies between the resonance parameters obtained and the values quoted by Angulo and Descouvemont [Ang01]. The total S-factor at astrophysical energies obtained in this analysis, $S(0)=1.12$ keV.b, is significantly lower than the one obtained with the phenomenological R-matrix analysis described earlier, and one quoted by Angulo and Descouvemont [Ang01], $S(0)=1.77\pm 0.20$ keV.b.

The reason for the discrepancies between S-factor values obtained for the $^{14}\text{N}(p, \gamma)^{15}\text{O}$ reaction, and also for the differences observed in the values obtained for the resonance parameters from different studies, is related to the uncertainties of the low energy experimental data, which do not allow a proper definition of the properties of the 6.79 MeV subthreshold state and the $\frac{1}{2}^+$ resonance at $E=0.262$ MeV. The ambiguities in the fitting procedure are expected to be resolved once the new experimental data, obtained by the ongoing experiments from the LUNA collaboration and TUNL, becomes available. These will significantly reduce the uncertainties in the low energy region, and allow for a much more reliable analysis of the $^{14}\text{N}(p, \gamma)^{15}\text{O}$ reaction.

With the application of the hybrid framework to the study of transfer and radiative capture reactions we proved the usefulness of this approach in the analysis of low energy nuclear reaction. Indeed, this work and the tool that was developed in its context, have created a significant number of research opportunities that will be pursued in the near future. These include the analysis of photon induced reactions, which are important in stellar environments and constitute a modern topic of research, the consideration of spin correlation coefficients in the analysis of the $^3\text{He}(d,p)^4\text{He}$ reaction, made possible by the new polarized target available at TUNL, and the analysis of the $^{12}\text{C}(\alpha, \gamma)^{16}\text{O}$ and $^7\text{Li}(p, \gamma)^8\text{Be}$ reactions, which were only briefly studied in this work.

Appendix A

Elastic scattering of spinless particles by a central potential

In the case of the elastic scattering of spinless particles the formalism becomes quite simple since one can drop the indices S_p , S_t and μ , that become zero, and also τ since we consider only elastic scattering. This case is however important to understand the application of the formalism to a general case.

The R-function

Considering the Schrödinger for the radial parts of the wave functions in the internal region for a given relative angular momentum, $R^{-1}u_L(R)$, at two different energies E_1 and E_2 :

$$\frac{d^2 u_1}{dR^2} + \frac{2m}{\hbar^2}(E_1 - V)u_1 = 0 \quad (\text{A.1})$$

$$\frac{d^2 u_2}{dR^2} + \frac{2m}{\hbar^2}(E_2 - V)u_2 = 0 \quad (\text{A.2})$$

where V includes the centrifugal term. Multiplying (A.1) by u_2 and (A.2) by u_1 , and integrating the difference of these equations from zero to the channel radius, one obtains the Green's theorem relation:

$$\left(u_2 \frac{du_1}{dR} - u_1 \frac{du_2}{dR} \right)_{R=a} + \frac{2m}{\hbar^2}(E_1 - E_2) \int_0^a u_1 u_2 dR = 0 \quad (\text{A.3})$$

since u should be zero at the origin for the radial term $R^{-1}u_L(R)$ to be finite.

For certain energies, E_λ , the solutions of the Schrödinger equation have zero derivative at the surface:

$$\left(\frac{du_\lambda}{dR}\right)_{R=a} = 0 \quad (\text{A.4})$$

These energies are energy eigenvalues and the solutions are eigenfunctions that satisfy the boundary condition (A.4). Using two of these eigenfunctions in the Green's theorem relation (A.3), one observes that these eigenfunctions form a orthogonal set of normalized radial functions in the internal region. The solutions of the Schrödinger equation for an arbitrary energy, E , may therefore be expanded in the internal region as a function of u_λ :

$$u_E(R) = \sum_{\lambda} A_\lambda u_\lambda, \quad 0 \leq R \leq a, \quad (\text{A.5})$$

where the expansion coefficients are, using (A.3):

$$A_\lambda = \int_0^a u_\lambda u_E dR = \frac{\hbar^2}{2m} \frac{u_\lambda(a)}{E_\lambda - E} \left(\frac{du_E}{dR}\right)_{R=a} \quad (\text{A.6})$$

With (A.6) one can write (A.5) in the form:

$$u_E(R) = G(R, a) \left(a \frac{du_E}{dR}\right)_{R=a} \quad (\text{A.7})$$

$$G(R, a) = \frac{\hbar^2}{2ma} \sum_{\lambda} \frac{u_\lambda(R) u_\lambda(a)}{E_\lambda - E} \quad (\text{A.8})$$

The Green function $G(R, a)$ relates the value of the wave function in the internal region with its derivative on the surface. Recalling (1.23-1.24) one can define the R-function as:

$$R = G(a, a) = \sum_{\lambda} \frac{\gamma_\lambda^2}{E_\lambda - E} = \frac{u_E(a)}{a \left(\frac{du_E}{dR}\right)_{R=a}} \quad (\text{A.9})$$

where $\gamma_\lambda = \sqrt{\frac{\hbar^2}{2ma}} u_E(a)$ is the square root of the reduced level widths.

The boundary condition

Equation (A.4) involves the choice of a particular boundary condition for the solutions of the Schrödinger equation. However, a more generic choice of boundary can be made, namely (2.1):

$$\left(\frac{R}{u_\lambda} \frac{du_\lambda}{dR}\right)_{R=a} = B \quad (\text{A.10})$$

where B is a real constant (independent of λ). By choosing this general boundary condition one should make appropriate changes to the expression obtained in this chapter [Lan58, Vog62]. In what concerns the formal aspects of the theory, the channel radius, a , and the boundary condition, B , are just parameters. However, in the implementation of the model special care should be taken in the choice of these parameters.

The scattering function

The general solution, Ψ_L , can be written in the external region as a linear combination of the incoming, \mathcal{I} , and outgoing, \mathcal{O} , waves (1.21) and (1.22):

$$\Psi_L = \mathcal{I}_L - U_L \mathcal{O}_L \quad (\text{A.11})$$

where U_L is the scattering function. The scattering function can be written in terms of the R-function since:

$$R_L = \left(\frac{u_L}{\rho_\alpha u'_L} \right)_{R=a} = \frac{I_L - U_L \mathcal{O}_L}{\rho_\alpha (I'_L - U_L \mathcal{O}'_L)} \quad (\text{A.12})$$

$$\Leftrightarrow U_L = \frac{I_L}{\mathcal{O}_L} \left(\frac{1 - L_L^* R_L}{1 - L_L R_L} \right) \quad (\text{A.13})$$

Since R_L is real, U_L can be written in terms of a phase shift δ_L :

$$U_L = e^{2i\delta_L} \quad (\text{A.14})$$

with

$$\delta_L = tg^{-1} \left(\frac{R_L P_L}{1 - R_L S_L} \right) - \phi_L + \omega_L \quad (\text{A.15})$$

where S_L is the shift function, P_L is the penetrability, ϕ_L is the hard-sphere phase shift, and ω_L is the Coulomb phase shift.

The Cross section

Considering the linear combination of solutions of the wave equation:

$$i\sqrt{\pi}k^{-1} \sum_L (2L+1)^{\frac{1}{2}} (\mathcal{I}_L - U_L \mathcal{O}_L) \quad (\text{A.16})$$

and adding and subtracting the term

$$\begin{aligned} \frac{e^{ikz}}{\sqrt{v}} \chi_1 \chi_2 &= \frac{k^{-1}}{v} \sum_L (2L+1) \frac{F_L(\rho)}{R} P_L(\cos\theta) \chi_1 \chi_2 \\ &= i\sqrt{\pi}k^{-1} \sum_L (2L+1)^{\frac{1}{2}} (\mathcal{I}_L - \mathcal{O}_L) \end{aligned} \quad (\text{A.17})$$

(where we used (1.21) and (1.22), with $\omega_c = 0$ - neglecting the Coulomb phase shift, and the partial wave expansion of the plane wave, and $P_L(\cos\theta)$ are the Legendre polynomials) one write a solution of the wave equation as

$$\frac{e^{ikz}}{\sqrt{v}} \chi_1 \chi_2 + i\sqrt{\pi} k^{-1} \sum_L (2L+1)^{\frac{1}{2}} (1-U_L) \mathcal{O}_L \quad (\text{A.18})$$

that corresponds to the sum of a plane wave, describing incident flux, with a term corresponding to the outgoing wave. The asymptotic form of this solution is

$$\frac{1}{\sqrt{v}} \left[e^{ikz} + \frac{e^{ikR}}{R} A(\theta) \right] \chi_1 \chi_2 \quad (\text{A.19})$$

where:

$$A(\theta) = \frac{1}{2} i k^{-1} \sum_L (2L+1) (1-U_L) P_L(\cos\theta) \quad (\text{A.20})$$

is the complex scattering amplitude. The elastic cross section per unit solid angle is therefore:

$$\sigma(\theta) = |A(\theta)|^2 = \frac{1}{4} k^{-2} \left| \sum_L (2L+1) (1-U_L) P_L(\cos\theta) \right|^2 \quad (\text{A.21})$$

The total cross section is obtained integrating the previous expression over the solid angle:

$$\sigma = \int \sigma(\theta) d\Omega = \pi k^{-2} \sum_L (2L+1) |1-U_L|^2 \quad (\text{A.22})$$

where, in the R-matrix formalism, U_L is given by eq. (A.13).

Appendix B

R–matrix formalism: 2–channels

Considering eqs. (A.1) and (A.2) written in matrix notation:

$$\begin{bmatrix} c_1 \frac{d^2}{dR^2} + (V_{11} - E) & V_{12} \\ V_{21} & c_2 \frac{d^2}{dR^2} + (V_{22} - E) \end{bmatrix} \begin{bmatrix} f_1 \\ f_2 \end{bmatrix} = 0 \quad (\text{B.1})$$

We denote

$$\begin{bmatrix} f_1^{(1)} \\ f_2^{(1)} \end{bmatrix} \quad \begin{bmatrix} f_1^{(2)} \\ f_2^{(2)} \end{bmatrix} \quad (\text{B.2})$$

as the solutions for energy E_1 and E_2 respectively, $\mathbf{u}^{(1)}$ and $\mathbf{u}^{(2)}$.

In analogy with the procedure followed in appendix A, we multiply eq. (B.1) for energy E_1 by the transposed of $u^{(2)}$ and subtract the product of eq. (B.1) for energy E_2 by the transposed of $u^{(1)}$:

$$\begin{aligned} & \mathbf{u}^{(2)T} \begin{bmatrix} c_1 \frac{d^2}{dR^2} + (V_{11} - E_1) & V_{12} \\ V_{21} & c_2 \frac{d^2}{dR^2} + (V_{22} - E_1) \end{bmatrix} \mathbf{u}^{(1)} \\ & - \mathbf{u}^{(1)T} \begin{bmatrix} c_1 \frac{d^2}{dR^2} + (V_{11} - E_2) & V_{12} \\ V_{21} & c_2 \frac{d^2}{dR^2} + (V_{22} - E_2) \end{bmatrix} \mathbf{u}^{(2)} = 0 \end{aligned} \quad (\text{B.3})$$

which corresponds to, with $V_{12} = V_{21}$:

$$\begin{aligned} & c_1 f_1^{(2)} \frac{d^2}{dR^2} f_1^{(1)} - E_1 f_1^{(2)} f_1^{(1)} + c_2 f_2^{(2)} \frac{d^2}{dR^2} f_2^{(1)} - E_1 f_2^{(2)} f_2^{(1)} \\ & - c_1 f_1^{(1)} \frac{d^2}{dR^2} f_1^{(2)} + E_2 f_1^{(2)} f_1^{(1)} - c_2 f_2^{(1)} \frac{d^2}{dR^2} f_2^{(2)} + E_2 f_2^{(1)} f_2^{(2)} = 0 \end{aligned} \quad (\text{B.4})$$

After rearranging the terms in the previous expression and integrating by parts in

the internal region, one obtains:

$$\begin{aligned} & c_1 \left(f_1^{(2)} \frac{d}{dR} f_1^{(1)} - f_1^{(1)} \frac{d}{dR} f_1^{(2)} \right)_{R=a} + (E_2 - E_1) \int_0^a f_1^{(1)} f_1^{(2)} dR \\ & + c_2 \left(f_2^{(2)} \frac{d}{dR} f_2^{(1)} - f_2^{(1)} \frac{d}{dR} f_2^{(2)} \right)_{R=a} + (E_2 - E_1) \int_0^a f_2^{(1)} f_2^{(2)} dR = 0 \end{aligned} \quad (\text{B.5})$$

For zero logarithmic derivative at $R = a$ and with $E_2 \neq E_1$, eq. (B.3) yields

$$\begin{aligned} & \int_0^a \left(f_1^{(1)} f_1^{(2)} + f_2^{(1)} f_2^{(2)} \right) dR = 0 \\ \Leftrightarrow & \int_0^a \mathbf{u}^{(1)} \cdot \mathbf{u}^{(2)} dR = 0 \end{aligned} \quad (\text{B.6})$$

so that, for a given energy E the solution of the Schrödinger equation can be expanded in the internal region, corresponding to eq. (A.5) in the one channel case:

$$\mathbf{u}^E(R) = \sum_{\lambda} A_{\lambda} \mathbf{u}^{\lambda}(R) \quad 0 < R < a \quad (\text{B.7})$$

where

$$\begin{aligned} A_{\lambda} &= \int_0^a \mathbf{u}^{\lambda} \cdot \mathbf{u}^E dR \\ &= \int_0^a \mathbf{u}^{\lambda T} \mathbf{u}^E dR \end{aligned} \quad (\text{B.8})$$

Writing eq. (B.5) for the energy E one obtains, using the boundary condition (A.4), one obtains

$$-c_1 \left(f_1^{\lambda} \frac{d}{dR} f_1^E \right)_{R=a} - c_2 \left(f_2^{\lambda} \frac{d}{dR} f_2^E \right)_{R=a} + (E - E_{\lambda}) \int_0^a \mathbf{u}^{\lambda} \cdot \mathbf{u}^E dR = 0 \quad (\text{B.9})$$

We therefore obtain for A_{λ}

$$A_{\lambda} = \frac{c_1}{E - E_{\lambda}} \left(f_1^{\lambda} \frac{d}{dR} f_1^E \right)_{R=a} + \frac{c_2}{E - E_{\lambda}} \left(f_2^{\lambda} \frac{d}{dR} f_2^E \right)_{R=a} \quad (\text{B.10})$$

which can be written in matrix notation:

$$A_{\lambda} = \frac{1}{E - E_{\lambda}} \mathbf{u}^{\lambda}(a) \cdot \left(\mathcal{C} \frac{d}{dR} \mathbf{u}^E(a) \right)_{R=a} \quad (\text{B.11})$$

where \mathcal{C} is the diagonal matrix of coefficients c_1 and c_2 :

$$\mathcal{C} = \begin{bmatrix} c_1 & 0 \\ 0 & c_2 \end{bmatrix} \quad (\text{B.12})$$

Inserting A_λ into eq. (B.7) one obtains

$$\begin{aligned}\mathbf{u}^E(R) &= \sum_{\lambda} \frac{1}{E - E_\lambda} \mathbf{u}^\lambda(R) \mathbf{u}^\lambda(a) \cdot \left(\mathcal{C} \frac{d}{dR} \mathbf{u}^E(a) \right)_{R=a} \\ &= G(R, a) \left(a \frac{d}{dR} \mathbf{u}^E(a) \right)_{R=a}\end{aligned}\quad (\text{B.13})$$

where

$$G(R, a) = \frac{1}{a} \sum_{\lambda} \frac{1}{E - E_\lambda} \mathbf{u}^\lambda(R) [\mathbf{u}^\lambda(a)]^T \mathcal{C} \quad (\text{B.14})$$

and therefore the R-matrix is

$$\begin{aligned}R &= G(a, a) \\ &= \frac{1}{a} \sum_{\lambda} \frac{1}{E - E_\lambda} \mathbf{u}^\lambda(a) [\mathbf{u}^\lambda(a)]^T \mathcal{C} \\ &= \frac{1}{a} \sum_{\lambda} \frac{1}{E - E_\lambda} \begin{bmatrix} c_1 (f_1^\lambda)^2 & c_2 f_1^\lambda f_2^\lambda \\ c_1 f_2^\lambda f_1^\lambda & c_2 (f_2^\lambda)^2 \end{bmatrix}\end{aligned}\quad (\text{B.15})$$

From (B.14) we obtain the relations for the elastic and reaction elements of the R-matrix, R_{11} and R_{12} respectively:

$$R_{11} = \frac{1}{a} \frac{1}{E - E_\lambda} c_1 (f_1^\lambda)^2 \quad (\text{B.16})$$

$$R_{21} = \frac{1}{a} \frac{1}{E - E_\lambda} c_1 f_1^\lambda f_2^\lambda \quad (\text{B.17})$$

Appendix C

Transfer couplings

A transfer process between an initial state with a projectile, a , and a target A , $\alpha' \equiv i = \{a + A\}$, and a final state, $\alpha' \equiv f = \{b + B\}$, represented by $A(a, b)B$ and shown schematically in figure C.1, involves the calculation of the following transition amplitude [Sat83]-16.37:

$$\begin{aligned}
 & T_{\alpha\alpha'} \\
 & \equiv T_{fi} \\
 & = \int \int dR_i dR_f \psi_{(L_f S_b)j_f S_B}^{J_f}(R_f) \langle (L_f S_b)j_f S_B; J_f | \mathbf{V} | (L_i S_a)j_i S_A; J_i \rangle \phi_{(L_i S_a)j_i S_A}^{J_i}(R_i)
 \end{aligned} \tag{C.1}$$

where $J_i = J_f$ since the interaction is rotational invariant, R_i and R_f are relative coordinates of the initial and final states respectively, $\phi_{(L_i S_a)j_i S_A}^{J_i}(R_i)$ are the distorted radial wave functions of the initial state, and $\psi_{(L_f S_b)j_f S_B}^{J_f}(R_f)$ are the distorted radial wave functions of the final state.

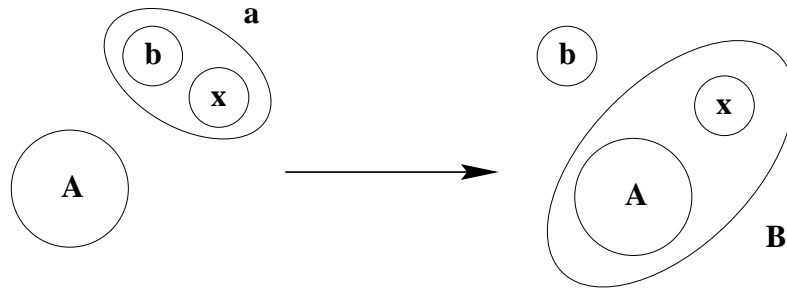


Figure C.1: Graphical description of the transfer process $A(a,b)B$.

The initial state has a composite projectile with internal coordinates $\mathbf{r}_{p,i} \equiv \{\mathbf{r}_p, \mathbf{r}_i\}$: $\chi_{S_a}(\mathbf{r}_p, \mathbf{r}_i) = |(L'_i s)j'_i S_b; S_a \rangle$, and the final state has a composite target with internal coordinates $\mathbf{r}_{t,f} \equiv \{\mathbf{r}_t, \mathbf{r}_f\}$: $\chi_{S_B}(\mathbf{r}_t, \mathbf{r}_f) = |(L'_f s)j'_f S_A; S_B \rangle$ [Tho88]. These coordinates are represented in figure C.2.

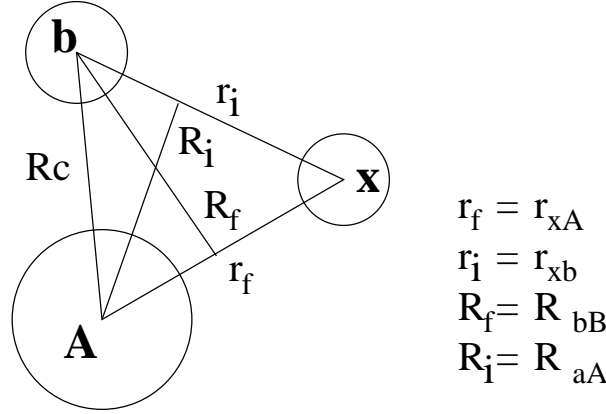


Figure C.2: Radial coordinates for the description of a transfer process A(a,b)B.

The interaction potential, \mathbf{V} , is in the prior form:

$$\mathbf{V}^{prior} = V_{(L'_f s)j'_f}(\mathbf{r}_f) + U_{cc}(R) - U_i(\mathbf{R}_i) \quad (\text{C.2})$$

and in the post form:

$$\mathbf{V}^{post} = V_{(L'_i s)j'_i}(\mathbf{r}_i) + U_{cc}(R) - U_f(\mathbf{R}_f) \quad (\text{C.3})$$

where $V_{(L'_f s)j'_f}(\mathbf{r}_f)$ is the potential that binds the target in the final state $\{A-x\}$, $V_{(L'_i s)j'_i}(\mathbf{r}_i)$ binds the projectile in the initial state $\{b-x\}$, $U_{cc}(R) \equiv U_{Ab}(R)$ is the “core-core” potential, $U_i(\mathbf{R}_i)$ is the distortive optical potential in the initial channel that generates $\phi_{(L_i S_a)j_i S_A}^{J_i}(R_i)$, and $U_f(\mathbf{R}_f)$ is the optical potential in the final channel.

The source function is therefore:

$$\begin{aligned} S_\alpha &\equiv S_\alpha(R_f) \\ &= \int dR_i \langle (L_f S_b)j_f S_B; J_f | \mathbf{V} | (L_i S_a)j_i S_A; J_i \rangle \phi_{(L_i S_a)j_i S_A}^{J_i}(R_i) \end{aligned} \quad (\text{C.4})$$

and evaluates a non-local integral operator since it operates on a function of R_i , $\phi_{(L_i S_a)j_i S_A}^{J_i}(R_i)$, to produce a function of R_f . One needs therefore to evaluate the non-local kernel $V_{\alpha,\alpha'}(R_i, R_f)$ that enters eq. (1.15). When the potential \mathbf{V} contains only scalar potentials, the kernel calculation can be reduced to the problem of finding $\mathbf{X}_{L'_f, L_f; L'_i, L_i}^\Lambda((R_i, R_f))$ such that, given [Tho88]

$$\begin{aligned}
& \langle (L_f S_b) j_f S_B; J_f | \mathbf{V} | (L_i S_a) j_i S_A; J_i \rangle \\
&= \sum_{\Lambda F} (-1)^{s+S_a-F} \hat{j}_f \hat{S}_A \hat{j}'_f \hat{F} \hat{S}_b \hat{\Lambda} \begin{Bmatrix} L_i & S_a & j_i \\ L'_i & s & j'_i \\ \Lambda & F & j_f \end{Bmatrix} W(S_B j'_i J_f j_i; S_A j_f) \\
& \quad W(L'_f s S_b S_a; j'_f F) W(L_f L'_f j_f F; \Lambda S_b) \langle L'_f L_f; \Lambda | \mathbf{V} | L'_i L_i; \Lambda \rangle \quad (\text{C.5})
\end{aligned}$$

the integral operator $\langle L'_f L_f; \Lambda | \mathbf{V} | L'_i L_i; \Lambda \rangle$ has the kernel function $\mathbf{X}_{L'_f, L_f; L'_i L_i}^\Lambda(R_f, R_i)$. Using (E.3) and (E.4), and performing a Legendre expansion the radial kernel function can be written as [Tho88]:

$$\begin{aligned}
& \mathbf{X}_{L'_f, L_f; L'_i L_i}^\Lambda(R_f, R_i) \\
&= \frac{|b|^3}{2} \sum_{nn'} c(L'_f n) c(L'_i n') R_f R_i (a R_f)^{L'_f - n} (b R_i)^{L'_i - n'} (a' R_f)^{L'_i - n'} (b' R_i)^{n'} \\
& \quad \sum_T \mathbf{q}_{L'_f, L'_i}^T(R_f, R_i) (2T+1) (-1)^{\Lambda+T+L_f+L_i} \hat{L}'_f \hat{L}'_i (L'_f - n) (L'_i - n') \hat{n} \hat{n}' \hat{L}_f \hat{L}_i \\
& \quad \sum_{KK'} (2K+1) (2K'+1) \begin{pmatrix} L'_f - n & n' & K \\ 0 & 0 & 0 \end{pmatrix} \begin{pmatrix} L'_i - n' & n & K' \\ 0 & 0 & 0 \end{pmatrix} \\
& \quad \begin{pmatrix} K & L_f & T \\ 0 & 0 & 0 \end{pmatrix} \begin{pmatrix} K' & L_i & T \\ 0 & 0 & 0 \end{pmatrix} \\
& \quad \sum_Q (2Q+1) W(L'_f L_f L'_i L_i; \Lambda Q) W(K L_f K' L_i; T Q) \\
& \quad \begin{pmatrix} L'_i & Q & L'_f \\ n' & K & L'_f - n \\ L'_i - n' & K' & n \end{pmatrix} \quad (\text{C.6})
\end{aligned}$$

where a, a', b and b' are the coefficients obtained from writing \mathbf{r}_i and \mathbf{r}_f as linear combinations of \mathbf{R}_i and \mathbf{R}_f : $\mathbf{r}_f = a\mathbf{R}_f + b\mathbf{R}_i$ and $\mathbf{r}_i = a'\mathbf{R}_f + b'\mathbf{R}_i$; and

$$\mathbf{q}_{L'_f, L'_i}^T(R_f, R_i) = \frac{1}{2} \int_{-1}^1 \mathbf{V} \frac{u_{L'_f s j'_f}(r)}{r^{L'_f+1}} \frac{u_{L'_i s j'_i}(r')}{r'^{L'_i+1}} P_T(u) du \quad (\text{C.7})$$

where $r_f = \sqrt{a^2 R_f^2 + b^2 R_i^2 + 2ab R_f R_i u}$ (analogously for r_i), u is the cosine of the angle between \mathbf{R}_f and \mathbf{R}_i , and $P_T(u)$ are the Legendre polynomials.

Appendix D

Madison and natural quantization frames

The vector components of the beam polarization in the projectile helicity frame are obtained by resolving $\hat{\mathbf{S}}$ into x , y and z components and multiplying by the vector polarization magnitude p_Z . In matrix notation this corresponds to:

$$\begin{aligned} \begin{bmatrix} p_x \\ p_y \\ p_z \end{bmatrix} &= \begin{bmatrix} U_{xx} & U_{xy} & -\sin \beta \cos \phi \\ U_{yx} & U_{yy} & \sin \beta \cos \phi \\ U_{zx} & U_{zy} & \cos \beta \end{bmatrix} \begin{bmatrix} 0 \\ 0 \\ p_Z \end{bmatrix} \\ \Leftrightarrow p_{xyz} &= U p_{XYZ} \end{aligned} \quad (\text{D.1})$$

Considering the case in which the incident beam polarization has the quantization axis (Z) as an axis of symmetry (thus $p_{XX} = p_{YY} = -\frac{1}{2}p_{ZZ}$), the second rank tensor in the X, Y, X system, pp_{XYZ} is expressed in the x, y, z system by the relation:

$$pp_{xyz} = U pp_{XYZ} \tilde{U} \quad (\text{D.2})$$

where the tilde indicates the transposed matrix.

The polarization tensor in the X, Y, Z frame is

$$\begin{aligned} pp_{XYZ} &= \begin{bmatrix} -\frac{1}{2}p_{ZZ} & 0 & 0 \\ 0 & -\frac{1}{2}p_{ZZ} & 0 \\ 0 & 0 & p_{ZZ} \end{bmatrix} \\ &= \frac{3}{2}p_{ZZ} \begin{bmatrix} 0 & 0 & 0 \\ 0 & 0 & 0 \\ 0 & 0 & 1 \end{bmatrix} - \frac{1}{2}p_{ZZ} \begin{bmatrix} 1 & 0 & 0 \\ 0 & 1 & 0 \\ 0 & 0 & 1 \end{bmatrix} \end{aligned} \quad (\text{D.3})$$

and therefore:

$$pp_{xyz} = \frac{3}{2}p_{ZZ} U \begin{bmatrix} 0 & 0 & 0 \\ 0 & 0 & 0 \\ 0 & 0 & 1 \end{bmatrix} \tilde{U} - \frac{1}{2}p_{ZZ} \begin{bmatrix} 1 & 0 & 0 \\ 0 & 1 & 0 \\ 0 & 0 & 1 \end{bmatrix} \quad (\text{D.4})$$

where the relation $U\tilde{U} = I$ was used.

On the other hand, the polarization tensor, pp_{xyz} , is formed from the expectation values of the operator (3.2):

$$pp_{xyz} = \begin{bmatrix} p_{xx} & p_{xy} & p_{xz} \\ p_{xy} & p_{yy} & p_{yz} \\ p_{xz} & p_{yz} & p_{zz} \end{bmatrix} \quad (\text{D.5})$$

and therefore from (D.2) one obtains the explicit relations for the vector and tensor polarizations in the projectile helicity frame:

$$p_{xx} = \left(\frac{3}{2}U_{xz}U_{xz} - \frac{1}{2}\right)p_{ZZ} = \frac{1}{2}(3\sin^2\beta \sin^2\phi - 1) p_{ZZ} \quad (\text{D.6})$$

$$p_{yy} = \left(\frac{3}{2}U_{yz}U_{yz} - \frac{1}{2}\right)p_{ZZ} = \frac{1}{2}(3\sin^2\beta \cos^2\phi - 1) p_{ZZ} \quad (\text{D.7})$$

$$p_{zz} = \left(\frac{3}{2}U_{zz}U_{zz} - \frac{1}{2}\right)p_{ZZ} = \frac{1}{2}(3\cos^2\beta - 1) p_{ZZ} \quad (\text{D.8})$$

$$p_{xy} = U_{yz}U_{xz}p_{ZZ} = -\frac{3}{2}\sin^2\beta \cos\phi \sin\phi p_{ZZ} \quad (\text{D.9})$$

$$p_{yz} = U_{yz}U_{zz}p_{ZZ} = \frac{3}{2}\sin\beta \cos\beta \cos\phi p_{ZZ} \quad (\text{D.10})$$

$$p_{xz} = U_{xz}U_{zz}p_{ZZ} = -\frac{3}{2}\sin\beta \cos\beta \sin\phi p_{ZZ} \quad (\text{D.11})$$

Appendix E

Properties of spherical harmonics and Racah algebra

General properties of spherical harmonics

The following properties of spherical harmonics have been used in this work:

$$Y_L^\mu(\alpha\hat{r}) = Y_L^\mu(\hat{r}) \quad (\text{E.1})$$

when α is a positive constant;

$$Y_L^\mu(-\hat{r}) = (-1)^L Y_L^\mu(\hat{r}) \quad (\text{E.2})$$

Expansion of spherical harmonics

Let $\mathbf{r} = a\mathbf{r}_a + b\mathbf{r}_b$, then the spherical harmonic $Y_L^\mu(\alpha\hat{r})$ can be expanded in terms of spherical harmonics of \mathbf{r}_a and \mathbf{r}_b [Tho79, Bri93]:

$$Y_L^\mu(\hat{r}) = \sqrt{4\pi} \sum_{n=0}^L \sum_{\lambda=-n}^n c(L, n) \frac{(ar_a)^{L-n} (br_b)^n}{r_a^L} (L - n\mu - \lambda, n\lambda | L\mu) Y_{L-n}^{\mu-\lambda}(\hat{r}_a) Y_n^\lambda(\hat{r}_b) \quad (\text{E.3})$$

where:

$$c(L, n) = \sqrt{\frac{1}{2n+1}} \binom{2L+1}{2n}^{\frac{1}{2}} \quad (\text{E.4})$$

$$\binom{x}{y} = \frac{x!}{y!(x-y)!} \quad (\text{E.5})$$

The first order term is simply $Y_L^\mu(\hat{r}_a)$, and by going to second order one obtains (with $a = b = 1$):

$$\begin{aligned} Y_L^\mu(\hat{r}) &= Y_L^\mu(\hat{r}_a) \\ &+ \frac{r_b}{r_a} \sum_{\lambda=-1}^1 \sqrt{\frac{4\pi}{3}} \binom{2L+1}{2}^{\frac{1}{2}} (L-1\mu-\lambda, 1\lambda|L\mu) Y_{L-1}^{\mu-\lambda}(\hat{r}_a) Y_1^\lambda(\hat{r}_b) \\ &\approx Y_L^\mu(\hat{r}_a) \end{aligned} \quad (\text{E.6})$$

and one sees that, if $r_b \ll r_a$, second and higher order terms may be neglected.

Vector spherical harmonics

The vector spherical harmonics $\mathbf{Y}(\theta, \phi)$ are vector functions of the angles only (independent of the radial coordinate r) which are simultaneous eigenfunctions of J_z and $J^2 = J_x^2 + J_y^2 + J_z^2$. Since the operators L and S commute, we can construct these vector spherical harmonics by using the vector addition law

$$\mathbf{Y}_{Jj j'}^M = \sum_{m=-j}^j \sum_{m'=-j'}^{j'} (jm, j'm'|JM) Y_j^m(1) Y_{j'}^{m'}(2) \quad (\text{E.7})$$

When we take $j'=S=1$ has the spin of the photon, then previous relation becomes

$$\mathbf{Y}_{Jl1}^M = \sum_{m'=-1}^1 (lM - m', 1m'|JM) Y_l^{M-m'}(\theta, \phi) \boldsymbol{\xi}_{m'} \quad (\text{E.8})$$

where $\boldsymbol{\xi}_{m'}$ are the elements of the spherical basis for S .

The gradient formula

$$\begin{aligned} \nabla(f(r)Y_L^\mu(\hat{r})) &= \left[\frac{L}{2L+1} \right]^{\frac{1}{2}} \left(\frac{df}{dr} + \frac{L+1}{r} f \right) \mathbf{Y}_{L1, L-1}^\mu(\hat{r}) \\ &- \left[\frac{L+1}{2L+1} \right]^{\frac{1}{2}} \left(\frac{df}{dr} - \frac{L}{r} f \right) \mathbf{Y}_{L1, L+1}^\mu(\hat{r}) \end{aligned} \quad (\text{E.9})$$

In the special case where $f(r)$ is the spherical Bessel function of order L , the following relations are useful:

$$\frac{d}{dr} j_L(r) = k j_{L-1}(kr) - \frac{L+1}{r} j_L(kr) \quad (\text{E.10})$$

$$\frac{d}{dr} j_L(r) = -k j_{L+1}(kr) + \frac{L}{r} j_L(kr) \quad (\text{E.11})$$

The Wigner-Eckart theorem

The Wigner-Eckart theorem used in this work is [Boh69]:

$$\langle L_2\mu_2|Y_{L\mu}|L_1\mu_1\rangle = \frac{(L_1\mu_1, L\mu|L_2\mu_2)}{\hat{L}_2} \langle L_2||Y_L||L_1\rangle \quad (\text{E.12})$$

and

$$\langle L_2||Y_L||L_1\rangle = \frac{\hat{L}\hat{L}_1}{\sqrt{4\pi}}(L_10, L0|L_20) \quad (\text{E.13})$$

Relation between reduced matrix element and $9j$ symbol

$$\begin{aligned} \langle (L'_1L'_2)L'|(A_{l_1}B_{l_2})_{(l_1l_2)l}|(L_1L_2)L\rangle &= \hat{l}\hat{L}\hat{L}' \begin{Bmatrix} L_1 & L_2 & L \\ l_1 & l_2 & l \\ L'_1 & L'_2 & L' \end{Bmatrix} \\ &\langle L'_1||A_{l_1}||L_1\rangle \langle L'_2||B_{l_2}||L_2\rangle \end{aligned} \quad (\text{E.14})$$

In this work we have dealt with the $l_2 = 0$ case, which considerably simplifies the expression.

$6j$, $9j$ symbols and Racah W -functions

The following relations were used in this work [Bri93]:

$$\begin{Bmatrix} a & b & c \\ d & e & f \\ g & h & 0 \end{Bmatrix} = \frac{\delta_{cf}\delta_{gh}(-1)^{c+g-a-e}W(abde; cg)}{\hat{c}\hat{g}} \quad (\text{E.15})$$

$$\begin{pmatrix} a & b & c \\ 0 & 0 & 0 \end{pmatrix} = \frac{(-1)^{b-a}}{\hat{c}}(a0, b0|c0) \quad (\text{E.16})$$

Relationships between the Racah W -functions and the Clebesh-Gordon coefficients

$$\begin{aligned} & \sum_{\beta} (a\alpha, b\beta|e\alpha + \beta)(e\alpha + \beta, d\gamma - \alpha - \beta|c\gamma)(b\beta, d\gamma - \alpha - \beta|f\gamma - \alpha) \\ &= (a\alpha, f\gamma - \alpha|c\gamma) [(2e + 1)(2f + 1)]^{\frac{1}{2}} W(abcd; ef) \end{aligned} \quad (\text{E.17})$$

Appendix F

Demonstration of expressions important for chapter 7

The calculation of the magnetization term for electric transitions, eq. (7.33), uses:

$$\begin{aligned}
& \int \nabla_i \times \left[\Psi_{J_f}^{M_f*} \mathbf{S}_i \Phi_{J_i, S_p, S_t}^{M_i, M_p, M_t} \right] \cdot \mathbf{A}_{L\nu}(\mathbf{r}; E) \, d\mathbf{r}_{1A} \\
&= \frac{-i}{k} \int \left[\Psi_{J_f}^{M_f*} \mathbf{S}_i \Phi_{J_i, S_p, S_t}^{M_i, M_p, M_t} \right] \cdot \nabla_i \times \nabla_i \times \mathbf{A}_{L\nu}(\mathbf{r}; M) \, d\mathbf{r}_{1A} \\
&= \frac{ik}{\sqrt{L(L+1)}} \int \left[\Psi_{J_f}^{M_f*} \mathbf{S}_i \Phi_{J_i, S_p, S_t}^{M_i, M_p, M_t} \right] \cdot \mathbf{L}j_L(kr_i) Y_L^\nu(\hat{r}_i) \, d\mathbf{r}_{1A} \\
&= \frac{i^2 k^{L+1}}{\sqrt{L(L+1)}(2L+1)!!} \int \left[\Psi_{J_f}^{M_f*} \mathbf{S}_i \Phi_{J_i, S_p, S_t}^{M_i, M_p, M_t} \right] \cdot \nabla (r_i^L Y_L^\nu(\hat{r}_i)) \times \mathbf{r}_i \, d\mathbf{r}_{1A} \\
&= -\frac{k^{L+1}}{\sqrt{L(L+1)}(2L+1)!!} \int \left[\Psi_{J_f}^{M_f*} \mathbf{S}_i \Phi_{J_i, S_p, S_t}^{M_i, M_p, M_t} \right] \times \mathbf{r}_i \cdot \nabla (r_i^L Y_L^\nu(\hat{r}_i)) \, d\mathbf{r}_{1A} \quad (\text{F.1})
\end{aligned}$$

(where we used eqs. (7.20) and (7.21), the gauge condition, and the fact that $\mathbf{A}_{L\nu}(\mathbf{r}; E)$ and $\mathbf{A}_{L\nu}(\mathbf{r}; M)$)

To calculate the reduced matrix element for electric transitions, eq. (7.48), we note that the transition operator is diagonal in the wave functions for projectile and target and use the relation between the reduced matrix element and $9j$ (E.14) symbols, obtaining for (7.47):

$$\begin{aligned}
& \langle \chi_{S_p''}^{M_p''} \chi_{S_t''}^{M_t''} \Psi_{J_f}^{M_f} | Q E_L^\mu(\mathbf{R}) | \Phi_{J_i, S_p, S_t}^{M_i, M_p, M_t} \rangle_{\mathbf{r}_{1A}} \chi_{S_p'}^{M_p'} \chi_{S_t'}^{M_t'} \rangle_{\mathbf{r}_{1A}} \\
&= \frac{4\pi}{k_p} \sum_{S_p'', j_f, L_f} \sum_{\substack{L_i, \mu_i, j_i, m_i \\ L_i', j_i', S_p', S_t'}} e^{i\sigma_{L_i} Y_{L_i}^{\mu_i}(\hat{k}_p)} i^{L_i'} (L_i \mu_i, S_p M_p | j_i m_i) (j_i m_i, S_t M_t | J_i M_i) \\
&\quad C_L (J_i M_i, L \mu | J_f M_f) \int R^2 \frac{\psi_{\alpha_f}^{J_f}(R)}{R} R^L \frac{\phi_{\alpha_i, \alpha_i}^{J_i}(R)}{R} dR \\
&\quad \hat{J}_i (-1)^{S_t' + L - j_i' - j_f} W(j_i' J_i j_f J_f; S_t' L) \\
&\quad \langle \chi_{S_p''}^{M_p''} | \chi_{S_p'}^{M_p'} \rangle_{\mathbf{r}_{1, p-1}} \langle (L_f S_p'') j_f || Y_L(\hat{R}) || (L_i' S_p') j_i' \rangle_{\hat{\mathbf{R}}} \tag{F.2}
\end{aligned}$$

where the $9j$ symbol was written in terms of the Racah W -function, eq. (E.15). Applying the same relations to the reduced matrix element of (F.2) one obtains:

$$\begin{aligned}
& \langle \chi_{S_p''}^{M_p''} \chi_{S_t''}^{M_t''} \Psi_{J_f}^{M_f} | Q E_L^\mu(\mathbf{R}) | \Phi_{J_i, S_p, S_t}^{M_i, M_p, M_t} \rangle_{\mathbf{r}_{1A}} \chi_{S_p'}^{M_p'} \chi_{S_t'}^{M_t'} \rangle_{\mathbf{r}_{1A}} \\
&= \frac{4\pi}{k_p} \sum_{j_f, L_f} \sum_{\substack{L_i, \mu_i, j_i, m_i \\ L_i', j_i', S_p', S_t'}} e^{i\sigma_{L_i} Y_{L_i}^{\mu_i}(\hat{k}_p)} i^{L_i'} (L_i \mu_i, S_p M_p | j_i m_i) (j_i m_i, S_t M_t | J_i M_i) \\
&\quad C_L (J_i M_i, L \mu | J_f M_f) \int R^2 \frac{\psi_{\alpha_f}^{J_f}(R)}{R} R^L \frac{\phi_{\alpha_i, \alpha_i}^{J_i}(R)}{R} dR \\
&\quad \hat{J}_i \hat{j}_i \hat{j}_f (-1)^{S_p' + S_t' - j_i' - L_i'} W(j_i' J_i j_f J_f; S_t' L) W(L_i' j_i' L_f j_f; S_p' L) \\
&\quad \langle L_f || Y_L(\hat{R}) || L_i' \rangle_{\hat{\mathbf{R}}} \tag{F.3}
\end{aligned}$$

$$\begin{aligned}
&= \frac{\sqrt{4\pi}}{k_p} \sum_{j_f, L_f} \sum_{\substack{L_i, \mu_i, j_i, m_i \\ L_i', j_i'}} e^{i\sigma_{L_i} Y_{L_i}^{\mu_i}(\hat{k}_p)} i^{L_i'} (L_i \mu_i, S_p M_p | j_i m_i) (j_i m_i, S_t M_t | J_i M_i) \\
&\quad C_L (J_i M_i, L \mu | J_f M_f) \int R^2 \frac{\psi_{\alpha_f}^{J_f}(R)}{R} R^L \frac{\phi_{\alpha_i, \alpha_i}^{J_i}(R)}{R} dR \\
&\quad \hat{J}_i \hat{j}_i' \hat{j}_f \hat{L} \hat{L}_i' \hat{L}_f (-1)^{S_p + S_t - j_i' - L_i' + L_f} \\
&\quad W(j_i' J_i j_f J_f; S_t L) W(L_i' j_i' L_f j_f; S_p L) \begin{pmatrix} L_f & L & L_i' \\ 0 & 0 & 0 \end{pmatrix} \tag{F.4}
\end{aligned}$$

where in the last step the reduced matrix element was written in terms of the $6j$ symbols using eqs. (E.13) and (E.16); and $S_{p(t)}$ were set to $S_{p(t)}$ respectively.

The calculations for the convective and magnetization current contributions to the magnetic matrix element, eqs. (7.50) and (7.51), use

$$\begin{aligned}
& \int \left[\Psi_{J_f}^{M_f*} \nabla_i \Phi_{J_i, S_p, S_t}^{M_i, M_p, M_t} - (\nabla_i \Psi_{J_f}^{M_f*}) \Phi_{J_i, S_p, S_t}^{M_i, M_p, M_t} \right] \cdot \mathbf{A}_{L\nu}(\mathbf{r}; M) \, d\mathbf{r}_{1A} \\
&= 2 \int \Psi_{J_f}^{M_f*} (\nabla_i \Phi_{J_i, S_p, S_t}^{M_i, M_p, M_t}) \cdot \mathbf{A}_{L\nu}(\mathbf{r}; M) \, d\mathbf{r}_{1A} \\
&= \frac{2k^L}{\sqrt{L(L+1)}(2L+1)!!} \int (\Psi_{J_f}^{M_f*} \nabla_i \Phi_{J_i, S_p, S_t}^{M_i, M_p, M_t}) \cdot \mathbf{L} r_i^L Y_L^\nu(\hat{r}_i) \, d\mathbf{r}_{1A} \\
&= \frac{2ik^L}{\sqrt{L(L+1)}(2L+1)!!} \int (\Psi_{J_f}^{M_f*} \nabla_i \Phi_{J_i, S_p, S_t}^{M_i, M_p, M_t}) \cdot \nabla_i (r_i^L Y_L^\nu(\hat{r}_i)) \times \mathbf{r}_i \, d\mathbf{r}_{1A} \\
&= \frac{2ik^L}{\sqrt{L(L+1)}(2L+1)!!} \int (\Psi_{J_f}^{M_f*} \mathbf{r}_i \times \nabla_i \Phi_{J_i, S_p, S_t}^{M_i, M_p, M_t}) \cdot \nabla_i (r_i^L Y_L^\nu(\hat{r}_i)) \, d\mathbf{r}_{1A} \\
&= -\frac{2k^L}{\sqrt{L(L+1)}(2L+1)!!} \int (\Psi_{J_f}^{M_f*} \mathbf{L}_i \Phi_{J_i, S_p, S_t}^{M_i, M_p, M_t}) \cdot \nabla_i (r_i^L Y_L^\nu(\hat{r}_i)) \, d\mathbf{r}_{1A} \quad (\text{F.5})
\end{aligned}$$

(where we used eqs. (7.20) and (7.21), the gauge condition, and integrated by parts to remove the gradient operator from $\Psi_{J_f}^{M_f*}$), and

$$\begin{aligned}
& \int \nabla_i \times \left[\Psi_{J_f}^{M_f*} \mathbf{S}_i \Phi_{J_i, S_p, S_t}^{M_i, M_p, M_t} \right] \cdot \mathbf{A}_{L\nu}(\mathbf{r}; M) \, d\mathbf{r}_{1A} \\
&= \int \left[\Psi_{J_f}^{M_f*} \mathbf{S}_i \Phi_{J_i, S_p, S_t}^{M_i, M_p, M_t} \right] \cdot \nabla_i \times \mathbf{A}_{L\nu}(\mathbf{r}; M) \, d\mathbf{r}_{1A} \\
&= \frac{k^L}{\sqrt{L(L+1)}(2L+1)!!} \int \left[\Psi_{J_f}^{M_f*} \mathbf{S}_i \Phi_{J_i, S_p, S_t}^{M_i, M_p, M_t} \right] \cdot \nabla_i \times (\mathbf{L} r_i^L Y_L^\nu(\hat{r}_i)) \, d\mathbf{r}_{1A} \\
&= \frac{ik^L}{(2L+1)!!} \sqrt{\frac{L+1}{L}} \int \left[\Psi_{J_f}^{M_f*} \mathbf{S}_i \Phi_{J_i, S_p, S_t}^{M_i, M_p, M_t} \right] \cdot \nabla_i (r_i^L Y_L^\nu(\hat{r}_i)) \, d\mathbf{r}_{1A} \quad (\text{F.6})
\end{aligned}$$

respectively.

To calculate the reduced matrix element for magnetic transitions, eq. (7.63), we note, as before, that the transition operator is diagonal in the wave functions for projectile and target and use the relation between the reduced matrix element and $9j$ (E.14) symbols, obtaining for (7.62):

$$\begin{aligned}
& \langle \chi_{S_p''}^{M_p''} \chi_{S_t''}^{M_t''} \Psi_{J_f}^{M_f} | Q M_L^\mu(\mathbf{R}) | \Phi_{J_i, S_p, S_t}^{M_i, M_p, M_t} \rangle \chi_{S_p'}^{M_p'} \chi_{S_t'}^{M_t'} \rangle_{\mathbf{r}_{1A}} \\
&= \frac{4\pi}{k_p} \sum_{S_p'', j_f, L_f} \sum_{\substack{L_i, \mu_i, j_i, m_i \\ L_i', j_i', S_p', S_t'}} e^{i\sigma_{L_i} Y_{L_i}^{\mu_i}(\hat{k}_p) i^{L_i'}} (L_i \mu_i, S_p M_p | j_i m_i) (j_i m_i, S_t M_t | J_i M_i) \\
&\quad \frac{2\mu_N}{L+1} C_L^m (J_i M_i, L \mu | J_f M_f) \int R^2 \frac{\psi_{\alpha_f}^{J_f}(R)}{R} R^{L-1} \frac{\phi_{\alpha_i, \alpha_i}^{J_i}(R)}{R} dR \\
&\quad \hat{J}_i (-1)^{S_i+L-j_i-J_f} W(j_i' J_i j_f J_f; S_t' L) \sqrt{L(2L+1)} \\
&\quad \langle \chi_{S_p''}^{M_p''} | \chi_{S_p'}^{M_p'} \rangle_{\mathbf{r}_{1, p-1}} \langle (L_f S_p'') j_f || [\mathbf{Y}_{L1L-1}(\hat{R}) \cdot \mathbf{L}_R] || (L_i' S_p') j_i \rangle_{\hat{\mathbf{R}}} \quad (\text{F.7})
\end{aligned}$$

where the $9j$ symbol was written in terms of the Racah W -function, eq. (E.15). Applying the same relations to the reduced matrix element of (F.7) one obtains:

$$\begin{aligned}
& \langle \chi_{S_p''}^{M_p''} \chi_{S_t''}^{M_t''} \Psi_{J_f}^{M_f} | Q M_L^\mu(\mathbf{R}) | \Phi_{J_i, S_p, S_t}^{M_i, M_p, M_t} \rangle \chi_{S_p'}^{M_p'} \chi_{S_t'}^{M_t'} \rangle_{\mathbf{r}_{1A}} \\
&= \frac{4\pi}{k_p} \sum_{j_f, L_f} \sum_{\substack{L_i, \mu_i, j_i, m_i \\ L_i', j_i'}} e^{i\sigma_{L_i} Y_{L_i}^{\mu_i}(\hat{k}_p) i^{L_i'}} (L_i \mu_i, S_p M_p | j_i m_i) (j_i m_i, S_t M_t | J_i M_i) \\
&\quad \frac{2\mu_N}{L+1} C_L^m (J_i M_i, L \mu | J_f M_f) \int R^2 \frac{\psi_{\alpha_f}^{J_f}(R)}{R} R^{L-1} \frac{\phi_{\alpha_i, \alpha_i}^{J_i}(R)}{R} dR \\
&\quad \hat{J}_i \hat{j}_i \hat{j}_f (-1)^{S_p+S_t-j_i-j_f-L_i-J_f} W(j_i' J_i j_f J_f; S_t' L) W(L_i' j_i' L_f j_f; S_p L) \\
&\quad \langle L_f || [\mathbf{Y}_{L1L-1}(\hat{R}) \cdot \mathbf{L}_R] || L_i' \rangle_{\hat{\mathbf{R}}} \quad (\text{F.8})
\end{aligned}$$

where $S_{p(t)}'$ were set to $S_{p(t)}$ respectively, since the central term of the transition operator does not allow spin excitation.

The reduce matrix element in (F.8) can be calculated using the Wigner-Eckart theorem (E.12):

$$\begin{aligned}
& \langle L_f || [\mathbf{Y}_{L1L-1}(\hat{R}) \cdot \mathbf{L}_R] || L_i' \rangle \\
&= \frac{\langle L_f | [\mathbf{Y}_{L1L-1}^q(\hat{R}) \cdot \mathbf{L}_R] | L_i' \rangle \hat{L}_f}{(L_i' \mu_i', L_q | L_f \mu_f)} \\
&= \frac{\hat{L}_f}{(L_i' \mu_i', L_q | L_f \mu_f)} \int d\Omega_R Y_{L_f}^{\mu_f*} \mathbf{Y}_{L1L-1}^q \cdot \mathbf{L}_R Y_{L_i'}^{\mu_i'} \\
&= \frac{\hat{L}_f \sqrt{L_i'(L_i'+1)}}{(L_i' \mu_i', L_q | L_f \mu_f)} \int d\Omega_R Y_{L_f}^{\mu_f*} \mathbf{Y}_{L1L-1}^q \cdot \mathbf{Y}_{L_i' 1 L_i'}^{\mu_i'} \quad (\text{F.9})
\end{aligned}$$

and using the definition of the spherical harmonics one obtains for (F.8):

$$\begin{aligned}
& \langle L_f || \left[\mathbf{Y}_{L_1 L-1}(\hat{R}) \cdot \mathbf{L}_R \right] || L'_i \rangle \\
&= \frac{\hat{L}_f \sqrt{L'_i(L'_i+1)}}{(L'_i \mu'_i, Lq | L_f \mu_f)} \\
& \quad \sum_{\mu} (-1)^{-\mu} (L-1q-\mu, 1\mu | Lq) (L'_i \mu'_i + \mu, 1-\mu | L'_i \mu'_i) \int d\Omega_R Y_{L_f}^{\mu_f *} Y_{L-1}^{q-\mu} Y_{L'_i}^{\mu'_i + \mu} \\
&= \frac{\hat{L}_f \sqrt{L'_i(L'_i+1)}}{(L'_i \mu'_i, Lq | L_f \mu_f)} \\
& \quad \sum_{\mu} (-1)^{-\mu} (L-1q-\mu, 1\mu | Lq) (L'_i \mu'_i + \mu, 1-\mu | L'_i \mu'_i) \langle L_f \mu_f | L-1q-\mu | L'_i \mu'_i + \mu \rangle \\
&= \frac{\hat{L}_i (k \hat{-} 1) \sqrt{L'_i(L'_i+1)}}{(L'_i \mu'_i, Lq | L_f \mu_f) \sqrt{4\pi}} (L_f 0, L-10 | L'_i 0) \\
& \quad \sum_{\mu} (-1)^{-\mu} (L-1q-\mu, 1\mu | Lq) (L'_i \mu'_i + \mu, 1-\mu | L'_i \mu'_i) (L'_i \mu'_i + \mu, L-1q-\mu | L_f \mu_f) \\
&= \frac{(2L'_i+1)(k \hat{-} 1) \hat{k} \sqrt{L'_i(L'_i+1)}}{\sqrt{4\pi}} (L_f 0, L-10 | L'_i 0) W(L'_i 1 L_f L-1; L'_i L) \quad (\text{F.10})
\end{aligned}$$

Bibliography

- [Ang01] C. Angulo and P. Descouvemont, *Rev. Mod. Phys.* **39**, (2001), 306.
- [AS91] F. Ajzenberg-Selove, *Nucl. Phys. A* **523**, (1991), 1.
- [Azu94] R. E. Azuma, L. Buchmann, F. C. Barker, C. A. Barnes, J. M. d'Auria, M. Dombisky, U. Giesen, K. P. Jackson, J. D. King, R. G. Korteling, P. McNeely, J. Powell, G. Roy, J. Vincent, T. R. Wang, S. S. M. Wong and P. R. Wrean, *Phys. Rev. C* **50**, (1994), 1194.
- [Ber02] P. F. Bertone *et al.*, *Phys. Rev. Lett.* **87**, (2002), 2001.
- [Bit90] M. Bittcher, W. Grüebler, V. König, P. A. Schmelzbach, B. Vuaridel and J. Ulbricht, *Few-Body Syst.* **9**, (1990), 165.
- [Bla58] J. M. Blatt and V. F. Weisskopf, *Theoretical Nuclear Physics*, John Wiley & Sons, 1958.
- [Boh69] A. Bohr and B. R. Mottelson, *Nuclear Structure Vol. I*, W.A. Benjamin, 1969.
- [Bra00] B. M. Braizinha, *A Reação $^{12}\text{C}(\alpha,\gamma)^{16}\text{O}$ a Energias Relevantes em Astrofísica*, Master's thesis, Universidade de Lisboa, FCUL, 2000.
- [Bra03] B. Braizinha *et al.*, in *Proceedings of the 17th International IUPAC Conference on Few-Body Problems in Physics*, 2003.
- [Bra04] B. Braizinha, C. R. Brune, A. M. Eiró, B. M. Fisher, H. J. Karwowski, D. S. Leonard, E. J. Ludwig, F. D. Santos and I. J. Thompson, *Phys. Rev. C* **69**, (2004), 0149.
- [Bri93] D. M. Brink and G. R. Satchler, *Angular Momentum*, Clarendon Press, Oxford, 1993.
- [Bro66] L. Brown, H. A. Christ and H. Rudin, *Nucl. Phys.* **79**, (1966), 459.
- [Bru01] C. R. Brune, W. H. Geist, H. J. Karwowski, E. J. Ludwig, K. D. Veal and M. H. Wood, *Phys. Rev. C* **63**, (2001), 044013.

- [Bur57] E. M. Burbidge, G. R. Burbidge, W. A. Fowler and F. Hoyle, *Rev. Mod. Phys.* **29**, (1957), 547.
- [Chr82] J. A. Christley and I. J. Thompson, *Comput. Phys. Commun.* **27**, (1982), 147.
- [Cle95] T. B. Clegg *et al.*, *Nucl. Instrum. Methods Phys. Res. A* **357**, (1995), 200.
- [Des00] P. Descouvemont, in *Astrophysica code*
URL <http://pntpm.ulb.ac.be/astro/>, 2000.
- [Eis88] J. M. Eisenber and W. Greiner, *Excitation Mechanisms of the Nucleus*, North-Holland, 1988.
- [Fle02] K. A. Fletcher, C. R. Brune, B. M. Fisher, R. P. Fitzgerald, H. J. Karwowski, D. S. Leonard, E. J. Ludwig, R. C. Runkle, M. H. Wood, W. H. Geist, K. D. Veal and G. M. Hale, *Phys. Rev. C* **66**, (2002), 057601.
- [Gei98] W. H. Geist, *The $^3\text{He}(d,p)^4\text{He}$ Reaction at Low energies*, Ph.D. thesis, The University of North Carolina at Chapel Hill, 1998.
- [Gei99] W. H. Geist, C. R. Brune, H. J. Karwowski, E. J. Ludwig, K. D. Veal and G. M. Hale, *Phys. Rev. C* **60**, (1999), 054003.
- [Gom01] J. Gomez-Camacho and R. C. Johnson, *Scattering*, (Pike & Sabatier, eds.), Academic Press (NY), 2001.
- [Gre95] W. Greiner and J. A. Maruhn, *Nuclear Models*, Springer, 1995.
- [Jam94] F. James, in *MINUIT - Function Minimization and Error Analysis Reference Manual*, Version 94.1
URL <http://wwwasdoc.web.cern.ch/wwwasdoc/minuit/minmain.html>, 1994.
- [Jen79] B. Jenny, W. Gruebler, V. König, P. A. Schmelzbach, R. Risler, H. R. Bürgi and D. O. Boerma, *Nucl. Phys. A* **324**, (1979), 99.
- [Joh73] C. H. Johnson, *Phys. Rev. C* **7**, (1973), 561.
- [Kap38] P. L. Kapur and R. E. Piers, *Proc. Roy. Soc. (London) A* **166**, (1938), 277.
- [Kie01] A. Kievsky, private communication, 2001.
- [Koo74] S. E. Koonin, T. A. Tombrello and G. Fox, *Nucl. Phys. A* **220**, (1974), 941.
- [Kra87] A. Krauss, H. W. Becker, H. P. Trautvetter, C. Rolfs and K. Brand, *Nucl. Phys. A* **465**, (1987), 150.
- [Lan58] A. M. Lane and R. G. Thomas, *Rev. Mod. Phys.* **30**, (1958), 257.

- [LUN04] LUNA, in
URL <http://axpd30.pd.infn.it/luna/>, 2004.
- [Mad71] Madison convention, in Proc. of the Third Int. Symp. on Polarization Phenomena in Nuclear Reactions, edited by H. H. Barschall and W. Haeberli, Madison, Wisconsin, (1971), page XXV.
- [Ohl72] G. G. Ohlsen, Rep. Prog. Phys. **35**, (1972), 717.
- [Pud95] B. S. Pudliner, V. R. Pandharipande, J. Carlson and R. B. Wiringa, Phys. Rev. Lett. **74**, (1995), 4396.
- [Rei68] R. Reid, Ann. Phys. **50**, (1968), 411.
- [Rod67] L. S. Rodberg and R. M. Thaler, Introduction to Quantum Theory of Scattering, Academic Press, 1967.
- [Ros58] M. E. Rose, Elementary Theory of Angular Momentum, John Wiley & Sons, 1958.
- [Sam99] J. M. Sampaio, Reação ${}^7\text{Li}(\bar{p},\gamma){}^8\text{Be}$ a Baixas Energias, Master's thesis, Universidade de Lisboa, FCUL, 1999.
- [San74] F. D. Santos, Nucl. Phys. A **236**, (1974), 90.
- [Sat83] G. R. Satchler, Direct Nuclear Reactions, Clarendon Press, Oxford, 1983.
- [Sch87] U. Schröder, H. W. Becker, G. Bogaert, J. Gorres, C. Rolfs, H. P. Trautvetter, R. E. Azuma, C. Campbell, J. D. King and J. Vise, Nucl. Phys. A **467**, (1987), 240.
- [Tho79] I. J. Thompson, Nuclear Cluster Reactions, Ph.D. thesis, University of Auckland, NZ, 1979.
- [Tho88] I. J. Thompson, Computer Physics Reports **7**, (1988), 167.
- [Tho01] I. J. Thompson, Scattering, (Pike & Sabatier, eds.), Academic Press (NY), 2001.
- [Tho04] I. J. Thompson, in FRESCO manual, University of Surrey
URL <http://www.fresco.org.uk>, 2004.
- [Til02] D. R. Tilley *et al.*, Nucl. Phys. A **708**, (2002), 3.
- [Viv98] M. Viviani, S. Rosati and A. Kievsky, Phys. Rev. Lett. **81**, (1998), 1580.
- [Vog62] E. Vogt, Rev. Mod. Phys. **34**, (1962), 723.
- [Wig47] E. P. Wigner and L. Eisenbud, Phys. Rev. **72**, (1947), 29.

- [Wir95] R. B. Wirlinga, V. G. J. Stoks and R. Schiavilla, *Phys. Rev. C* **51**, (1995), 38.
- [Woo02] M. H. Wood, C. R. Brune, B. M. Fisher, H. J. Karwowski, D. S. Leonard, E. J. Ludwig, A. Kievsky, S. Rosati and M. Viviani, *Phys. Rev. C* **65**, (2002), 034002.
- [Yam04] K. Yamada *et al.*, *Phys. Lett. B* **579**, (2004), 265.
- [Zie00] J. F. Ziegler and J. P. Biersack, in *Stopping and Range of Ions in Matter*
URL <http://www.research.ibm.com/ionbeams/>, SRIM-2000.